Alma Mater Studiorum – Università di Bologna
in cotutela con Universitat Politécnica de Valencia

DOTTORATO DI RICERCA IN

Chimica

Ciclo XXXIV

Settore Concorsuale: 03/C2

Settore Scientifico Disciplinare: CHIM/04

Valorization of bio-alcohols into added value chemicals

Presentata da: GIULIA BALESTRA

Coordinatore Dottorato

Prof.ssa D.TONELLI

Supervisori

Prof. F. CAVANI
Prof. J. M. LOPEZ NIETO

Co – Supervisore

Dr. T.TABANELLI
Prof.ssa S.ALBONETTI

Esame finale anno 2022

The research presented in this PhD thesis was carried out in the Department of Industrial Chemistry "Toso Montanari" of the University of Bologna (Unibo) and in the "Istituto de Teqnologia Quimica" (ITQ) of the "Universitat Politecnica de Valencia" (UPV) within the cotutelle agreement between Unibo in Italy and UPV in Spain.

RELAZIONE ATTIVITÀ SVOLTE:

Durante i tre anni di dottorato sono state svolte le seguenti attività:

CORSI:

- "Spettroscopia applicata" (4 CFU), tenuto dal Prof. F. Tamassia;
- "FROM IP MANAGEMENT TO TECHNOLOGY TRANSFER FOR BUSINESS" (3CFU), tenuto da Prof. Reschiglian;
- "Workshop on Academic Writing and Publishing", Enago Academy;
- "Complementi di Chimica Inorganica",(3 CFU);
- "Share Food, Cut Waste", corso on-line Politecnico di Milano;
- "Personal Risk Reduction In Insecure Contexts", corso on-line Politecnico di Milano.
- "Communication skills for engineering scholars", corso on-line Politecnico di Milano.
- "Being a researcher (in Information Science and Technology)", corso on-line Politecnico di Milano.
- 09/2020-2021 - Abroad period for the Co-tutelle program in the "Instituto de Tecnología Química" (ITQ) of the "Universitat Politècnica de València-Consejo Superior de Investigaciones Científicas"(UPV-CSIC) in Valencia, Spain.

CONGRESSI:

- 7° Workshop Nazionale GRUPPO INTERDIVISIONALE GREEN CHEMISTRY- CHIMICA SOSTENIBILE, Padova, 05/07/2019 – Presentazione di Poster: "Studio della riduzione catalitica di 5-(idrossimetil)-2-furaldeide";
- XXI Congresso Nazionale della Divisione di Chimica Industriale della Società Chimica Italiana - Salerno 27/08/2019 – Poster presentation:·" Study of the catalytic hydrogenation of 5-(hydroxymethyl)furfural";
- CIS2019 – "Chemistry meets Industry and Society", Salerno (Grand Hotel), 28-30/08/2019 – Poster presentation: "Sustainable bio-products: study of the catalytic hydrogenation of 5-(hydroxymethyl)furfural";
- CATBIOR 2019 - 5th International Congress on Catalysis for Biorefineries 2019, Turku, 23-27/09/2019 – Poster presentation: "Study of the catalytic hydrogenation of 5-(hydroxymethyl)furfural";
- XXVII Congresso Nazionale della Società Chimica Italiana" (CIS2021), Web-congress, from 14 till 23 September 2021– Poster presentation: "The catalytic hydrogenation of 5-(hydroxymethyl)furfural: a comparison between batch and continuous flow approaches";
- "Reunión Bienal de la Sociedad Española de Catálisis (SECAT 2021), Valencia, from 18 untill 20 October 2021– Poster presentation: "Alkali doped sepiolite as catalyst for bio-ethanol gas-phase conversion".

SCUOLE:

- International Winter School "INNOVATIVE CATALYSIS AND SUSTAINABILITY - Scientific and Socio-Economic Aspects", Palazzo delle Feste, Bardonecchia 07-11/01/2019 – Presentazione di Poster:" Study of the catalytic hydrogenation of 5-(hydroxymethyl)furfural";
- Sinchem Winter School 2020, Dipartimento Chimica Industriale "Toso Montanari"04-06/02/2020.

PUBBLICATIONS

//

KEY WORDS

Bio-Ethanol

Guerbet

Butanol

Bio-fuels

Hydroxyapatite

Zirconia

Sepiolite

Heterogeneous Catalyst

Gas-phase

Continuous-flow processes

ABSTRACT

Fossil fuels reserves are running out and their usage is known to be the main contributor to climate change and global warming. Therefore, the transition toward alternative sources of energy and chemicals products more sustainable and environment friendly is critically important. Biomass-derived ethanol (bio-ethanol) production is believed to grow worldwide in the near future and its conversion into added value derivatives is becoming more and more attractive. The present research work focused on the valorisation and upgrading of bio-ethanol over heterogeneous catalysts in a lab-scale continuous gas-flow system.

Firstly, in the laboratories of the Department of Industrial Chemistry of the University of Bologna (Unibo), the catalytic ethanol gas-phase conversion was studied over hydroxyapatite (HAP) based catalysts. Catalytic tests have been carried out in the temperature range 300-600°C by feeding an ethanol/He mixture into a quartz lab-scale fixed bed reactor of pelletized catalyst. The focus was placed on enhancing the formation of higher condensation products in order to obtain an organic mixture with application as bio-fuel. After choosing the reaction conditions, ion-exchanged hydroxyapatite with transition metals (i.e., Fe, Cu) and alkaline earth metal (i.e., Sr) have been synthetized and tested. While the transition metal-exchanged HAP acted essentially as acid catalysts, yielding mainly the dehydration product of ethanol, ethylene, the Sr-HAP catalyst led to the formation of a complex reaction mixture the composition of which need further optimization in order to fill the requisite to be used as fuel-blend.

Then, in the laboratories of the Institute of Chemical Technologies (ITQ) of the Polytechnic University of Valencia (UPV), the study focused on two different catalytic materials, zirconium oxide and the natural clay sepiolite. Both the materials have been tested into the ethanol transformation carrying out the catalytic tests in the temperature range 300–450 °C by feeding an ethanol/N_2 mixture into a quartz lab-scale fixed bed reactor of pelletized catalyst.

Zirconium-oxide based catalysts have been prepared through two different methods, precipitation and hydrothermal, by varying some synthetic parameters (i.e., pH, the nature of the base) and by adding a transition metal as dopant agent (i.e., Ti and Y). The presence of a dopant into the zirconia structure favoured the stabilization of the tetragonal or cubic phase against the monoclinic one. All samples exhibited acidic behaviour. Interestingly, 5%mol Ti-doped zirconia exhibited a different catalytic behaviour yielding diethyl ether as major product at 300°C, while all the others samples produced mainly ethylene, both dehydration products of ethanol.

The effect of acid-base properties of sepiolite, using alkali metals (i.e., Na, K, Cs) with different metal loading (i.e., 2, 4, 5, 7, 14 wt%) as promoters, and of the redox properties of sepiolite-supported CuO or NiO, on the catalytic conversion of ethanol into *n*-butanol has been investigated. Thermal treated sepiolite samples mainly acted as acid catalyst, yielding preferentially the dehydration products of

ethanol (ethylene and diethyl ether). While the presence of a transition metal did not favoured *n*-butanol production, the presence of an alkali metal into the catalytic system appeared to be crucial for *n*-butanol formation. Best results in terms of activity (ethanol conversion, 59%) and *n*-butanol selectivity (30%) where obtained at 400ºC and a contact time, W/F, of 2 g/mL·s over the catalyst consisting of sepiolite calcinated at 500ºC modified with 7 wt% of cesium.

In order to understand the relationship between the catalytic performance and their physicochemical characteristics, all the tested catalysts have been deeply characterized by XRD, N_2 physisorption, CO_2 and NH_3- TPD, TGA, DR UV-Vis, SEM-EDX and RAMAN spectroscopy.

RESUMEN

Las reservas de combustibles fósiles se están acabando, y se sabe que su empleo es uno de los mayores responsables del cambio climático y al calentamiento global. Es por ello, que la transición hacia el empleo de fuentes de energía alternativas y la producción de productos químicos más adecuados y amigables con el ambiente posee una importancia crítica. Se espera que la producción mundial de etanol, derivado de la biomasa (bioetanol), se incremente en un futuro cercano, por lo que su transformación en productos químicos con un valor añadido se está convirtiendo cada vez en un proceso más atractivo. El presente trabajo de investigación está centrado en la valorización y la mejora del bioetanol, empleando catalizadores heterogéneos, en un reactor de flujo continuo a escala de laboratorio.

En primer lugar, en los laboratorios del Departamento de Química Industrial de la Universidad de Bolonia (Unibo), se ha estudiado la conversión catalítica del etanol en fase gaseosa sobre catalizadores basados en hidroxiapatitas (HAP). Los ensayos catalíticos se llevaron a cabo alimentando un reactor de lecho fijo a escala de laboratorio, empleando el catalizador en forma de pellets y una mezcla de etanol/He, en el rango de temperatura de 300-600 ºC. El interés se focalizó en la formación de productos de alta condensación, con el fin de obtener una mezcla orgánica que pueda ser empleada como bio-combustible. Tras seleccionar las condiciones de reacción, se sintetizaron y probaron diferentes hidroxiapatitas con capacidad de intercambio iónico que poseen metales de transición (Fe, Cu) y metales alcalinotérreos (Sr) en su composición. Mientras que las HAP conteniendo metales de transición actúan esencialmente como catalizadores ácidos, produciendo principalmente el producto de la deshidratación del etanol, el etileno, el catalizador de Sr-HAP permite la formación de una mezcla de reacción compleja, la cual necesita de una mayor optimización para cumplir con los requisitos adecuados para su posterior empleo como biofuel.

A continuación, en los laboratorios del Instituto de Tecnología Química (ITQ) de la Universidad Politécnica de Valencia (UPV), el estudio se centró en dos materiales catalíticos diferentes, el óxido de zirconio y la sepiolita, una arcilla natural abundante en España. Ambos materiales se han probados para la transformación de etanol, en el rango de temperatura de 300-450 ºC, empleando un reactor de lecho fijo a escala laboratorio, con el catalizador en forma de pellets, y usando una mezcla de etanol/N_2.

Los catalizadores con óxido de zirconio se prepararon mediante dos métodos diferentes, precipitación e hidrotermal, variando algunos de los parámetros de síntesis (pH, naturaleza de la base), y empleando algunos metales de transición como elementos dopantes (Ti, Y). La presencia de un elemento dopante en la estructura de la zirconia favorece la estabilización de las fases tetragonal y cúbica frente a fase monoclínica. Todas las muestras exhibieron un comportamiento ácido. Resulta interesante que la zirconia dopada con 5%mol de Ti exhibe un comportamiento

catalítico diferente, produciendo el dietiléter como principal producto a 300ºC, mientras que los otros catalizadores producen principalmente etileno, ambos, productos de la deshidratación del etanol.

Por otra parte, se ha estudiado el efecto de las propiedades ácido-base de la sepiolita, modificada con metales alcalinos (Na, K, Cs) y cargas de metal variables (2, 4, 5, 7, 14 wt%), y de las propiedades redox de la sepiolita, como soporte de CuO o NiO, sobre la conversión catalítica de etanol a *n*-butanol. Las sepiolitas tratadas térmicamente actúan principalmente como catalizadores ácidos, produciendo preferentemente productos de deshidratación del etanol (etileno y dietiléter). Mientras que la presencia de un metal de transición no favorece la producción de *n*-butanol, la presencia de un metal alcalino en el sistema catalítico parece ser crucial para la formación de *n*-butanol. Los mejores resultados en términos de actividad (conversión de etanol, 59%) y selectividad (30%) de *n*-butanol se han obtenido a 400 ºC y un tiempo de contacto, W/F, de 2 g/mL·s, con el catalizador basado en sepiolita calcinada a 500 ºC, y modificada con 7 wt% de cesio, mediante impregnación en fase acuosa.

Para entender la relación entre el rendimiento catalítico y las características fisicoquímicas del catalizador, todos los catalizadores empleados fueron caracterizados mediante DRX, fisisorción de N_2, TPD de NH_3 o CO_2, ATG, DR UV-Vis, MEB-EDX y espectrocopia Raman.

RESUM

Les reserves de combustibles fòssils s'estan acabant, i se sap que el seu ús és un dels majors responsables del canvi climàtic i al calfament global. És per això, que la transició cap a l'ús de fonts d'energia alternatives i la producció de productes químics més adequats i amigables amb l'ambient posseeix una importància crítica. S'espera que la producció mundial d'etanol, derivat de la biomassa (bioetanol), s'incremente en un futur pròxim, i la seua conversió en productes químics amb un valor afegit s'està convertint cada vegada en un procés més atractiu. El present treball de recerca està centrat en la valorització i la millora del bioetanol, emprant catalitzadors heterogenis, en un reactor de flux continu a escala de laboratori.

En primer lloc, en els laboratoris del Departament de Química Industrial de la Universitat de Bolonya (Unibo), s'ha estudiat la conversió catalítica de l'etanol en fase gasosa sobre catalitzadors basats en hidroxiapatites (HAP). Els assajos catalítics es van dur a terme alimentant un reactor de llit fix, a escala de laboratori, contenint el catalitzador en forma de pèl·lets amb una mescla d'etanol/He, en el rang de temperatura de 300-600 °C. L'interés es va focalitzar en la formació de productes d'alta condensació, amb la finalitat d'obtindre una mescla orgànica que puga ser emprada com a bio-combustible. Després de seleccionar les condicions de reacció, es van sintetitzar i van provar diferents hidroxiapatites amb capacitat d'intercanvi iònic que posseeixen metalls de transició (Fe, Cu) i metalls alcalinotérreos (Sr) en la seua composició. Mentre que les HAP contenint metalls de transició actuen essencialment com a catalitzadors àcids produint principalment el producte de la deshidratació de l'etanol, l'etilé, el catalitzador de Sr-HAP permet la formació d'una mescla de reacció complexa, la qual necessita d'una major optimització per a complir amb els requisits adequats per a la seua posterior ocupació com biofuel.

A continuació, en els laboratoris de l'Institut de Tecnologia Química (ITQ) de la Universitat Politècnica de València (UPV), l'estudi es va centrar en dos materials catalítics diferents, l'òxid de zirconio i sepiolita, una argila natural abundant a Espanya. Tots dos materials s'han provats per a la transformació d'etanol en el rang de temperatura de 300-450 °C, emprant un reactor de llit fix a escala laboratori, contenint el catalitzador en forma de pèl·lets, i usant una mescla d'etanol/N_2

Els catalitzadors amb òxid de zirconio es van preparar mitjançant dos mètodes diferents, precipitació i hidrotermal, variant alguns dels paràmetres de síntesis (pH, naturalesa de la base), i emprant alguns metalls de transició com a elements dopants (Ti, Y). La presència d'un element dopant en l'estructura de la zircònia afavoreix l'estabilització de les fases tetragonal i cúbica enfront de fase monoclínica Totes les mostres van exhibir un comportament àcid. Resulta interessant que la zircònia dopada amb 5%mol de Ti exhibisca un comportament catalític diferent, produint el dietiléter com a principal producte a 300 °C, mentre que les altres mostres produeixen principalment etilé, tots dos, productes de la deshidratació de l'etanol.

D'altra banda s'ha estudiat l'efecte de les propietats àcid-base de la sepiolita, modificada amb metalls alcalins (Na, K, Cs) i càrregues de metall variables (2, 4, 5, 7, 14 wt%), i de les propietats redox de la sepiolita, com a suport de CuO o NiO, sobre la conversió catalítica d'etanol a *n*-butanol. Les sepiolitas tractades tèrmicament actuen principalment com a catalitzadors àcids, produint principalment productes de deshidratació de l'etanol (etilé i *dietiléter). Mentre que la presència d'un metall de transició no afavoreix la producció de *n*-butanol, la presència d'un metall alcalí en el sistema catalític sembla ser crucial per a la formació del *n*-butanol. Els millors resultats en termes d'activitat (conversió d'etanol, 59%) i selectivitat (30%) de *n*-butanol s'han obtingut a 400°C i un temps de contacte, W/F, de 2 g/ml·s amb el catalitzador compost de sepiolita calcinada a 500 °C, i modificada amb 7 wt% de Cs.

Per a entendre la relació entre el rendiment catalític i les seues característiques fisicoquímiques del catalitzador, tots els catalitzadors emprats van ser caracteritzats en profunditat mitjançant DRX, fisisorción de N_2, TPD de NH3 o CO_2, ATG, DR UV-Vis, MEB-EDX i espectrocopia Raman.

Table of Contents

NOMENCLATURE

AA = Acetaldehyde

BD = Butadiene

BuA = Butyraldehyde

BuOH = *n*-butanol

CH_4 = Methane

CO_2 = Carbon Dioxide

DEE = Diethyl ether

EDX = Energy Dispersive X-Ray Spectrometry

EtOH = Ethanol

HAP = Hydroxyapatite

H_2 = Hydrogen

MPV = Meerwein–Ponndorf–Verley reaction

N_2 = Nitrogen

NH_3 = Ammonia

SEM = Scanning Electron Microscopy

S = Selectivity

Sep = Natural Sepiolite

Sep@500 = Sepiolite calcined at 500ºC

Sep@700 = Sepiolite calcined at 700ºC

TGA = Thermogravimetric Analysis

ToN= Time on Stream

TPD = Temperature Programmed Desorption

Y = Yield

X = Conversion

XRD = X-Ray Diffraction

W/F = Weight/Flow, contact time

WHSV = Weight hourly space velocity

ZrO_2 = zirconium oxide

AKNOWLEDGEMENTS

1 INTRODUCTION

1.1 GREEN CHEMISTRY and BIOREFINERY

Fossil fuels (petroleum, natural gas, and coal) inevitable depletion and related adverse effects (e.g., the rising greenhouse gas concentrations in the atmosphere, global warming, ocean acidification and rising sea levels..) have meant that new approaches toward production of fuels and chemicals have been developed.[1] In the early 1990s in the USA it was introduced the concept of "Green Chemistry", that has been defined as "the utilization of a set of principles that reduces or eliminates the use or generation of hazardous substances in the design, manufacture and application of chemical products." [2] In practice, it focuses on production and employment of chemicals that have little or no pollution potentials or environmental risks, with process both economically and technologically feasible.[3] Paul Anastas and John Warner in 1998, developed the following list of the "Twelve principle of Green Chemistry", shaping a framework for making a greener chemical, process, or product [2]:

1. Waste prevention is better than treatment or clean-up
2. Chemical synthesis should maximize the incorporation of all starting materials
3. Chemical synthesis ideally should use and generate non-hazardous substances
4. Chemical products should be designed to be nontoxic
5. Catalysts are superior to reagents
6. The use of auxiliaries should be minimized
7. Energy demands in chemical syntheses should be minimized
8. Raw materials increasingly should be renewable
9. Derivations should be minimized
10. Chemical products should break down into innocuous products
11. Chemical processes require better control
12. Substances should have minimum potential for accidents

Together with the concept of green chemistry, the concept of sustainable chemistry has to be taken into account and it is based on "the maintenance and continuation of an ecological-sound development". [4] In 2015 the United Nations created a "universal call to action to end poverty, protect the planet, and ensure that all people enjoy peace and prosperity by 2030" that comprises 17 goals known as the Sustainable Development Goals (SDGs). This framework is being adopted by governments, industry, and many other organizations worldwide and both the concepts of green and sustainable chemistry have gained significant attention due to their potential to promote and

consolidate a transition towards more sustainable societies and to help achieve the SDGs and their targets.[3,5]

In this regard, the use of renewable resources for the generation of energy and production of chemicals is considered a major imperative in the 21st century[1], especially considering the massive amount of advantages related with bio-based products. Indeed, exploiting bio resources has the potential to reduce greenhouse gas emissions (carbon-neutral nature)[5], inherently allows to use renewable and expendable resources and to develop sustainable industrial production. The classical petroleum oil refinery from which chemicals have been mainly produced so far is related with the emission of carbon-based greenhouse gases.[6] With the imperative of getting away from petrochemicals, the use of biomass as a chemical feedstock will become more and more important.

Biomass is the final product of the photosynthetic process in which nature stores solar energy converting it into a great variety of chemicals. [7]It consists of a mixture of organic materials mainly composed of cellulose, hemicellulose, lignin and, in minor part, of lipids, proteins, simple sugars and starches.[8] Biomass also contains inorganic constituents and a fraction of water. From an elemental point of view, the 90% of its dry weight is composed mainly by carbon (51wt%) and oxygen (42wt%). In addition, there are trace amounts of hydrogen (5wt.%), nitrogen (0.9wt.%) and chlorine (0.01–2wt.%).[9] According to the Directive 2009/28/EC of the European Parliament and of the Council of 23 April 2009, the term "biomass" means "the biodegradable fraction of products, waste and residues from biological origin from agriculture (including vegetal and animal substances), forestry and related industries including fisheries and aquaculture, as well as the biodegradable fraction of industrial and municipal waste". [10] Employing biomass as raw material could close the carbon cycle. For this reason the future chemical industries might increasingly rely on 'biorefinery'[11], a concept strictly connected to the one of "bio-economy" which "encompasses the production of renewable biological resources and the conversion of these resources and waste streams into value added products, such as food, feed, bio-based products and bioenergy". [12]

Biorefinery is a sustainable means of generating multiple bioenergy products from various biomass feedstocks through the incorporation of relevant conversion technologies. With the increased attention of circular economy in the past half-decade with the emphasis globally addressing economic, environmental, and social aspects to the industrial-sector, biorefinery acts as a strategic mechanism for the realization of a circular bioeconomy.[13] Ideally, biorefinery takes part of the integrated biomass zero-emission cycle (Figure 1).[14] Indeed, it exploits biomass and the products CO_2 and ash that are recycled producing biofuels, heat, electricity and oxygenated organic chemicals such as alcohols, esters and carboxylic acids, from which bio-material can be produced. [14]
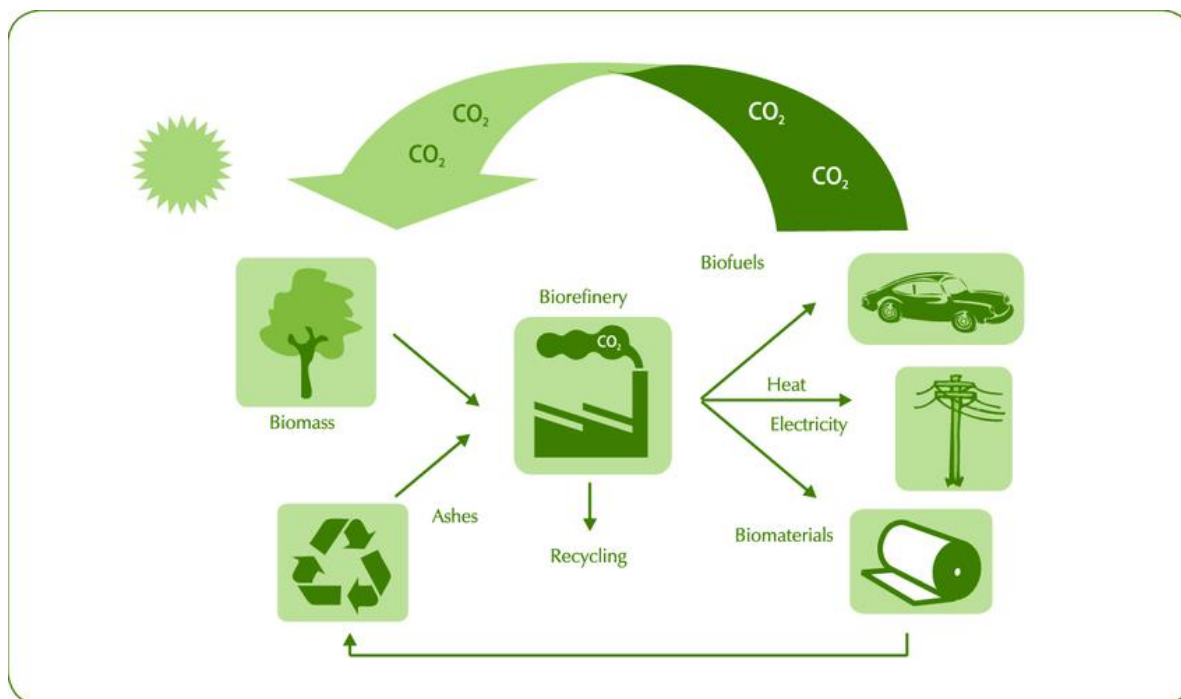
Figure 1   Complete integrated biomass-biofuel-biomaterial-bioenergy cycle. [15]

Catalysis, together with biotechnologies and thermochemistry, enables designing a network of chemical transformations for upgrading biomass-derived compounds to a variety of chemicals, the so-called "biomass valorization".[16] Catalysis has been already a core technology in the fossil fuel based economy and more than the 90% of industrial chemical processes involve catalytic steps. In this optic, both heterogeneous and homogeneous catalysis technology will also have a key role in the transition to a biobased economy. [16,17] In particular, catalytic processes find employment into the conversion of the so-called biomass derived "platform molecules" into added value products and/or intermediates within the biorefineries. These platform molecules, which correspond to the 'commodities' in a petro-based refinery, are obtained from biomass raw material previously treated. Those pre-processes encompass steps of fractionation, extraction and purification as well as deconstruction of the natural polymers. Then followed by bioprocessing to yield short molecules with most commonly less than 6 carbon atoms.[16] Figure 2 outlines the possible routes of biomass valorisation.
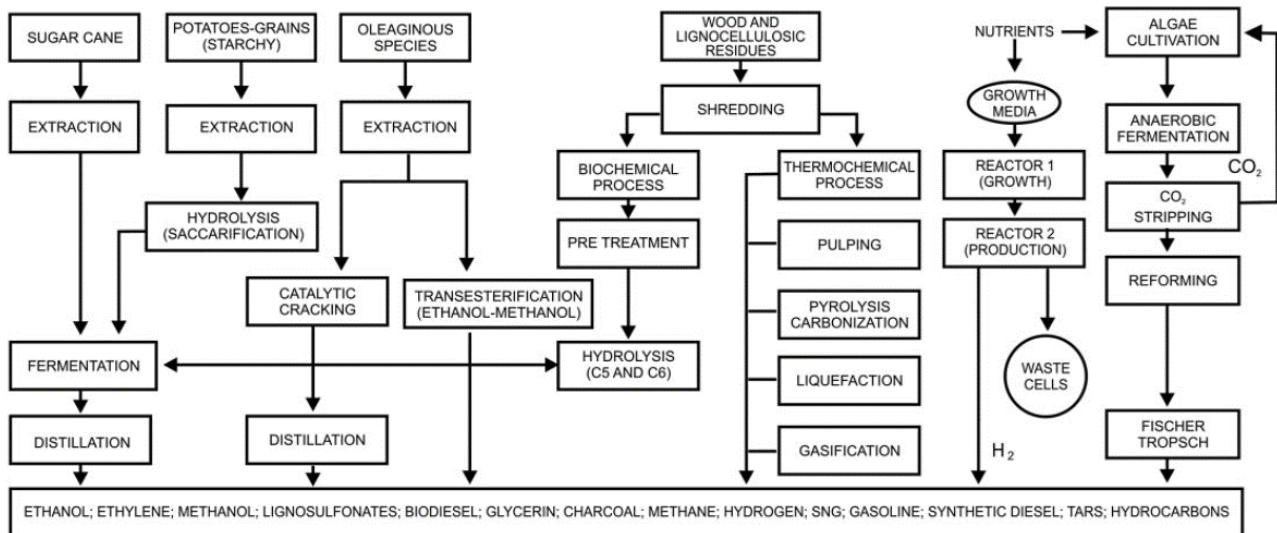
Figure 2   Possible routes and processes for biomass refining.[7]

1.1.1   BIO-FUEL

As stated before, biomass has received considerable attention as a sustainable feedstock that can replace diminishing fossil fuels, being an abundant and carbon-neutral renewable energy resource for the production of biofuels.[1,18]

Bio-fuels are liquid or gaseous fuels derived from plant matter and residues, such as agricultural crops, municipal wastes and agricultural and forestry by-products. In particular, liquid biofuels are unique in their similarity to the currently preferred fuel sources. Their application does not require extensive changes to the transportation infrastructure and the internal combustion engine. For example, bioethanol and biodiesel are currently used commercially as blending agents for petroleum-derived gasoline and Diesel fuels.[1] However, in order to properly replace fossil fuels, several technological advances are needed to increase the photosynthetic yields and improve the agriculture activities as well as the processing plants components to achieve a positive net energy ratio inside the biorefinery concept. In addition, it is important to avoid competitions among agricultural production intended to food supply.[7] Regardless, the overall approach to convert biomass into hydrocarbon fuels is mainly based on two lines: to reduce the substantial oxygen content of the parent feedstock to improve energy density and to create C–C bonds between biomass-derived intermediates to increase the molecular weight of the final hydrocarbon product. [1]

Current strategies for the production of biofuels and useful heat from biomass are shown in Fig.3. The mechanical processes lead to concentration, compression and reduction of biomass humidity. Then, two groups of chemical technologies are employed to alter the composition of the raw material and generate products that are better suited to their end uses. One group, made up with combustion,

gasification and pyrolysis is called "thermochemical conversions", where raw materials are treated at high temperatures. Gasification of biomass occurs at high temperature, 600-1000⁰C or higher, in the presence of an oxidizing agent such as air, steam, or oxygen. Syngas, a mixture containing mainly CO, CO_2, H_2 and H_2O, is the product of the gasification of coal or biomass, allowing the utilization of a wider range of biomass types including low-cost organic wastes, without the need for specific fractionation. [19] Then, the "biochemical processes" that are carried out in high water content conditions and ambient temperatures can yields hydrocarbon fuels.[15] For example, fermentation converts sugars into alcohol that can be directly used as fuel, or in principle can be used as the raw material of a biorefinery plant for further upgrading. Triglycerides, derived from oil seeds, are used to be converted into biodiesel through transesterification processes. [14]
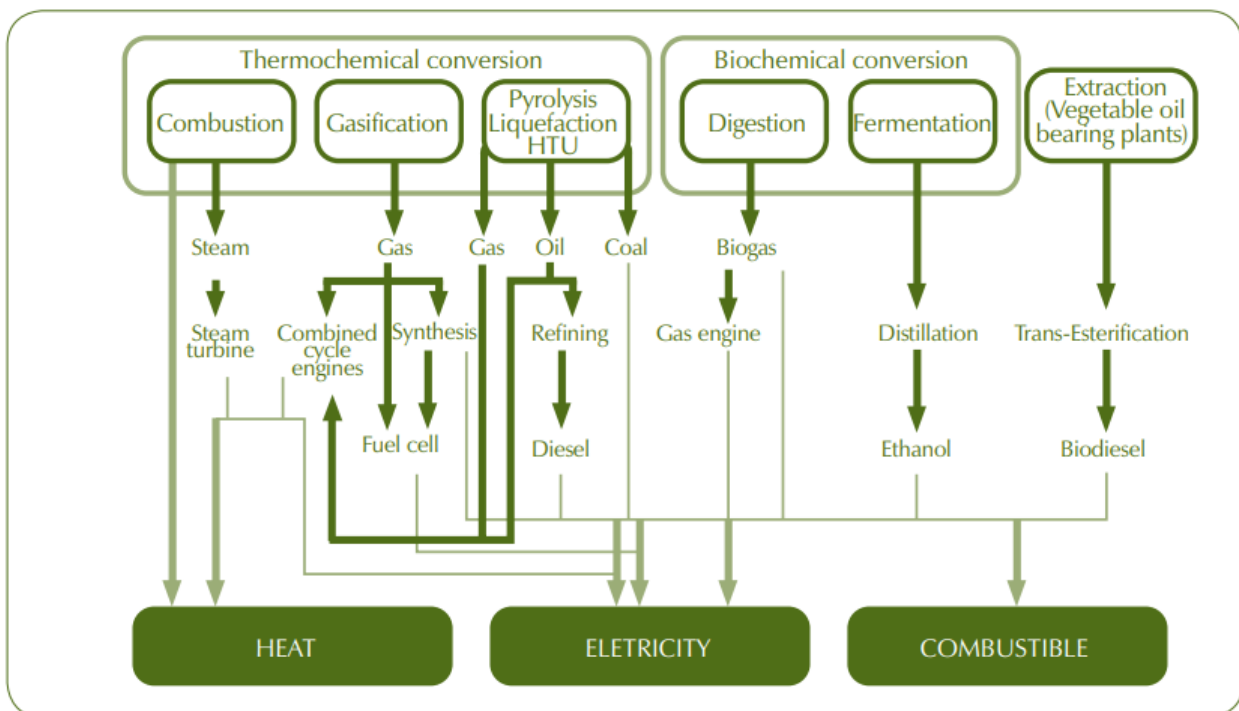
Figure 3   Technological routes for the production of bioenergy [15]

Biofuels, i.e. cellulosic bioethanol, *n*-butanol and biodiesel, are therefore of considerable interest to researchers, industrial partners and governments. In particular, bioethanol is considered a promising drop-in fuel, which could provide an alternative to petrol in the transport sector. [20] It can be directly used as a transportation fuel or it can be blended with gasoline. Bio-ethanol can be mixed with gasoline (mainly in 10% ethanol concentration, known as E10) and burned in traditional combustion engines without any modifications needed. In Brazil, the world's largest exporter of bio-ethanol, it is used pure or blended with gasoline in a mixture called gasohol (24% bio-ethanol and 76% gasoline).[21] In addition, due to the increasing demand of heavy middle-distillate fuels, the exploitation of ethanol as renewable feedstock to produce hydrocarbon mixture has become more and more attractive.

1.2 BIO-ETHANOL and bio-alcohols

Among various biofuels, platform molecule and end-use products derived from biomass, bio-ethanol is the most important one. [22] In recent years, the amount of ethanol produced has increased significantly, mostly due to the rising demand for bio renewable alternatives to petroleum-based fuels and chemicals. [23] It is estimated that up to 30% of the transportation fuels will be derived from biomass by the year of 2030 in order to limit CO_2 emissions, and cellulosic ethanol will be a leading player as it can be used not only as a renewable fuel itself but also as a starting material for producing other hydrocarbon fuels. [22]

Ethanol is currently produced both as a petrochemical, through the hydration of ethylene and via biological processes. The main part of the production of bio-ethanol is still obtained by a 1st generation fermentation process, meaning from fermentation of carbohydrates such as starch and sugars.[24,25] But, in order to be truly sustainable, its production should not compete with food production. Therefore, much researches focused on the development of more efficient technologies starting from low-cost and non-food biomass sources, such as from lignocellulosic feedstock (second generation bio-ethanol). [7,26–31] For large scale production of bio-ethanol, first, sugars are obtained from enzymatic saccharification or hydrolysis of carbohydrates, such as cellulose and starch. Then, the following steps lead to ethanol production: microbial (yeast) fermentation of sugars, distillation, dehydration, and denaturation. [32] In addition, promising results are reported for ethanol production from algal feedstock (third generation)[7,16,26–31] and even by fermentation of syngas. [33–38] Several papers describe the chemocatalytic conversion of syngas into ethanol and higher alcohols.[39,40] Three different pathways from syngas to ethanol are reported: direct selective hydrogenation of CO over a solid catalyst, homologation of methanol which involves reductive carbonylation on a redox catalyst, or a classical methanol synthesis reaction followed by carbonylation to acetic acid and subsequent hydrogenation to ethanol. [41] Noteworthy, the quality of the obtained bioethanol is completely the same as the one produced from petrochemical feedstock[42] and, since it contains carbon recycled from the atmosphere by photosynthesis, it is classified as carbon neutral in the Kyoto Protocol adopted by the United Nations Framework Convention on Climate Change, COP3 (1997). [43–45]

To date, bioethanol, has dominated the bio-gasoline market, used on its own or as a blend with conventional fuels. The addition of up to 10% ethanol is believed not to affect present gasoline-based vehicle engines, and 10% ethanol-containing gasoline (gasohol) is sold as E10 in the United States, while in Brazil 22-26% ethanol is already included in gasoline sold for general use. However, ethanol is characterized by a relatively low vapour pressure, has a lower energy density (70% that of gasoline), it readily absorbs water leading to separation and dilution problems in storage tanks, and it is corrosive to current engine technology and fuel infrastructure. Indeed, even the E10 fuel has the defeat of evaporative emissions and increased aldehyde emissions. Moreover, for gasoline

containing 85% ethanol (E85) and for 100% ethanol fuel, a specially designed car engine is necessary and the fuel efficiencies for hybrid cars using the E85 mixture are only 75% compared to the standard cars. Hence, using ethanol blended with gasoline presents several drawbacks that can be overcome by using higher alcohols with better fuel properties.[41]

Accordingly, *n*-butanol is essentially noncorrosive, immiscible with water, and its energetic value (29.2 MJ/L) is higher than the one of ethanol (19.6 MJ/L), and the 90% of that of gasoline. [46,47] This improved performance has led to *n*-butanol being termed an "advanced biofuel", and the commercial availability of this material as a green drop-in alternative to gasoline is gaining ground. Nevertheless, *n*-butanol is a valuable product with many application as solvent, additive in many commercial products or as chemical intermediate, for instance is a crucial building block for acrylic acid and acrylic esters. [47,48] Its petrochemical-based route of synthesis, the so-called Oxo process, involves several reaction steps, some of which use homogeneous catalysts and non-renewable resources such as propylene and CO.[47] Hence, alternative way for the bulk synthesis of *n*-butanol from bio-sustainable feedstock have been taken into account recently. Bio-butanol can be obtained through the ABE (Acetone, Butanol and Ethanol) fermentation process, where this organic mixture is produced by the use of strains of the bacterium Clostridium acetobutylicum. However, it's a challenging fermentation process limited by the toxicity of *n*-butanol itself, with low conversion and modest selectivity.[49,50] An attractive alternative approach to obtain bio-butanol is to catalytically convert or upgrade widely available bio-ethanol through the so called "Guerbet reaction", which enables C−C bond formation between alcohols.[51,52] In addition, through the Guerbet route higher alcohols than *n*-butanol can be produced, both linear and branched (mainly 2-alkil alcohols named "Guerbet alcohols"), that can be considered an added benefit since higher alcohols have an appropriate energy density to be combined with gasoline (e.g., the energy densities of 1-hexanol and 1-octanol are the 94% and 99% of that of gasoline, respectively) [53] or to be employed in fuel blends for diesel engines. [54] In particular, the branched Guerbet alcohols have a much lower melting point than their linear counterparts. They are used for the synthesis of functional liquids that have to remain fluid at very low temperatures, like some lubricants or hydraulic fluids for aircrafts, but also for its use as jet fuel precursors. [55] Then, they can have a wide range of applications in cosmetics and detergent formulations.[52] However, large-scale production of such alcohols from renewable biomass is still a great challenge, but the Guerbet chemistry represents an interesting opportunity even due to the rapidly growing availability of renewable alcohols. [53]

Overall, along with fuels market, ethanol is used in the beverage market, in the formulation of industrial products (e.g., cosmetics, pharmaceuticals and inks).[16] In chemistry, ethanol is widely used both as a solvent and as platform molecule for the synthesis of other products. Therefore, ethanol is often regarded as the most important C_2 platform molecule because, even if being a very simple molecule, a prosperous chemistry can be derived from ethanol used as a platform molecule and it is

considered as a key compound in biorefineries [16] [14,16] In the next chapter, some of the main reactions starting from ethanol reported in the literature will be examined.

1.2.1 ETHANOL as building block

Being one of the largest bulk-biochemical, which can be used as additive blend with gasoline but also for synthetizing value-added chemicals and advanced fuels. In particular, ethanol can be converted into other important chemicals such as acetaldehyde, ethylene ethyl ether, 1,3-butadiene, *n*-butanol, ethyl acetate, acetone, propylene and isobutene. In addition, bio-ethanol can be upgraded to advanced fuels including hydrogen (by steam reforming) and higher hydrocarbons.[56] (Figure 4).
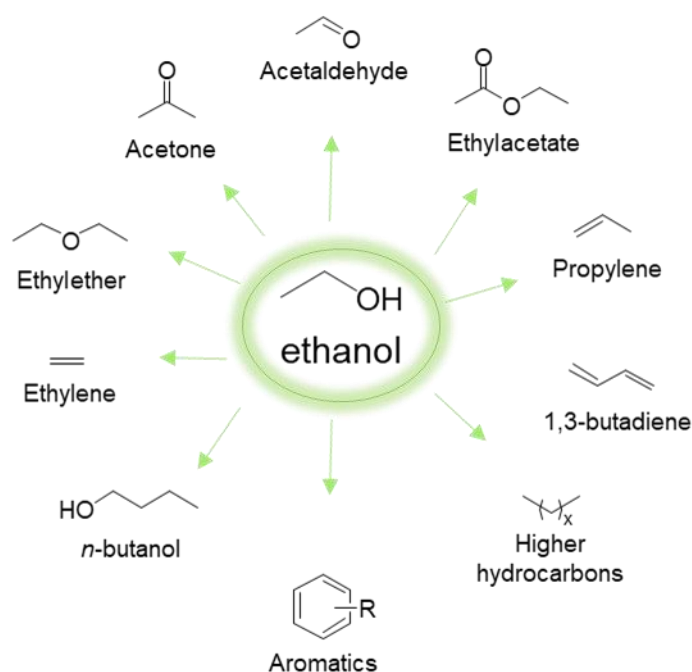
Figure 4　　Ethanol as building block.

By varying the nature of the catalyst employed and the reaction conditions, many different products can be obtained. Regarding the heterogeneous conversion of ethanol, the general first surface molecular unit has been identified as the ethoxy group forming on the catalyst surface by ethanol dissociative adsorption. [57,58,59] Then, depending on the nature of the catalyst, different products can be formed. Generally, ethylene or ethyl ether are formed on acidic catalysts. When acid sites are located near to basic sites, the ethoxy group can lose hydride species and producing acetaldehyde, from which aldol-like condensations can take place. The low selectivity frequently observed in ethanol conversion is mainly caused by its high versatility, especially when performed over complex multifunctional catalysts. In fact, complex catalytic materials have, together with the desired

functionality, also undesired functionalities. Hence, an optimized catalyst design with well-balanced functionalities is crucial to selectively transform ethanol into the target product.

1.2.1.1 Ethanol to higher alcohols: the Guerbet reaction

Ethanol can undergo coupling reaction yielding *n*-butanol and higher alcohols through the so-called Guerbet route. [60] The main reaction mechanisms proposed for the Guerbet reaction are two: one based on the direct ethanol condensation ("direct route") and one based on aldol condensation ("aldol-condensation route"). Figure 5 depicts the two routes to forming *n*-butanol starting from ethanol, the direct one (in red) and the aldol-condensation one (in green). The issue is still object of debate, especially when the ethanol upgrading reaction it is studied over heterogeneous basic catalysts, as shown by the presence of several alternative mechanisms proposed in the literature. This variety is related to the different reaction conditions performed over different catalytic systems characterized by diverse physicochemical properties, so it's difficult to reach a universal conclusion. [61]
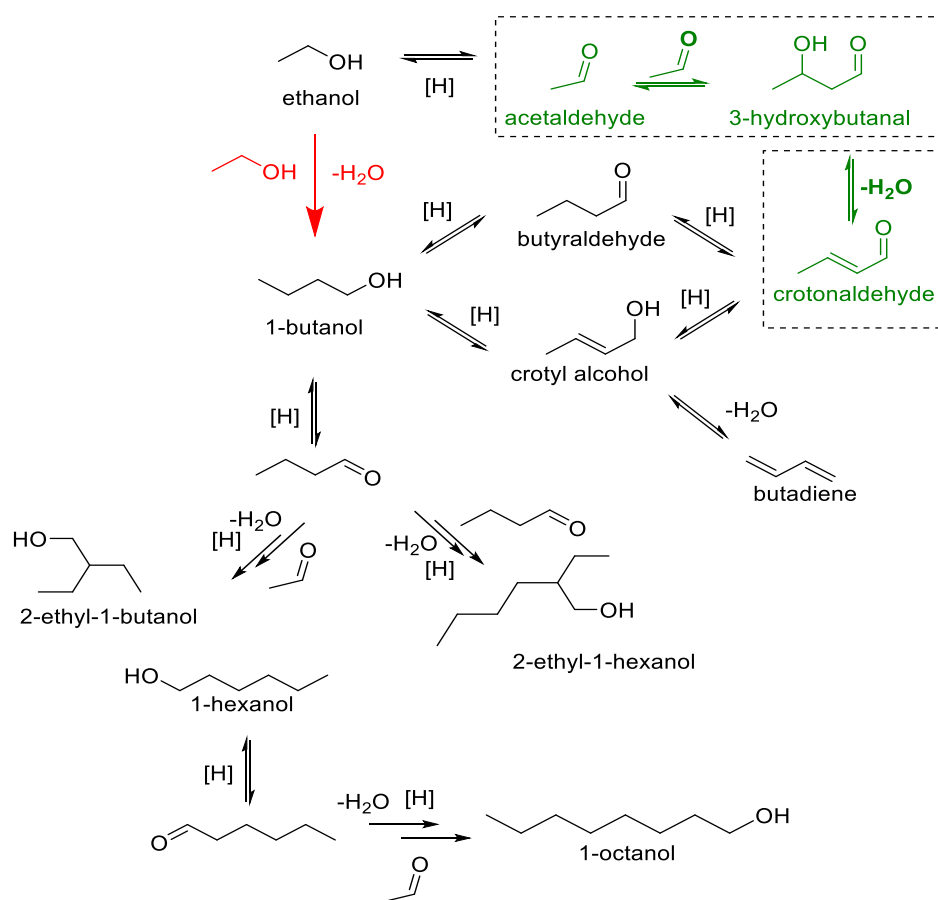
Figure 5 Generally accepted pathway for ethanol transformation through Guerbet routes to higher alcohols (in red is highlighted the direct route, in green is highlighted the aldol-condensation reaction from acetaldehyde).

Although different reaction mechanisms have been proposed, the most commonly accepted one is the aldol-condensation route (Figure 5). The mechanism starts with the dehydrogenation of ethanol over basic or redox active sites producing acetaldehyde, commonly reported as the key intermediate. Acetaldehyde can then undergo to the aldol condensation to yield 3-hydroxybutanal (acetaldol). Then the reduction of the aldol can occur through the H-transfer mechanism from ethanol, the Meerwein–Ponndorf–Verley (MPV) reaction.[65] Nonetheless, the in-situ formed hydrogen (from ethanol dehydrogenation) might also play a role as reducing agent. However, other mechanistic options have been reported: acetaldol may undergo reduction by ethanol to form 1,3-butanediol, the dehydration of which possibly leads to either crotyl alcohol or 3-butene-2-ol. Notably, both compounds can be further dehydrated into butadiene (Lebedev process on bifunctional acid-base catalysts). [64] The fact that it has been observed that at least one of both reacting alcohols requires an α-methylene group in order to undergo Guerbet condensation supports the aldol-type mechanism since it is a requisite for the formation of the aldol condensation product. [66]

On the other hand, some studies performed over basic heterogeneous catalysts suggested the direct condensation route, which involves the condensation of two ethanol molecules with no intermediate gaseous compounds. The main direct pathway is suggested to occur by direct coupling of two ethanol molecules with dehydration occurring by the elimination of the hydroxyl of one molecule and the hydrogen attached to the α-carbon of the second one (Figure 6, A). Then, the direct condensation of an alcohol with its corresponding aldehyde and consecutive hydrogenation of the higher aldehyde so-formed (Figure 6, B) or condenstion with its enol form (Figure 6, C) are reported as minor reaction pathways. [46,48,48,62,63]
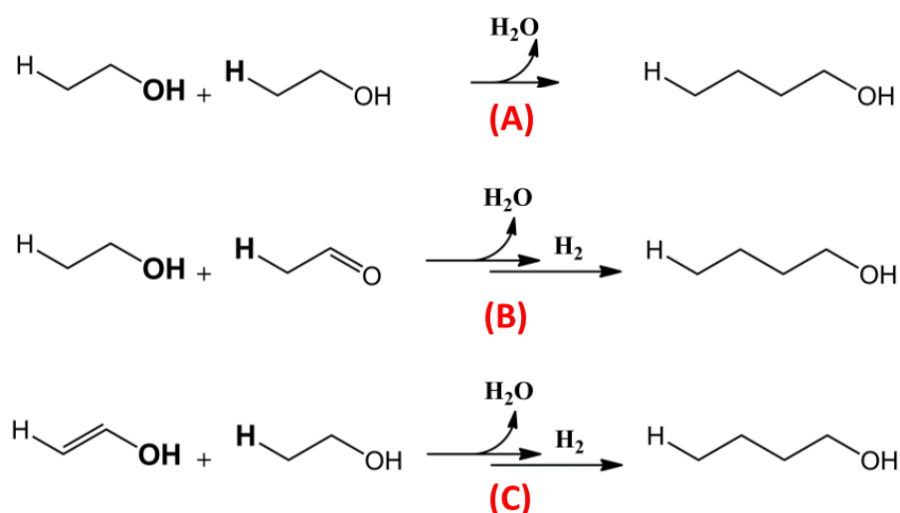
Figure 6   Schematic representation of the direct condensation mechanisms for ethanol. A) main mechanism; B) and C) minor mechanisms proposed for the direct condensation.[60]

Similarly to the mechanism A in Figure 6, Chieregato et al.[64] proposed a direct mechanism in 2015. By conducting kinetic experiments in combination with in situ infrared spectroscopy (DRIFTS), MS

and DFT calculations, they formulate a new mechanism for transformation of ethanol into *n*-butanol, explaining the formation of the Guerbet alcohols as kinetic primary product. Their mechanism is based on the formation of a carbanion specie on the catalyst surface which directly attacks another ethanol molecule with elimination of water leading to the direct formation of *n*-butanol. In this way, they discharged the key role of the intermediate products characterizing the aldol-route (i.e., acetaldol and crotonaldehyde).

Anyway, regardless the mechanism, one molecule of water is formed for every molecule of *n*-butanol produced. In general, through the Guerbet route, a higher alcohol containing the double number of the reagent alcohols is produced; hence the Guerbet reaction product of ethanol is *n*-butanol. Similarly, a mixture of *n*-butanol and ethanol can react to form 2-ethylhexanol (by condensation of two molecules of *n*-butanol), *n*-butanol (by condensation of two molecules of ethanol), *n*-hexanol and 2-ethylbutanol (by condensation of a molecule of *n*-butanol with a molecule of ethanol). Therefore, if at least one of the two materials undergoing condensation contains a α-methylene group, a certain amount of condensation reactions can occur between the alcohols present in the reaction environment yielding a series of higher molecular weight alcohols. [51]

Taking into account the most-accepted pathway, which is the "aldol condensation route", some general thermodynamic consideration can be made. Indeed, from a thermodynamic point of view, the intermediate reaction steps show different behaviours: dehydrogenation is endothermic, favoured at temperature above 300ºC, while hydrogenation is exothermic and favoured at temperature lower than 300ºC. The aldol condensation reaction (highlighted in green in the scheme reported in Figure 5) even if is slightly exothermic, is favoured in the temperature range 150-550ºC, showing a negative ΔG value. [60] As a consequence, the reaction temperature should be chosen considering kinetic factors in order to optimize the yield of the Guerbet alcohols.

The aldol-condensation reaction step in generally is catalysed by basic, acidic or amphoteric catalysts and occur through the formation of an enol or an enolate. By being slightly exothermic, can be the rate determining step while performing the reaction at high temperature. [52] Assuming that the subsequent hydrogenation step takes place with H_2 (g) as hydrogenation agent, the catalytic systems requires a hydrogenation-dehydrogenation active site to facilitate it such as transition metals, otherwise, higher reaction temperatures are needed due to the higher activation energy. [67] On catalytic systems that do not possess transition metals, the hydrogenation reaction is proposed to occur by transfer hydrogenation mechanism like the Meerwein–Ponndorf–Verley (MPV) reduction, in which the hydrogen is directly transferred to the unsaturated aldol from the reagent alcohol. [68] Since a plurality of reaction is involved, the process is particularly sensitive and unpredictable. Accordingly, it is imperative to develop a multifunctional catalytic system focusing on properly tuning both proportion and strength of the different active sites in order to maximize the production of the target alcohol. Indeed, the relatively complex Guerbet reaction requires the use of catalysts that

exhibits simultaneously acidic (for the dehydration step), basic (for the aldol-condesation) and/or dehydrogenation/hydrogenation properties. Unfortunately, a lot of side reactions can take place, resulting in the formation of other compounds, such as esters, ketones and carboxylic acids. In this way, the process efficiency is lowered and the catalytic system can be poisoned. Indeed, it is known that the Guerbet reaction generates numerous by-products, Figure 7 depicts some of the possible side reactions that can take place. [63,69,70]

For instance, on acid sites the dehydration of the starting alcohols might occur leading to the olefin (ethylene, if starting from ethanol) and to ether (ethyl ether) formations.[71] Dehydrations reactions, are also required in a part of the Guerbet aldol-condensation route, where the enol is dehydrated leading to the formation of the α,β-unsaturated alcohol. [72,73] In addition, the subsequent dehydration of the latter alcohol, can lead to the formation of conjugated olefins, and this route is frequently reported as the reaction mechanism for the formation of 1,3-butadiene (Lebedev, Figure 5). [74] Butadiene formation from ethanol will be better examined in section X.

Over solid bases (e.g., alkaline earth oxides), the esterification of acetaldehyde or higher aldehydes can occur (Tischenko reaction), leading to the formation of ethyl acetate or higher esters. [75,76] Indeed, esters can be formed via hydride shift, through the Tischenko reaction, and also through the Cannizzaro reaction. The latter includes the reduction of an alkanal species to the alkanol, the oxidation of another alkanal molecule to carboxylic acid, and their subsequent bimolecular reactions. [77,78] Decomposition of esters [79] and coupling of carboxylates [80] are reported in the literature as possible ways to form ketones co-producing CO_2. [81,82] The presence of CO_2 associated with ketones formation has been reported as detrimental for the Guerbet condensation. [83] Anyway, ketones can be formed even as isomer of the aldol intermediate product or its subsequent dehydration and hydrogenation. [77] Some aromatic compounds can be formed by cyclization reactions of conjugated C=C bonds. Indeed, alkyl-substituted aryl compounds are often observed as side products in Guerbet reaction. [69,83] In general, many heavy products with different nature, mainly aldehydes, esters and ketones, can be formed as a results of further condensation reactions.
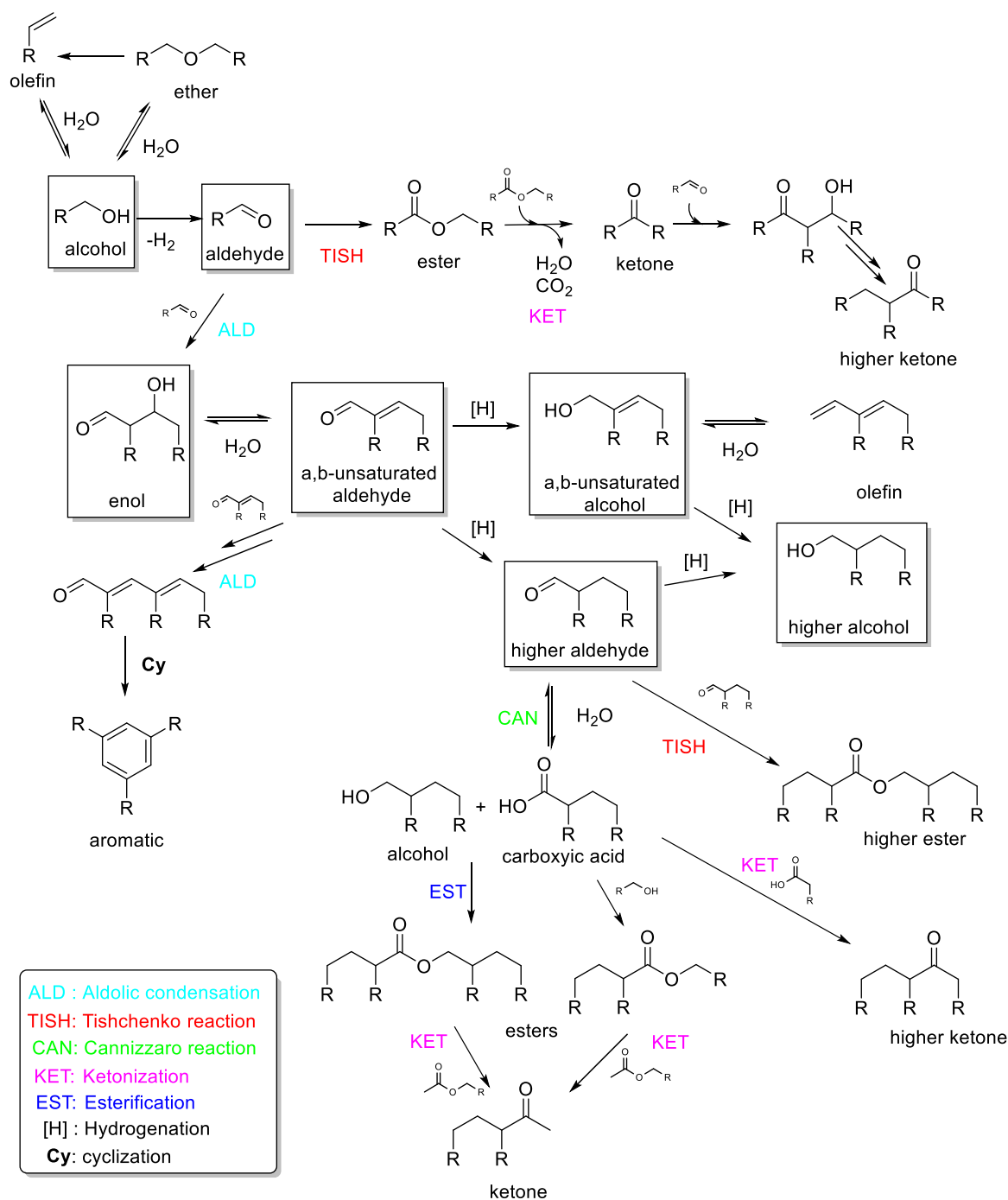
Figure 7 Scheme of the side reactions pathway. The Guerbet products are framed.

A variety of homogeneous, homogeneous/ heterogeneous, and heterogeneous catalyst systems have been studied for the Guerbet reaction. Most of the homogeneous systems employed uses basic catalysts such as alkaline catalysts or systems modified by homogenously or heterogeneously addition of a metal to accelerate the dehydrogenation and hydrogenation steps. [84] Many metal-organic complexes (Ir[85], Ru[53], Rh[86]) have been used as catalytic system showing high performance toward Guerbet reactions, allowing to obtain *n*-butanol and Guerbet alcohols with high selectivity values (>80%).[86,87] Overall, homogeneous catalysts generally offer the best performance in terms of

selectivity, but they exhibit many drawbacks since they imposes thorough purification of the product stream as well as recovery of the basic compound together with waste treatment. Also, these bases induce metal leaching, corrosion of reactor vessels and are often deactivated by the co-produced water resulting in incomplete conversions and by-products formation. [88] Homogeneous catalysts thus can be used as a model systems for the heterogeneous ones which provide many advantages in terms of separation and so production processes costs.[84] Indeed, completely heterogeneous catalytic systems are easily separated from the reaction mixture using filtration, therefore, the product contamination is reduced. Also, ideally they can be reused many times without comprehensive regeneration, they do not cause corrosion nor metal leaching. [89] They can be fixed in a catalyst bed, thus facilitating continuous operation e.g. in a simple plug flow reactor set-up. This allows for easier integration with subsequent post-treatment steps such as an extra hydrogenation step or purification by distillation.

The realization of the vapour-phase condensation flow system opens new routes for industrial production of *n*-butanol from bioethanol. Indeed, performing the reaction in vapour phase allows higher temperatures to be reached without pressure build-up, which generally imposes practical limitations to liquid phase systems such as autoclave. At high temperatures, typically 350-450°C, the basic catalyst also catalyses the dehydrogenation and hydrogenation reactions.[60] Therefore, there are many studies describing high temperature vapour phase reactions performed over catalysts devoid of transition metals as active phase. Indeed, the most studied heterogeneous catalyst by far is the basic magnesium oxide, which owing to its superior activity and selectivity has often been used as a reference catalyst for studying Guerbet mechanism. [59,90–93] Tsuchida et al. [59] proposed a dehydrogenation mechanism of ethanol over MgO surface, where Mg^{2+}-O^- pairs is believed to be the active site for hydrogen abstraction (Figure 8): ethanol is dissociatively adsorbed to ethoxide on Mg (Lewis acid sites) and to proton-like hydrogen on ionically bound O (hard basic sites) near these acid sites. The acetaldehyde is formed by dissociation of the ethoxide realising H_2.
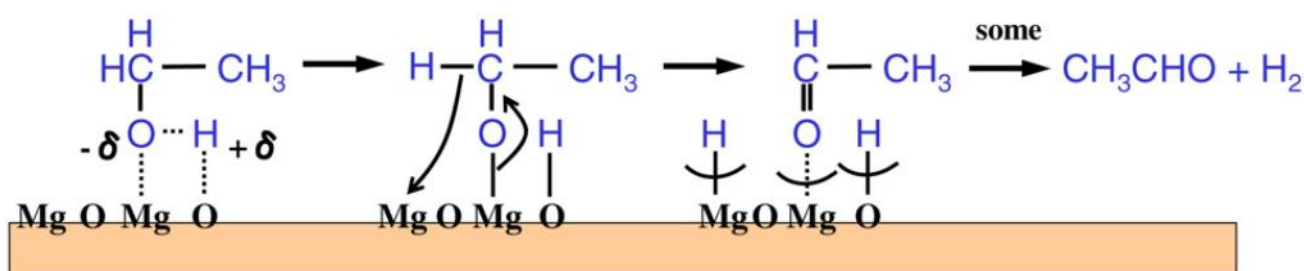
Figure 8   Dehydrogenation mechanism from ethanol on MgO catalyst.[59]

Regardless, the Guerbet reaction has been studied over many different heterogeneous catalysts, including mixed metal oxides [63], hydrotalcite[94], cation exchanged zeolites[46] and supported metal catalysts. They have been studied both in gas and liquid phase, for example, via a one-pot liquid-

phase reaction, different metals (Ru, Rh, Pd, Pt, Au, Ni, Ag) over alumina were reported to produce *n*-butanol from ethanol.[95]

Furthermore, it has been carried out using hydroxyapatite (HAP) that has been shown to be the most active catalyst with high selectivity toward *n*-butanol.[96] In general, there is an inverse relation between *n*-butanol selectivity and ethanol conversion yield, indeed, the highest selectivity of 82% was obtained over Sr-P hydroxyapatite[97] with an ethanol conversion of 4%, while working at 300ºC. Earley and co-workers [98] managed to obtain a better compromise between *n*-butanol selectivity (45%) and ethanol conversion (67%) over Cu/CeO$_2$ catalyst in a continuous flow supercritical CO$_2$ reactor, but the process has the drawback of being more cost effective.

Both the studies over the Mg/Al mixed oxide and HAP based catalysts led to some analogous conclusion about the relation between basic and acidic catalytic sites. By varying the Mg/Al-ratios, hence changing the acid-base properties, the selectivity can be optimized towards dehydrogenation, aldolization and hydride-shifts. Strong acid sites are to be avoided for its dehydration property, yet a moderate amount of acidity facilitates coupling of the intermediates. Indeed, while basic sites are required to generate carbanion species by abstraction of hydrogen, the acid sites are needed for acetaldehyde adsorption that then produces the acetaldol by reaction with the carbanion species. [63] Similarly, Tsuchida et al. [59] found that by varying the Ca/P ratio in HAP its acid-base properties can be optimized toward *n*-butanol selectivity.

In general, a fine-tuning of both the strength (weak acid sites are preferred)[93] and the amount of acid-base sites (the selectivity to *n*-butanol is favoured by high number of strong basic sites)[99] is crucial to obtain high *n*-butanol yield. Hence, both acid and basic sites are needed, in particular adjacent acid and medium basic sites are needed in order to generate the intermediate compounds in ethanol conversion through Guerbet route. [99] Many authors reported the necessity of a specific superficial atomic arrangement in order to adsorb two molecules of acetaldehyde, remove a proton from one of these aldehydes, and promote the nucleophilic attack. Hence, to promote aldol condensation, the catalyst surface should consist of one basic site adjacent to two acids sites.[59,63,100]

1.2.1.2 Ethanol to hydrocarbon fuels

The dependence on fossil fuels for the production of energy is particularly drastic concerning the transportation sector, which relies almost entirely (95%) on petroleum-derived liquid hydrocarbon fuels (gasoline, diesel and jet fuels). [101] Gasoline is a volatile (boiling points between 30 and 220 °C) and inflammable complex mixture of olefinic, paraffinic, naphthenic, and aromatic hydrocarbons in the C$_4$-C$_{12}$ range. It incorporates low contents of oxygenates and traces of sulfur, nitrogen, and metals, which introduce instability to the final mixture. Its variable compositions determines its physicochemical properties and relative engine performance.[102] For example, gasoline produced by

catalytic reforming (with high content of aromatic hydrocarbons and isoparaffins) and by catalytic cracking (with high olefins content) are characterized by low self-ignition point and consequently high octane values. Improved combustion characteristics can be achieved by addition of oxygen-containing additives (alcohol and tertiary ethers) instead of aromatic hydrocarbons. Methyl tertiary butyl ether (MTBE) and ethanol are most widely used oxygen-containing compounds for octane rating improvement. MTBE dominates markets in Europe and USA, but its application is decreasing due to its solubility with water and toxicity of its dissociation products. [103]

Gasoline is the world's major automotive fuel and influences each country's economy and energy strategy. Nevertheless, the demand for gasoline is also projected to decrease over the next few decades, while the worldwide demand for heavier C_8–C_{22} distillate fuels such as jet fuel and diesel is projected to increase.[104] In 2016 the International Civil Aviation Organization (ICAO) reported that 2% of global CO_2 emissions can be attributed to the aviation sector and with increasing demand, the aviation industry could become a significant fossil-based CO_2 emitter by 2050.[105] Table 1 resumes the main properties featuring petroleum derived fuels and ethanol.

Table 1. *Fuels properties, from Ref.* [106]

Fuel	Density [g/mL]	Net heating value [MJ/L]	Carbon range	Freezing point [ºC]	Boiling point [ºC]	Flash point [ºC]	Max aromatic content [vol%]	Cetane
Gasoline	0.735	31.8	4–12	–	40–215	−45	35	–
Jet (A-1)	0.808	34.1	8–16	<−47	140–300	>38	25	–
Diesel	0.85	36.2	10–22	−17	170–370	>52	35	>40
EtOH	0.789	21.1	2	−114	78	13	–	8

The most common jet fuel (Jet A-1) is a complex mixture of hydrocarbons in the C_9–C_{16} range, composed by linear alkanes (providing energy density); slightly branched alkanes or isoalkanes (lowering freezing point); cycloalkanes/naphtanes; and aromatics (≤ 25 %)[107]. (Figure 9). The carbon length and relative amount of each families of hydrocarbons have to be controlled in order to provide to jet fuel the desired properties. [108,109] It must have high flash points (to reduce fire hazard on board), low freeze points (to ensure good cold flow properties at high altitudes and log international flights), high energy density (to minimize fuel storage room), and good sealing properties (to avoid fuel leakage on board). [107] A certain amount of aromatics is mandatory to promote the swelling of elastomeric valves in fuel systems, thereby ensuring proper sealing.[110] Above this amount (exactly 25%)[111], aromatics do not provide beneficial effects to the jet fuel, negatively affecting the combustion performance of the fuel. In addition it have been observed that aromatics contribute considerably to non-volatile particulate matter emissions (i.e. soot). [112] A fuel must have a flash point

of at least 38 °C to be classified as Jet A-1, and aviation fuels have a higher volumetric energy density (net heating value = 34.1 MJ l−1) than does gasoline (31.8 MJ l−1). In general, jet fuel specifications are stricter than those of gasoline or diesel, which are typically more regionally determined.
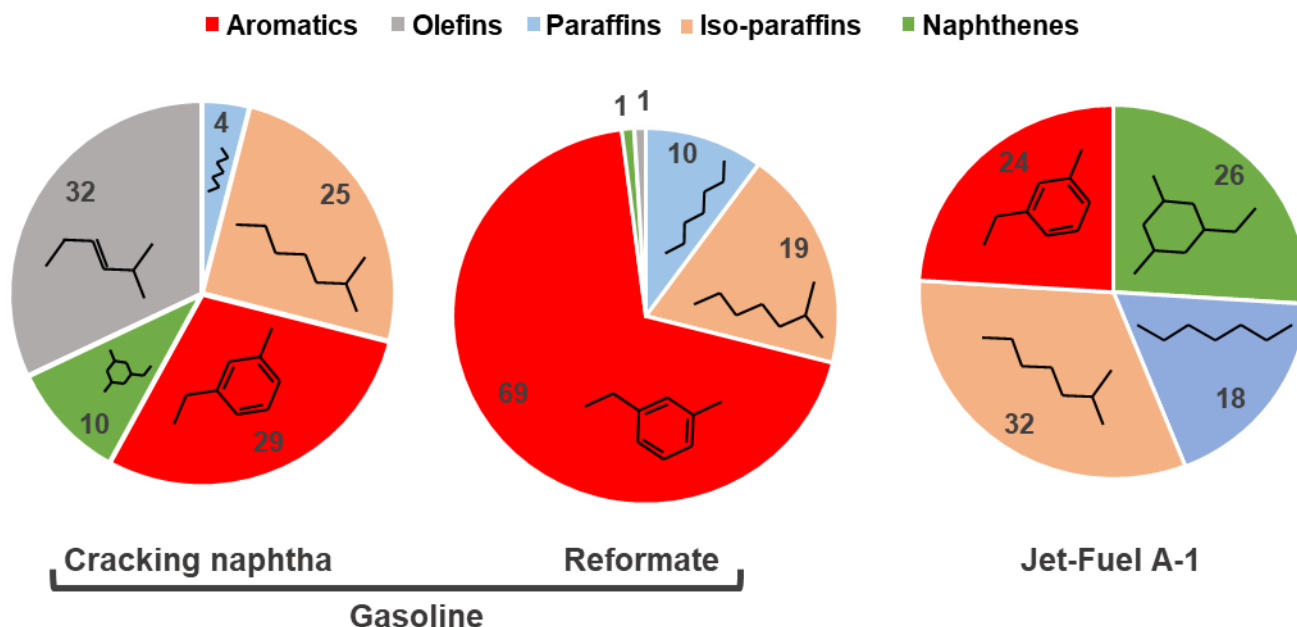
Figure 9   Average chemical composition of gasoline (from carking naphtha and reforming)[103] and jet fuel Jet A-1.[101]

Given the fact that hydrocarbon fuels are mainly produced from crude oil and considering the issues related to its usage (e.g., diminishing petroleum reserves, energy security concerns, realise of CO_2 in the atmosphere as primary cause of global warming), the shift from fossil-based to renewable-based fuels is needed.[101,113] The existing liquid biofuels most widely used are the crop-based bioethanol and biodiesel, produced by transesterification and fermentation technologies respectively. [114] However, their implementation has inherently issues related to their nature, requiring proper engines and infrastructure. Hydrocarbon biofuels that are "drop-in replacements" for conventional petroleum-derived transportation fuels, since chemically identical, are expected to gradually supplant ethanol and biodiesel. [113,113] Considering the lignocellulosic biomass, it can be converted to syngas through gasification which can then be converted to fuel hydrocarbons by Fischer–Tropsch conversion. Otherwise, the alcohols derived by fermentation of sugars and ethanol in particular, can be upgraded to hydrocarbon fuels (C_{3+} hydrocarbons) undergoing several chemical transformations. [69,115,116] The valorisation of ethanol into longer chain hydrocarbons mixtures (resembling the gasoline composition) has gained importance in both industry and academic researches. Technologies for converting alcohols and other oxygenates to jet fuel are being developed by several companies, still at laboratory and pilot level, and most of them by partnering

bio-alcohol producers and companies able to perform the upgrading.[101,107] For instance, Vertimass is currently commercializing a process for making bioderived jet fuel and BTEX (benzene, toluene, ethylbenzene, and toluene) from ethanol. [117] While Gevo and BioChemtes [118] cooperated to convert bioalcohols into jet fuels in the C_{12}–C_{16} range.

The main strategies to transform ethanol into hydrocarbon mixtures and can be gathered into two different approaches.[119] The first one, the most studied, involves acid-catalysed ethanol dehydration to ethylene followed by olefin oligomerization over solid acids, mainly zeolites. Then through hydrogenation it is possible to obtain a mixture suitable to be used as gasoline or jet fuel. However, one of the challenges of this process is to tailor the catalyst composition in order to control the product distribution. Ethylene oligomerization is slow and requires operative temperature above 300 °C where undesirable side-reactions including cracking, hydrogen transfer, and aromatization can take place, lowering the overall selectivity. [120,121] As a result, such processes are limited to producing mainly C_3–C_8 paraffins and C_6–C_{12} aromatics, species suitable for use in gasoline or in the chemical industry (e.g. BTEX).[122] This first approach is a process similar to much more studied technology named methanol-to-gasoline (MTG) developed by Mobil Corp. (now Exxon Mobil Corp.)[123] on HZSM-5 zeolite. Hence this approach has been frequently named the ethanol-to-gasoline process (ETG) and is based on the so-called "hydrocarbon pool" mechanism. [42,124,125] According to this model, the overall process is catalysed not only by the zeolite itself, but also by the organic compounds retained within the voids, that constitute the "hydrocarbon pool" mainly composed by alkyl substituted aromatics compounds, that participate to the reactions as co-catalysts.[106] In this case the main factors affecting the product distribution are the Si/Al ratio of the zeolites, which affects the surface acidity of the catalyst and consequently the reaction temperature required. The main obstacles encountered with this approach are related to the catalysts deactivation due to the extensive coke formation and the competition between cracking and oligomerization reactions, limiting the yield in longer chain hydrocarbons. The control of heavier products formation has been reported to be easily obtained through a two-step oligomerization. Pacific Northwest National Laboratory (PNNL) has developed a two-step oligomerization process that converted ethanol into isobutene/propene-rich gas mixture over $Zn_1Zr_{2.5}O_z$ catalyst, followed by oligomerization over solid acid resin (Amberlyst-36), obtaining a gasoline-range hydrocarbon mixture. They managed to obtain a jet-range hydrocarbons by separating the light gases (i.e., H_2, CO_2, etc.) from olefins before performing the oligomerization step.[126]

The other approach to convert ethanol into middle distillate hydrocarbons is based on ethanol dehydrogenation followed by aldolization. In this context, when heterogeneous bifunctional acid/base catalyst is used, such as a hydroxyapatite, the ethanol could be converted into higher hydrocarbons, namely longer chains alcohols, through a completely different synthetic mechanism generally based on the Guerbet condensation reaction, the mechanism of which has been deepened in the previous section section 1.2.1.1. In particular, this approach has been applied by Ueda et al.

[23,69] over hydroxyapatite based catalysts, this topic is further detailed in section 1.3.1. In general, the main challenge with using Guerbet coupling to forma C-C bonds and produce distillate-range molecules is reaching high conversions while maintaining high selectivities for the alcohol products. Nevertheless, *n*-butanol and higher alcohols produced can be directly used as fuels or can be subsequently dehydrated to mixed olefins, which can be used to make jet range fuel via oligomerization reactions.

1.2.1.3 Ethanol dehydration

The dehydration products of ethanol are diethyl ether (DEE) and ethylene, and the reaction is catalysed by various solid acid catalysts such as silica-alumina and zeolites. Ethylene and diethyl ether are important products for the chemical and petroleum industries. [127,128] Ethylene is one of the most demanded intermediate chemicals, widely used in the industrial synthesis of polymers and a variety of other valuable products of organic chemistry, due to its high reactivity. When derived by fossil fuels, its production is based on steam cracking of petroleum liquids and natural gases. However, this process is exothermic and requires high reaction temperatures (780–1200°C) and the use of steam as a heat transfer agent at a ratio of 1: 1. The overall process releases great amounts of carbon dioxide into the atmosphere. [129,130] Catalytic dehydration of ethanol is an alternative ecological route for production of ethylene, which reduces the greenhouse gas emissions and dependency on limited fossil fuels.[72,73,131] Diethyl ether is a valuable chemical and an attractive motor vehicle fuel alternative [132] since it has excellent transportation fuel properties (cetane number > 125). [133,134]. Good burning properties of DEE make it a promising alternative fuel or fuel additive for diesel fuel[132]. Also, blending of DEE with ethanol was reported to improve the cold start problem of ethanol fueled cars.

When ethanol reacts on solid acid catalysts, the products generally found are ethylene, water and diethylether. There is no general agreement in the literature on the reaction pathway, that has been observed to depend to some extent on the catalyst used, but it can be resumed as reported in Figure 10. Where ethylene could be formed by a consecutive intramolecular dehydration reaction where DEE acts ad intermediated obtained by interdehydration of two molecules of ethanol; ethyelene and ethyl ether are products of parallel reactions or both parallel and consecutive reactions take place. [135]
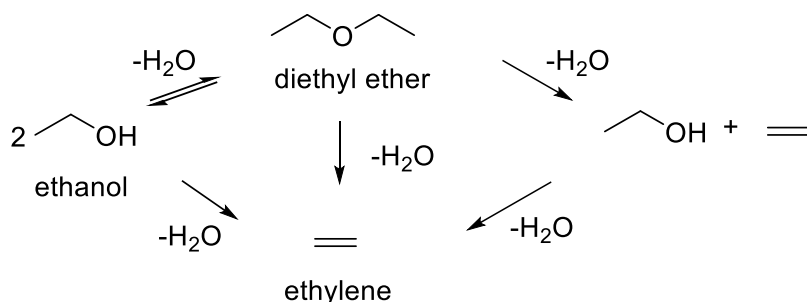
Figure 10   Ethanol dehydration pathways. [135]

Reaction temperature plays an important role in the product distribution since the two reactions have an opposite thermodynamic behaviour. The production of ethylene is endothermic and the highest selectivity towards ethylene is obtained at 300–500 ºC. Higher temperatures shift the reaction towards acetaldehyde production, while the slightly exothermic production of diethyl ether (DEE) is only favoured below at lower temperatures.[72,73,131,136] For these reasons, the potential to achieveof DEE with high yields is quite low in a conventional flow reactor.[136] From the catalytic point of view, the activity and respective selectivity between DEE and ethylene has been correlated with both the amount and strength of the acidic centres of the catalysts employed. [137] It has been observed that generally, ethanol is adsorbed on the catalysts surface as ethoxy group, that then can crack over acidic catalyst-producing ethylene by an elimination reaction or can react as a nucleophile, which attacks un-dissociated ethanol producing diethyl ether. [136] In addition, the mechanism of the dehydration of ethanol reaction suggested that two separate types of sites are responsible for the ethylene and DEE formation. Generally, it has been observed that low-temperatures and medium strength of acid sites favour DEE production.[138,139]

1.2.1.4 Ethanol to butadiene

Butadiene is one of the most important bulk chemicals produced in the petrochemical industry, widely used in the production of polymers and polymer intermediates. [140] It is mainly produced as a by-product of ethylene steam cracking of naphtha or by the catalytic or oxidative dehydrogenation of *n*-butane and *n*-butene respectively. [141]

Butadiene production from ethanol has gained interests in recent years and is often considered as product of a parallel reaction to the Guerbet reaction pathway.[74,142] The most encountered processes that lead to butadiene production starting from ethanol are made up by one or two steps. The two-step process which is called "Ostromislensky process" and is based on a first dehydrogenation step of ethanol yielding acetaldehyde and a second one where acetaldehyde and ethanol react over a tantala promoted silica catalyst to yield butadiene.[32] Then, the one-step process, the so-called "Lebedev process" which requires a bifunctional catalyst, exhibiting both dehydrating and

dehydrogenating activity. [143] Lebedev first proposed a radical mechanism but in recent years all the reaction mechanism for both processes proposed considers acetaldehyde as the key intermediate and its conversion toward crotonaldehyde. [74] Indeed, Toussaint and co-workers[144] proposed a mechanism based on the aldol condensation between two acetaldehyde molecules formed upon ethanol dehydrogenation. The overall mechanism includes the formation of acetaldol via the aldol condensation of two acetaldehyde molecules, followed by dehydration of the aldol to crotonaldehyde, in accordance with the reaction mechanism showed in figure 11. Then crotonaldehyde is reduced via Meerwein–Pondorf–Verley mechanism(MPV) mechanism to crotylalcohol, where ethanol (or any other alcohol present in the system) served as a hydrogen donor, requiring the participation of acid and basic sites. [32,145] Finally, the dehydration of crotylalcohol yield butadiene. However, there are different perspectives and mechanism proposed, even concerning the rate controlling stage of the reaction.[143]
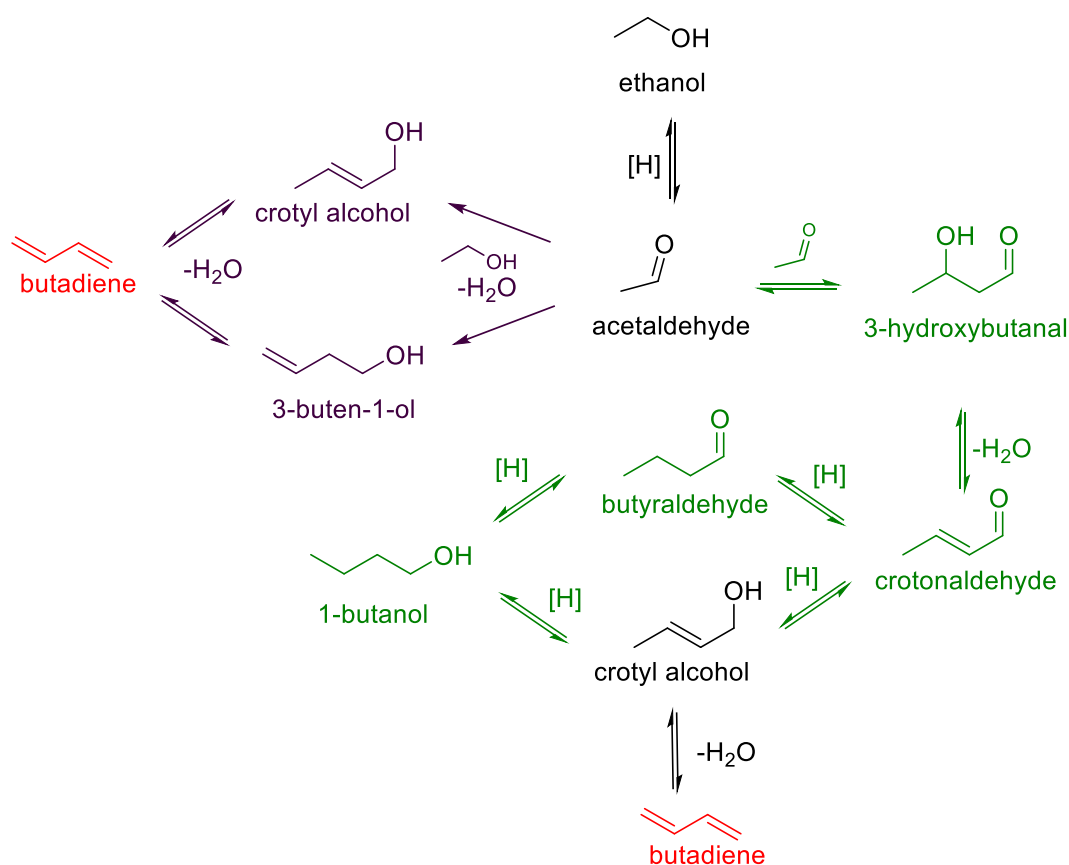
Figure 11   Mechanism formation of butadiene from ethanol. In purple the alkenols route, in green the aldol-condensation route.

Recently, Chieregato et al. [64], by studying the ethanol conversion over MgO, proposed the direct route of *n*-butanol formation. Accordingly, they proposed a different reaction mechanism for butadiene production as well, suggesting that is is formed by condensation between ethanol and acetaldehyde, leading to alkenols (mainly crotyl alcohol) which are then dehydrated into butadiene.

Similarly to the Guerbet reaction, a multifunctional catalyst with balanced basic, acid and redox properties is required for the reactions of condensation, dehydration and hydrogenation. Over the years, butadiene formation from ethanol has been studied over many catalytic systems (e.g., ZrO_2-Fe_2O_3, doped Al_2O_3, metal oxide-promoted MgO-SiO_2 (e.g., CuO, NiO, ZnO) , metal modified sepiolite, Zn-containing talc and zeolite-based catalysts). [146–149] For instance, Angelici et al. [148] managed to obtain butadiene with 53% of selectivity while performing the reaction at 425ºC over a CuO/SiO_2–MgO catalyst. They stated that the addition of CuO as a promoter on the physical mixture of SiO_2–MgO systems improved butadiene yield and that the nature of the CuO played a crucial role in butadiene formation (i.e., cluster-like species of CuO), that is strictly related to the synthesis method applied. Nevertheless, the main issues generally encountered were the formation of the many side products, lowering the overall yield and the negative effect of water produced on the surface of the catalyst.

1.3 CATALYSTS

1.3.1   Hydroxyapatite

Calcium hydroxyapatite (Ca-HAP, $Ca_{10-x}(PO_4)_{6-x}(HPO_4)_x(OH)_{2-x}$), with 0< x≤1) is the basic mineral constituent of human bone and tooth enamel. [150] Naturally, it can be extracted from mineral rocks, biogenic products (e.g., eggshells, mussel shells) and bio-wastes (e.g., fish bones, mammal bones). Otherwise, it can be synthetized by wet chemical methods (i.e., precipitation, sol-gel technique, hydrolysis, hydrothermal, emulsion method) starting from its inorganic precursors (e.g., calcium hydroxide, calcium nitrate, phosphoric acid, ammonium phosphate). [151]

The stoichiometric HAP contains calcium (Ca) and phosphorus (P) at a molar ratio of 1.67 (Ca/P) and a H_2O content of 1.79 wt %.However, HAP in human bones is usually nonstoichiometric due to Ca deficiency with Ca/P ratios varying from 1.5 to 1.67, which affects the biological and mechanical properties of HAP .[150] Indeed, it is easy to find HAP in its non-stoichiometric composition caused by the relationship in size between its Ca^{2+} and P^{5+} ions, which allows HAP structure to tolerate a certain degree of substitution of ions during crystal formation, for this reason HAP is classified as a distorted apatite. [23,69] Its structure (Figure 12) comprises three-dimensional networks of hexagonally packed tetrahedral PO_4^{3-} ions. These ions make a first channel around Ca^{2+} ions [type 1 Ca, "Ca1"] with a diameter of 2.5 Å, Ca1 is coordinated to 9 oxygen atoms. [61] A second channel with a diameter of 3.5 Å, bordered by triangular Ca^{2+} ions [type 2 Ca, "Ca2"], hosts the OH^- species along the c-axis, C2 is coordinated to 7 oxygen atoms.[61,152] "Non-stoichiometric hydroxyapatite" is represented by the formula Ca $_{10-Z}(HPO_4)_Z(PO_4)_{6-Z}(OH)_{2-Z}\cdot nH_2O$; 0 < Z ≤ 1, n= 0-2.5, with OH- sites that can be partially

substituted with H_2O. It is characterized by the presence of a vacancy defect in cationic site and OH. In addition, the non-stoichiometry affects the crystallinity, that is lower the further hydroxyapatite is from stoichiometry and simultaneously, its solubility increases.[153] Thus, hydroxyapatite surface exposes different functional groups, acting as acid and basic sites and conferring a peculiar amphoteric character, which can be more or less pronounced depending on the HAP composition, in particular on the Ca/P ratio.[154] In addition, it has the intrinsic capability to exchange the Ca^{2+} ions and to distribute some other metal ions analogously to zeolites allows one to obtain interesting functionalized materials with modulated number and strength of acid and basic sites.[152,23,69] Both cationic and anionic substitutions can take place. Several cations can substitute calcium ions in either type1 and type 2 Ca positions or in both positions simultaneously, for instance, Ca (II) can be exchanged with Mg(II), Sr(II), Ba(II), Co(II), Cd(II), Cu(II), Fe (III), Ce(III), Eu (III).[155–158] Similarly, several anions can replace either OH^- or PO_4^{3-} ions or both, for example the trivalent anion PO_4^{3-} can be exchanged with SO_4^{3-}, MnO_4^{3-}. [152,153,159]
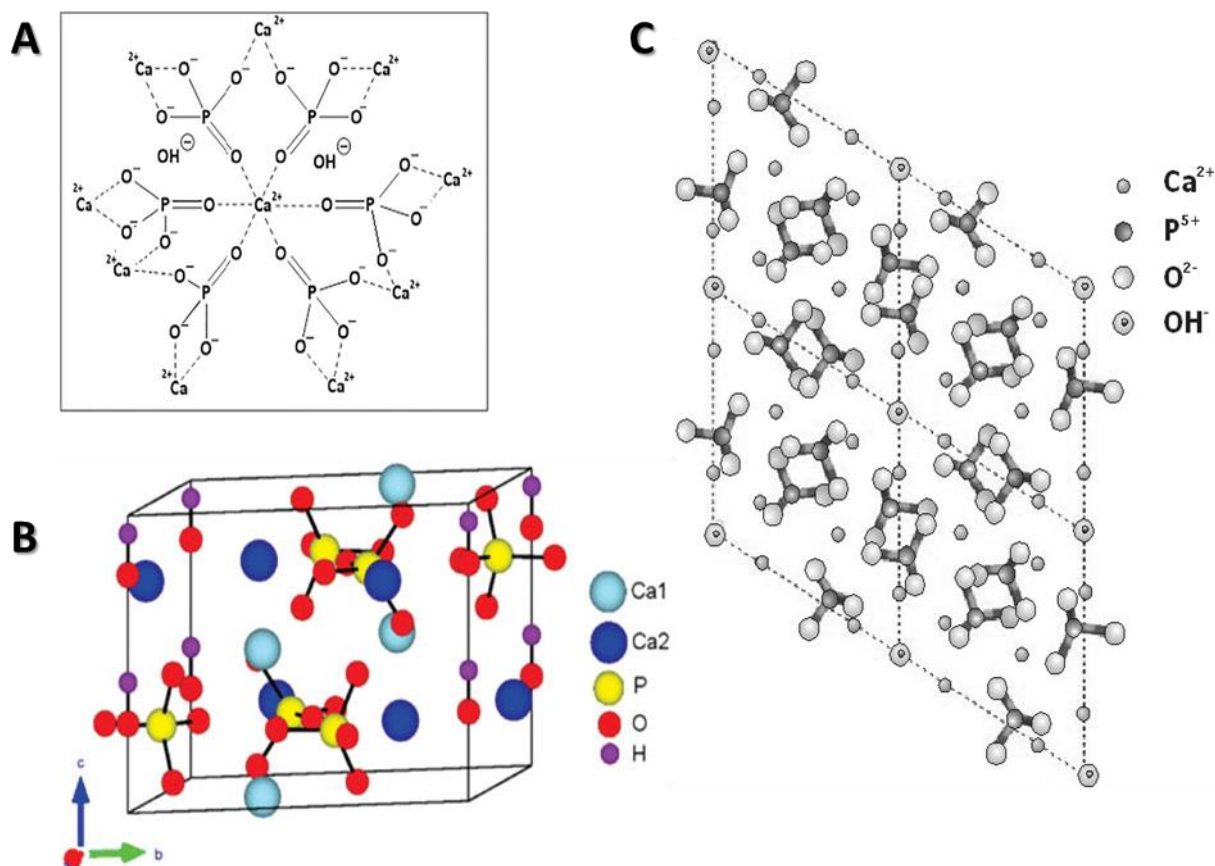
Figure 12 A) Structure of hydroxyapatite, [160] B) Hexagonal unit cell of SHAp[150], C) Crystal structure of hydroxyapatite.[161]

Besides its ion-exchange ability, HAP has a remarkable thermal stability, allowing to be processed at high temperature (up to 800ºC) without undergoing physical modifications, letting it be really suitable to be used as heterogeneous catalyst to perform gas-phase reaction. In addition, its

functionalization with metal species could lead to multifunctional catalysts that would benefit from the combination of the electron transfer capacity and Lewis acidity associated with the metal centres and of the amphoteric surface properties of HAP. [162]

Me-HAP based catalysts been used for environmental protection reactions, such as the abatement of volatile organic compounds and denitrifications (i.e., de-VOCs and de-NOx). [162] Then, it has been observed quite effective for the C-C coupling reactions. In particular, it incorporates the ideal multifunctionality to be used as multifunctional catalyst for the ethanol Guerbet condensation. In this regard, it has been extensively employed by several authors and it has been shown to be the most active catalyst with high selectivity toward *n*-butanol.[96,58,59,163] The highest selectivity obtained up to now has been 82% over a Sr-substitued HAP, at 300ºC and atmospheric pressure, nevertheless, it was related to a low value of EtOH conversion of 4%.[97] In addition, Silvester et al. [61] managed to obtain an overall alcohols selectivity of 76.4% with 13% of ethanol conversion over a 100 mol% Sr substitued apatite, by working at 350ºC and GHSV = 5000 mL·h⁻1·g⁻1. The same research group [164] in a former study, obtained a total alcohols selectivity of 83% over a carbonate containing apatite (Hap-CO$_3$).

Ho et al. [58] studied the mechanism of *n*-butanol formation starting from ethanol over HAP catalyst. They stated that ethanol is adsorbed by dissociative adsorption on the Ca-O sites forming ethoxide and hydroxyl species on the surface that lead to the formation of acetaldehyde which migrates to the neighbouring sites CaO/PO$_4^{3-}$ undergoing aldol-condensation and yielding crotonaldehyde. The two hydrogenation steps that yield *n*-butanol take place by hydrogen transfer from ethanol via Meerwein-Ponndorf-Verley (MPV) reduction. The mechanism hypnotized is depicted in Figure 13. Nevertheless, the acid-base cooperation was found to accelerate the aldol condensation rates.
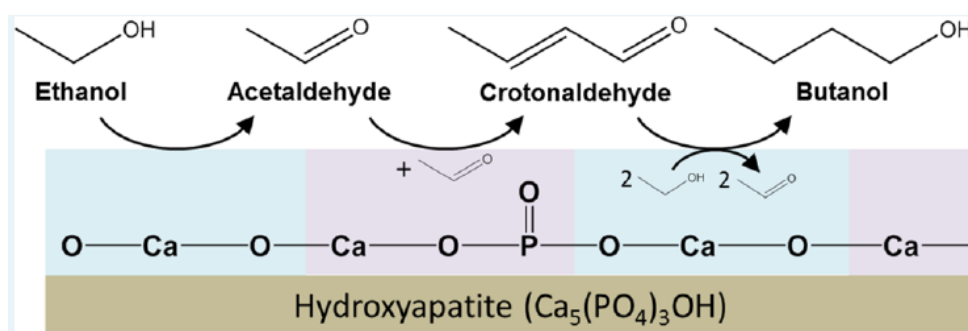
Figure 13   Ethanol Guerbet conversion over hydroxyapatite catalyst. [58]

Ogo et al. and Silverster et al.[61,164] investigated the effects of ion-substitution on the catalytic activity of ion-exhanged HAP. The substitution with VO4^{3-} anions increases its selectivity for acetaldehyde dimerization to crotonaldehyde, while by exchanging CO3 $^{2-}$ anions and Sr^{2+} in the HAP structure, it was highlighted the importance of balancing acid and base sites in order to enhance the selectivity for the Guerbet coupling of ethanol. In particular, it was found an optimal ratio of 4 between acid and

basic sites over a series of Sr-substitued hydroxyapatite[61], while HAP with predominantly acid sites functions as a dehydration catalyst. [63] Nevertheless, the extent of ethanol conversion has been strictly related to the surface area of the catalyst. [61]

Due to the well-known good performance of HAP in the ethanol Guerbet coupling reaction, it has been recently used as "Guerbet catalyst" in a patented process. In detail, Sakuma et al. [165], patented a two step approach for producing a mixture of hydrocarbon of C_4-C_{12} resembling gasoline starting from ethanol. They fed ethanol from the top of a two fixed bed reactor consisting of "Guerbet catalyst" such as HAP (the first bed) producing a longer chain compounds mixture and a hydrogenation catalyst (the second bed) to reduce it. They used hydrogen as carrier gas or they fed hydrogen only in the second step and they even studied the reaction by using only the hydrogen generated in the first step as hydrogenation agent for the second step using helium as carrier gas in this case. They conducted the first step at 1-200 atm, 100-600°C and using a contact time of 0.1-600 seconds whereas the second step was conducted at 1-200 atm, 0-400°C.

In the context of pushing the Guerbet reaction toward the production of higher alcohols and condensed products, Tsuchida et al. [23,69] studied the ethanol gas phase conversion over HAP and by working at 500ºC they obtained a product mixtures from C_2 to around C_{12} hydrocarbons. The obtained liquid contained oxygenates such as alcohols, aldehydes, and ketones, which are not found in commercial gasoline, and at the same time, aromatics such as benzene, toluene, and xylene, in smaller quantities than in commercial gasoline. They suggested a new mechanism for the synthesis of biogasoline from ethanol consisting of two consecutive reactions: the propagation of ethanol (to produce Guerbet alcohols) followed by dehydration/dehydrogenation of the generated alcohols (i.e., 2-ethyl-1-butanol; n-hexanol; 2-ethyl-1-hexanol; n-octanol; two kinds of branched C10 alcohols and n-decanol). They observed that with high Ca/P ratios, close to stoichiometry, the good acidic/basic sites ratio can promote the dehydrogenation properties of the catalyst (i.e., lower Ca/P led to higher acidity). Indeed, using nonstoichiometric HAP as catalysts for the conversion of ethanol brought to hydrocarbon fuels (up to C12) containing, in addition to non-oxygenated hydrocarbons, a fraction of oxygenated hydrocarbons (alcohols, aldehydes). [69] Conducting ethanol conversion over HAP with a Ca/P ratio of 1.64 at a contact time of 1.78 s and a reaction temperature of 300°C resulted in a *n*-butanol selectivity as high as 76%. [23] In 2008, Tsuchida et al. managed to synthetize biogasoline from ethanol in one step over a highly active nonstoichiometric HAP catalyst.[69] The biogasoline produced has a research octane number of 99 and contains dienes and oxygenates almost entirely absent from the product of MTG or ETG over a zeolite catalyst. They found that the ratio of oxygenates in the biogasoline could be adjusted by changing the reaction conditions (mainly reaction temperature).

In 2017, Quintana et al.[166] prepared a carbonate hydroxyapatite by precipitation (i.e., B-type CHAP [$Ca_{10-x/2}(PO_4)_{6-x}(CO_3)_x(OH)_2$]) and tested for ethanol conversion. They managed to obtain a

hydrocarbon fuel mixture with carbon chain lengths in the range C_4-C_{18+} with high yield (97%). The carbon chain lengths obtained was quite higher than those reported in the literature (e.g., C_4-C_{10+}) on HZSM-5[167] and nonstoichiometric HAP catalysts[69], suggesting that carbonate ions may play an important role in the formation and breakage of C-C, C-H and C-O bonds, favouring the production of large hydrocarbon molecules.

1.3.2   Zirconia

Several studies have been performed on the structures and properties of oxides surfaces, in order to understand the roles that oxides play in the catalytic processes. Among various metal oxides, zirconia (ZrO_2) is of particular interest and has received widespread attention thanks to its ideal mechanical and chemical stability. Moreover, zirconia also possesses excellent properties of high melting point, high electrical resistivity, high refractive index and low thermal expansion coefficient, and therefore is considered as one of the most important ceramic materials[168]. In nature, zirconium oxide occurs as the mineral baddeleyite. The normal procedure used to prepare zirconia consists of calcination of the zirconium hydroxide (hydroxylated gel) which is prepared by hydrolysis of zirconium salts. This gel presents two different kinds of OH$^-$ group, terminal and bridged, the ratio of which depends mainly on the precursor used to form the gel. The polymorphic nature of ZrO_2 is well known and has been subject of many studies. [169] Zirconia has three polymorphs: monoclinic (T<1000ºC), tetragonal (T>1170ºC) and cubic phases (T>2370ºC). In addition, it can even exists as an amorphous solid. The final crystal structure of ZrO_2 is strictly affected by the preparation method. [170] Nevertheless, the monoclinic phase is thermodynamically stable at room temperature, while the tetragonal and cubic phases are metastable. [171] The transition from the monoclinic phase to the tetragonal phase starts around 1050 °C, completing around 1170 °C. During this transformation, the volume decreases of 3–5%. A metastable tetragonal phase can be obtained by quenching to room temperature[172]. The crystal structures related to these phases are shown in Fig. 14
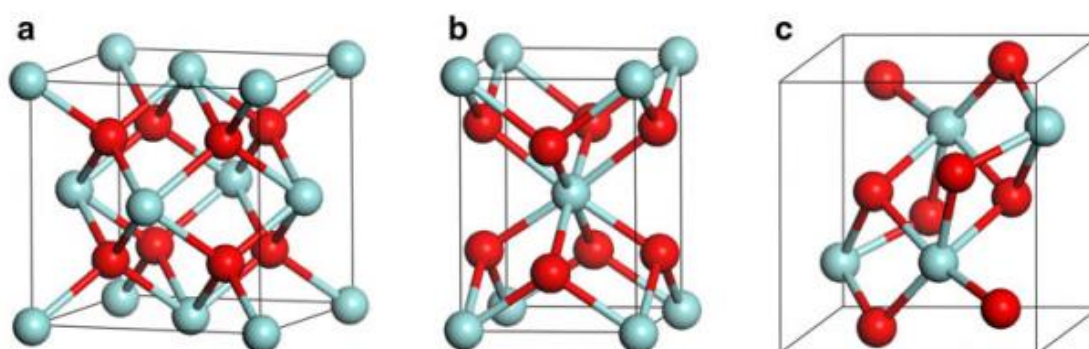

Figure 14   Crystal structures of ZrO2: a) cubic; b) tetragonal and c) monoclinic. Red and blue spheres correspond to oxygen and zirconium atoms respectively[168]

The cubic ZrO_2 has an ideal fluorite structure (Fig. 14a). The Zr cations are situated at the corners of the cubic elementary cell as well as at the halves of the [110] directions, in a face-centred cubic (fcc) lattice. The oxygen anions lie at the quarters of [111] directions, which are the tetrahedral interstitial sites associated with this fcc lattice. In this structure, each Zr cation is coordinated to eight equivalent nearest-neighbour oxygen anions at the corners of a cube, and each O anions is tetrahedrally coordinated to four Zr cations[173]. Consequently, zirconium and oxygen are octahedrally and tetrahedrally coordinated, respectively. The unite cell contains one zirconium and two oxygen atoms with Zr–O distances of ≈ 2.2 Å.[174] The tetragonal ZrO_2 possesses a distorted cubic structure (Fig. 14b), obtained by displacing opposite pairs of oxygen atoms alternatively up and down along the [001] direction. In the tetragonal ZrO_2, each Zr cation is still surrounded by eight oxygen anions, with four oxygen neighbours arranged in a flattened tetrahedron at a short Zr–O distance, 2.065 Å, and the rest in an elongated tetrahedron rotated 90° at 2.455 Å from Zr. Each oxygen anion is bonded to two Zr cations at 2.065 Å, and two more Zr cations are 2.455 Å away[175]. Finally, monoclinic zirconia has a lower symmetry and a more complex geometric structure. The primitive cell contains four ZrO_2, so 12 atoms (Fig. 14c). Each Zr cation is in sevenfold coordination to oxygen anions, and there are two non-equivalent oxygen sites: threefold O_I and fourfold O_{II}[176]. There is a large dispersion of interatomic Zr–O distances, with average values of 2.07 Å and 2.21 Å for Zr–O_I and Zr–O_{II}, respectively. Zirconia also has a high-pressure (10 GPa) orthorhombic structure which can be stabilized at atmospheric pressure by addition of >12 mol% of niobia or tantala or a mixture of them[177]. Stable lower oxides of zirconium are not known, although oxygen dissolved in the zirconium metal lattice has led to the identification of some superstructures as $ZrO_{0.3}$[178]. While stabilized zirconias are insulators at room temperature, at elevated temperatures the vacancies in the anion lattice allow oxygen ions to diffuse and the zirconia becomes a solid electrolyte with applications in oxygen sensors and high-temperature fuel cells[172]. Zirconium monoxide, ZrO, has been observed in mass spectrographic measurements[179].

Zirconia has both acidic and basic properties, that depend greatly on both the synthetic procedure and the calcination temperature.[180] Moreover, it is possible to control the acid−base properties of zirconium oxide by modifying the phase composition because it was shown that various crystalline modifications of zirconia differ in acid−base characteristics. In particular, it was found that tetragonal ZrO_2 is characterized by higher basicity than the stable monoclinic phase.[181] The various crystal forms of ZrO_2 reflect how the hydroxide was prepared and treated. In this sense, a gel with a high proportion of bridged OH groups gives the tetragonal form, while if terminal OH groups are predominant in the gel, the monoclinic form is formed.[182] In the literature there are many hypotheses and theories about the factors that can stabilize the metastable phases tetragonal (*t*) and/or cubic (*c*) form versus the monoclinic (*m*) one. [183] For instance, the tetragonal phase may be stabilized by using additives. Lanthanum or yttrium oxides as well as sulphate ions are frequently used for this purpose.[184] The cubic phase of zirconia can be stabilized down to room temperature by the addition

of magnesia, calcia, yttria, or rare earth oxides, whose presence creates vacancies in the zirconium anion lattice. These stabilized zirconium oxides contain from 3% yttria to 8% of calcia[172].

The flexible amphoteric character, the high thermal stability, the versatility to modifications, the non-toxicity and its relative low cos are all promising characteristics for zirconia to be used as catalytic material. [182,185] Indeed, it has been widely used also in heterogeneous catalysis. In particular, it has been used in many catalytic reactions as catalysts itself or as catalyst support, as well as an additive to improve the catalytic performances of other catalysts[168]. For example, the addition of zirconia to ceria (CeO_2) can greatly increase the "oxygen storage" property of ceria[186]. At the same time, ceria has been added as stabilizer for the tetragonal ZrO_2. The ZrO_2–CeO_2 mixed oxide catalyst containing 10 wt% of ceria showed enhanced basicity and promoted the Guerbet route favouring the *n*-butanol formation. [187] In this context, bare zirconia has been showed to act as acid catalyst and its Lewis surface acidity directs the ethanol preferentially toward its dehydration into ethylene.[92] By contrast, when its tetragonal phase is stabilized by yttrium addition, zirconia showed great activity toward *n*-butanol formation, obtaining a 16.8 % yield at 300ºC.[181]

Generally, zirconia can be used to catalyse a wide variety of reactions including the alkene isomerization[188], the Meerwein-Ponndorf-Verley reduction reactions with an alcohol as H-donor [189,190], aldol condensation [191], alcohol dehydration and alcohol dehydrogenation [192–194] and hydrocarbon hydrogenation, dehydrogenation, cracking, hydrodesulfurization[195]. As previously mentioned, ZrO_2 has also been used as a support in several catalytic reactions. For example CO oxidation[196–198], low-temperature water–gas-shift (WGS) reactions[199,200] and selective hydrogenation of unsaturated organic compounds[201].

1.3.3   Sepiolite

Sepiolite is a typical fibrous Mg-rich silicate mineral belonging to the clay family, with the fiber length up to several micrometres. [202] In nature, sepiolite usually precipitates from water bodies undergoing evaporation but it can precipitate also from interstitial fluids sediments. It occurs in two forms and is designated as α-sepiolite, derived by hydrothermal process, and β-sepiolite from precipitation. [203] Besides the formation processes, sepiolite can originate from magnesium–silicate substrates or pre-existing minerals during diagenesis. The widest accepted mechanism for sepiolite formation is the direct precipitation from solutions containing dissolved ionic species (silica and magnesium).[204,205] The reserve of sepiolite in the world is estimated to be 8000 million tons, and the largest mine of sepiolite is located in Spain, with the total reserve over 3800 million tons.[203] The most well-known Spanish sepiolite deposit is that of Vallecas-Vicálvaro on the outskirts of Madrid, where the sepiolite was formed mainly by neoformation in a continental environment of Miocene age.[206] In general, clay minerals may be one-dimensional, such as sepiolite, and two-dimensional. They have special crystal

structures with a variety of physicochemical properties, such as expansion of the interlayer space, cation exchange, small particle size, high surface area, and so forth. They are naturally occurring, cheap, eco-friendly, non toxic and abundantly available. [207] Thus, considering the "Green and Sustainable Development" concept, sepiolite gained both industrial and academic attention. [203]

Sepiolite is a hydrated magnesium silicate having an internal structure of channels which can accommodate zeolitic water and other molecules structure (Figure 15), its structure was firstly described in 1995 by Nagy and Bradley.[202,208] Its molecular formula is $Mg_8Si_{12}O_{30}(OH)_4(H_2O)_4 \cdot 8H_2O$, with stoichiometric variations in the number of protons, surface hydroxyl groups and crystallization water molecules, depending on the origin and taking into account the peculiar properties thereof.[209]
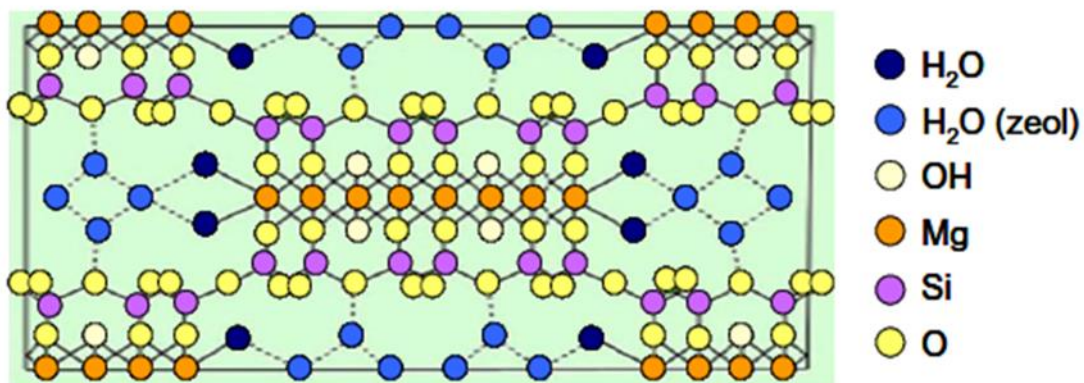
Figure 15   Structure of sepiolite. [210]

Sepiolite exhibits microfibrous morphology, showing an alternation of blocks and tunnels that grow up in the fibre direction. Each structural block is composed of two tetrahedral silica sheets linked by means of oxygen atoms to a central sheet of magnesium oxide-hydroxide, so that the tetrahedral sheet is continuous, but with the directions of the apical end of the silica tetrahedrons of the adjacent ribbons inverted. Along the fibre axis, each ribbon alternates with channels (or "zeolitic tunnels") that are filled with weakly bound zeolitic water and exchangeable cations (Figure 16). Theoretically, every octahedral site of the ideal sepiolite is occupied by Mg(II) cations. The magnesium ion in sepiolite crystal is exchangeable with various transition metal ions. [211] In the formation process of sepiolite, octahedral Mg(II) cations are easily substituted by Al(III) and/or Fe(III), which may cause the generation of negative charges and formation of structural defects. Moreover, the substitution of tetrahedral Si(IV) cations by Al(III) is also possible. It is for these reasons that a considerable number of exchangeable cations exist in the channels to compensate for the structural negative charges. [212] There are three types of water in sepiolite structure: in addition to zeolitic water molecules present in the channels, crystal water is bonded by hydrogen bonds at the external surface and the coordination of octahedral cations is completed by coordination H_2O molecules (Figure 16B).[213] At the edges of the tunnels opened to the external surface of the sepiolite particles, several silanol

groups (Si-OH) are present, which, together with structural H_2O molecules, are the active hydrogen-bonding sides of sepiolite. This special crystal structure makes sepiolite having large specific areas and high surface activity. [203] In principle, these clay minerals can accommodate larger molecules between their layers than rigid framework silicates (zeolites) could do.[214] Those characteristics together with its fibrous crystal morphology and active silanol groups, give sepiolite excellent adsorption, reinforcing, and supporter functions. Therefore, sepiolite has been applied widely in many areas, e.g. adsorption, catalysis, polymer composites. [203,215,216]
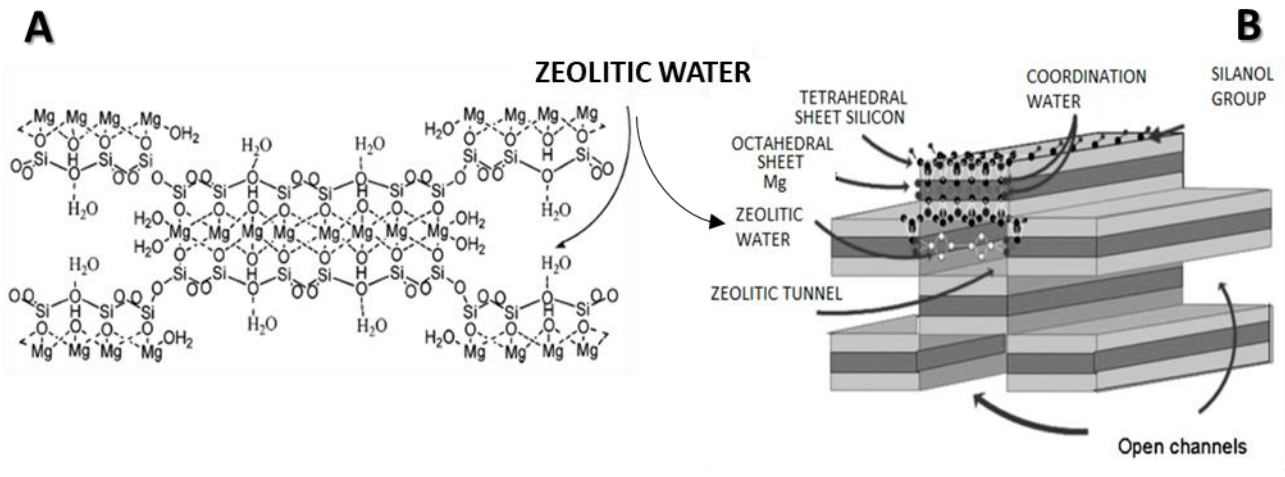
Figure 16 (A) Structure of sepiolite, zeolitic water. [213] (B)Crystalline structure and fiber structure of sepiolite.[217]

Sepiolite structure can be modified and regulated through different methods including thermal activation, acid activation, cationic exchange, and organic modification.[203] When sepiolite is heated in air at temperatures greater than 200ºC, micropores are destroyed, and the surface area is decreased. [208] In particular, the water molecules contained into its structure can be released after thermal treatment at different temperatures, and thus the structure, specific surface area, pore size, and surface activity of sepiolite will be changed.[203,210,218] There are several studies about the calcination temperature effect over the sepiolite structure.[218,219] Some temperature intervals of sepiolite thermal treatment have been individuated: i) the first one at 25–250 °C for dehydration of the zeolitic or channel water, ii) 250–400 °C and iii) 400–600 °C for the respective first [218] and second dehydration stages of the crystalline water, iv) 600–700 °C for the chemical removal of the structural hydroxyls, and v) 800–900 °C for collapse of the crystal.[219] During the first stage in the temperature range 250-400°C, the sepiolite structure is maintained but adsorbed water and water bonded to exchangeable cations in the raw material are removed and a new phase of "sepiolite dihydrate" ($Mg_8Si_{12}O_{30} (OH)_4 \cdot (H_2O)_2$) is formed[219] (Figure 17A, eq2). Then "sepiolite anhydrate" ($Mg_8Si_{12}O_{30} (OH)_4$) in formed in the second dehydration stage by heating the sepiolite up to 550°C (Figure 17A,

eq.3). After heating of the sample up to 850°C the formation of enstatite ($MgSiO_3$) and silica by the degradation of sepiolite anhydrite consisting of its dehydroxylation (Figure 17A, eq.4) takes place.

A

(25-250ºC) (1) $Mg_8Si_{12}O_{30}(OH)_4 \cdot (H_2O)_4 \cdot nH_2O \rightarrow Mg_8Si_{12}O_{30}(OH)_4 \cdot (H_2O)_4 + nH_2O$

(250-400ºC) (2) $Mg_8Si_{12}O_{30}(OH)_4 \cdot (H_2O)_4 \rightarrow Mg_8Si_{12}O_{30}(OH)_4 \cdot (H_2O)_2 + 2H_2O$

(400-600ºC) (3) $Mg_8Si_{12}O_{30}(OH)_4 \cdot (H_2O)_2 \rightarrow Mg_8Si_{12}O_{30}(OH)_4 + 2H_2O$

(T>600ºC) (4) $Mg_8Si_{12}O_{30}(OH)_4 \rightarrow 8MgSiO_3 + 4SiO_2 + 2H_2O$

B
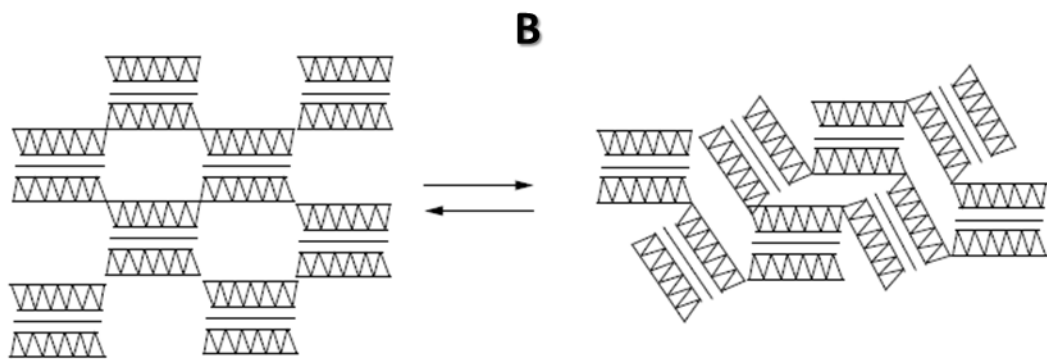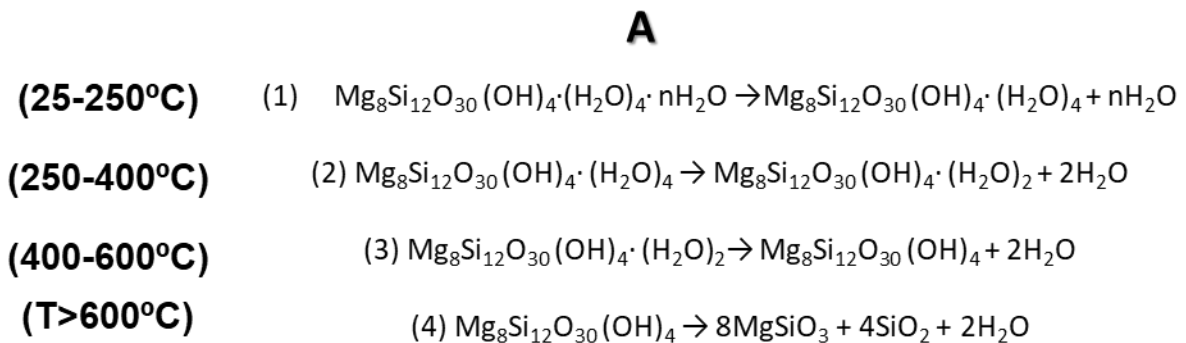
Figure 17   Thermal treatment of sepiolite. A) Phase changes with thermal treatment. B) Structure folding after thermal treatment. [220]

Sepiolite structure can be "activated" by acid treatment with HCl, H_2SO_4, and HNO_3 which can lead to an alteration of its surface area and activity, dissolving soluble imputiries and changing the Lewis and Brönsted surface acid centers.[221] M. Myriam et al [222] found that the mild acid attack results in a progressive dissolution of the octahedral cations, such as Al(III), Mg(II), Fe(III), and Fe(II), accompanied by an obvious increase of the micro- and meso-porosities and specific surface area of sepiolite. Modification of sepiolite with metal salts can be achieved by a cationic exchange process, where the metal ions (M) can substitute the tetrahedral and/or octahedral cations (i.e., Si[IV], Al[III] and Mg[II]), leading to the formation of a series of M^+-sepiolite materials with active acidic or alkali sites. In general, acidic or alkali strength of the obtained ion-exchanged sepiolite is influenced by nature of different metals ions. [203] J. Perez Pariente et al [223] prepared modified sepiolites, with aluminium, chromium or protons substituting octahedral magnesium. By measuring the surface acidity with pyridine adsorption, they noticed that has been created Brønsted acidity and also hydrothermal stability increased. Some alkali treatment have been patented[209,224] and in general, alkali exchanged sepiolite has been used as basic catalyst.[225–227] From those studies emerged that the ion-exchange capability of sepiolite can be enhanced by treating it with base. Previous reports in the literature have demonstrated that the basic strength of the alkali-exchanged sepiolites

increases in the order $Na^+ < K^+ < Cs^+$.[225] Corma et al [226] prepared a sodium-sepiolite based catalyst. By using the obtained system as support for impregnating palladium phase, they found that upon magnesium to sodium exchange, the sepiolite increased its basic strength and that the resulting $PdCl_2$/NaSep sample exhibited a notable activity for the Heck reaction.

Sepiolite has de ideal properties to be used as catalysis support such as its fibrous crystal morphology, large specific surface area, and good surface reactivity. Indeed, it has been utilized as catalyst support for various catalytic reaction systems including methanation of CO_2 with H_2, synthesis of light olefins from CO_2 hydrogenation, purification of ammonia synthesis feed gas by methanation method and for oxidation reactions.[228] In recent years, a variety of catalysts have been prepared by loading active components such as metals (i.e., Zn, Cu, Mo, Ag, Ti) and their alloys, metal oxides, solid acids, and other metal compounds onto sepiolite.[220] Degirmenbasi et al. [228] used its K-impregnated form to catalyse the transesterification of oil to biodiesel, finding the catalyst quite stable upon five reaction cycles. They explained such stability by the special structure of sepiolite, less prone to leaching. [228]

Between its catalysis application, when sepiolite has been employed as heterogeneous catalyst for ethanol conversion the formation of 1,3-butadiene has been observed quite often. For example, A. J. Dandy and M. S. Nadiye - Tabbiruka [208] studied the catalytic activity of natural sepiolite for the dehydration and dehydrogenation of ethanol at 150 - 300°C using a flow reactor (before reaction the catalysts was treated under hydrogen flow at 150°C for 3h). Sepiolite acted as bifunctional catalyst; indeed they observed the formation of water, carbon dioxide, ethene, acetaldehyde, diethyl ether, butadiene and crotonaldehyde with the proportions changing with temperature. In 1981, Kitayama Y. and Michishita A. studied the catalytic conversion of ethanol over Manganese supported on sepiolite. [229] They got a butadiene maximum yield of 33.4% with complete conversion of ethanol with the manganese contents of Mn-sepiolite(II) of 79 mol% for the reaction performed at 300°C for 7 h. Kitayama, Y. et al [211] studied the catalytic conversion of ethanol over a ZnO supported over sepiolite, synthetized by ion-exchange. They found that, while only acidic sites existed on sepiolite, both acidic and basic sites were produced by supporting ZnO on sepiolite. This bifunctional characteristic has been claimed as crucial for the production of 1,3 butadiene. Gruver et al [230] prepared an ammonium-exchanged aluminated sepiolite and a silver-exchanged aluminated sepiolite (6wt%) and they tested them in the ethanol conversion in a gas flow reaction system. Over the Al-sepiolite, diethyl ether and ethylene were the main products. Also, they observed a significant selectivity toward acetaldehyde, which they related to the presence of lewis acid sites over the catalyst surface that could even catalyse the dehydrogenation reaction. Interestingly, they found that the modification of the previous catalyst with the dispersion of Ag led to the formation of a bifunctional catalytic system that brought to the formation of butadiene. They connected the formation of butadiene to two possible routes: the aldol condensation reaction followed by hydrogenation and the Prins routes [231], an acid or lewis acid

catalyzed reaction of addition aldehydes or ketones to alkenes via an oxonium ion, between acetaldehyde and ethylene.

A. Corma et al [135] shown that when Al^{3+} is introduced in the octahedral sheet by exchanging Mg^{2+} ions, sepiolite develops medium and strong acidity and becomes quite an active catalyst for the dehydration of ethanol, with a reaction pathway and kinetics characteristic of a strong acid catalyst. They tested in a gas-flow system a Al-exchanged sepiolite with an Al content of 2.60 wt% in a temperature range of 300-400°C, obtaining mainly ethyl ether and ethylene. Chen et al [232] prepared by co-precipitation synthesis a sepiolite supported cobalt-cerium catalyst, where the Ce was added to strengthen catalytic performance. By testing the multicomponent Co-xCe/SEP catalysts in the ethanol steam reforming they found that the Ce amount influenced the catalyst performance in terms of activity and stability and the Co-0.3Ce/SEP has been optimized to reach 90.8% carbon conversion and over 69.1% H_2 yield at S/C=3, T=600 °C and WHSV=21.5 h^{-1}.

2 AIMS OF THE WORKS

The aim of the work presented and discussed in this thesis was to exploit the versatile nature of bio-ethanol in being converted into various added-value chemical compounds and hydrocarbon mixtures by studying its valorisation over heterogeneous catalysts of a different nature. In particular, it was intentional to investigate the catalytic gas-phase conversion of bio-ethanol into added value derivatives. The objectives can be divided by means of the nature of heterogeneous catalyst employed:

1.   To investigate the gas-phase catalytic conversion of bio-ethanol into hydrocarbon fuels via the Guerbet condensation route. To do so, a commercial hydroxyapatite sample has been used as catalyst and modified by ion-exchange method, varying its acidic/basic and redox properties. (Experimental work at UniBo).

2.   To investigate the influence of the synthetic strategies on zirconia oxide formation and the resulted effects of its surface properties on the catalytic ethanol gas-phase conversion. (Experimental work at ITQ).

3.   To investigate the gas-phase catalytic conversion of bio-ethanol through the Guerbet route over the natural clay Sepiolite catalyst. In order to modulate the acid-base surface characteristics of the clay, a crucial catalyst's feature that has to be optimized for the complex Guerbet reaction mechanism, sepiolite has been modified by impregnation with different alkali-metals salts. (Experimental work at ITQ).

3 MATERIALS AND METHODS

The herein presented PhD thesis resumes the work carried out as a joint PhD programme ("Cotutelle") between two institutions, the laboratories of the Department of Industrial Chemistry "Toso Montanari" in the University of Bologna and the laboratories of the "Istituto de Teqnologia Quimica" (ITQ) of the "Universitat Politecnica de Valencia" (UPV). Accordingly, this chapter will be divided in two parts, describing the different facilities and procedures used at the two institutions.

3.1 Upgrading of ethanol to bio-fuel mixtures at UNIBO

3.1.1 Materials used

Table 1. *Summary of the materials utilized to perform the experiments.*

Compound	MW (g/mol)	Supplier
$Ca_{10}(OH)_2(PO_4)_6$, 34-40% Ca	1004.67	Alfa Aesar
$Cu(NO_3)_2 \cdot 3H_2O$	241.60	Carlo Erba
$Sr(NO_3)_2$ anhydrous	211.63	Alfa Aesar
$Fe(NO_3)_3 \cdot 9H_2O$	404.00	VWR chemicals
$Cu(NO_3)_2 \cdot 2,5H_2O$	232,59	Aldrich
HNO_3	63.01	Aldrich
Absolute ethanol	46,07	Aldrich
n-butanol	74.12	Aldrich
Crotyl alcohol	72.11	Aldrich
2-Ethyl-1-butanol	102.10	Aldrich
Hexanol	102.18	Aldrich
2-Ethyl-1-hexanol	130.23	Aldrich
Octanol	130.23	Aldrich
Decanol	158.28	Aldrich
Acetaldehyde	44.05	Aldrich
Ethyl Ether	74.12	Aldrich
Acetone	58.08	Aldrich
Butyraldehyde	72.10	Aldrich
Ethyl Acetate	88.10	Aldrich
Butyl-benzene	134.22	Aldrich
1,2,4 Trimethyl benzene	120.19	Aldrich
o-Xylene	106.16	Aldrich
Ethyl benzene	106.167	Aldrich
Toluene	92.14	Aldrich
Hexanal	100.16	Aldrich
Decanal	156.2	Aldrich

3.1.2 Catalytic tests: general procedure

3.1.2.1 Reaction system

The catalytic activity was studied in a gas phase continuous-flow quartz reactor working at atmospheric pressure. The amount of catalyst, loaded as pellet (20-40 mesh), was kept constant at 0,6 g for the most of the catalytic tests; however, in some reactions the quantity of the catalyst was varied in order to study the effect of the contact time, calculated as volume of catalyst (mL) divided for the total feed flow (mL/s). The activity of the catalysts was investigated in respect to the time on stream. The inlet gas feed composition was maintained at 5 mol% EtOH in He (95 mol %) unless otherwise stated. These tests were conducted via vaporization of the liquid ethanol that was fed by means of a syringe pump (KPS 100 Syringe Pump) into a stainless steel heated line to obtain an instant vaporization. That heated line has an inlet with the carrier gas (He) and is connected with a tubular quartz reactor (length 600 mm, inner diameter 11 mm) containing the catalyst. The reactor was placed inside a furnace and its inlet and outlet were covered with heating tapes equipped with an electrical resistance to regulate the inlet (230°C) and outlet (230°C) temperature, the same treatments was used for the connecting line between the reactor outlet and the on-line GC inlet valves (both at 260°C). Indeed, the outlet gas stream was analyzed with an on-line Agilent 6890A gas-chromatograph. The latter was equipped with two TCD detectors and the products were separated using a PLOT-Q (30 m x 0.32 mm x 20 µm) column and a DB-1701 (30 m x 0.53 mm x 1 µm) column. Figure 1 represents the scheme of the reaction plant.

The main products that might derive from the reaction were calibrated. Some samples of the reaction products were analyzed by means of a gas chromatograph coupled with a mass spectrometer (GC-MS), in order to identify unknown by-products.
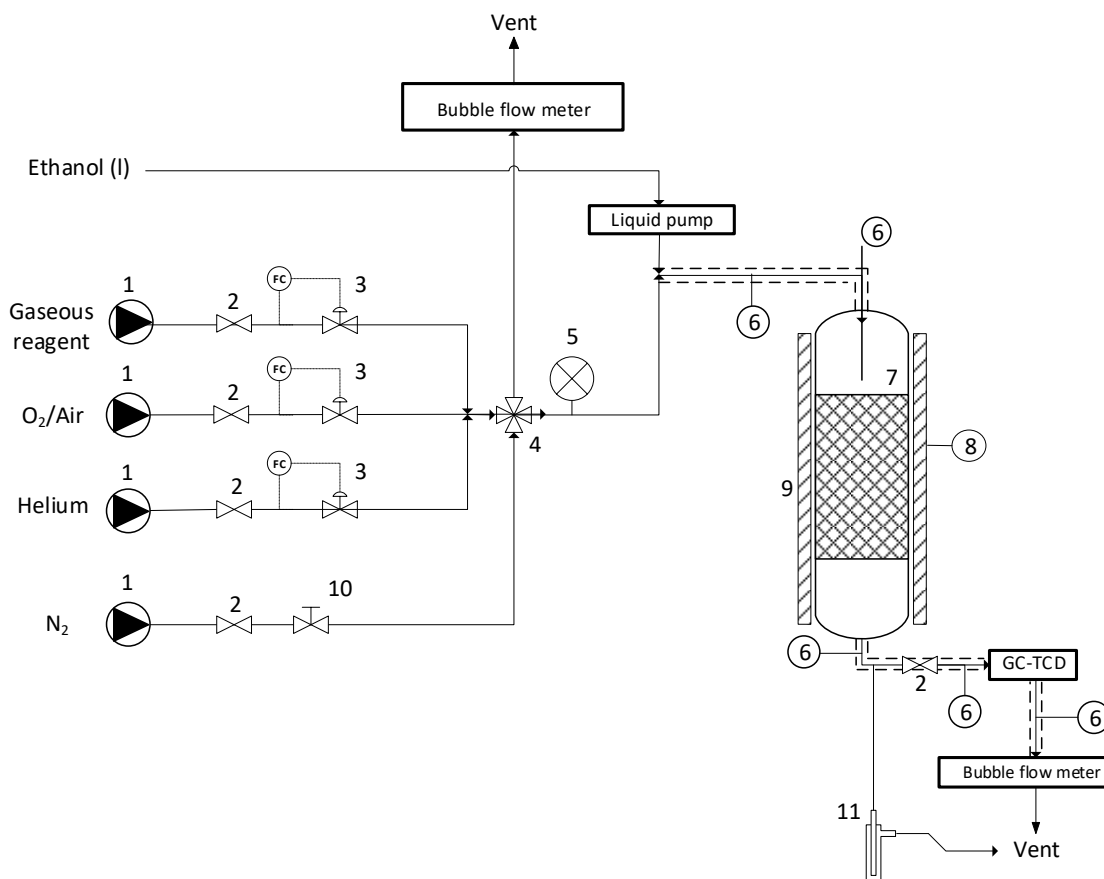
Figure 1   Plant scheme. 1: Gases; 2: On/off valve; 3. Mass flow meters; 4: Four ways valve; 5: Manometer; 6: Thermocouple; 7: Reactor; 8: Temperature control; 9: Reactor oven; 10: Needle valve; 11: Gas bubbler; --- : heated line.

The conversion (X%), yields (Y%), selectivities (S%) and the carbon balance (%) were calculated as follow:

$$\chi\% = \frac{mol_{EtOH}^{in} - mol_{EtOH}^{out}}{mol_{EtOH}^{in}} \times 100$$

$$Y_p\% = \frac{C_{atom}^{p} \cdot mol_{p}^{out}}{C_{atom}^{EtOH} \cdot mol_{EtOH}^{in}} \times 100$$

$$S_p\% = \frac{Y_p}{\chi} \times 100$$

$$Carbon\ balance = \frac{\sum_i Y_{p_i}}{\chi} \times 100$$

The contact time τ (s) was calculated as the ratio between the volume of the catalyst loaded in the reactor (V_{CAT}, mL) and the total volumetric gas flow ($\dot{V}$, mL/min) at the related reaction temperature:

$$\tau = \frac{V_{catalyst}}{\dot{V}_{total}} \times 60$$

3.1.3 Compounds analysis and quantification

3.1.3.1 Qualitative analysis - GC-MS

Qualitative analyses were performed by manual injection of sample into the GC-MS system. This gas-chromatograph (Agilent 6890N coupled with mass spectrometer Agilent Technologies 5973 Inert) was equipped with an HP-5ms (30m x 250 μm x 0.25 μm) capillary column and the injection was made with a split ratio of 50:1 using He as carrier with a flow of 1 mL/min. The following temperature ramp was employed: hold at 45 °C for 7 minutes, ramp to 250°C at 5°C/min then held for 5 minutes.

3.1.3.2 Quantitative analysis

In order to analyse the composition of the outlet stream gas, the reaction system was equipped with an on-line gas chromatograph. The instrument was supplied with two different columns, both connected with a dedicated TCD detector. In particular the lighter products such as CO_2, ethylene, butadiene,1-butene, 2-butene, CH_4 and ethane were analysed using a PLOT-Q (30 m x 0.32 mm x 20 μm) column; while the heavier products (namely alcohols, aldehydes, esters and aromatics) were quantified using a DB-1701 (30 m x 0.53 mm x 1 μm) column. The analytical method was optimized with the aim of separate the components that could be produced in the reaction taking into account the total time needed for the analysis. With helium as carrier, the flow in the column was 1.4 mL/min in the HP-PLOT Q and 1.6 mL/min in the DB-1701 column. The temperature program of the method is depicted in Figure 2; in this way the total method lasted for 38.8 min.
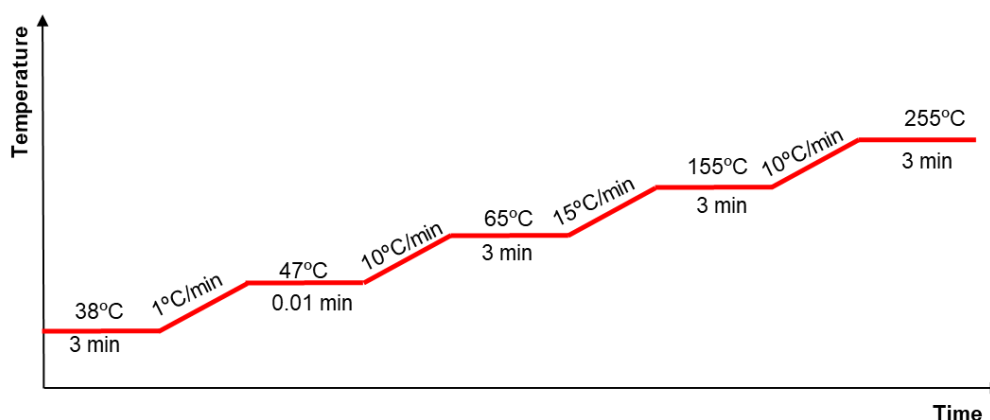
Figure 2   Temperature ramp of the on-line GC analysis.

After performing some catalytic tests, the calibration of the chemical compounds was expanded to some aromatic compounds and to higher aldehydes. Specifically, butyl-benzene, 1,2,4 trimethyl benzene, o-xylene, ethyl benzene, toluene, hexanal and decanal standards were used to perform the calibration, realized by feeding every liquid mixture of the standard compounds with the syringe pump into the empty reactor heated at 300°C. In this way, the vaporized compounds were analysed directly through the on-line gas chromatograph, simulating the reaction conditions.

After that, the quantification of the so-called "other products" was revised and calculated as follows: the products were gathered into three groups named "Light others", "Mid others" and "Heavy others" considering the retention times of the peaks obtained during the on-line analysis, specifically (Figure 3):

- Light others, C_4-C_6, (alkenes, alkenols, benzene, light ethers, ketones): from 0 to 15.6 minutes;
- Mid others, C_6-C_{10} (alkenes, alkenols, xylenes, styrene, methylated phenols, ketones; alkylated aromatics compounds): from 15.6 to 25,6 minutes;
- Heavy others, C_{10}-C_{16}, (alkenes, alkenols, alkylated aromatics compounds, alkylated phenols) from 25,7 till the end of the analysis.

LIGHT OTHERS   MID OTHERS   HEAVY OTHERS
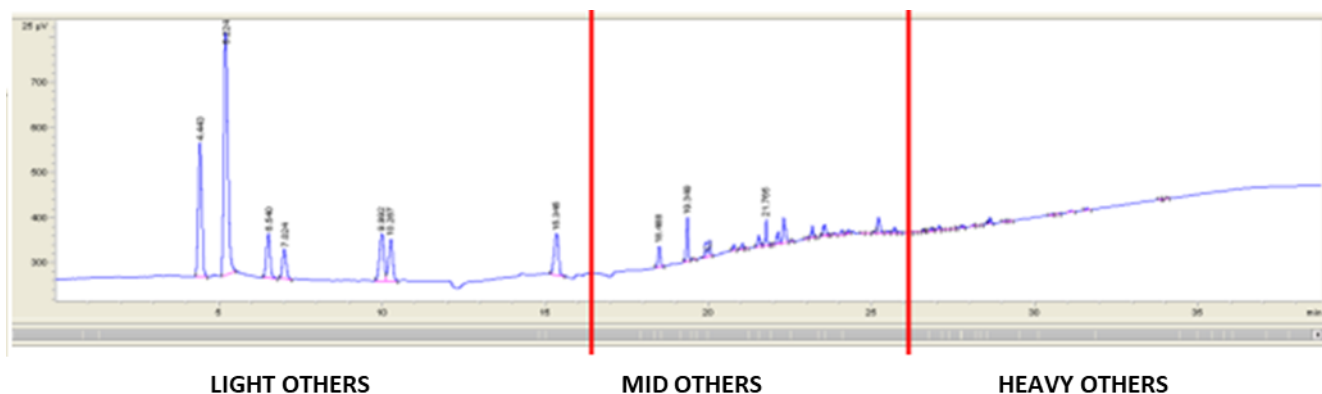
Figure 3   Example of a chromatogram obtained with the GC on-line while performing a reaction that brought to the production of a wide distribution of products.

The response factor of each groups was obtained by the arithmetic average of the ones known related to the calibrated compounds that are retained into the relative period, regardless the functional group of the molecules. The stoichiometric coefficient considered for each group was extrapolated from the ones known and detected through the GC-MS analysis. In this way the yields of the three groups of other products was calculated as follows:

$$Y_{LIGHT\ OTHERS}\% = \frac{6 \cdot mol_p^{out}}{C_{atom}^{EtOH} \cdot mol_{EtOH}^{in}} \times 100$$

$$Y_{MID\ OTHERS}\% = \frac{9 \cdot mol_p^{out}}{C_{atom}^{EtOH} \cdot mol_{EtOH}^{in}} \times 100$$

$$Y_{HEAVY\ OTHERS}\% = \frac{14 \cdot mol_p^{out}}{C_{atom}^{EtOH} \cdot mol_{EtOH}^{in}} \times 100$$

3.1.4 Catalysts Synthesis

The catalysts were characterized by means of powder X-ray diffraction (XRD) in order to check the crystallinity of the material. Some MP-AES analysis of the filtration waters were made in order to check the amount of metals exchanged during the catalyst synthesis; those analysis results were used to compute the amount of metal loading of the synthetized catalysts. Their specific surface area was determined by nitrogen physisorption using the BET equation. Moreover, the characterization of acid and basic sites of the catalytic surface was performed with TPD analysis using NH_3 and CO_2 as probe molecules for the determination of acid and basic sites respectively.

3.1.4.1 Hydroxyapatite (HAP)

A commercial Ca Hydroxyapatite (provided by Alfa Aesar, Calcium phosphate tribasic, 34-40% Ca) was selected for the preliminary catalytic investigations. The powder was calcined at 600°C in a muffle furnace under static air (10°C/min ramp until 600°C, and then kept for 2 hours). The calcined powder was pressurized with a manual hydraulic press and then crushed to a particle size of 20 to 40 mesh (841-400 μm) in order to be used in the quartz reactor of an inner diameter of 11 mm.

3.1.4.1.1 Ion-exchanged Ca-HAP

Calcium hydroxyapatite (Ca-HAP, $Ca_{10-x}(PO_4)_{6-x}(HPO_4)_x(OH)_{2-x}$), with $0 < x \leq 1$) crystallizes in the hexagonal system, space group P63/m, its structure comprises three-dimensional networks of hexagonally packed tetrahedral PO_4^{3-} ions. These ions make a first channel around Ca^{2+} ions [type 1 Ca] with a diameter of 2.5 Å. A second channel with a diameter of 3.5 Å, bordered by triangular Ca^{2+} ions [type 2 Ca], hosts the OH^- species along the c-axis. [152] This structure is flexible to both cationic and anionic substitutions, several cations can substitute calcium ions in either type1 and type 2 Ca positions or in both positions simultaneously. Similarly, several anions can replace either OH^- or PO_4^{3-} ions or both. [152,159] This intrinsic capability to exchange the Ca^{2+} ions and to allocate some other metal ions analogously to zeolites, allow to obtaining interesting functionalized materials with modulated number and strength of acid and basic sites.[152]

A commercial Ca Hydroxyapatite (Ca-HAP) (provided by Alfa Aesar, Calcium phosphate tribasic, 34-40% Ca) was modified by means of ion-exchange method.[233] By means of this post-synthetic method, it possible to introduce new ions into the HAP structure modifying its surface composition without alteration of the bulk properties.[234] In this way, the acid/base properties or dehydrogenation properties of the HAP surface can be modified. [235] In particular, samples of Fe, Cu and Sr-HAP were prepared following a synthesis method found in literature [236], after that they were characterized with different techniques and then tested in the gas-phase reaction system for the conversion of ethanol to higher analogues. All the exchanged hydroxyapatite catalysts are symbolized as Me-HAP samples.

3.1.4.1.1.1   Cu-HAP and Sr-HAP – Ion exchange

Both copper and strontium-modified HAP were prepared by conventional ion exchange (I.E.) procedure. [237] Regarding the Cu-HAP, its synthesis was performed as follows: 6 g of HAP powder was dried at 120°C overnight and then added to 250 mL of 0.02 M Cu(II) nitrate solution (Cu $(NO_3)_2 \cdot 3H_2O$, 99,5%, Carlo Erba) under vigorous magnetic stirring at 40°C for 20h. After filtration, thorough washing with 2L of hot water (40 °C) and drying at 120 °C for 16 h, a light-blue-green coloured sample was recovered. This sample was calcined at 600°C in a muffle furnace under static air (10°C/min ramp until 600°C, and then kept for 2 hours), obtaining a green-brown powder. The calcined powder was pressurized with a manual hydraulic press and then crushed to a particle size of 20 to 40 mesh (841-400 μm) in order to be used in the quartz reactor of an inner diameter of 11 mm.

The Sr-HAP was prepared by following the same procedure, using strontium (II) nitrate ($Sr(NO_3)_2$ anhydrous, Alfa Aesar) as metal precursor. In this case, both fresh and calcined samples consisted in white powders.

3.1.4.1.1.2   Fe-HAP – Flash Ion Exchange

The iron-loaded samples were prepared by a modified ion exchange procedure [237], in which very short contact time of HAP in the Fe-solution took place, in order to prevent morphological and structural damages to HAP . In a typical preparation, 250 mL of 0.02 M iron (III) nitrate ($Fe(NO_3)_3 \cdot 9H_2O$, VWR chemicals) solution was heated to 40 °C, then the pH was adjusted to ~3 by HNO_3 addition for preventing the precipitation of iron (III) hydroxide. HAP powder (~6 g, previously dried at 120 °C, overnight) was added to the iron solution and the suspension was maintained under stirring at 40 °C for 15 min. The sample was then filtered, thoroughly washed with 2 L of hot water (40°C) , dried at 120 °C overnight, obtaining a yellow powder. After that, the sample was finally calcined at

600 °C for 2 h in static air, becoming an orange-brown powder that was then pressurized with a manual hydraulic press and crushed to a particle size of 20 to 40 mesh (841-400 µm).

3.1.5 Catalysts characterization

The catalysts were characterized by means of powder X-ray diffraction (XRD) in order to check the crystallinity of the material. Some MP-AES analysis of the filtration waters were made in order to check the amount of metals exchanged during the catalyst synthesis; those analysis results were used to compute the amount of metal loading of the synthetized catalysts. Their specific surface area was determined by nitrogen physisorption using the BET equation. Moreover, the characterization of acid and basic sites of the catalytic surface was performed with TPD analysis using NH_3 and CO_2 as probe molecules for the determination of acid and basic sites respectively.

3.1.5.1 X-Ray spectroscopy (XRD)

X Rays Diffractometry (XRD) is one of the main techniques used to study the bulk properties of solid samples.

The most important features that can be determined with this technique are:

► Crystallinity of the solid;
► Crystallites dimensions;
► Phases;
► Atoms present in the structure and cell parameters.

A beam of X rays is directed to the solid sample, the incident radiation is diffracted in some specific direction which depends on the solid characteristics, in particular on the Bragg's law:

$$n\lambda = 2d\sin\theta$$

Where:

► n is a whole number,
► λ is the wavelength of the incident X rays,
► d is the interplanar distance within the crystal,
► θ is the angle of incidence.

The diffracted ray's intensity is plotted versus the diffraction angle.

The Bragg's law shows that each diffraction peak corresponds to a specific interplanar distance d; analysing this parameter is possible to identify the corresponding phase, comparing the obtained diffractogram with the JCPDS databank.

It is possible to calculate the average crystallites size (D, nm) of each phase with the following equation (Scherrer equation)[238].

$$D = \frac{B\lambda}{\beta(1/2)\cos\theta}$$

Where:

- ► B =0.9 (Scherrer constant);
- ► β1/2 = full width at half maximum (FWHM) in radians;
- ► θ is peak position, radians;
- ► λ is the wavelength of the incident X ray (nm); λ(CuKα) = 0.154nm.

The Scherrer equation relates the width of a powder diffraction peak to the average (by volume) dimensions of crystallites in a polycrystalline powder.

It is possible to correlate the crystallinity of a mineral with the related XRS pattern obtained. For the purpose of application, the crystallinity of a mineral could be simply represented by the crystallite size or equivalent to the FWHM of a typical reflection of XRD pattern concerned. In general, the bigger the crystal is, the better the crystallinity, and the sharper and more isolated the XRD reflections are. In recent years, many researchers have demonstrated this consideration of crystallinity in their publications—for example, broad XRD peak means low crystallinity [239], narrower XRD peak indicates an increase in the crystallinity [240], the appearances of narrow and different XRD peaks mark more crystalline [241], and the lower XRD peak indicated a lower degree of crystallinity[242].

The X-ray diffraction (XRD) analysis of the sample was carried out using a PANalytical X'Pert diffractometer equipped with a copper anode (λmean= 0.15418 nm) and a fast X'Celerator detector. Wide-angle diffractogram was collected over 2θ range from 5 to 80° with a step size of 0.05° and counting time 15s.

3.1.5.2 N₂ Adsorption/desorption isotherms (BET)

The catalyst's surface area is the ratio between the exposed surface and its mass; it is commonly expressed in **m²/g**.

Surface area is one of the most important parameters used to characterize a material from the catalytic point of view.

The surface area value is obtained measuring the quantity of physisorbed gas at a known temperature. The most common gas for this purpose is N_2; for that, physisorption is usually carried out at 77 K, which is the nitrogen boiling point. This process has several advantages:

► It occurs spontaneously;
► It has a low specificity, letting the gas occupy all the sample's surface without preferential sites;
► It is fast;
► It is reversible.

First of all, physisorbed products on the solid's surface are eliminated by increasing the temperature and place the sample under vacuum, after that the sample is submerged in a liquid nitrogen dewar to decrease the temperature to 77K. A nitrogen flow is provided by the instrument, starting its adsorption. The instrument measures the thermal conductivity difference between the initial gas and the one after the adsorption. Since nitrogen is adsorbed by the solid's surface, the final conductivity will decrease. At the end of the analysis, the instrument plots the adsorbed amount versus the relative pressure, giving an adsorption isotherm.

This technique is based on the BET model (due to Brunauer, Emmett, and Teller), an extension of the Langmuir method, the Langmuir assumptions are:

► The adsorption process has a kinetic behaviour;
► The adsorption rate is equal to the desorption rate;
► The heat of adsorption is constant and does not depend on the degree of coverage;
► Gas molecules behave ideally;
► Only a monolayer is formed;
► All surface sites are equivalent;
► There is no interaction between the adsorbate's molecules, and they can't move.

The BET model assumptions are:

► The surface is homogeneous;
► There are no lateral interactions between molecules;
► All the surface sites have the same adsorption energy for the adsorbate;
► Multilayers can be formed, and their adsorption energy is the same;
► The theory can be applied to all the layers.

The BET equation is:

$$\frac{P}{V(P_0 - P)} = \frac{1}{V_m C} + \frac{P(C-1)}{V_m C P_0}$$

Where:

► V=Total adsorbate volume

► Vm=Monolayer volume

► P=adsorbant pressure

► Po=adsorbant vapor pressure

► C= BET constant

This linear equation can be used to calculate the monolayer volume (Vm) by which is possible to calculate the sample specific surface area (S_{BET}):

$$S_{BET} = \frac{\frac{V_m}{V_0} * N_A * A_{N_2}}{g}$$

► V_0= Adsorbant molar volume

► N_A= Avogadro number

► A_{N2}= N_2 molecular cross-sectional area

► g= Mass of the sample

The specific surface area of the catalysts was determined by N_2 absorption–desorption at liquid N_2 temperature using a Sorpty 1750 Fison instrument. Around 0.2 g of the sample was typically used for the measurement, and the sample was outgassed at 150°C before N_2 absorption.

3.1.5.3 Temperature Programmed Desorption (TPD)

Temperature programmed desorption (TPD) technique allows one to study the interaction of reaction gases with solid surfaces, thereby being a powerful tool for both the evaluation of active sites on catalyst surfaces and the understanding of the mechanisms of catalytic reactions including adsorption, surface reaction and desorption. When ammonia and carbon oxide are used as probe molecules, the acidity and the basicity respectively of the materials are investigated.

The experiments were performed in an Autochem II (Micrometrics) instrument with catalyst in pellets (calcined) for the analysis of the acid/base properties of catalyst. The sample was placed in a quartz tubular reactor and pre-treated under 30 mL/min He flow to the calcination temperature (600°C) for 60 min, in order to remove adsorbed H_2O and CO_2 from the catalyst surface prior to adsorption. Then the catalyst was cooled down to 40°C and 100°C for CO_2-TPD and the NH_3-TPD analysis, respectively. NH_3 was adsorbed at 100°C to eliminate the contribution of very weak acid sites and improve the spectrum resolution. In this way, the catalyst surface was saturated with the probe molecule for 1 h (flow rate of 30 mL/min of 10 vol. % of CO_2 or NH_3 in He). Both physisorbed CO_2 and NH_3 were removed by flowing He (30 mL/min) for 60 min. Then, the sample was heated at 10°C/min up to 600°C and the desorbed probe molecules were monitored and recorded using TCD

detector and an online mass spectrometer (Cirrus 2, MKS instruments) which was calibrated by manual injections of pure CO_2 (m/z= 44) and NH_3 (m/z=17) pulses.

3.1.5.4 Thermogravimetric analysis (TGA)

Using a SDT Q 600 instrument, TG/DT analyses were performed over fresh and spent catalysts in order to identify the amount of heavy compounds absorbed on the catalyst surface. 20mg of the sample was typically used for the measurement and the temperature increased from room temperature up to 1000°C, with a heating rate of 10°C/min in air flow (100 mL/min).

3.1.5.5 MP-AES analysis

In order to evaluate the obtained metal loading of the hydroxyapatite-based catalyst prepared via ion exchange, the filtrate solution was analysed with MP-AES technique. In this way the amount of Fe^{2+}, Cu^{2+} or Sr^{2+} detected in the solution (measuring the absorbance at 325 nm, 372 nm and 431 nm, respectively) was used to calculate the actual metal loading obtained for the prepared catalyst. The analyses were made using a MP-AES instrument (Agilent 4210 MP-AES). After calibration with standard solutions, the concentration of the determined metal-ion of the filtrate waters was evaluated and then related to the amount of the metal deposited over the HAP support.

3.2 Catalytic gas-phase ethanol valorisation at ITQ- UPV

During the research period spent in the laboratory of "Instituto de Tecnologia Química" (ITQ) of the "Universitat Politecnica de Valencia" (UPV), the work focused on two main topics that can be gathered for the nature of the catalysts: i) zirconia based catalysts; and ii) natural sepiolite based catalysts. All the catalytic systems have been characterized by means of different techniques and tested in a lab-scale fixed bed gas-flow reactor to evaluate their activity in the gas-phase ethanol conversion. In the following section the characterization techniques and instruments used as well as the reactor and analysis systems used will be widely explained.

3.2.1   Materials used

Table 1. *Summary of the materials utilized to perform the experiments.*

Compound	MW (g/mol)	Supplier
$ZrO(NO_3)_2$ hydrate	231,22	Aldrich
$(NH_4)_2Ce(NO_3)_6 \cdot 6H_2O$	348,23	Aldrich
$Y(NO_3)_3 \cdot 6H_2O$	383,01	Aldrich
$TiOSO_4$ hydrate	159,93	Riedel-de Haen
$Cu(NO_3)_2 \cdot 2,5H_2O$	232,59	Aldrich
NaOH pellets	39,99	Merck
NH_4OH	25%w in H_2O	Aldrich
Urea	60,06	Aldrich
Absolute ethanol	46,07	Scharlab
Natural Sepiolite	-	Tolsa, S.A.
Na_2CO_3 (99.8%)	105,99	Aldrich
K_2CO_3 (99%)	138,21	Aldrich
Cs_2CO_3 (99%)	325,82	Aldrich
$Ni(NO_3)_2 \cdot 6H_2O$	290,79	Aldrich

3.2.2   Catalytic tests: general procedure

3.2.2.1 Reaction system

The catalytic tests were performed in gas phase continuous-flow quartz reactor, with a 330mm length and an internal and external diameter of 10 and 12 mm respectively, working at atmospheric pressure.

The inlet gas feed composition was maintained at 5 mol% EtOH in N_2 (95 mol %). The tests were conducted via vaporization of the liquid ethanol that was fed by means of a syringe pump into a stainless steel heated line to obtain an instant vaporization. That heated line had an inlet with the carrier gas (N_2) and was connected to the tubular quartz reactor containing the catalyst (with a particle dimension of 0,25-0,6 mm). The reactor was placed inside an oven and its inlet and outlet were covered with heating tapes equipped with an electrical resistance to regulate the inlet (160°C) and outlet (180°C) temperature, the same treatments was used for the connecting line between the reactor outlet and the on-line GC inlet valves (both at 180°C). Indeed, the outlet gas stream was analysed with an on-line Agilent 7890A gas-chromatograph. The latter was equipped with two columns a Rt-U-Bond (30 m x 530 um x 20 um) column and a HP-FFAP Polyethylene glycol (50 m x 320 um x 0,5 um) connected with two detectors, a TCD and a FID, respectively. Figure 1 represents the scheme of the reaction plant.
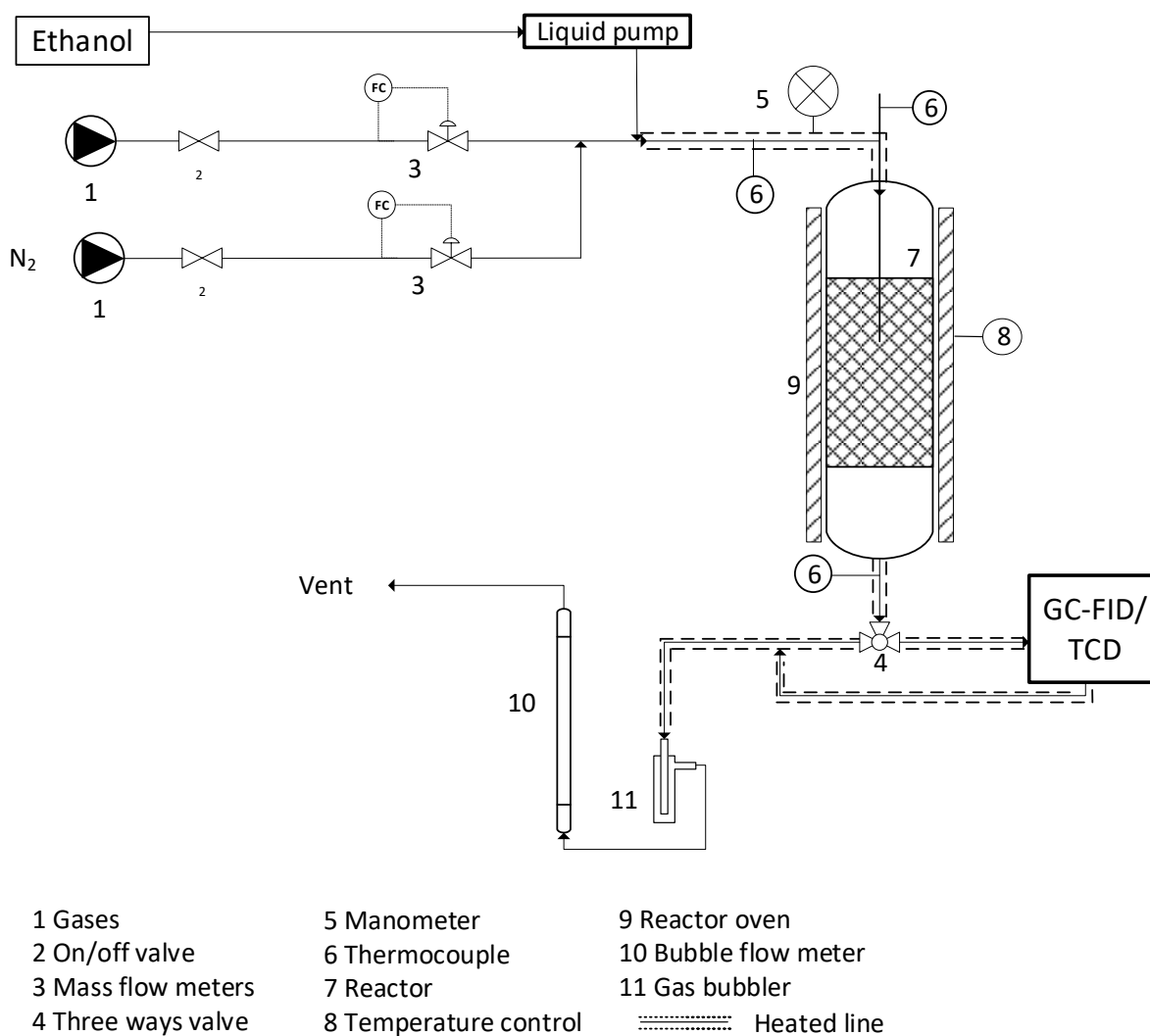
Figure 1   Plant scheme.

1 Gases	5 Manometer	9 Reactor oven
2 On/off valve	6 Thermocouple	10 Bubble flow meter
3 Mass flow meters	7 Reactor	11 Gas bubbler
4 Three ways valve	8 Temperature control	▭▭▭ Heated line

The main products that might derive from the reaction were calibrated. Some samples of the reaction products were analysed by means of a gas chromatograph coupled with a mass spectrometer (GC-MS), in order to identify unknown by-products.

3.2.3 Compounds analysis and quantification

In that section the analytical method used to identify and quantify the reaction products is described. The most common performance indicators (conversion, X; yields, Y and selectivity, S) have been calculated. The gaseous outflowing stream was analysed with an on-line GC system, while to identify some unknown outcoming products, an aliquot of gaseous stream was manually sampled with a gas-syringe and injected to a GC-MS system.

3.2.3.1 Quantitative analysis

The utilised gas-chromatograph is an Agilent 7890A GC System, equipped with two different columns, connected to a Thermal Conductivity Detector (TCD) and using He as carrier gas:

i) An Agilent 19091F-115, HP-FFAP Polyethylene glycol (50 m x 320 um x 0,5 um) column connected to a Flame Ionization Detector (FID) was used to quantify the volatile hydrocarbons and the oxygenated compounds such as acetaldehyde, ethyl ether, acetone, ethyl acetate, *n*-butanol, 2-pentanone, butyraldehyde and the higher alcohols, namely 2-ethyl butanol, hexanol, 2.ethyl hexanol and 1-octanol.

ii) For the separation and quantification of the light products (ethylene, ethane, CO_2, butadiene) an Agilent 19750 column, Rt-U-Bond (30 m x 530 um x 20 um), was used.
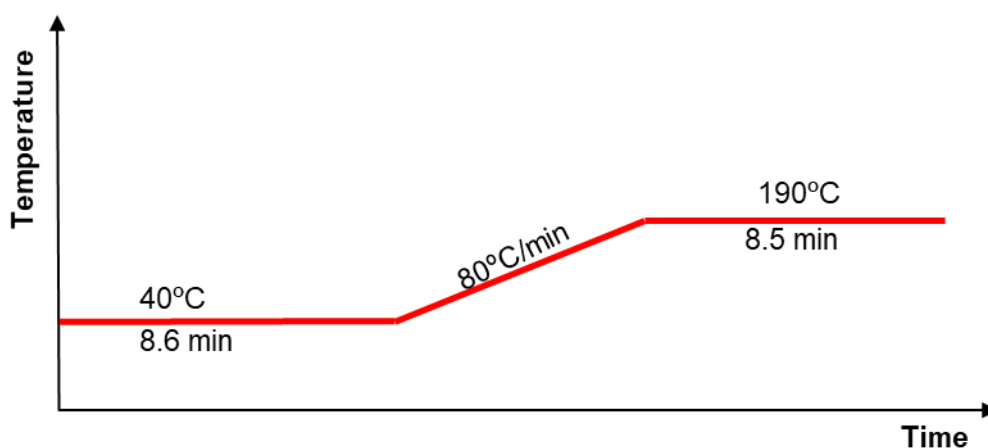
Figure 2   Temperature ramp of the on-line GC analysis.

The oven temperature was kept at 40 °C for 8,6 min, then the temperature was increased with an 80°C/min rate to 190°C and kept at this temperature for 8,5 min, reaching a total runtime of 18,975 min (Figure 2).FID was kept at 300°C with 450 mL/min air flow and 40 mL/min H2 flow. TCD was kept at 250°C with a reference flow of 22 mL/min and a He flow of 4,5 mL/min. FID works burning the molecules exiting from the column in a hydrogen/oxidant flame, the formed ions are collected and analysed giving a signal proportional to the analyte's quantity. TCD evaluates the thermal conductivity of the flow, since most of the compounds have a smaller thermal conductivity than the carrier gases (He or H). This difference will increase the temperature of a resistor, causing a change in resistance of that filament and a consequent change in voltage due to a Wheatstone bridge. That change in voltage is proportional to the analyte's concentration in the gas flow. This detector was used to quantify the same products of the FID, and the products that cannot be detected with FID such as N_2, CO, CO_2, ethylene and ethane.

In order to quantify ethanol conversion and the principal products yields and selectivity, the reagent and the obtained products have been calibrated by using standard compounds. Each product was calibrated measuring the area of the peak and plotting it versus its volumetric concentration. In this way, response factors of each component have been calculated. For each product, a response factor relative to ethanol was calculated by dividing the product's response factor by the ethanol one. In the following table, the quantified products, their relative response factors (Fij), and their retention time are indicated, specifying the detector utilised for the calibration.

Table 2. *Analytic parameters utilized in the reaction products quantification into the GC-online system.*

	Detector	Retention time [min]	Relative Response Factor to EtOH
EtOH	TCD	11,8	1,00
Acetaldehyde	FID	5,6	1,33
Ethyl ether	FID	5,1	1,33
Acetone	FID	6,8	3,33
Ethyl acetate	FID	8,7	6,67
n-Butanol	FID	14,0	6,67
Butadiene	TCD	11,3	1,13
Ethylene	TCD	2,9	1,00
CO_2	TCD	2,9	1,00
2-Pentanone	FID	10,75	6,67
Butyraldehyde	FID	8,75	3,33
2-ethyl butanol	FID	15,6	13,33
1-hexanol	FID	15.9	10,00
2-ethyl hexanol	FID	16.7	16,67
1-octanol	FID	17.3	16,67

The following formulas have been utilized for the main performance indicators calculation, such as conversion (X, %) of ethanol (j) and selectivity (S, %) of the main products (i).

➢ i= calibrated compound; j= EtOH;

➢ $C_i = x_i \left(\frac{mol_i}{mol_{TOT}} \times 100 \right)$;

➢ $Fi = \frac{Ai}{Ci}$; $Fij = \frac{Fi}{Fj}$;

➢ $X_{EtOH} = \frac{\Sigma \left(\frac{Ai}{Fij} \times \frac{wi}{wj} \right)}{\Sigma \left(\frac{Ai}{Fij} \times \frac{wi}{wj} \right) + AEtOH} \times 100$;

➢ $S_i = \frac{\frac{Ai}{Fij}}{\Sigma \left(\frac{Ai}{Fij} \times \frac{wi}{wj} \right)} \times 100$;

➢ w_i, w_j= stoichiometric coefficients.

Not all the reaction products have been identified and calibrated, the unidentified products, named "NID others" have been quantified by means of an artificial response factor calculated through mathematical average of the ones obtained from standards calibration. Considering their retention times into the obtained on-line chromatogram, an average stoichiometric coefficients of 4 has been considered. Given that these are approximate values it is possible that within experimental tests, they will be underestimated or overestimated but since they were generally secondary products, the intrinsic error was considered acceptable.

The contact time, W/F (in g_{CAT}/mL·s), and the weight hourly space velocity, WHSV (in g/(g_{CAT}·h)), that are defined as the ratio between the mass of the catalyst loaded in the reactor (g_{CAT}) and the total volumetric gas flow ($\dot{V}$, mL/min) and as the mass flow rate of ethanol ($\dot{m}$, g/h) divided by the weight of catalyst (g_{CAT}) respectively, were calculated with the following formulas:

$$W/F = \frac{w_{catalyst}}{\dot{V}_{total}} \times 60$$

$$WHSV = \frac{\dot{m}}{w_{catalyst}}$$

3.2.3.2 Qualitative analysis - GC-MS

Since several peaks have been detected during the GC analysis of the reaction mixture in all the reaction tests, a qualitative analysis of the outlet flow was planned. By the help of a gas-syringe, a sample of the gaseous products flow was taken from a rubber septum placed after the reaction zone and injected to a GC-MS for the analysis. GC-MS analysis couples two different techniques: gas chromatography (GC) firstly separates the compounds present in the mixture, subsequently, mass spectrometry (MS) ionizes and breaks the compounds, detecting them depending on the mass-to-charge ratio. The coupling of these two techniques allows to identify the molecules that have a similar retention time in gas chromatography and molecules with similar pattern at the mass spectrometry.

The utilized instrument was an Agilent 6890N GC System connected to a Mass Selective Detector 5973 Network. The GC was equipped with an Agilent 19091S-433 column, HP-5MS (5%Phenyl Methyl Siloxane) (30 m x 250 um x 0,25 um); the inlet was a Split-Splitless kept at 250°C, the carrier gas was He. During the elution time, the temperature was initially kept for 5 min at 50°C, then raised with a 3°C/min rate until reaching 80°C, 1 min of isotherm at this temperature completes the elution.

3.2.4 Catalysts Synthesis and Characterization

3.2.4.1 Zirconia catalysts synthesis

In order to evaluate the effect of the synthesis techniques on the catalyst properties, several zirconium oxide catalysts have been prepared with three different methods: hydrothermal[243], precipitation[244] and urea-precipitation. Several synthetic parameters have been studied:

- Synthetic method;
- Precipitating agent;
- pH of the synthesis;
- Dopant addition.

Y, Ti, and Ce have been selected as possible dopants for the zirconia catalyst. A certain amount of one of these elements has been added to the zirconyl nitrate water solution by using respectively: $Y(NO_3)_4$, $TiOSO_4$, and $(NH_4)_2Ce(NO_3)_6$. The metal precursors solution has been prepared in order to have a Zr:Dopant molar ratio of 95:5. Before performing the reaction, all the calcined samples have been shaped into 0,25-0,6 mm pellets.

3.2.4.1.1 Hydrothermal method

The hydrothermal method synthesis was performed as found in literature and was performed as follows. 20 mL of a 0.5M water solution of zirconyl nitrate has been prepared and hydrolysed with a basic solution. Two different precipitating agents have been used: 25% aqueous ammonia solution and 5M NaOH water solution. The precipitating agent has been added until reaching a certain pH value between 7 and 13, measured with a SevenMulti™ Mettler Toledo pH-meter. The obtained mixture has been placed into an ultrasonicator for 30 minutes, after that, 8 mL of absolute ethanol were added. The mixture has been placed into a Teflon-lined autoclave for the hydrothermal treatment in an oven at 175°C for 24 h. After, the mixture has been filtered under vacuum and abundantly washed with water and/or absolute ethanol. Finally, the obtained solid has been dried overnight at 100°C and calcined at 500°C for 3 h (2°C/min) in air.

3.2.4.1.2 . Precipitation method

A 0.5 M water solution of zirconyl nitrate has been prepared and hydrolysed with a basic solution. Two different precipitating agents have been used: 25% aqueous ammonia solution and 5M NaOH water solution. The precipitating agent has been added until reaching a certain pH value between 7

and 13, measured with a SevenMulti™ Mettler Toledo pH-meter and stirred at constant pH for 1 h. Finally, the obtained mixture was filtered under vacuum and abundantly washed with water and/or absolute ethanol, the solid has been dried overnight at 100°C and calcined at 500°C for 3 h (2°C/min) in air. The synthetic method used is the same as Corma et al[244].

3.2.4.1.3 Urea precipitation method

The samples have been prepared weighting 5g of zirconyl nitrate dihydrate and a 12,2g of urea to reach a $n_{UREA}/n_{METALS} = 10$. These components have been dissolved in 80 mL of milliq water. This solution have been heated in reflux condition (around 100°C) for 16 h or 88 h. After cooling at room temperature, the solution pH have been measured with a SevenMulti™ Mettler Toledo pH-meter, the mixture have been filtered under vacuum and abundantly washed with water. The obtained solid have been dried overnight at 100°C and calcined at 500°C for 3h (2°C/min) in air. Since the synthesis pH is given by the urea thermal hydrolisis, to obtain different pH values from the one obtained by temperature increasing, the pH has been raised before thermal hydrolisis using a 3 M NaOH water solution.

3.2.4.2 MgO synthesis

Magnesium oxide was synthetized by precipitation method [245]. The precipitation has been conducted at pH 5 with a NH_4OH 1.3 M solution, of a magnesium acetate $Mg(CH_3COO)_2 \cdot 4H_2O$ solution with an oxalic acid $C_2O_4H_2 \cdot 2H_2O$ solution, the magnesium oxalate $\beta\text{-}MgC_2O_4$ precipitate immediately. The solid obtained was filters, washed, and dried at 80°C overnight. Then, the obtained solid have been calcined at 700°C for 3 h with a 2°C/min ramp, obtaining the magnesium oxide MgO. The obtained MgO have been shaped into 0.25-0.6 mm pellets before testing into the reaction system.

3.2.4.3 Sepiolite catalysts preparation

Sepiolite catalysts were prepared starting from a sample of sepiolite natural (Sepiolite 11AS-13) provided by Tolsa, S.A.

The samples of sepiolite based catalysts were prepared using different synthetic methods: the ion-exchange capability of sepiolite was exploited in order to modify the sepiolite support, as well as active phase was added by incipient wetness impregnation or by wet impregnation.

All the sepiolite catalysts samples have been calcined at different temperature (500ºC or 700º). In general, the heating treatment have been performed by keeping the temperature for 3h with a

heating ramp of 2°C/min. Before performing the reaction, all the calcined samples have been shaped into 0.25-0.6 mm pellets.

3.2.4.3.1 Incipient wetness impregnation

The sepiolite supported catalysts were prepared by an impregnation procedure using an appropriate amount of aqueous metal hydroxide/carbonate solutions (incipient wetness method) after a previous measure of the mud point of the support. The required weight of the alkali-metal precursor was dissolved in the minimum amount of water to wet the dry sepiolite supports before a slurry is obtained. The aqueous solution was added to the support dropwise and the powdery solid was manually mixed in order to accomplish the maximum homogeneity. (Figure3)

Then, the solids were dried at 100ºC (16 h) and calcined in air at 500ºC for 3h with a heating ramp of 2ºC/min. The catalysts were pelletized and sieved into 0.25-0.6 mm pellets before testing into the reaction system.
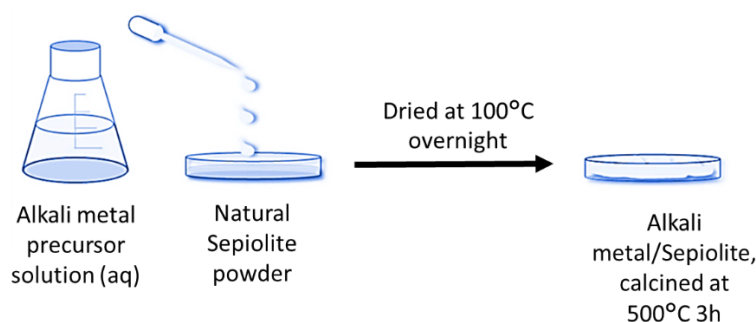
Figure 3   Incipient wetness impregnation catalyst synthesis.

In particular, the following catalysts have been synthetized:

- 2Na/Sep@500, 5Na/Sep@500, 2Na/Sep@700, 5Na/Sep@700, 0.5Na/5CuO/Sep@500;
- 2K/Sep@500, 5K/Sep@500,
- 2Cs/Sep@500, 4Cs/Sep@500, 7Cs/Sep@500, 14Cs/Sep@500.

The general symbols for the catalysts used was XMe/Sep@Y, where X was the number of the metal amount expressed as weight percent (wt %), Me the alkali metal concerned and Y the calcination temperature of the sepiolite support.

3.2.4.3.2 Wet impregnation

Copper was deposited over the sepiolite supports by wet impregnation. Copper nitrate $Cu(NO_3)_2 \cdot 2.5H_2O$ or nickel nitrate $Ni(NO_3)_2 \cdot 6H_2O$ have been used as metal precursor for the

preparation of the metal solution. The support was added to the metal solution and stirred for 2 hours in a rotavapor at 60°C without vacuum. After 2h the vacuum was added in order to remove the excess of water and then the sample was recovered and dried overnight at 100°C in furnace. The catalyst was calcined at 500°C for 5 h with a 2°C/min heating ramp. The resulting catalysts were all pelletized and sieved into 0.25-0.6 mm pellets before testing into the reaction system.

In particular, the following catalysts have been synthetized:

- CuO/MgO 5wt%, CuO/Sep@500 5 wt%, CuO/Sep@700 5 wt%, CuO/Sep@700 5 wt% CuO/Sep@500 10 wt%, CuO/2Na/Sep@500 5 wt%, CuO/2Na/Sep@500 10 wt%,
- NiO/2Na/Sep@500 5 wt%.

3.2.4.4 Powder X-ray diffraction patterns (XRD)

XRD analysis has been carried out at room temperature with a PANalytical X'Pert PRO equipped with a Cu Kα radiation and a X'Celerator detector in Bragg-Brentano operating at 40 keV and 30 mA.

In order to compare the phases obtained in the different zirconia samples synthetized, this characterization technique has been used to evaluate their tetragonal fraction (%t). It was calculated according to the so-called "Garvie Nicholson", used to estimate the monoclinic (m-ZrO_2) and the tetragonal (t-ZrO_2) phases content in a zirconia sample. [169,246,247] This technique uses the relation between the reflections intensities in the diffraction patterns of the ($\bar{1}11$) plane of m-ZrO_2 and the (101) plane of t-ZrO_2. Accordingly, the tetragonal fraction has been calculated applying the following equation[247]:

$$\%t = \frac{It(101)}{It(101) + 1.6\,Im(\bar{1}11)} \times 100$$

Samples Preparation:

XRD samples have been prepared grinding the solid to analyse in an agate mortar. The grinded solid has been placed into a steel sample holder and introduced into the diffractometer, which was equipped with an auto-sampler.

3.2.4.5 Raman

The Raman effect is one of the possible results of the interaction between light and matter. If the photon energy is not sufficiently high to give an electronic transition of the target molecule, it can be scattered in three different ways:

► Elastic scattering
► Inelastic scattering

In the first case, the photon energy after the interaction does not decrease, leading to a Rayleigh scattering. When inelastic scattering occurs, the photon can remove or increase the target molecule's energy. These types of inelastic interactions lead respectively to Stokes scattering and Anti-Stokes scattering. The energy gain in Stokes scattering is vibrational energy, when it is lost gives Anti-Stokes scattering. [248] The change in the radiation's energy is characteristic of the target molecule and independent on the incident radiation's energy. Raman spectroscopy is a non-destructive technique, which studies the inelastic scattering of the monochromatic radiation by the use of laser with a wavelength within visible, near IR or near UV regions. In particular, the molecular vibrations variation of the specimen's bonds is investigated to get structural information about the sample [249].

The Raman spectroscope is composed of:

► A sample holder;
► A laser light source;
► A collection optic for the scattered photons;
► A monochromator;
► A detector for the measurement of the Raman signals relative intensities, at different wavelengths;
► A computer.

The most interesting band section to analyse for the zirconium oxide is the one between 100-900 cm^{-1}. Since the XRD cannot let us distinguish the tetragonal from the cubic phase of zirconia, Raman spectroscopy has been used as a complementary technique. Raman spectra were obtained with a Renishaw 1000 In Via spectroscope, equipped with an Olympus microscope. The light source was a 20W Ar laser with a wavelength of 512 nm.

Sample Preparation:
The analysis has been carried out on grinded calcined catalyst samples.

3.2.4.6 Scanning Electron Microscopy (SEM) and energy-dispersive X-ray Spectroscopy (EDX)

Energy dispersive X-ray spectroscopy (EDS or EDX) is a standard method for identifying and quantifying elemental compositions in a very small sample of material (even a few cubic micro meters).[250] EDX spectroscopy, as well as the previously discussed X-Rays Diffraction, is a characterization technique which studies the X-Rays radiations obtained after the interaction between an electron beam with a specimen.[251,252] When the beams hits the sample, it can remove a core electron creating an electron hole. An electron of a higher level can fill the hole emitting a radiation in the X-Ray region, with a wavelength which depends on the energy difference between the higher and lower level of this electronic transition. Since each element of the periodic table presents a unique atomic structure, the obtained spectrum will be unique for each element. In Fig.4, a scheme of the used instrument is presented. The output of this kind of analysis is a graph in which on the x axis the energies of the emitted X-Rays are indicated, on the y axis the intensity revealed by the detector. Each peak formed can be attributed to a specific element, allowing to know the sample's composition. This procedure is called energy dispersive X-ray spectroscopy (EDS) and is useful for analysing the composition of the surface of a specimen.

Scanning electron microscopy (SEM) micrographs were collected in a JEOL 6300 microscope operating at 20 kV. The quantitative EDX analysis was performed using an Oxford LINK ISIS System with the SEMQUANT program. In this work, Energy Dispersive Spectroscopy was used to perform a semi-quantitative analysis of the elements.
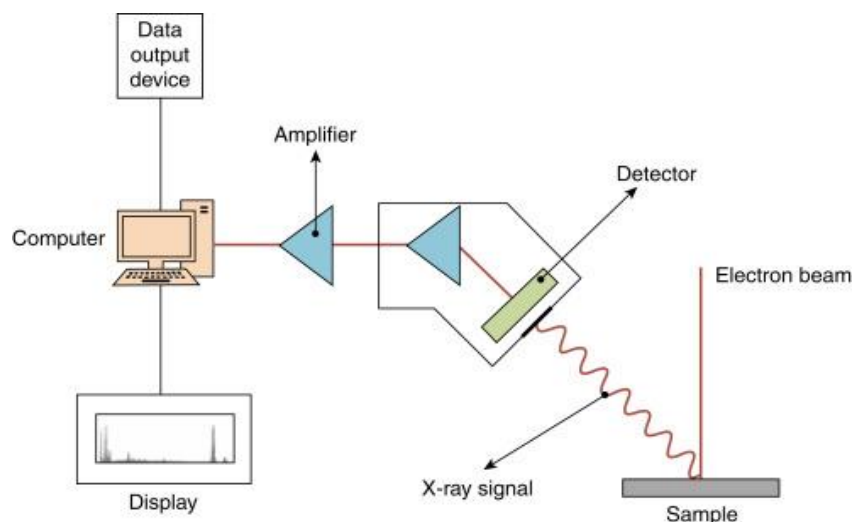

Figure 4   EDX Spectroscope scheme.[252]

3.2.4.7 N₂ Adsorption/desorption isotherms (BET)

Surface areas were obtained from N2 adsorption isotherms using the BET method; a Micromeritics ASAP 2000 instrument was used. Samples were degassed in situ under vacuum at a 250 °C temperature. Surface areas were calculated by the Brunauer–Emmett–Teller (BET) method and pore volumes were obtained by the Barrett–Joyner–Halenda (BJH) method.

3.2.4.8 Temperature Programmed Desorption (TPD)

The temperature-programmed desorption of ammonia (TPD-NH₃) experiments have been carried out as follows:

- ► Sample Pre-treatment;
- ► Ammonia pulse-adsorption;
- ► Physisorbed ammonia desorption;
- ► Chemisorbed ammonia desorption following a temperature profile.

The instrument used was a TPD/2900 apparatus from Micromeritics. 0,30 g of sample were pre-treated in an Ar stream at 350 °C for 1 h. Ammonia was chemisorbed by pulses at 100 °C until equilibrium was reached. Then, the sample was fluxed with a He stream for 15 min, prior to increasing the temperature up to 500 °C in a helium stream of 100 mL min^{-1} and using a heating rate of 10 °C min^{-1}. The NH₃ desorption was monitored with a thermal conductivity detector (TCD) and a mass-spectrometer following the characteristic mass of ammonia at 15 a.m.u.

Temperature programmed desorption of CO_2 (TPD-CO_2) experiments were performed in an Autochem II (Micrometrics) instrument with catalyst in pellets (calcined) for the analysis of the base properties of catalyst. The sample was placed in a quartz tubular reactor and pre-treated under 30 mL/min He flow to the calcination temperature (500°C) for 60 min, in order to remove adsorbed H_2O and CO_2 from the catalyst surface prior to adsorption. Then the catalyst was cooled down to 40°C and the catalyst surface was saturated with the probe molecule for 1 h (flow rate of 30 mL/min of 10 v/v % of CO_2 He). Physisorbed CO_2 was removed by flowing He (30 mL/min) for 60 min. Then, the sample was heated at 10°C/min up to 500°C and the desorbed probe molecules were monitored and recorded using TCD detector.

3.2.4.9 Thermogravimetric analysis (TGA)

TGA allows to measure the weight losses that occurs during a pre-set thermic profile in a controlled atmosphere. This parameter can be extremely useful to choose the right calcination conditions. TGA

is usually coupled with DSC (Differential Scanning Calorimetry), which measures the heat flow during the thermic profile. The sample is usually loaded in an inert pot which is placed in a balance, another identical empty inert pot is placed in another balance as a reference. During the analysis, the instrument keeps the sample's temperature equal to the reference one. When a phase transition occurs, that can be exothermic or endothermic, the sample requires respectively a heat removal or a heat addition to keep the same temperature as the reference. DSC measures the energy needed to keep the sample and the reference at the same temperature. Combining the TGA and DSC results it is possible to predict which phase transformation occurred at a specific temperature value. The instrument used for the analysis was a NETZSCH STA 449 F3 Jupiter® that permits the simultaneous measurement of weight changes and thermal effects. The samples have been analysed with the same program. They have been heated up to 800°C starting from room temperature, with a 10°C/min ramp. For both the catalyst spent and the solid precursors, the selected atmosphere were air.

<u>Sample Preparation</u>

TGA/DTA samples do not need a complex preparation, the powder of the precursor's or the spent catalyst pellets have been analysed without any previous treatment.

The thermogravimetric (TG) and differential thermal analysis (DTA) curves for the samples were simultaneously recorded in air at a heating rate 10 K min^{-1} using a Setaram (Labsys SETSYS-1780) instrument.

3.2.4.10   *Diffuse reflectance UV-visible spectroscopy (DRS-UV-vis)*

UV–vis spectroscopic characterization of solid catalysts can provide information on the catalyst's oxidation state and coordination in metals and metal oxides, band gap in semiconductors, particle size and shape and surface adsorption in metal nanoparticles via surface plasmon resonance, among others. [253] Analysis made via diffuse reflectance (DRS-UV-vis), which is a surface analytical technique, are particularly convenient because they do not require sample preparation. [253] Hence, it uses photons as a probing medium (i.e. light, varying in wavelength from the near-UV through the visible to the IR region) that interact with strongly absorbing materials (e.g., metals, alloys, semiconductors, etc) in the first 10–20 nm of the sample surface.[254] If the material has electronic energy levels that are separated by an energy in the visible region, then it may absorb some of light energy to move electrons from the filled energy level (valence band) into this empty level (conduction band). The information obtained by DR spectroscopy is related to the energies which valence (or conduction) electrons absorb from interaction with photon. The relative optical spectra result from electron transitions between broad, outer electron bands, resulting in peaks broader than the ones that can be obtained from other tecniques such as X-ray Fluorescence (XRF). [254] This technique can be used to study the local environment and oxidation state of transition metals. [255] Diffuse reflectance

spectra in the UV-visible region were collected with a Shimadzu UV-2010 PC spectrophotometer equipped with a reflectance attachment.

4 RESULTS AND DISCUSSION

4.1 The continuous-flow upgrading of ethanol to bio-fuel mixtures- UNIBO

The first part of my PhD period has been accomplished into the laboratories of the Department of Industrial Chemistry "Toso Montanari", of the University of Bologna. The topic of the whole research has been the valorisation of ethanol through its gas-phase conversion over heterogeneous catalysts into added value products. The heterogeneous catalysts object of this first part of the thesis have been hydroxyapatite-based materials.

As extensively discussed in the introduction sections (Chapter 1.2.1.1) the conversion of EtOH to *n*-butanol is better known as Guerbet reaction. The reaction pathway through which it takes place is still a matter of debate and different results have been obtained over materials of different nature. Nevertheless, the most accepted mechanism rely on the aldol condensation of the dehydrogenation product of the alcohol reagent and subsequent hydrogenation of the condensed products. Accordingly, the resulting higher alcohol can undergo the same mechanism and yield longer chains alcohols, both linear and branched. As a result, by optimizing the reaction conditions it could be possible to obtain a longer chain organic mixture that, after undergoing the appropriate treatments, has comparable characteristics with the ones of gasoline (C_4-C_{10}) [256] or even jet-fuel (C_9-C_{16})[257]. In order to catalyse this complex reaction mechanism, the presence of both acid/basic and redox sites on the surface of the catalyst is mandatory. Among the multifunctional materials studied, hydroxyapatite has been widely used due to its good performances obtained by several authors. [59,69,258,259]

In this work, a commercial CaHAP has been employed and then modified by ion-exchange (as explained in Section X) to study the ethanol gas-phase conversion through the Guerbet route while trying to favouring consecutive condensation reactions and obtaining longer carbon chain hydrocarbons.

4.1.1 Catalysts characterization

4.1.1.1 Thermogravimetric analyses (TGA)

The results of the TGA analysis performed over the pellets of calcium hydroxyapatite are depicted in Figure 1. The two weight losses that can be noticed in the analysis carried out over the fresh sample (Figure 1A) are related to the dehydration of the hydroxyapatite, that is a gradual process. Indeed, as found in literature [260,261], hydroxyapatite has two types of water in its structure: adsorbed

and lattice water. Adsorbed water is lost in a reversible manner from 25 to 200°C. Lattice water is irreversibly lost at the temperature from 200°C to 400°C, which causes a contraction in *a*-lattice dimension during heating. At higher temperature (~800°C) the hydroxyapatite gradually dehydrates loosing OH$^-$ ions and then, around 1000-1360ºC transforms to OHAP (oxyhydroxyapatite, where a bivalent oxygen ion and a vacancy substitute two monovalent OH$^-$, $Ca_{10}(PO_4)_6(OH)_{2-x}O_x\square_x$, where $\square$ stands for the vacancy).
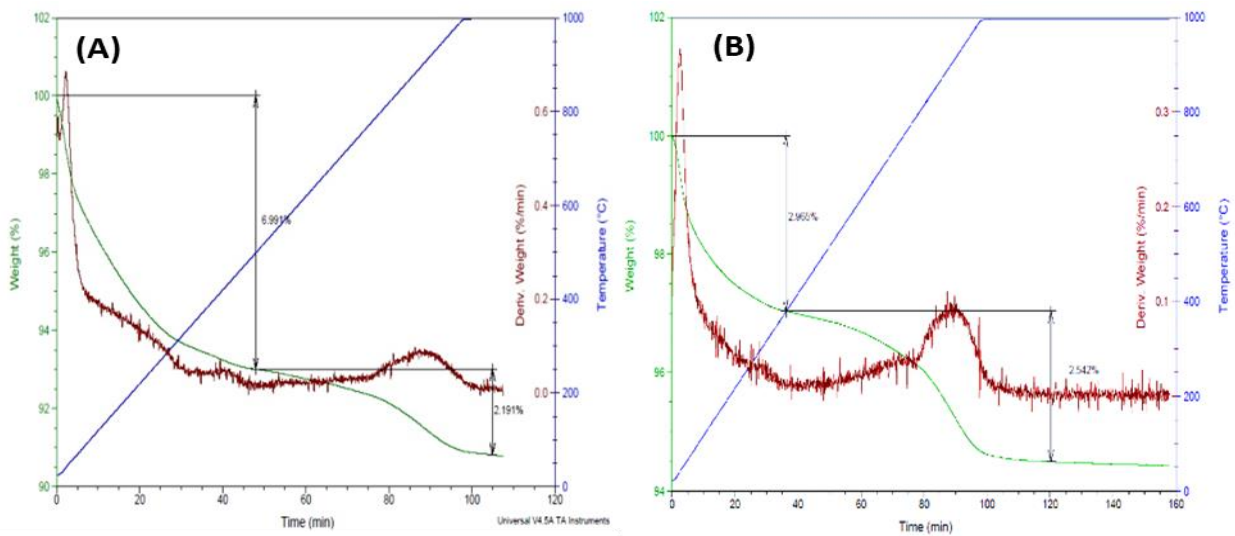
Figure 1   TGA results heating commercial Ca hydroxyapatite from room temperature until 1000°C. A) Fresh Ca-HAP B) Ca-HAP calcined at 600ºC.

Figure 1B shows the TGA results obtained heating the calcined Ca HAP pellets. Since this sample has been already treated with heat at 600°C for 2 hours, the first weight lost (2.97%) is smaller than the one obtained treating the fresh one (6.9%), because even if it should have lost all the adsorbed water, a bit of it has been re-adsorbed during storage. This suggests that calcined samples should be stored in desiccator.

4.1.1.2 X-ray diffraction analyses (XRD)

4.1.1.2.1 Ca-HAP
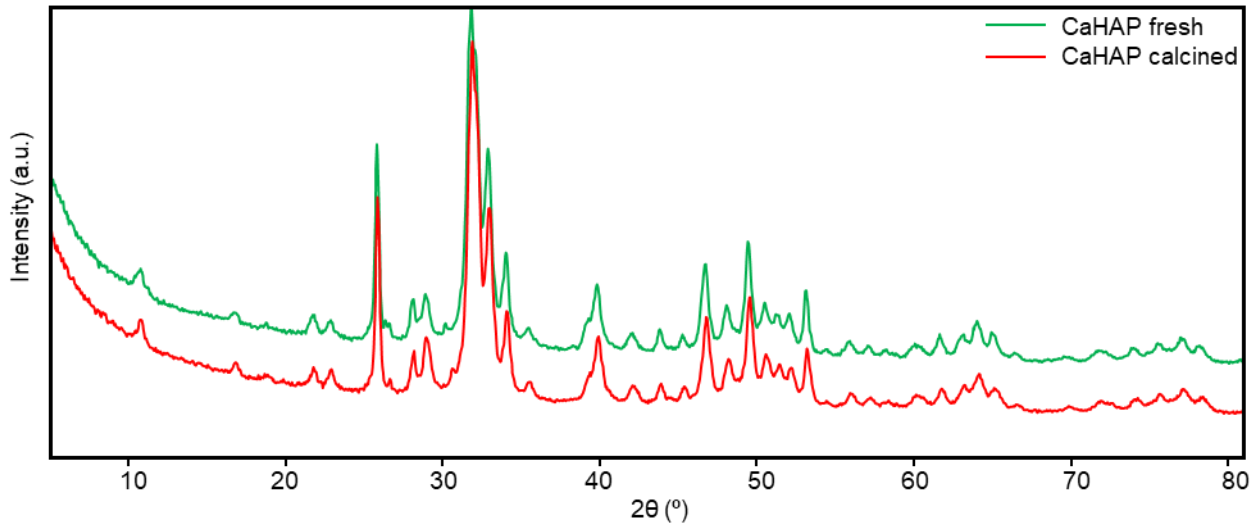
Figure 2   XRD patterns of Ca HAP fresh and calcined.

Figure 2 shows the powder diffraction pattern for Ca HAP fresh (green) and calcined at 600°C for 2 hours (red) .The diffraction peaks of the samples of Ca HAP match with the XRD standard reference of the synthetic hydroxyapatite – HAP, ICDD#24-0033. This confirms that calcination did not altered the molecular structure of the HAP sample.

4.1.1.2.2 Ion-exchanged HAP
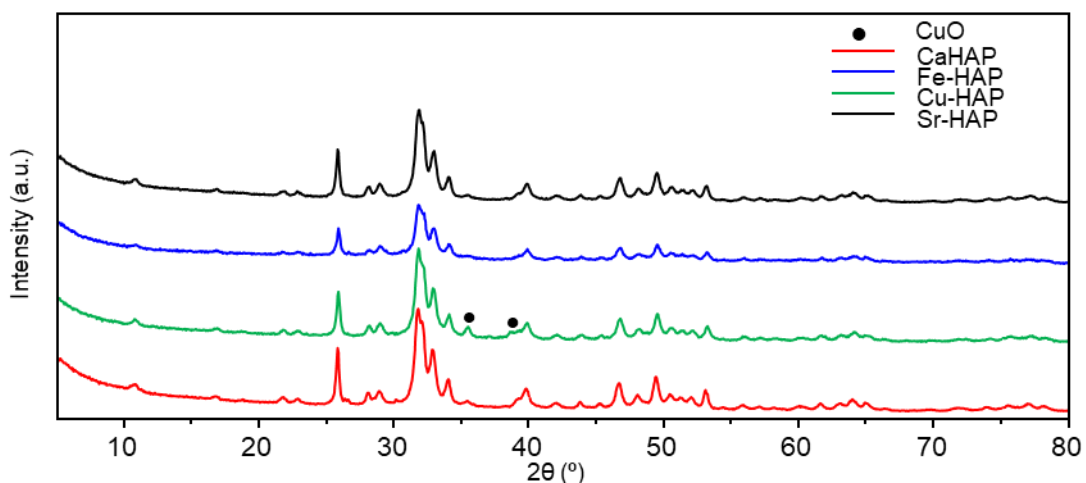
Figure 3   XRD patterns of ion-exchanged HAP samples.

Figure 3 depicts the XRD patterns of the Me-HAP exchanged samples, prepared as explained in Section 3.1.4. All Me-HAP exchanged samples, excepting for the Cu-HAP, showed XRD patterns

analogous to the structure of the commercial Ca-HAP without any additional peaks that could be related to the presence of other, segregated, phases. These results lead to the considerations that the metal ions substituted the calcium ones in the exchange positions of HAP (type 1 and type 2 Ca ions) [236]. The iron-exchanged hydroxyapatite (blue line) showed a slight decrease of crystallinity with shorter diffraction peaks.

Regarding the diffraction patterns of Cu-HAP, some additional peaks related to the formation of CuO aggregates were detected, so in this case not all the copper, calculated by means of MP-AES, is present in the HAP structure by ion-exchange but also segregated as oxide on the external surface of the material.

4.1.1.3 Bet, specific surface area

In Table 1 are summarized the results obtained with the BET area measurements. No changes in surface area after calcination nor palletisation were detected in the Ca-HAP.

In addition, after the ion-exchange process both Cu-HAP and Sr-HAP resulted with a lower specific superficial area, compared to the pristine Ca-HAP, while the Fe-HAP sample showed a slightly higher area. This increase of specific area can be related to dissolution-precipitation of HAP due to the pH of the solution during catalyst preparation.[262] This data is in accordance with XRD results showing a decrease of crystallinity of the hydroxyapatite after ion- exchanging with iron.

Table 1. *BET area measurement results.*

	A sup [m^2/g]
Ca HAP commercial, calcined	63
Ca-HAP (20-40), calcined	65
Ca HAP pellets (20-40), calcined	63
Fe-HAP 4 wt% (20-40), calcined	73
Cu-HAP 5 wt% (20-40), calcined	45
Sr-HAP 1.6 wt% (20-40), calcined	40

4.1.1.4 Temperature-programmed desorption (TPD)

Temperature programmed desorption of ammonia (TPD-NH_3) and carbon dioxide (TPD-CO_2) experiments were performed to explore the surface acidity and basicity of the samples, respectively (Fig. 4 and Table 2). The NH_3-TPD profiles and amount of NH_3 desorbed from the catalysts can be considered as the acid strength distribution and the number of acid sites on the catalyst, including both the Brønsted and Lewis acid sites, respectively.[263] Generally, according to the acidic strength determined using the temperature of NH_3 desorption, the solid acid sites can be classified into three types: weak (150–300 °C), moderate (300–450°C) and strong (450–650 °C) acid sites. [137] Similarly, the weak strength basic sites are related to curves that shows a maximum at temperature lower than 170ºC, the ones between 170 and 270ºC are assigned to medium strength basic sites, and finally,

the ones above 270ºC are strong basic sites.[99] Recorded spectra may be further deconvoluted by a Gaussian peak fitting method into separate peaks to be then attributed to different strength acid sites.

It is well known the bi-functionality of hydroxyapatite having both acid and basic sites in a single-crystal lattice (with the ability to promote dehydration and dehydrogenation reactions of ethanol in this specific case). [264] According to E. G. Rodrigues et al. [265] stoichiometric hydroxyapatite presents 2 types of basic sites and one of acidic site. With the temperature programmed desorption (TPD) of carbon dioxide CO_2 (red line, Figure 4A) it was possible to detect a higher concentration of weak basic sites for the Ca-HAP, corresponding to the desorption at 180°C and a second smaller peak at 260°C of medium strength basic sites. It can been noted a third small desorption peak at higher temperature (around 500ºC) that can be attributed to lattice OH^- groups in the apatite structure, indeed the CO_2 evolved at higher temperatures can predominantly be linked to the reaction of CO_2 with basic OH^- groups ($CO_2 + 2OH^- \rightarrow CO_3^{2-} + H_2O$). [265,266] In the NH_3 desorption profile (red line, Figure 4B) only a single peak centred at 200°C can be noted related to the presence of well-defined Lewis acid sites according to E. G. Rodrigues et al. [265]
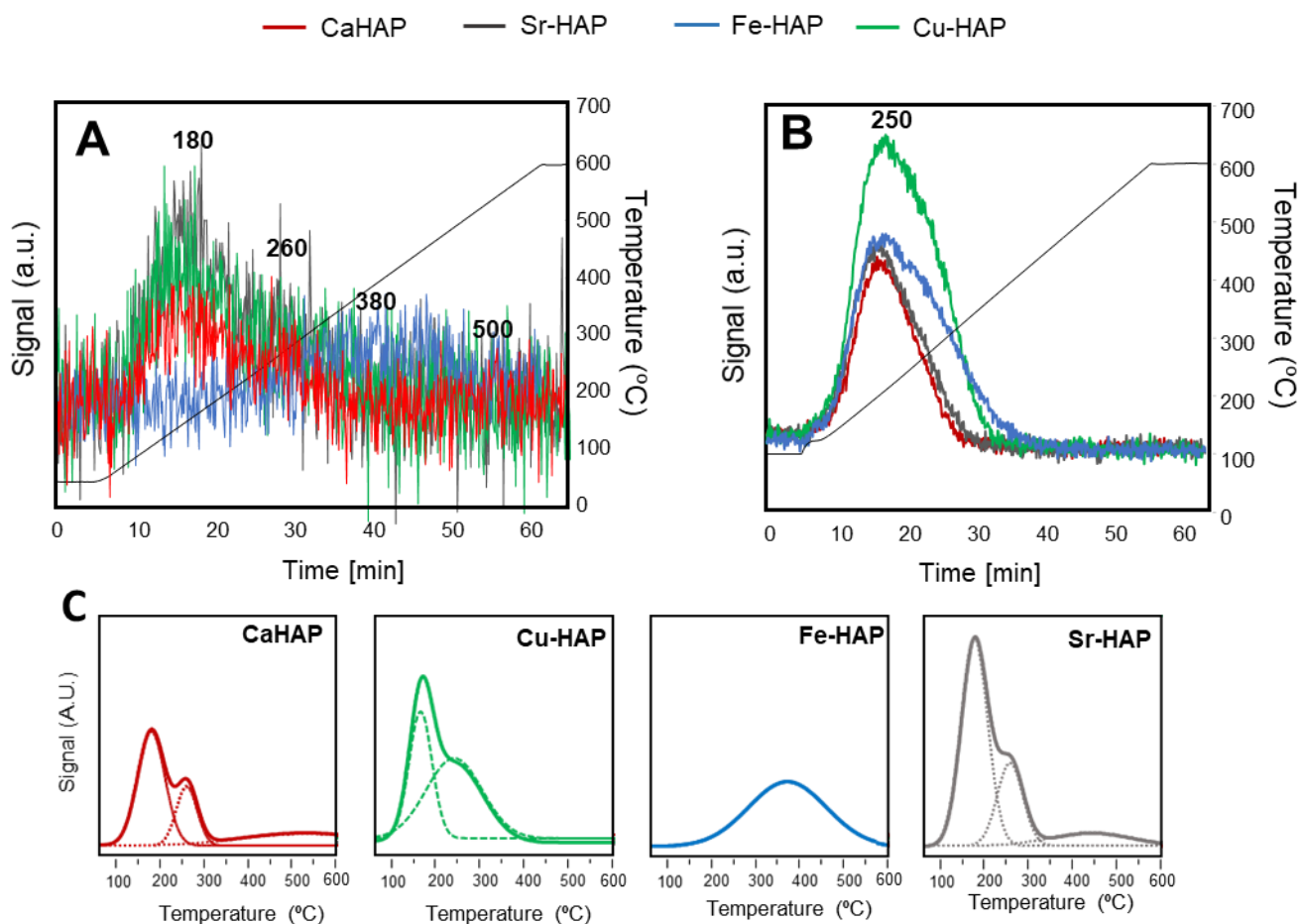

Figure 4   TPD profiles of the hydroxyapatite catalysts. Profile of the signals expressed as [µmol$_{PROBEMOLECULE}$/m$_2$]. (A): TPD-CO_2; (B): TPD-NH_3; (C): TPD-CO_2 deconvoluted.

The ion exchange modification of Ca-HAP led to some modifications of its acidic and basic characteristics. Table 2 summarizes the results obtained from the temperature programmed desorption analysis in terms of the amount of ammonia or carbon dioxide adsorbed (µmol NH_3/g cat or µmol CO_2/g cat). In general, the exchange of Ca ions with the Fe or Cu ones led to the formation of new acid sites leading to a higher adsorption of the probe molecule NH_3, those results are in accordance with literature [237]. According to Silvester et al.[266], the exchange between Ca^{2+} ions with the strontium ones led to a decrease of acidity, but from the analysis performed over the Sr-HAP sample, a slight increase of the acidity even in this case has been observed.

On the other hand, the TPD-CO_2 analyses showed that the exchange of Ca ions with other ions didn't lead to remarkable effects on the overall basicity of the material, in general quite low, as it can be observed in Table 4. The only exception that can be noticed is related to the Fe-exchanged HAP where a slight decrease of the adsorbed CO_2 from 17 to 11 µmol /g_{CAT} has been observed together with a desorption peak at higher temperature (380ºC), showing the formation of a small amount of stronger basic sites (Figure 4A, and deconvoluted Fig,4C). Overall, considering the changes in the acidic and basic properties of the materials, the exchange with a transition metals (i.e. Fe or Cu) led to a general increase of the acidity/basicity ratio of the catalyst surface. In contrast, the Sr-HAP sample presented a lower value of that ratio (i.e., 9,4 instead of 13,7), showing an indirect growth of the basic properties of the material over the acidic ones, in accordance with literature. [266]

Table 2. *TPD- NH_3 and TPD- CO_2 results.*

	S_{BET}	Acidity		Basicity		Acidity/Basicity ratio
	[m^2/g]	[$µmol_{NH3}$/g_{CAT}]	[$µmol_{NH3}$/m^2]	[$µmol_{CO2}$/g_{CAT}]	[$µmolCO_2$/m^2]	(A/B ratio)
Ca HAP	63	262	4.1	17	0.3	13.7
Fe HAP 4 wt%	73	483	6.6	11	0.2	33.0
Cu HAP 5 wt%	45	371	8.3	22	0.5	16.6
Sr HAP 1.6 wt%	40	189	4.7	22	0.5	9.4

4.1.1.5 MP – AES analysis

Cu, Fe and Sr loading was checked by measuring the relative absorbance of the filtrate waters to compute the residual metal concentration. In this way it has been possible to relate those data with the effective metal loading of the catalyst: Cu HAP ca. 5 wt%, Fe HAP ca. 4wt% and Sr HAP ca. 1.6 wt%.

4.1.2 Catalytic tests

The commercial Ca HAP was used as benchmark catalyst for the preliminary catalytic investigations. At the beginning, the effect of the reaction temperature was studied in condition of constant feed flow. To do so, many reaction parameters like the catalyst volume, the feed flow, the pressure and the reactants composition were kept constant. By keeping the feed flow constant using the same amount of catalyst, the contact time (calculated as V_{CAT}/F_{TOT}, mL/(mL/s)) varied in the reactions made at different reaction temperature between 0.35 and 0.23 seconds; while the so-called pseudo contact time (pseudo τ, W/F), calculated as the weight of catalyst divided by the total volumetric flow of the gaseous mixture at room temperature, was kept constant. For this reason, at a later time also the effect of the contact time was studied at 450°C by keeping all the other parameters (EtOH concentration, temperature and pressure) unvaried.

A typical reaction was performed as follows: the reactor charged with the catalyst was pre-heated at 100°C, at this temperature the vaporized ethanol was fed and analysed with the on-line GC in order to evaluate the exact starting concentration of the reagent. After that, the temperature of the furnace was set to the desired temperature and when was reached, the reaction started. For each reaction, fresh new catalyst was loaded inside the reactor.

Several blank tests were performed by feeding ethanol into the reactor, in the absence of the catalytic bed, in the range of the desired temperatures (300 - 600 °C). Ethanol conversion was negligible until 600°C, at this temperature ethanol conversion was around 10% with the concomitant formation of acetaldehyde.

4.1.2.1 Ca-HAP – Reaction temperature effect

The study of the temperature effect was performed maintaining the W/F around 0.5 g/mL·s by feeding the 5 %v/v EtOH/He gaseous mixture at a constant flow of around 60 ml/min throughout the reactor charged with 0.5 g of fresh catalyst. In this way the contact time was altered by the effect of the reaction temperature ranging from 0.35 s for the lowest T of 300°C to 0.23 s at 600°C.

4.1.2.1.1 Effect of reaction temperature over selectivity of products as function of the time on stream (ToN)

The effect of the reaction temperature was investigated in the range 300-600°C. The obtained results are summarised from Figure 5 to Figure 12. In particular, ethanol conversion, the carbon balance (reported as the sum of the yields of quantified products divided for the ethanol conversion, ΣY/X) and the selectivity of the main products are reported referred to the time on stream (ToN, h). In order to better summarize the results, the selectivity of the products were gathered as follows: C_4 (olefins):

butadiene, 1-butene, 2-butene-cis and 2-butene-trans; C_2-C_3: ethylene, ethane, propylene and propane; C_1: methane and carbon dioxide; C_4 aldehydes: butyraldehyde and crotonaldehyde; Guerbet alcohols: hexanol, 2-ethyl-butanol, octanol, 2-ethyl-esanol, decanol. On the other hand, the selectivity of both *n*-butanol and acetaldehyde have been directly reported on the graphs. As the reaction temperature increased, the same did the complexity of the composition of the out stream mixture in terms of amount of formed reaction products. These products were identified through GC-MS qualitative analysis, observing the formation of aldehydes (C_4-C_9), ketones (C_4-C_9), alkyl substituted aromatic compounds (C_7-C_{10}) and some alkenes. Those compounds were quantified using an artificial response factor evaluated from the available commercial samples and are gathered in the graphs as "others". Figure 12 depicts the catalytic results obtained at 300ºC.
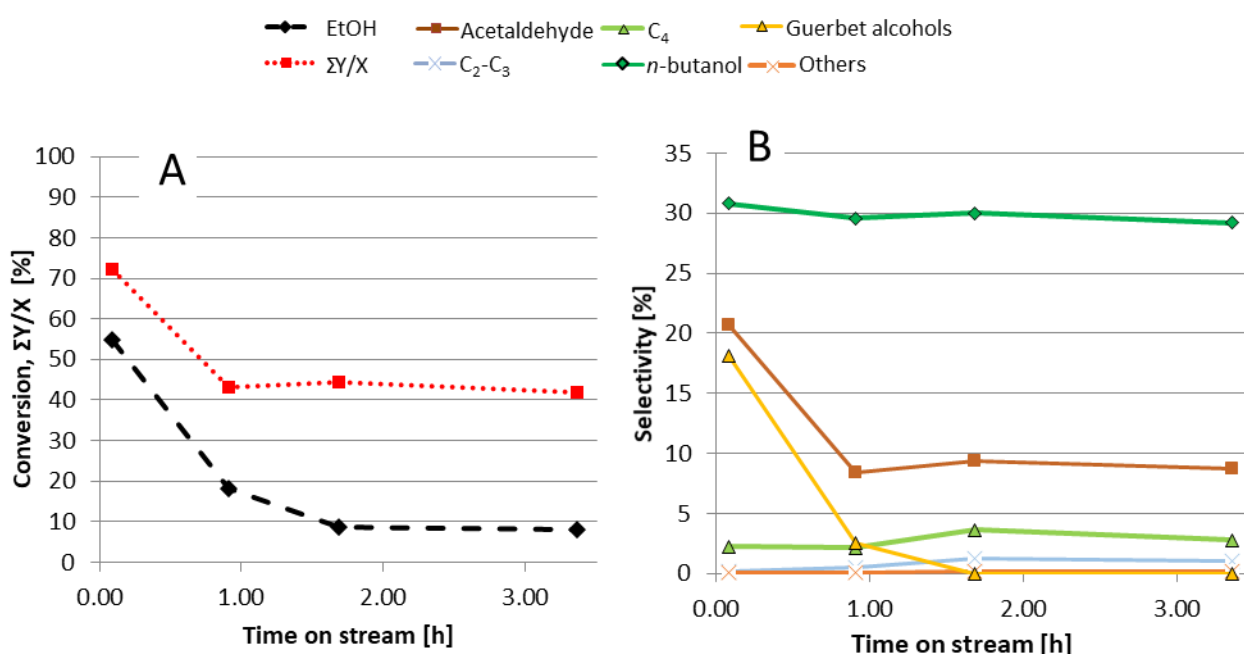
Figure 5   Catalytic results obtained in the Ethanol conversion over Ca HAP. Reaction conditions: EtOH 5% v/v in He, T= **300°**C, P= 1 atm, τ= 0.35 s. A) Ethanol conversion and carbon balance ΣY/X as a function of the time on stream. B) Products selectivity as a function of the time on stream.

At 300°C, after an initial value of around 55%, since 90 minutes of reaction the conversion decreased to 10% remaining stable with the time on stream. The main products obtained in those conditions are related to ethanol dehydrogenation (acetaldehyde) and to the Guerbet reaction namely *n*-butanol and higher alcohols (hexanol, 2-ethyl-butanol, octanol, 2-ethyl-esanol, decanol), grouped in the graphs as "Guerbet alcohols". In particular, the selectivity of *n*-butanol is predominant. Indeed, its selectivity at 300°C was around 30% and constant for all the time on stream investigated while the carbon balance decreased to a low steady value of around 40% with the time on stream. This deficit in carbon balance needs further investigation since couldn't be explained with carbonaceous deposition investigated with TGA analysis (see section 4.1.1.1).
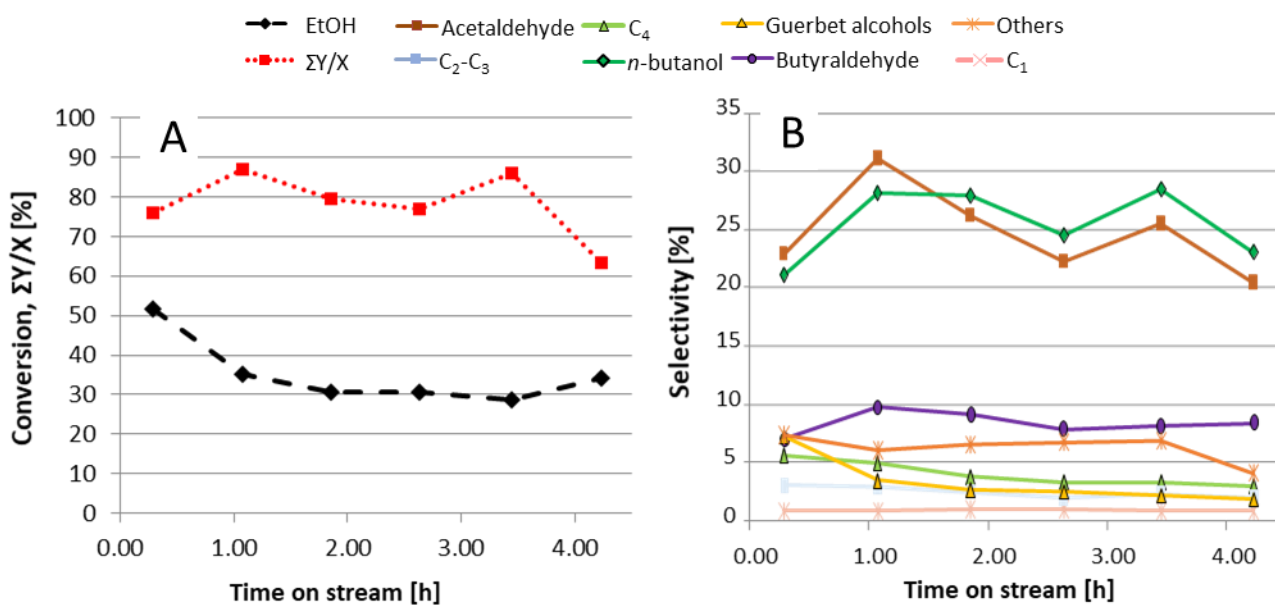
Figure 6 Catalytic results obtained in the Ethanol conversion over Ca HAP. Reaction conditions: EtOH 5% v/v in He, T= 400°C, P= 1 atm, τ= 0.30 s. A) Ethanol conversion and carbon balance ΣY/X as a function of the time on stream. B) Products selectivity as a function of the time on stream.

At 400°C (Figure 13) ethanol conversion reach the stationary state at around 30% after 1 hour of time of stream. Interestingly, both the conversion and the carbon balance seemed to reach a steady value of 30% and 80%, respectively. Even in this case, the main products were still acetaldehyde and *n*-butanol, of which the selectivity profiles showed a similar trend over the time on stream, fluctuating around a value of 25%. Even butyraldehyde and crotonaldehyde were produced in a considerable amount (around 7%). In this condition some higher Guerbet alcohols were formed in small quantity even if their selectivity decreased with the time of stream. Moreover, also the formation of "others" products started to be detectable, mainly at the beginning of the reaction. Indeed, the overall selectivity of those products reached an initial value of 7% decreasing with the time of stream. The changing observed in the products distribution with the time on stream are probably due to a partial deactivation of the catalyst caused by heavier carbonaceous compounds depositions on the catalyst surface.
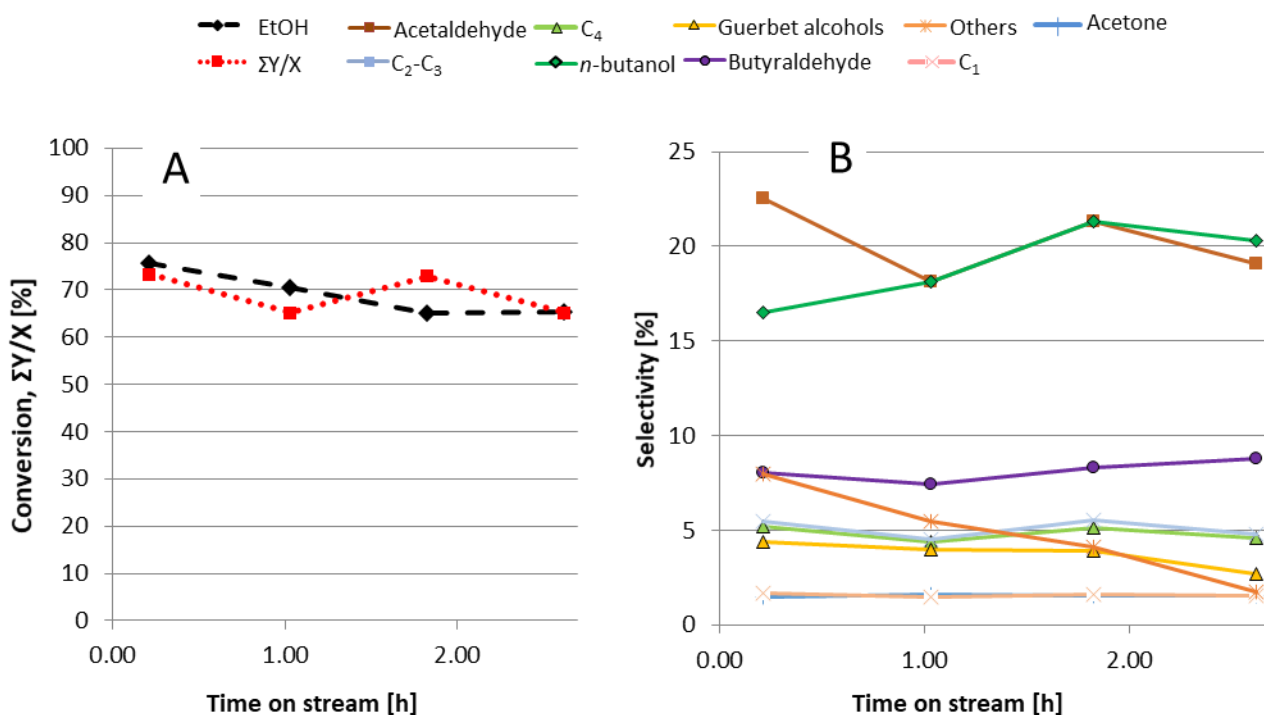
Figure 7   Catalytic results obtained in the Ethanol conversion over Ca HAP. Reaction conditions: EtOH 5% v/v in He, T= 450°C, P= 1 atm, τ= 0.28 s. A) Ethanol conversion and carbon balance ΣY/X as a function of the time on stream. B) Products selectivity as a function of the time on stream.

Figure 7 reports the results obtained at 450°C, where similar trends to the one obtained at 400°C can be noticed. As expected, the kinetic is favoured at higher temperature; as a result, the conversion of ethanol reached a greater value of around 65%. Interestingly, the products distribution does not seem to be strongly affected by the increase of reaction temperature compared to 400°C; however, both the higher conversion and the improved carbon balance allowed to increase the yields into the target Guerbet products. Nevertheless, a slight decrease of EtOH conversion with the time on stream can be noticed, namely from 75% to around 65% after 2,5 hours. Although the distribution of the main products have not been considerably affected from the time on stream, a slight increase of the C_4 aldehydes and a concomitant decrease of the "other" products can be observed. This could again suggest a partial deactivation of the catalyst with the time on stream, where consecutive side-reactions which start from butyraldehyde and/or crotonaldehyde are progressively suppressed. At 450ºC acetone has been detected, its formation could be related to a two consecutive reactions starting from acetaldehyde. The dehydrogenation step of ethanol yielding the corresponding aldehyde, acetaldehyde, has been found as necessary first step for the "alcohols ketonization" reaction to happen.[81] Indeed, the reaction mechanism that is likely to take place to from acteone is the following: firstly, acetaldehyde underwent Cannizzaro or Tishchenko-like disproportionation reactions, producing the related acid, alcohols or ester, respectively. The same ester can undergo hydrolysis yielding the corresponding acid. [82] Then, the acids underwent decarboxylative

72

condensation (i.e. ketonization) reaction, producing non-symmetric or symmetric ketones with the evolution of carbon dioxide as co-product (Scheme 1).
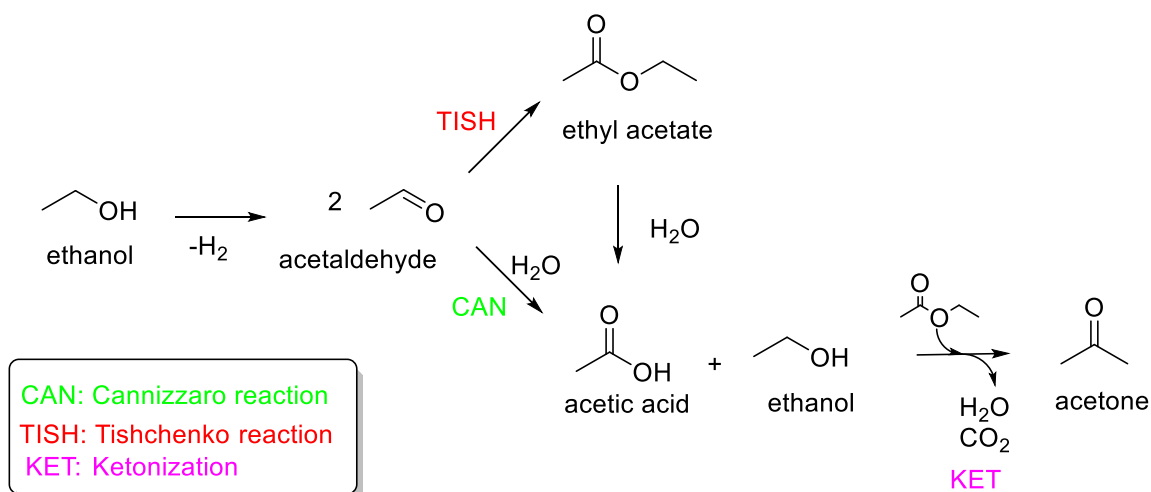
Scheme 1. Reaction mechanism of ethanol toward acetone. Adapted from Ref. [81]

Thanks to the manual injection into the GC-MS of gaseous samples collected during reactions, it was possible to identify most of the compounds constituting the group named "others" and it was found that is made up of different classes of compounds. Figure 8 shows the complex chromatograph obtained by a manual injection into the GC-MS obtained after 75 minutes of time on stream during reaction performed at 450°C. In Figure 9 some of the compounds detected and gathered in the group named "others" are shown. Higher aldehydes (as 2-ethylbutanal, hexanal) were detected, which were formed through the consecutive Guerbet reaction pathway. Furthermore, higher dienes as hexadiene and 1,3-butadiene-2-ethyl were recognized, probably formed through the Lebedev mechanism.[146] Some ketones were noticed (pentanone, hexanone, heptanone, nonanone), the formation of which can be related to the mechanism showed in Scheme 1. Otherwise, ketone formation could be related to another two-step reaction[166]: first the carbonylation of olefins that forms carboxylic acid and then two carboxylic acids react obtaining the ketones by ketonization reaction. A significant amount of alkyl substituted cyclic and aromatics compounds (i.e., xylene, ethyl-benzene, benzene-1,2-diethyl, butylbenzene and ciclohexane-4-methyl) was noticed. The formation of aromatic compounds probably started from ethylene that underwent aromatization that requires acid sites in the catalyst surface.[267]
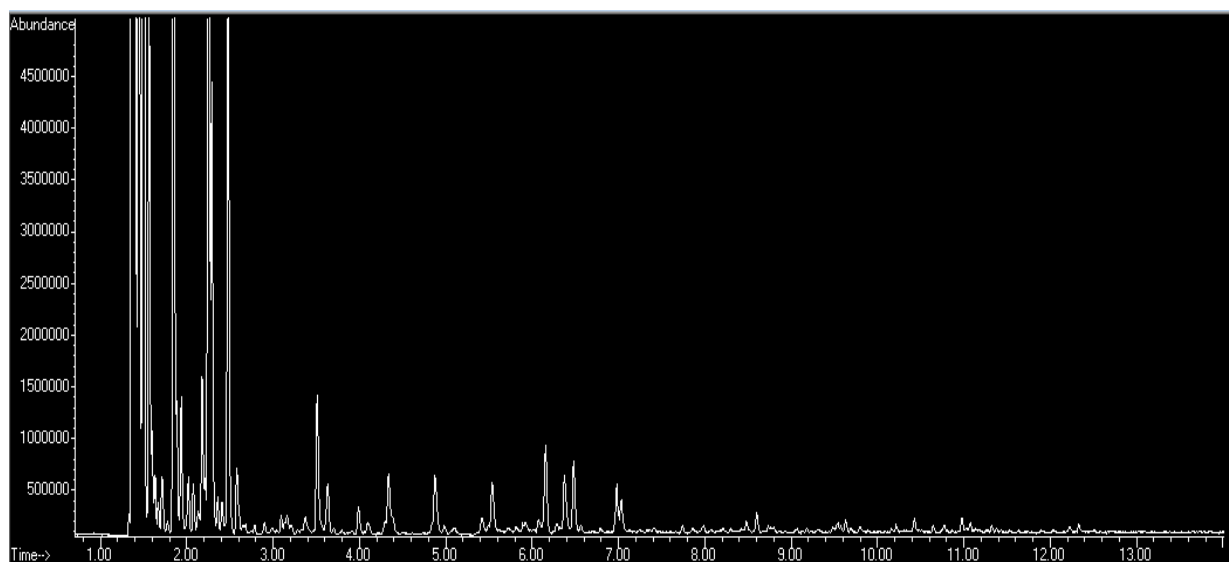
Figure 8   Chromatogram obtained after injection of a sample of the outlet gas stream of the reactor during reaction a 450°C.
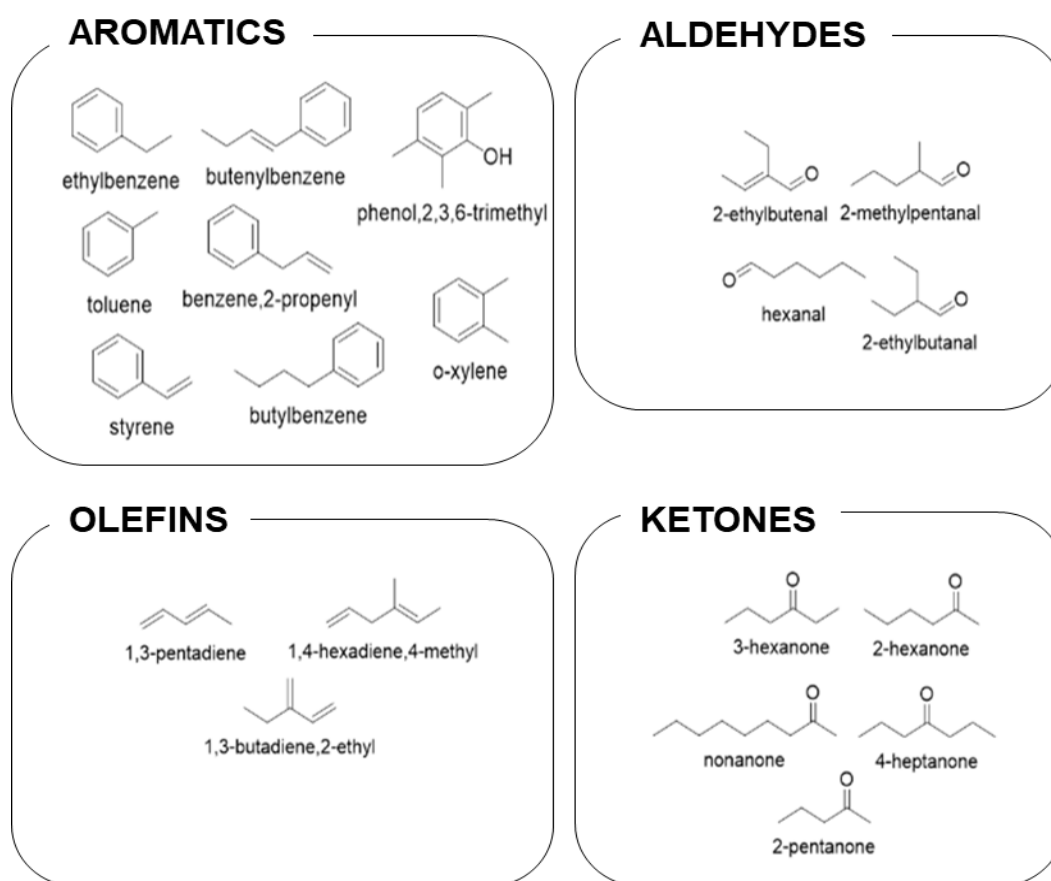
Figure 9   Some of the compounds detected through the manual injection into the GC-MS.

Finally, at 500°C the conversion of ethanol was completed (100%) from the beginning and endured over the time of stream with a carbon balance slightly constant around 65% (Figure 10). The increase of reaction temperature favoured the production of other products but even the formation of C_3 and

74

C_4 unsaturated compounds, as well as of CO_2, that is the co-product of the formation of acetone (and probably higher ketones) from ketonization reactions.
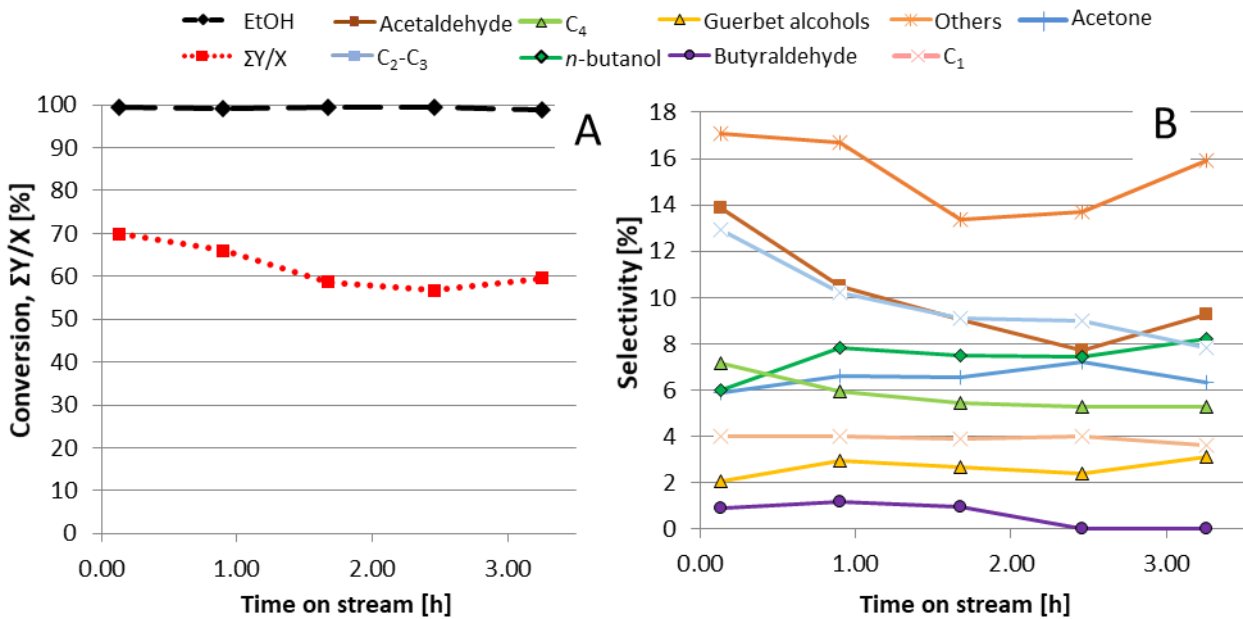
Figure 10   Catalytic results obtained in the Ethanol conversion over Ca HAP. Reaction conditions: EtOH 5% v/v in He, T= 500°C, P= 1 atm, τ= 0.27 s. A) Ethanol conversion and carbon balance ΣY/X as a function of the time on stream. B) Products selectivity as a function of the time on stream.

Figure 11 reports the catalytic results obtained at 550°C. After 190 minutes of time on stream, the conversion of ethanol, initially completed, decreased to 96% while the carbon balance fluctuated around 70%. In this case, the product distribution is similar to the one obtained at 500°C even if when the conversion decreased so did the selectivity of the "others" products while the ones of acetaldehyde, *n*-butanol and butyraldehyde increased, all factors that indicated a partial deactivation of the catalyst with the time on stream.
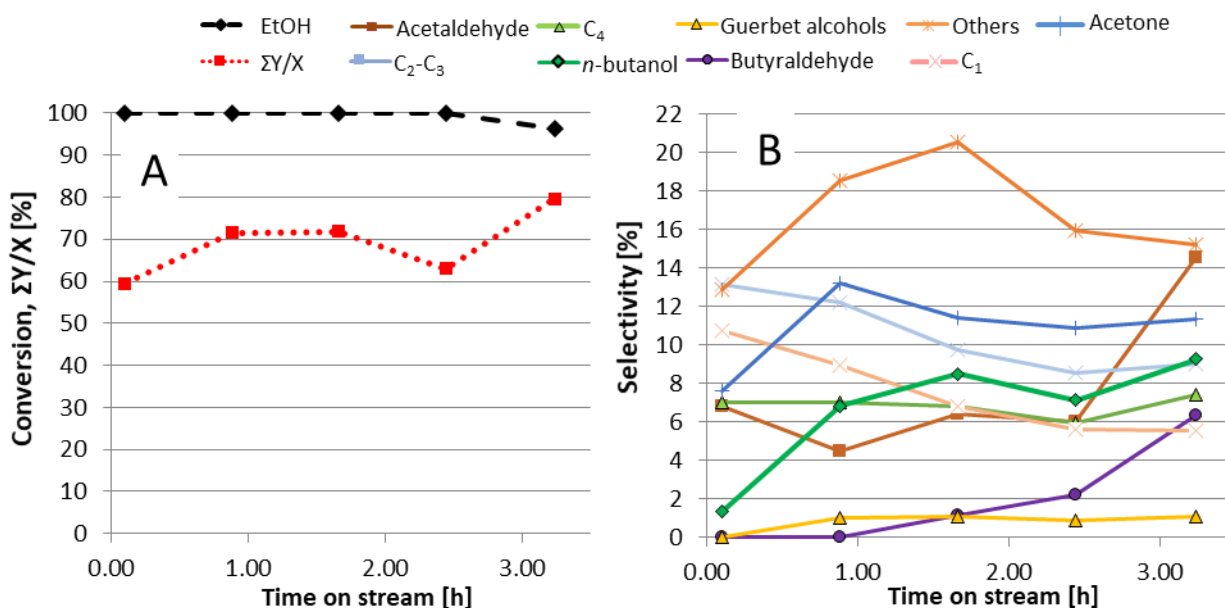
Figure 11   Catalytic results obtained in the Ethanol conversion over Ca HAP. Reaction conditions: EtOH 5% v/v in He, T= 550°C, P= 1 atm, τ= 0.25 s. A) Ethanol conversion and carbon balance ΣY/X as a function of the time on stream. B) Products selectivity as a function of the time on stream.

Interestingly, at 600°C, the ethanol conversion rapidly drop from 100% to 25% over the time of stream, probably due to a quick deactivation of the catalyst as a result of hydrocarbon decomposition to hydrogen-poor compounds, i.e. coke (Figure 12). Indeed, the spent catalyst was completely black after reaction. On the other hand, the carbon balance increased during the reaction from 42% to 93% after 160 minutes. At this temperature, *n*-butanol was not formed while the main reaction products were acetaldehyde (reaching a value of selectivity of 70%) and ethylene (with a selectivity of ~ 20%). They are both products of endothermic reactions, i.e. dehydrogenation and dehydration. Accordingly, their production could be favoured at higher temperature. The catalytic results suggest that heavier products have been rapidly produced from ethylene and acetaldehyde as intermediates resulting in the deactivation of the catalyst for coke deposition on its surface.
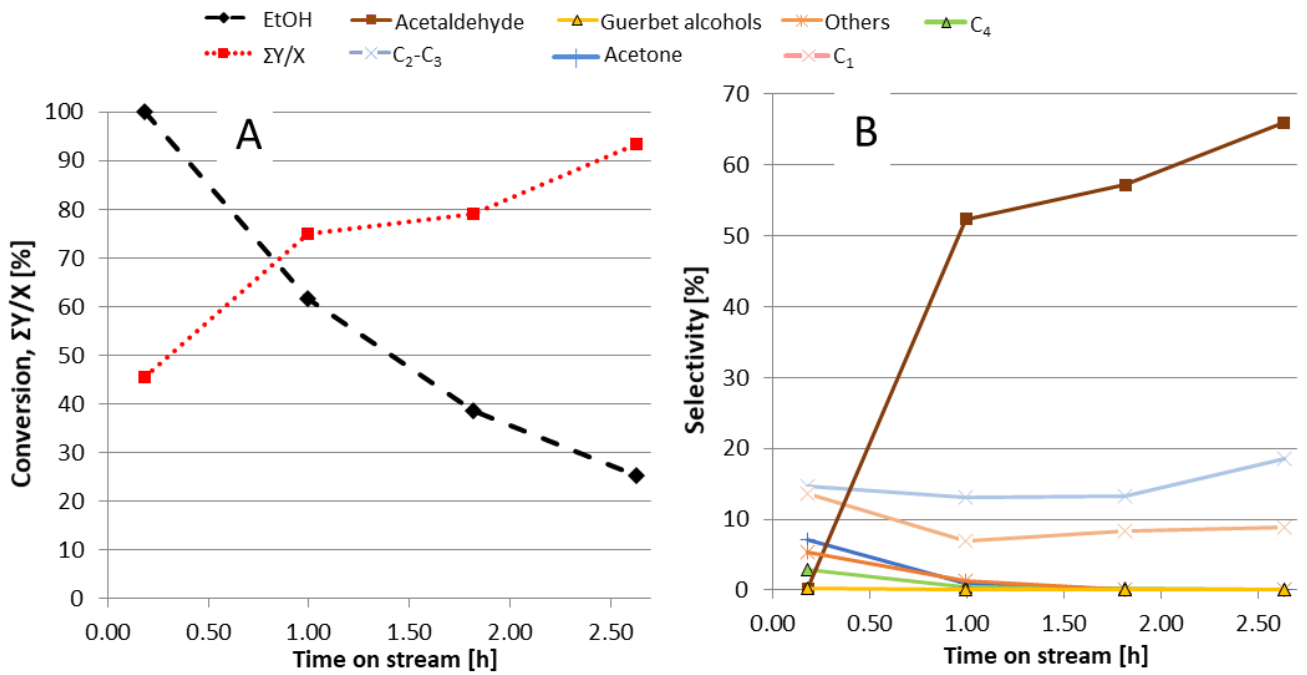
Figure 12   Catalytic results obtained in the Ethanol conversion over Ca HAP. Reaction conditions: EtOH 5% v/v in He, T= 600°C, P= 1 atm, τ= 0.23 s. A) Ethanol conversion and carbon balance $\Sigma Y/X$ as a function of the time on stream. B) Products selectivity as a function of the time on stream.

4.1.2.1.2 The effect of the reaction temperature: overview

In Figure 13 are depicted the trends of the conversion of EtOH, the carbon balance and the selectivity of the quantified products as function of the reaction temperature. In this case, the showed data are an arithmetic average of all the results obtained at each temperature avoiding the first point of reactivity in order to show what happened in the stationary state.
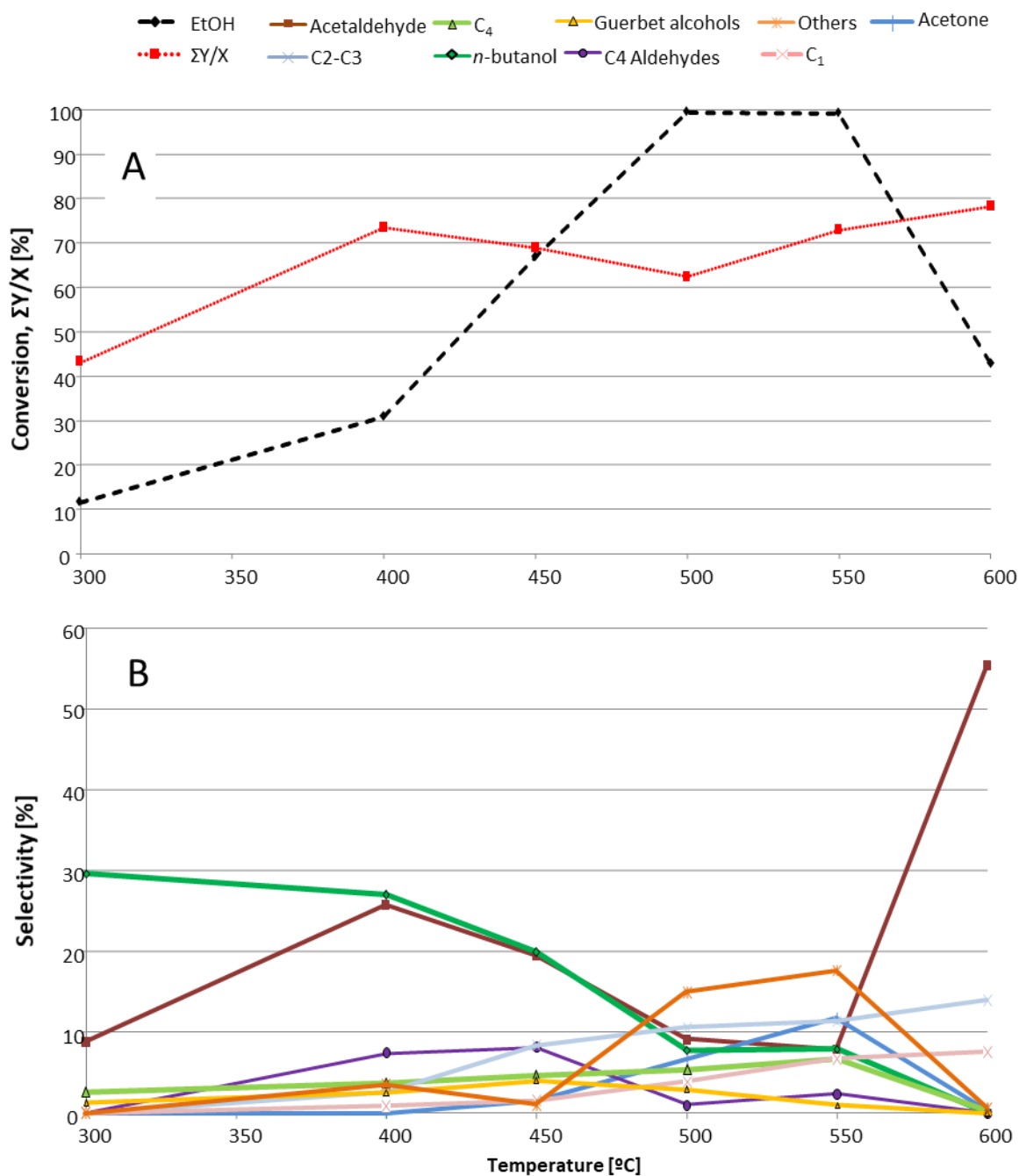
Figure 13 AVERAGE CATALYTIC RESULTS in terms of conversion of EtOH, carbon balance and selectivity of products as a function of reaction temperature, for the ethanol gas-phase conversion over Ca-HAP catalyst. Reaction conditions: p= 1 atm, EtOH 5% v/v in He, Ftotal= 60 ml/min, mcat= 0.5 g A) Ethanol conversion and carbon balance ΣY/X as a function of the time on stream. B) Products selectivity as a function of the time on stream.

With increasing temperature, the conversion of EtOH increased from 11 % at 300°C to complete conversion (100%) at 500°C, as expected from a kinetic point of view. Surprisingly, at 600°C the conversion decreased to 42 %. These results are in accordance with J.J Lovón-Quintana et al. [264] who obtained a decreasing conversion of EtOH over a modified hydroxyapatite after increasing

temperature from 550°C to 600°C. Anyway, the reason of this drop in ethanol conversion at 600°C could be related to a quick deactivation of the catalyst due to coke deposition.

The carbon balance showed an upward trend with increasing reaction temperature, indeed at 300°C it was about 40% and then it fluctuated around 70%. In general, in those reaction conditions, the main reaction products were *n*-butanol and acetaldehyde. The *n*-butanol selectivity showed a decreasing trend over the reaction temperature, with a maximum value of 30% at the lower temperature studied (300°C) that decreased to 0% at 600°C. Acetaldehyde selectivity varied with reaction temperature and the main difference to the one of *n*-butanol is noticeable at 600°C where it was the main product with a value of 55%. Since acetaldehyde is the dehydrogenation product of ethanol, which is an endothermic reaction favoured at higher temperature, this result is in accordance with the thermodynamics. In the temperature range 300-450°C the selectivity toward Guerbet reaction products was remarkable while an increase of reaction temperature seems to favour the production of side products that were identified as mainly aromatic compounds. It is worth to notice that with increasing reaction temperature the production of ethylene (grouped in C2-C3) linearly increased, so did the one of C1 compounds, mainly methane.

Since it has been observed a general progressive deactivation with the time on stream, the same results of the effects of the reaction temperature have been computed by plotting the first point of reactivity, that is the one in which can be noticed the activity of the fresh catalyst before deactivation. In those conditions, the effect of the reaction temperature is better pointed out, as can be observed in Figure 14. The effect of the reaction temperature on the selectivity of *n*-butanol is revealed, which decreased from 30% to 0% with increasing temperature from 300 to 600ºC.

By considering the results obtained over the fresh catalyst, the trends of Guerbet alcohols is noted, with a decreasing trend from 17% at 300°C to 0 % at 600%. The trend of selectivity of acetaldehyde differs from the average one showed in the previous Fig. 13, in particular considering the lowest and the highest temperature studied. Indeed, at 300°C the starting value is higher (20%) than the one obtained after the partial deactivation of the catalyst (10%). In contrast, at higher temperature (i.e., 600ºC) the selectivity of acetaldehyde was initially very low (i.e., almost 0%) while after the deactivation of the catalyst it became the main reaction product, reaching a selectivity value of 55%. Generally, at medium reaction temperature (400-550°C), as the reactivity reached a stable value over the time on stream very quickly, the results reported with the average values calculated and with the first point of reactivity were very similar. On the contrary, at lower (300ºC) and higher temperatures (600ºC), the deactivation had a greater effect on the products distribution, the two kind of results reported were rather different; such as the selectivity of both acetaldehyde and Guerbet alcohols.
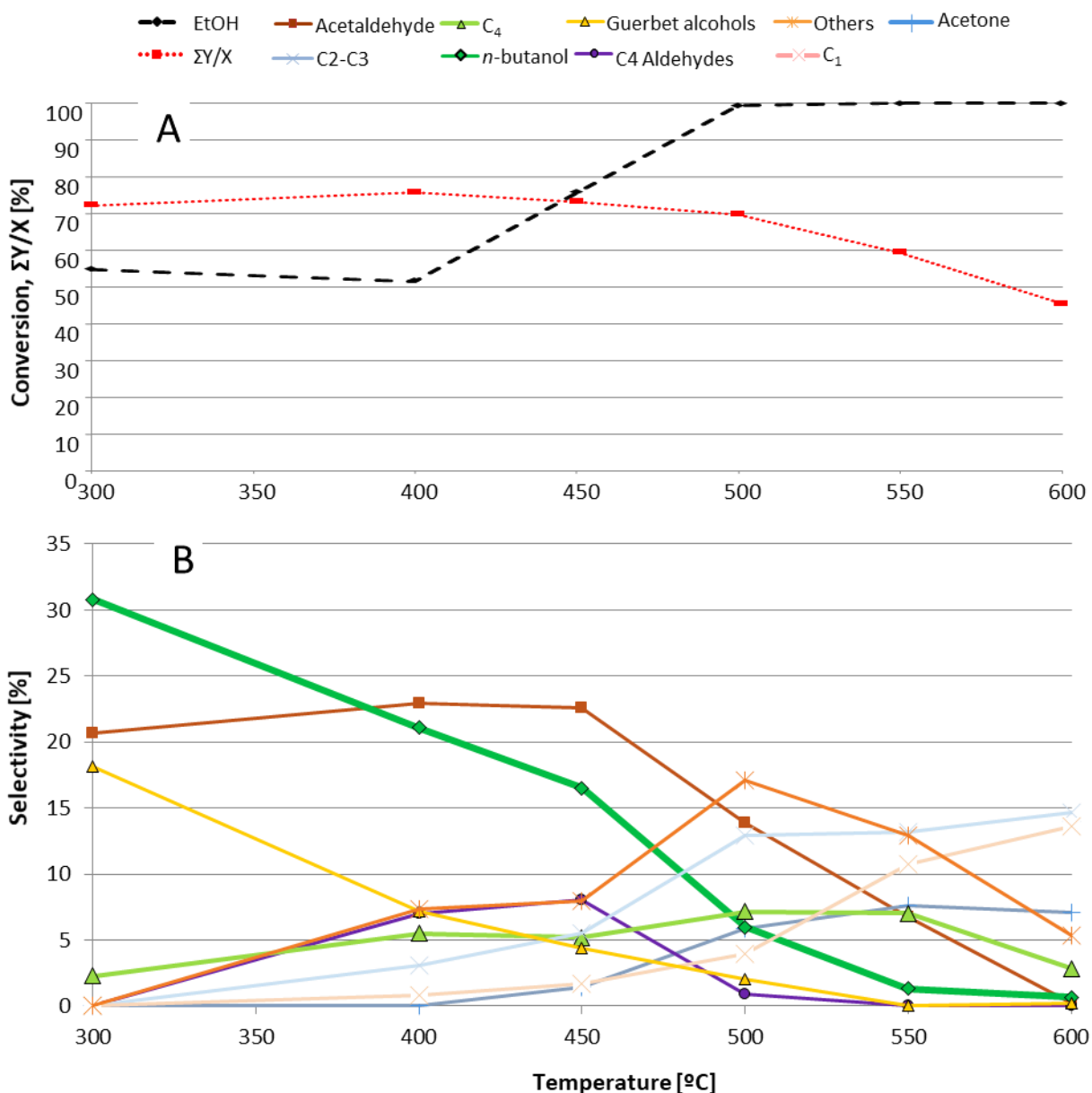
Figure 14 Results obtained over the fresh catalyst, in terms of conversion of EtOH, carbon balance and selectivity of the quantified products as a function of reaction temperature. Reaction conditions: p= 1 atm, EtOH 5% v/v in He, Ftotal= 60 ml/min, mcat= 0.5 g. A) Ethanol conversion and carbon balance ΣY/X as a function of the time on stream. B) Products selectivity as a function of the time on stream.

To deepen the possible causes of catalyst deactivation, some Thermogravimetric analysis (TGA) under an air flow of 100 ml/min (10°C/min of ramp until 100°C followed of an isothermal for 1 h) were performed over the spent catalysts after reaction. Figure 15 shows a representative thermogram obtained with the catalyst spent after the reaction performed at 550°. This Ca HAP sample exhibits three different stages of mass loss, the first around 200°C can be related to the dehydration of adsorbed water. The last mass loss that started around 800°C is the same observed with the fresh

catalyst. (see section 4.1.1.1). The middle stage of mass loss from 200°C to 600°C can be related to the loss of carbonaceous residues adsorbed over the surface of the catalyst.
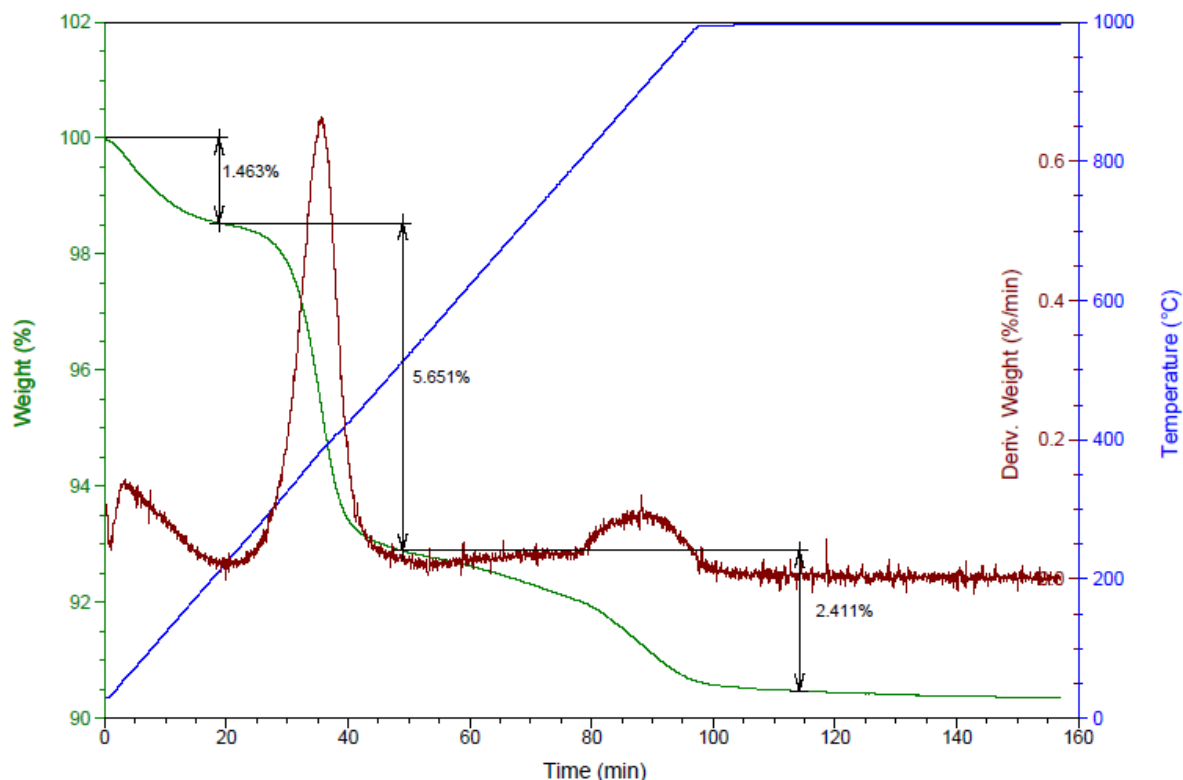
Figure 15   TGA results with Ca HAP spent catalyst after the reaction performed at the reaction temperature of 500°C.

Table 3 summarized the results obtained from the TGA analysis of all the spent catalysts after the reactions performed at different temperatures and the weight loss tabulated is the one attributed to the carbonaceous residues (i.e. coke). The increase of this weight loss with rising reaction temperature can be related to a general higher coke formation, this trend resemble the one observed for the carbon loss as can be noticed in Figure 14 The highest coke content was observed over the spent catalyst used in the reaction performed at 600ºC, this result is in line with the catalytic results (Figure 12), where a high rate of deactivation can be noticed.

Table 3.   *Thermogravimetric analysis (TGA) of the spent catalysts performed under flow of air.*

Reaction temperature [°C]	Overall time on stream [min]	Weight loss [%]	Temperature of desorption [°C]	Mass of heavy compounds deposited per minutes[g/min]
300	202	2.37	377	5.87E-05
400	254	1.9	368	3.74E-05
450	157	1.6	372	5.10E-05
500	196	2.1	383	2.79E-05
550	194	5.7	384	1.46E-04
600	158	6.8	386	2.15E-04

The weight loss obtained from the TGA analysis can be referred to the deposition of heavy organic compounds over the catalytic surface during the reaction. In this way, it is possible to quantify the total mass of the deposited organic compounds over the catalyst during the time on stream. However, these values alone does not explain completely the deficit in the carbon balance.
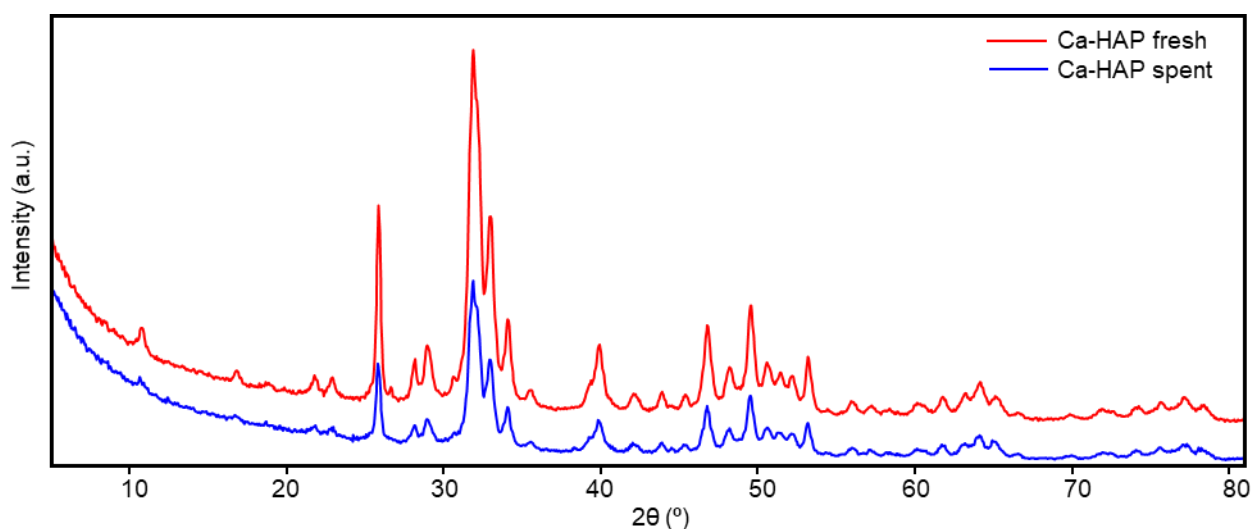
Figure 16   XRD patterns of Ca-HAP fresh and spent.

Figure 16 shows the powder diffraction pattern for Ca-HAP catalyst before reaction (Ca-HAP fresh, red line) and after the reaction performed at 600°C (Ca-HAP spent, blue). The XRD analysis made over the spent catalyst after the reaction performed at 600°C showed a decrease in the crystallinity of the material without any significant change in the crystal phase or segregation of any components.

4.1.2.2 Ca-HAP – Contact time effect

From the previous tests, the best catalytic result, in terms of catalyst activity and relative carbon balance, has been achieved at 450°C. Indeed, at 450°C an EtOH conversion of 70% with a carbon balance of 70% have been obtained, with reasonable selectivity of Guerbet products. Indeed, in those conditions, the main products were Guerbet alcohols (or related aldehydes) with medium length chain. For all these reasons, 450°C was chosen as suitable reaction temperature for the investigation of the effect of contact time on the product distributions. In fact, by increasing contact time it could be possible to promote the consecutive condensation reactions of higher aldehydes, finally favouring the formation of products characterised by a longer carbon chain. Specifically, the contact time employed have been τ= 0.28, 0.56, 0.94s.
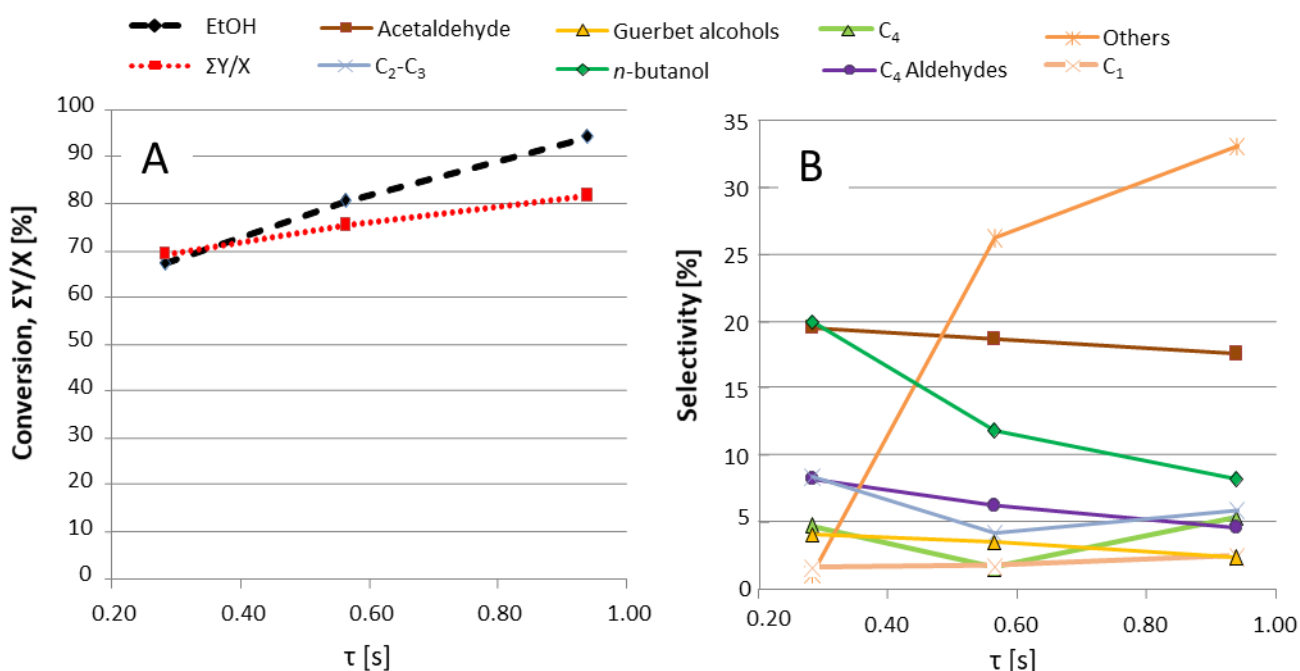
Figure 17   Catalytic results obtained in the Ethanol conversion over Ca HAP. Reaction conditions: EtOH 5% v/v in He, T= 450°C, P= 1 atm, τ= 0.28, 0.56, 0.94 s. A) Ethanol conversion and carbon balance ΣY/X as a function of the time on stream. B) Products selectivity as a function of the time on stream.

The results reported in Figure 17 represents an arithmetic average of all the results obtained at each τ avoiding the very first hour of reaction (time in which, generally, is reached the steady state, as observed in previous tests). As expected, the increase of the contact time led to a slight increase of ethanol conversion values (from 68% to 92 %). However, also an impressive increase in the selectivity of other products (mainly aromatic compounds) with a concomitant drop in both *n*-butanol and C4 aldehydes selectivity was observed. On the other hand, the selectivity toward acetaldehyde was almost unaffected by the contact time. These results are probably suggesting that consecutive reaction on *n*-butanol and C4 aldehydes can occurs for longer contact time leading to the formation

to unsaturated compounds that can undergo radical oligomerisation or Diels Alder reaction toward the formation of aromatic compounds (mainly ethyl benzene, toluene and xylenes).

Figure 18 depicts the results obtained at the highest contact time studied (0.94 s) as a function of the time on stream. Even in this case ethanol conversion (initially 95%) decreased a bit with the time on stream but after 1 hour it reached a stable value of 80% and the carbon balance remained almost stable to 75-80% for all time on stream studied. In general, after 1 hour of time of stream the reaction mixture was composed by almost a 25% of the others products, 20% of acetaldehyde, 12% of *n*-butanol, 7% of C4 aldehyde, 5% of Guerbet alcohols and the lighter products were produced in a very low quantity. Anyway, the slight decrease of the other products selectivity could be related to the use of an average response factor that could underestimate some products.
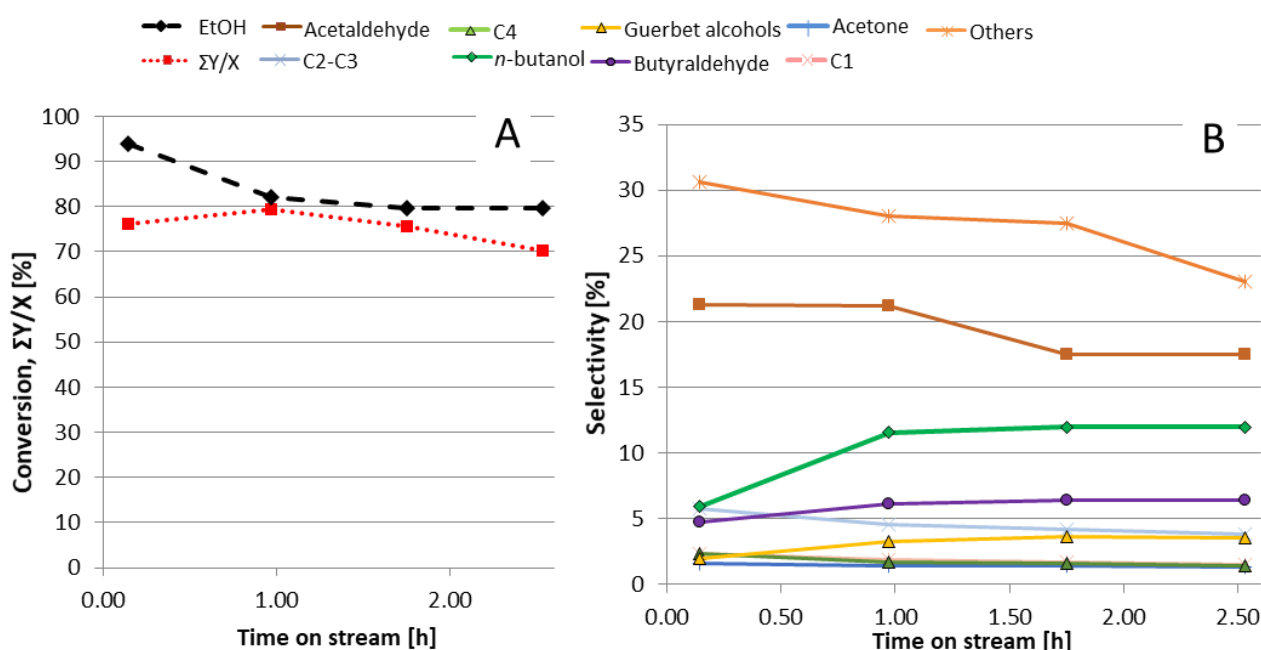
Figure 18   Catalytic results obtained in the Ethanol conversion over Ca HAP. Reaction conditions: EtOH 5% v/v in He, T= 450°C, P= 1 atm, τ=0.94 s. A) Ethanol conversion and carbon balance ΣY/X as a function of the time on stream. B) Products selectivity as a function of the time on stream.

4.1.2.2.1 Ca-HAP results resume

In summary, as expected ethanol conversion increased with increasing temperature reaching the value of 100% at 500°C. The conversion drop observed at 600°C has been related to a rapid deactivation of the catalyst due to the formation of heavy carbonaceous compounds over the surface. In addition, a partial deactivation of the Ca-HAP over the time on stream has been generally observed in all the reaction condition tested.

Generally, as can be observed in Figure 13-14, the products distribution depends significantly on the reaction temperature. With increasing temperature, the production of other products, mainly aromatic compounds, became relevant. In addition, the production of ethanol dehydration product, ethylene, increased with increasing temperature. It is well known that the latter reaction requires acid catalyst. Furthermore, ethylene is the key intermediate for the formation of aromatic hydrocarbons as it happens in the Ethanol to Gasoline (ETG) process, which consists in feeding ethanol over an acid heterogeneous catalysts, namely zeolite with the structure of HZSM-5.[268] The just mentioned process comprises ethanol dehydration to ethylene and ethylene oligomerization to higher hydrocarbon. The aromatization of ethylene involves a complex network of reactions consisting in ethylene oligomerization and cracking of the formed higher olefins, followed by dehydrogenation and cyclisation over Brønsted acid sites.[267] The fact that aromatic compound formation was favoured at higher temperature observed while performing the catalytic tests is in accordance with literature.[267]

At 450°C both the ethanol conversion and the carbon balance reached a value of around 70%. In addition, at this temperature the main products were *n*-butanol, acetaldehyde, and other Guerbet alcohols such as hexanol, 2-ethyl-butanol, octanol and 2-ethyl-hexanol as well as butyraldehyde. By studying the effect of the contact time at this reaction temperature, it was noticed that as the contact time increased so did the production of other products. Even if some of the other products detected through injection into the GC-MS were higher aldehydes and ketones, the nature of most of them was aromatic. However, Ca-HAP presented partial deactivation over the time on stream in all the reaction conditions tested with the concomitant formation of a considerable amount of aromatic compounds while trying to push the reaction to the production higher molecules.

Accordingly, the following reaction conditions have been chosen to study the catalytic activity of the ion-exchanged hydroxyapatite synthetized: 450°C, 0.6 s of contact time and continuously feeding ethanol in a helium stream (EtOH 5 mol%).

4.1.2.3 Ion-Exchanged HAP

4.1.2.3.1 Fe-HAP and Cu-HAP

The first ion-exchanged hydroxyapatite that was tested for the target reaction was Fe-HAP 4 wt%. Figure 19 reports the results obtained in terms of ethanol conversion, carbon balance (reported as the sum of the yields of quantified products divided for the ethanol conversion, ΣY/X) and the selectivity of the main products as a function of the time on stream [h]. In this case, the insertion of a transition metal with redox properties in the catalytic system led only to a slight increase in the formation of the dehydrogenation product of ethanol, acetaldehyde. Nonetheless, the main products obtained was ethylene with yields around 50%. This is typically an acid catalysed reaction and the results are in accordance with the one obtained by TPD-NH$_3$ analysis that showed an increased

acidity of the catalyst surface after ion-exchange reaction between Ca^{2+} and Fe^{3+} ions. Interestingly, it is possible to notice that the selectivity of C4 (butadiene and unsaturated butenes) increased with the time on stream reaching the value of 10% after 2.5h. Anyway, in these conditions, Fe-HAP was very active allowing a stable, complete conversion of ethanol for more than 2.5 hours.
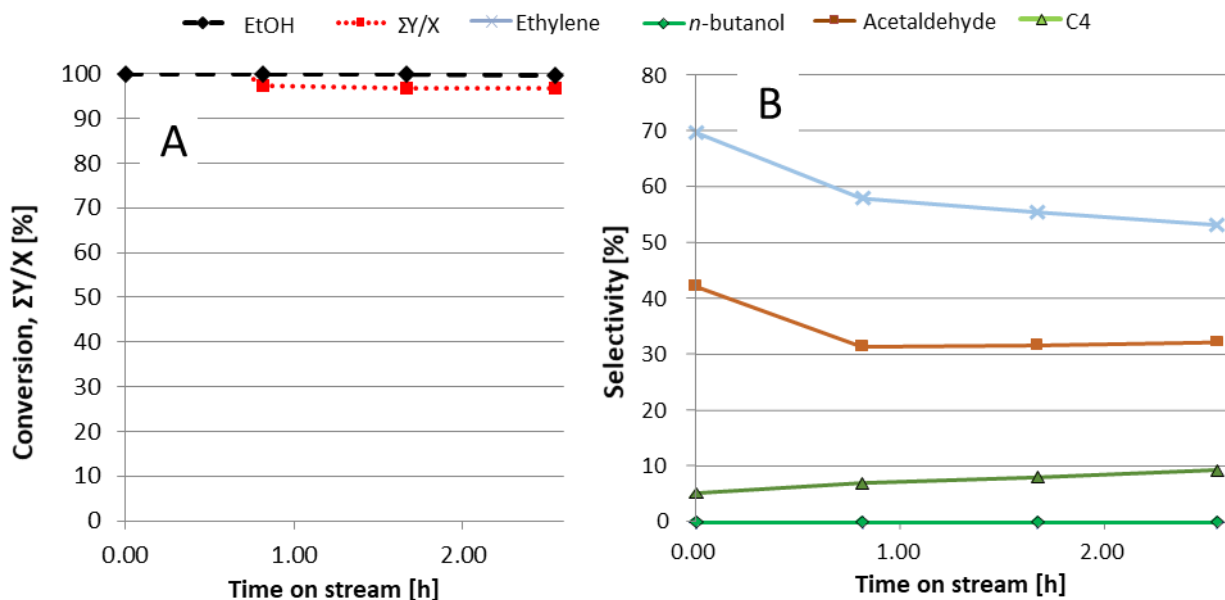
Figure 19   Catalytic results obtained in the Ethanol conversion over Fe-HAP. Reaction conditions: EtOH 5% v/v in He, T= 450°C, P= 1 atm, τ= 0,6 s. "C4": butadiene, 1-butene, 2-butene-cis and 2-butene-trans. A) Ethanol conversion and carbon balance ΣY/X as a function of the time on stream. B) Products selectivity as a function of the time on stream.

Figure 20 depicts the catalytic results obtained over the Cu-HAP 5wt% catalyst. As it is possible to notice from the figure, the effect of the addition of copper into the catalytic system is similar to the one of iron: even in this case the two main products were acetaldehyde and ethylene (with yield above 60%) with a steady, complete conversion of ethanol. The selectivity of the products obtained over the transition metal-exchanged hydroxyapatite seemed not influenced by the nature of the metal, indeed they were obtained with similar values when testing in the same reaction conditions the two catalysts. Nevertheless, since the main activity was acidic in nature, and no consecutive condensation reactions have been catalysed, no further experiments have been performed over those materials.
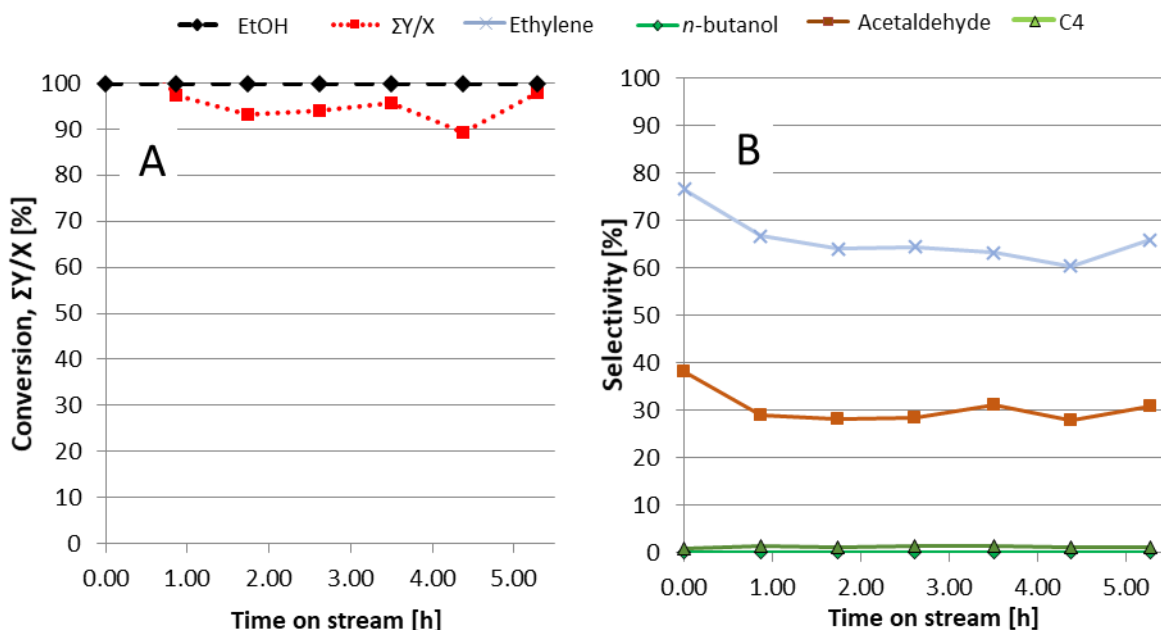
Figure 20   Catalytic results obtained in the Ethanol conversion over Cu-HAP. Reaction conditions: EtOH 5% v/v in He, T= 450°C, P= 1 atm, τ= 0,6 s. "C4": butadiene, 1-butene, 2-butene-cis and 2-butene-trans. A) Ethanol conversion and carbon balance ΣY/X as a function of the time on stream. B) Products selectivity as a function of the time on stream.

4.1.2.3.2 Sr-HAP

The Sr-HAP 1.6 wt% catalyst was tested in the same conditions explained before and the results obtained are shown in Figure 21. The reaction mixture obtained in this case was pretty complex. In order to better summarize the results, the selectivity of the products were gathered as follows: "C4": butadiene, 1-butene, 2-butene-cis and 2-butene-trans; "C1": carbon dioxide; "C4 aldehydes": butyraldehyde and crotonaldehyde; "Guerbet alcohols": hexanol, 2-ethyl-butanol, octanol, 2-ethyl-esanol, decanol. In addition, new compounds groups have been used to quantify the reaction products after optimizing the analytical method by calibrations of new standards, as explained in Section 3.1.3. Therefore, the group name "Aromatics" corresponds mainly to toluene, *o*-xylene, ethyl-benzene, butyl benzene and the one named "Higher aldehydes" is the summed contribution of both hexanal and decanal. In addition, the quantification of other unknown products has been improved in order to better understand the results of the catalytic tests. More specifically, the unknown compounds have been gathered in "Light" (i.e., C_4-C_6), "Mid" (i.e., C_6-C_{10}) and "Heavy Others" (C_{10}-C_{16}), accordingly to their retention times in the chromatogram.

Interestingly, the Sr-exchanged hydroxyapatite was pretty active, with an ethanol conversion of around 90% and a carbon balance of 70%. From Figure 21, it can be noticed a complex reaction mixture. *n*-Butanol and C_4 aldehydes selectivity slightly increased with the time on stream, probably due to a partial deactivation of the catalyst. Indeed, at the same time, there was a concomitant

decrease of the formation of heavy compounds (mainly aromatics, as it will be deepened later in this section). These results are probably suggesting that even in this case, consecutive reactions on *n*-butanol and C_4 aldehydes can occur leading to the formation to unsaturated compound that can undergo to radical oligomerization or Diels Alder reactions toward the formation of aromatic compounds (mainly benzene, ethyl benzene, toluene and xylene).
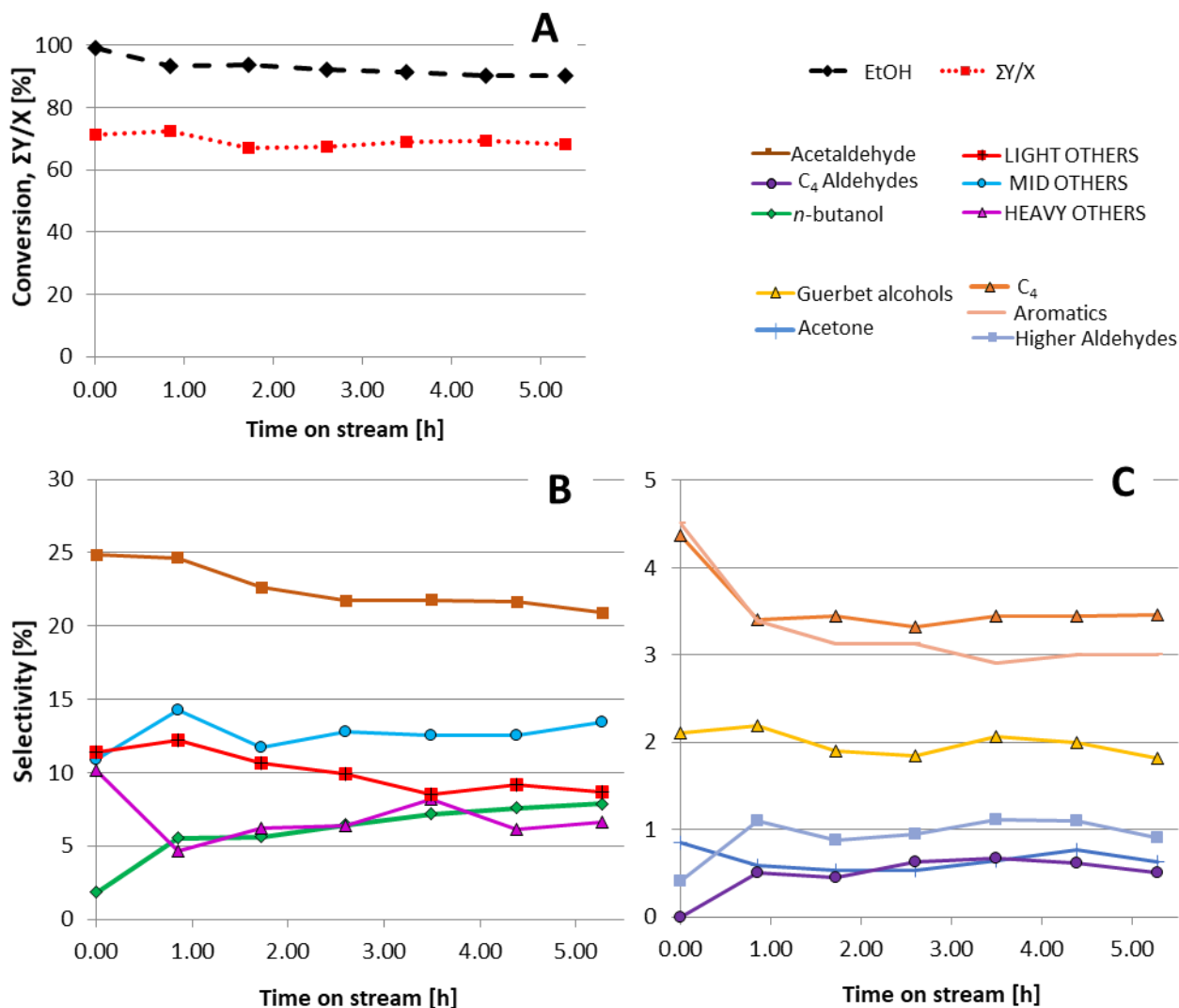

Figure 21 Catalytic results obtained in the Ethanol conversion over Sr-HAP. Reaction conditions: EtOH 5% v/v in He, T= 450°C, P= 1 atm, τ= 0,6 s. "C4": butadiene, 1-butene, 2-butene-cis and 2-butene-trans; "C1": methane and carbon dioxide; "C4 aldehydes": butyraldehyde and crotonaldehyde; "Guerbet alcohols": hexanol, 2-ethyl-butanol, octanol, 2-ethyl-esanol, decanol. Higher aldehydes: hexanal, decanal; Aromatics: toluene, o-xylene; "Light, Mid and Heavy Others": other unknown products gathered by retention times in the chromatogram. A) Ethanol conversion and carbon balance ΣY/X as a function of the time on stream. B) Main products selectivity as a function of the time on stream. C) Minor products selectivity as a function of the time on stream.

Thank to offline sampling and injection into the GC-MS system, some of the other products were identified (Figure 22-23). Higher aldehydes (as 2-ethylbutanal, hexanal, decanal) were detected,

which were formed through the consecutive Guerbet reaction pathway. Furthermore, higher dienes as hexadiene and 2,4-octadiene were recognized, probably formed through a Lebedev-type mechanism.[269] Some ketones were noticed (pentanone, heptanone), the formation of which can be related to a sequential reactions [264], as showed in Scheme1. A significant amount of alkyl substituted aromatics and cyclic compounds (such as xylene, ethyl-benzene, benzene-1,2-diethyl, butyl benzene and ciclohexane-4-methyl) was noticed. The formation of aromatic compounds can arise from three different pathways: i) ethylene aromatization[267]; ii) radical or Diels-Alder type reactions between conjugated dienes compounds (such as butadiene) and a dienophile (such as ethylene) and subsequent dehydrogenation of the cyclic compounds[270]; iii) the cyclization reactions of conjugated C=C bonds of higher aldehydes.[59]

Scheme 2 depicts the possible reactions pathways that can happen over the Ca-HAP and Sr-HAP catalysts leading to the formation of the complex reaction mixture observed.
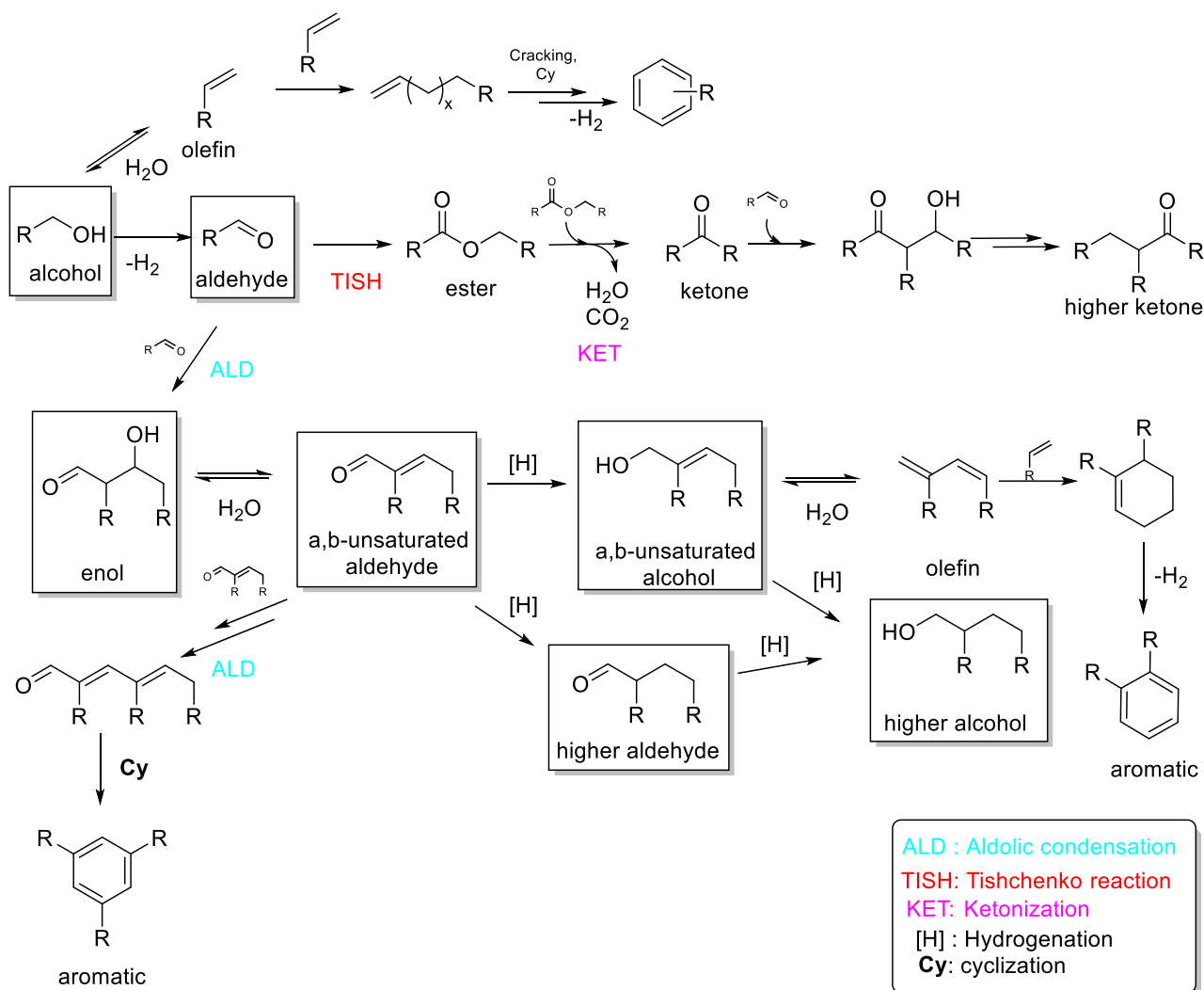
Scheme 2. Reaction pathway for the formation of the main products detected into the reaction mixture. The Guerbet-derived products are framed.

89

From off-line GC-MS analysis, it was possible to extrapolate the percentage composition of the gaseous reaction mixture, sampled at around 4.5 h of time on stream. Figure 22 and 23 show the compounds present in the highest amount detected by analysing the gaseous out-flowing reaction mixture using both Ca-HAP and Sr-HAP as heterogeneous catalysts. Although the latter catalytic system seemed promising for the production of higher molecules (such as decanal), the production of aromatic compounds seemed to be predominant, around the 33%.
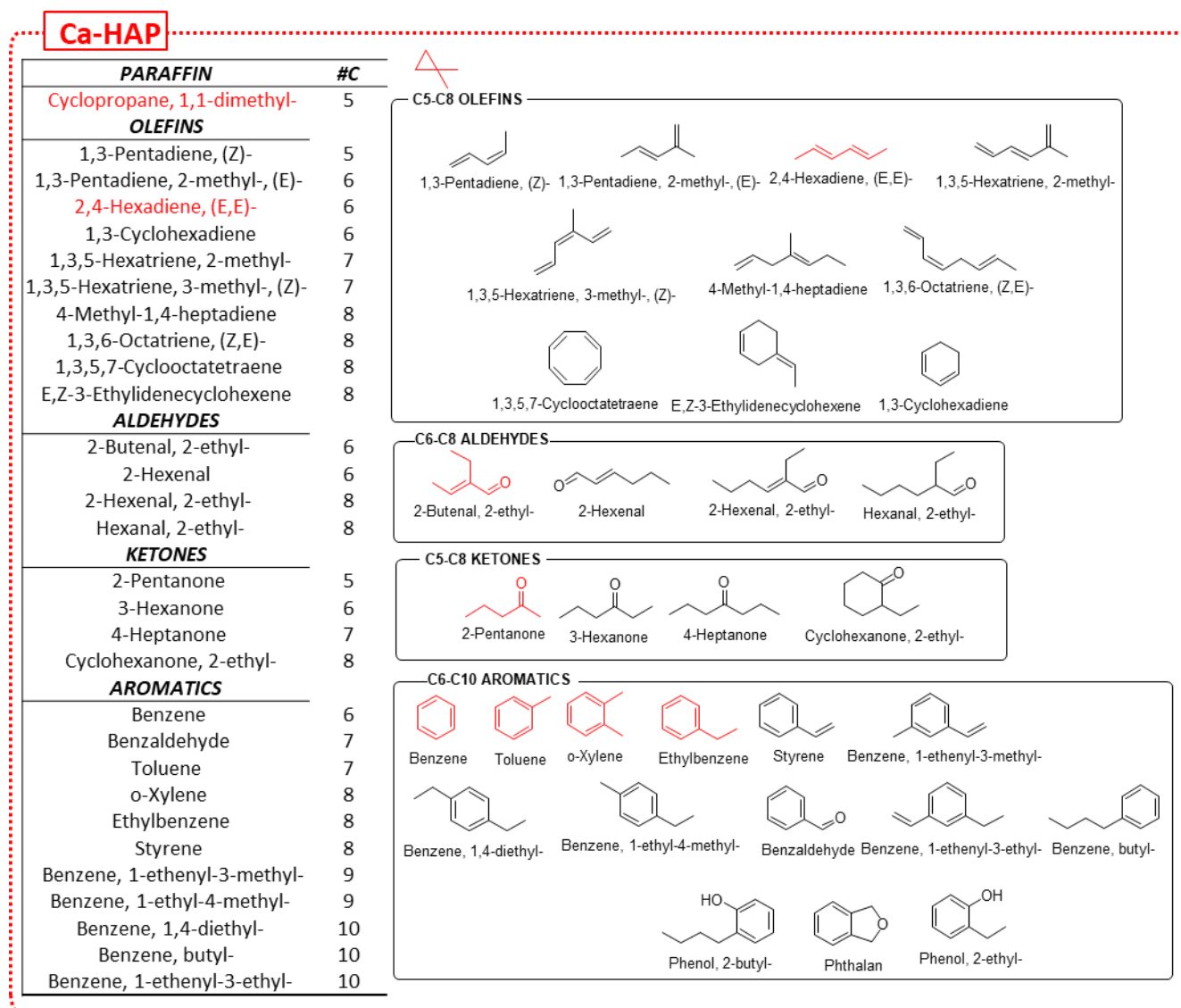
Figure 22   Compounds detected by manual injection into the GC-MS analysis system of a reaction-mixture sample obtained for the ethanol gas-phase conversion over Ca-HAP catalyst (in red are highlighted the prevalent ones).

Sr-HAP

PARAFFIN	#C
Cyclopropane, 1,1-dimethyl-	5
OLEFINS	
1,3-Pentadiene, (Z)-	5
2,4-Hexadiene, (E,E)-	6
1,3-Cyclopentadiene, 1-methyl-	6
1,3-Cyclohexadiene	6
1,3,5-Heptatriene, (E,E)-	7
1,3-Cycloheptadiene	7
1,3,6-Heptatriene, 5-methyl-, (E)-	8
E,Z-3-Ethylidenecyclohexene	8
1,3,6-Octatriene, (Z,E)-	8
1,3,5,7-Cyclooctatetraene	8
ALDEHYDES	
2-Butenal, 2-ethyl-	6
Butanal, 2-ethyl-	6
2-Hexenal	6
2-Hexenal, 2-ethyl-	8
Hexanal, 2-ethyl-	8
Decanal	10
2-Octenal, 2-butyl-	12
KETONES	
2-Pentanone	5
3-Hexanone	6
4-Heptanone	7
Cyclohexanone, 2-ethyl-	8
4-Nonanone	9
AROMATICS	
Benzene	6
Toluene	7
o-Xylene	8
Ethylbenzene	8
Styrene	8
Phenol, 2-ethyl-	8
Benzaldehyde, 2-methyl-	8
Benzene, 1-ethenyl-3-methyl-	9
Benzene, butyl-	10
Benzene, (2-methyl-1-propenyl)-	10
Phenol, 2-methyl-5-(1-methylethyl)	10
Benzene, 1,4-diethyl-	10
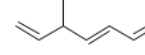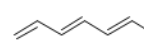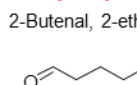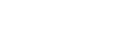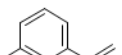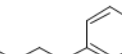
Figure 23 Compounds detected by manual injection into the GC-MS analysis system of a reaction mixture sample obtained for the ethanol gas-phase reaction over Sr-HAP catalyst (in red are highlighted the prevalent ones).

91

4.1.2.3.2.1 *Effect of ethanol feeding concentration*

The presence of longer chain compounds, such as decanal, into the reaction mixture while performing the ethanol gas-phase conversion over the Sr-HAP catalyst at 450ºC and 0.6 s of contact time has been noticed. Therefore, attempts have been made in enhancing the formation of higher products by consecutive reactions by studying the effect of reaction parameters such as the contact time and the starting concentration of ethanol.

The first strategy adopted was based on increasing the ethanol feeding concentration in order to try to enhance the production of the heavy other products, i.e. by increasing the density of ethanol and/or acetaldehyde over the catalyst surface thus promoting the condensations reactions. The effect of the ethanol feeding concentration was studied in the range of 5, 10 and 20% v/v in He over the Sr-HAP catalyst. The obtained results are summarised from Figure 24 until Figure 31.

By feeding a 10% v/v ethanol in helium mixture at 450°C and 0.6 s of contact time, both conversion of ethanol and the carbon balance fluctuated around 85% (Figure 24). Even in this case the main product obtained was the ethanol dehydrogenation product, acetaldehyde, with a selectivity value of around 25%. It can be noticed an increasing trend of the selectivity of the mid and heavy "other" compounds with the time on stream. Since they gather many different compounds, it is not easy to relate this trend to a specific product but it is likely that they encompassed intermediate products that initially were converted to consecutive products. With the time on stream the catalyst partially deactivated and the selectivity of those intermediate other products increased.

Figure 24   Catalytic results obtained in the Ethanol conversion over Sr-HAP. Reaction conditions: EtOH **10%** v/v in He, T= 450°C, P= 1 atm, τ= **0.6** s. "C4": butadiene, 1-butene, 2-butene-cis and 2-butene-trans; "C1": carbon dioxide; "C4 aldehydes": butyraldehyde and crotonaldehyde; "Guerbet alcohols": hexanol, 2-ethyl-butanol, octanol, 2-ethyl-esanol, decanol; "Aromatics": toluene, o-xylene, ethyl-benzene, butyl benzene; "Light, Mid and Heavy Others": other unknown products gathered by retention times in the chromatogram. A) Ethanol conversion and carbon balance ΣY/X as a function of the time on stream. B) Main products selectivity as a function of the time on stream. C) Minor products selectivity as a function of the time on stream.

Figure 25 shows the results obtained while feeding a 20% v/v ethanol in helium mixture. Both the conversion and the carbon balance seemed to reach a steady value of about 80%. Even in this case, the main product was still acetaldehyde of which the selectivity profiles showed a similar trend over the time on stream, fluctuating around a value of 25%. Both the selectivity of light and mid others reached almost the 8% while the one of the heavy products was near the 5%. In this case, even the so-called C4 alcohols, that are unsaturated alcohols intermediate products, were detectable probably due to the higher starting concentration of the reagent.
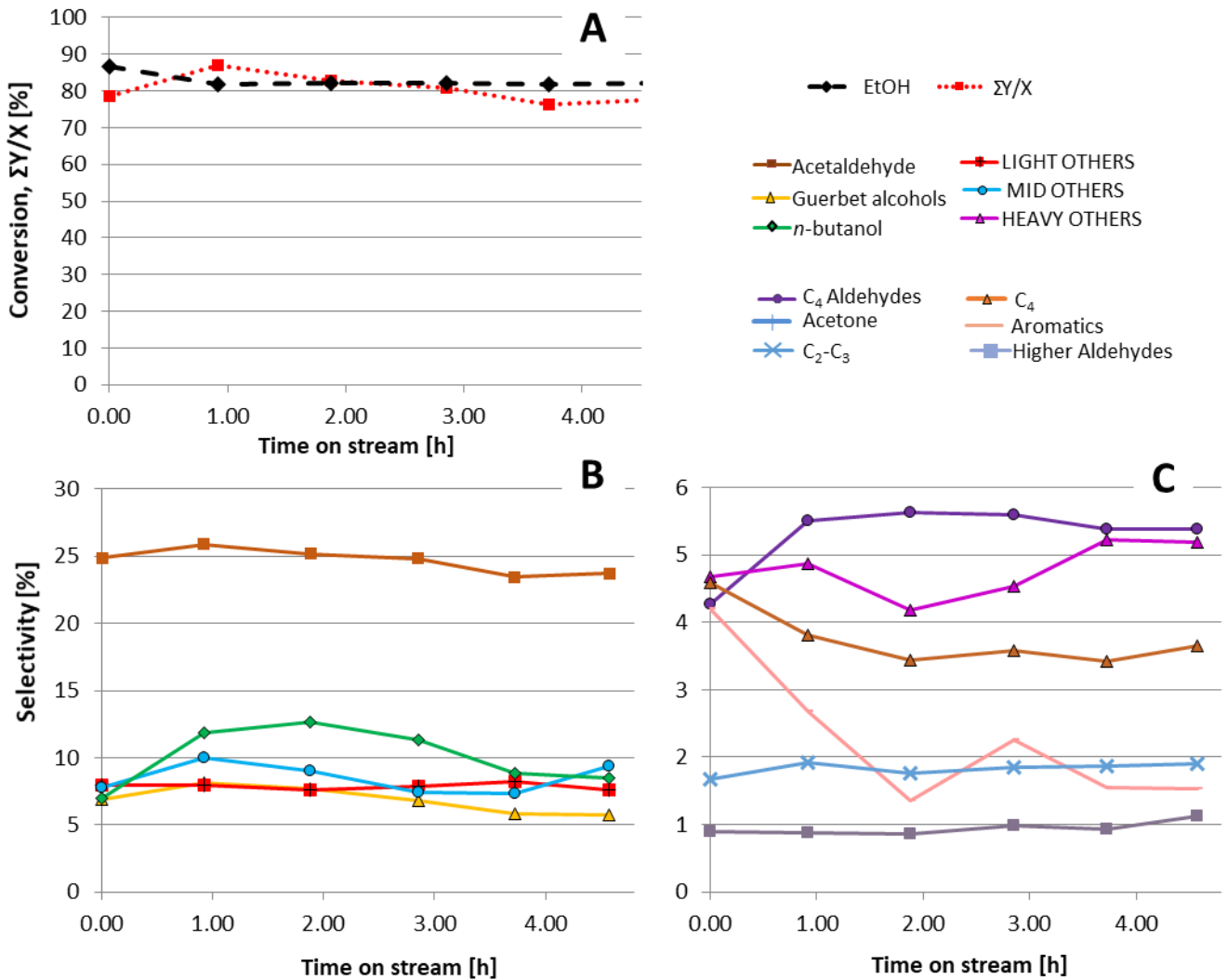
93

Figure 25 Catalytic results obtained in the Ethanol conversion over Sr-HAP. Reaction conditions: EtOH **20**% v/v in He, T= 450°C, P= 1 atm, τ= **0.6** s. "C4": butadiene, 1-butene, 2-butene-cis and 2-butene-trans; "C1": carbon dioxide; "C4 aldehydes": butyraldehyde and crotonaldehyde; "Guerbet alcohols": hexanol, 2-ethyl-butanol, octanol, 2-ethyl-esanol; "Higher aldehydes": hexanal, decanal; "Aromatics": toluene, o-xylene, ethyl-benzene, butyl benzene; "C4 alcohols": crotylalcohol, 3-buten-1-ol; "Light, Mid and Heavy Others": other unknown products gathered by retention times in the chromatogram.

Figure 26 and Figure 27 depict the trends of the conversion of ethanol, carbon balance and the selectivity of the other products as a function of the feeding concentration of ethanol. The results showed correspond to the average value obtained after reaching the steady state, after around 1,5 h. With increasing feeding concentration of ethanol, its conversion decreased as expected, while the carbon balance presented a maximum with a feeding mixture of 10% ethanol in helium. Since the carbon balance was calculated considering even the yields of the "others" products, that are quantified with an average response factor, it is possible that this difference depends on a defective quantification. Anyway, by feeding ethanol with a concentration of 10% v/v in He, the highest value of the selectivity of medium (C_6-C_{10}) and heavy (C_{10}-C_{16}) other products was reached: 16%, and

8.5%, respectively. Figure 27 highlights the results obtained with an EtOH concentration of 10 % v/v by grouping the "Mid" and "Heavy" other products, their cumulative selectivity in those conditions reached the 25%. Indeed, higher molecules were detected through offline injections into the GC-MS system. Nevertheless, the nature of the compounds detected was mainly aromatic.
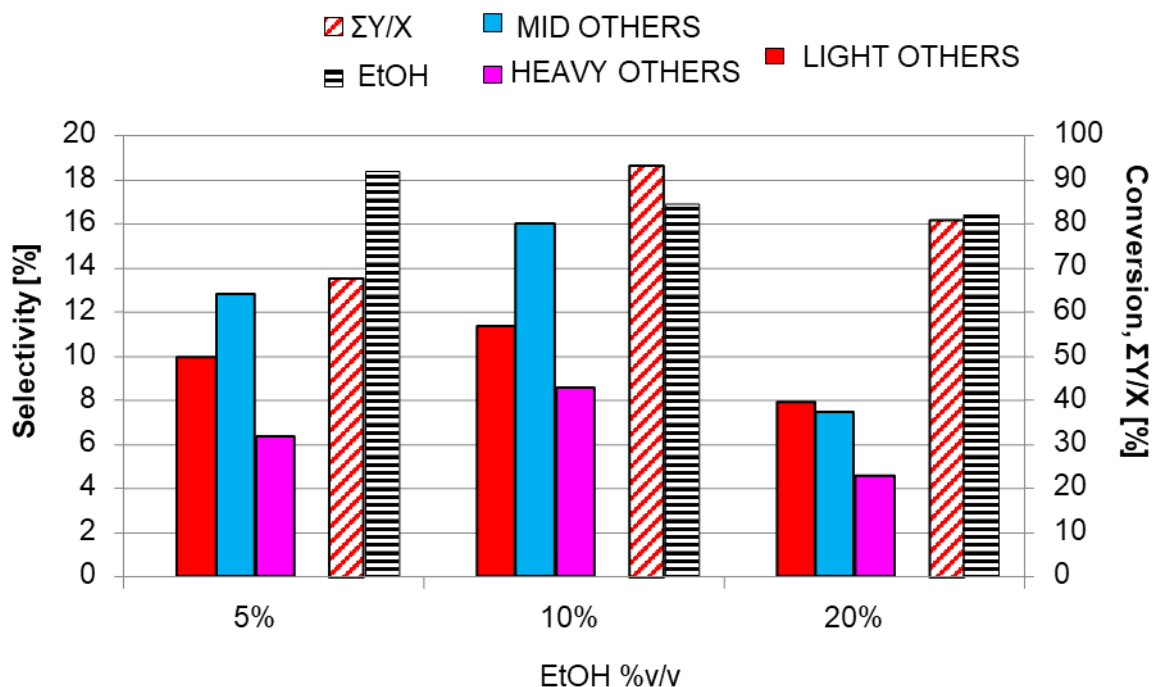
Figure 26 Effect of the ethanol feeding concentration over the ethanol conversion and the carbon balance, expressed as the sum of the products yields divided by the ethanol conversion. Catalytic results obtained in the Ethanol conversion over Sr HAP. Reaction conditions: EtOH 5-10-20 % v/v in He, T= 450°C, P= 1 atm, τ= 0.6 s.
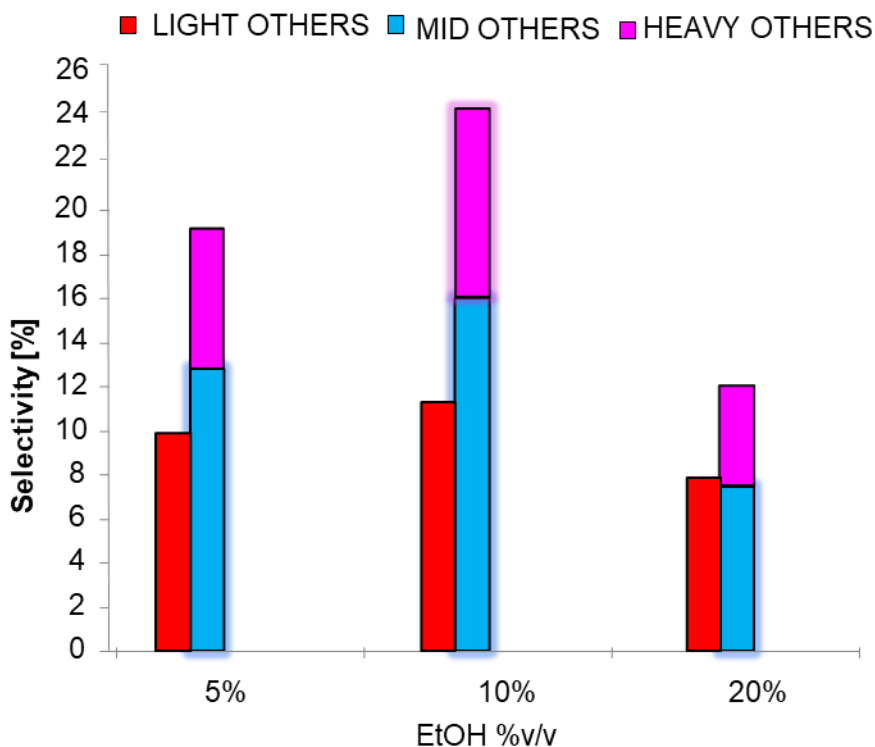
**Figure 27**   Effect of the ethanol feeding concentration over the selectivity of the so-called others products. Catalytic results obtained in the Ethanol conversion over Sr-HAP. Reaction conditions: EtOH 5-10-20 % v/v in He, T= 450°C, P= 1 atm, τ= 0.6 s.

4.1.2.3.2.2 *Effect of the contact time*

Another way to favour the formation of consecutive reactions, thus fostering the production of heavier compounds, could be represented by the increase of the contact time of the reactants over the catalyst. Indeed, by increasing the contact time it could be possible to promote the condensation reactions of even the higher aldehydes produced from ethanol, finally favouring the formation of products characterised by a longer carbon chain.

In order to study the effect of the contact time (τ), the feeding flows of both ethanol and helium were adjusted so that the 5% v/v of ethanol was maintained and the quantity of the catalyst charged was modified obtaining a contact time doubled compared to the previous tests (new τ: 1.2 s). Figure 28 depicts the results obtained in those last conditions.

Complete conversion of ethanol was reached, so rising the contact time led to an increase of the ethanol conversion, as expected (a comparison of the results obtained by varying the contact time is showed in figure 29). The carbon balance value was around 65% and wasn't affected by the higher contact time. Regarding the products distribution, again the main product was acetaldehyde, even if in this case its selectivity was lower than in the other cases: it fluctuated around 20% while in the previous cases it fluctuated around 25%. In those conditions the performances seemed almost stable with the time on stream, except for the selectivity of the medium others that increased from 4% to

8.5% after 1.6 h of time on stream. This trend can be related to the artificial response factor that could underestimate some products and overestimate other products.
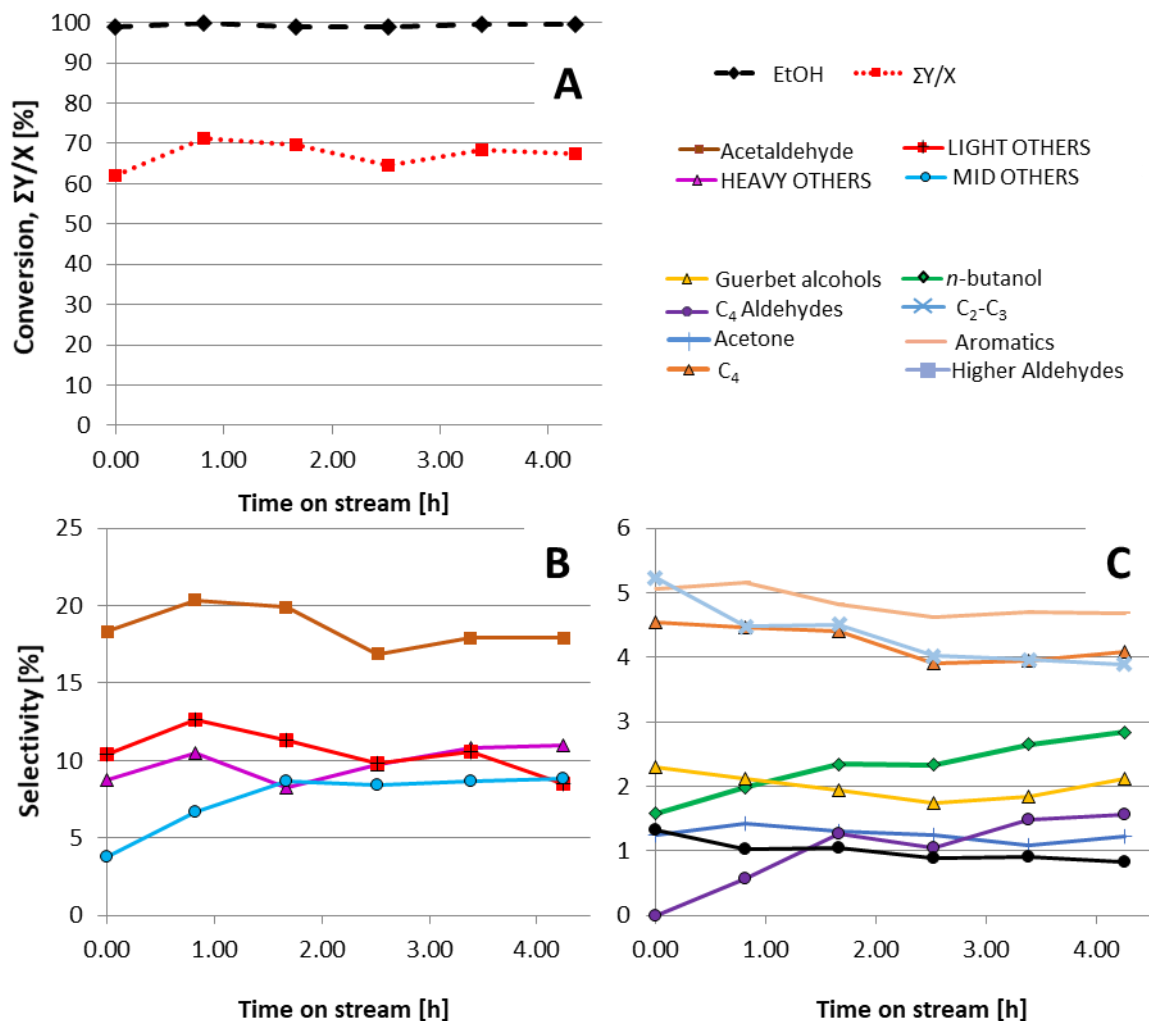

Figure 28   Catalytic results obtained in the Ethanol conversion over Sr-HAP. Reaction conditions: EtOH **5**% v/v in He, T= 450°C, P= 1 atm, τ= **1.2** s. "C4": butadiene, 1-butene, 2-butene-cis and 2-butene-trans; "C4 aldehydes": butyraldehyde and crotonaldehyde; "Guerbet alcohols": hexanol, 2-ethyl-butanol, octanol, 2-ethyl-esanol, decanol; "Aromatics": toluene, o-xylene; "Light, Mid and Heavy Others": other unknown products gathered by retention times in the chromatogram.

The effect of the contact time over the selectivity in the other products can be easily noticed in Figure 29: by doubling the contact time the selectivity of the "heavy" products increased from 6 to almost 10%; probably due to the conversion of intermediate products gathered in the "medium others" group the selectivity of which decreased from almost 12% to 8.5% with increasing contact time.
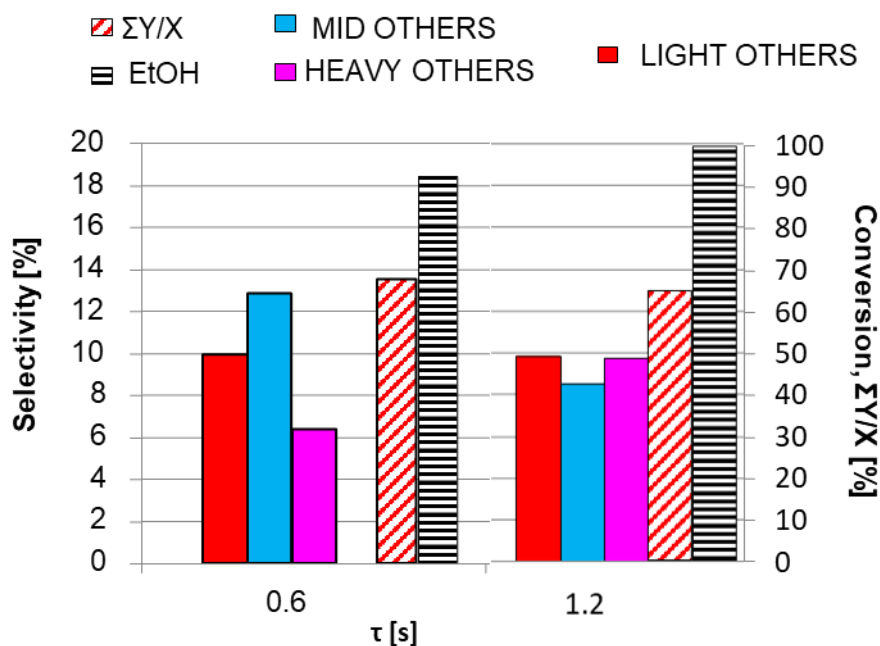
Figure 29   Effect of the contact time over the ethanol conversion, the carbon balance (ΣY/X) and the selectivity of the other products.. Catalytic results obtained in the Ethanol conversion over Sr-HAP. Reaction conditions: EtOH **5 %** v/v in He, T= 450°C, P= 1 atm, τ= 0.6 - 1.2 s.

It has been observed that by feeding EtOH with a concentration of 10 v/v% and by working with a contact time of 1.2 s, the formation of heavy products is favoured. Accordingly, a catalytic test combining those conditions has been performed, i.e., by feeding ethanol, 10 %v/v in He, over Sr-HAP at 450ºC and with 1.2s as contact time. The catalytic results are depicted in Figure 30 and Figure 31.

Figure 30   Catalytic results obtained in the Ethanol conversion over Sr-HAP. Reaction conditions: EtOH **10**% v/v in He, T= 450°C, P= 1 atm, τ= **1.2** s. "C2-C3": ethylene, ethane, propylene; "C4": butadiene, 1-butene, 2-butene-cis and 2-butene-trans; "C4 aldehydes": butyraldehyde and crotonaldehyde; "Guerbet alcohols": hexanol, 2-ethyl-butanol, octanol, 2-ethyl-esanol, decanol; "Aromatics": toluene, o-xylene; "Light, Mid and Heavy Others": other unknown products gathered by retention times in the chromatogram.

Unexpected results have been obtained while performing the reaction with the reaction conditions just described. Indeed, instead of favouring the formation of heavier products by increasing the contact time and the ethanol feeding concentration, those mentioned conditions led to an increase of the lighter part of the other unknown products, of which the selectivity raised from 11 to 19% by doubling the contact time (Figure 31). At the same time, the average formation of the heaviest part of them seemed decreased by rising the contact time. Nevertheless, the trends of the products selectivity with the time on stream could suggest a rapid partial deactivation of the catalyst. For instance, an abrupt decrease from 13 to 7% in the first hour of time on stream of the "heavy other"

99

products selectivity can be noticed, the formation of which could be related to the "medium" ones as intermediate since their selectivity simultaneously increased. (Figure 30).
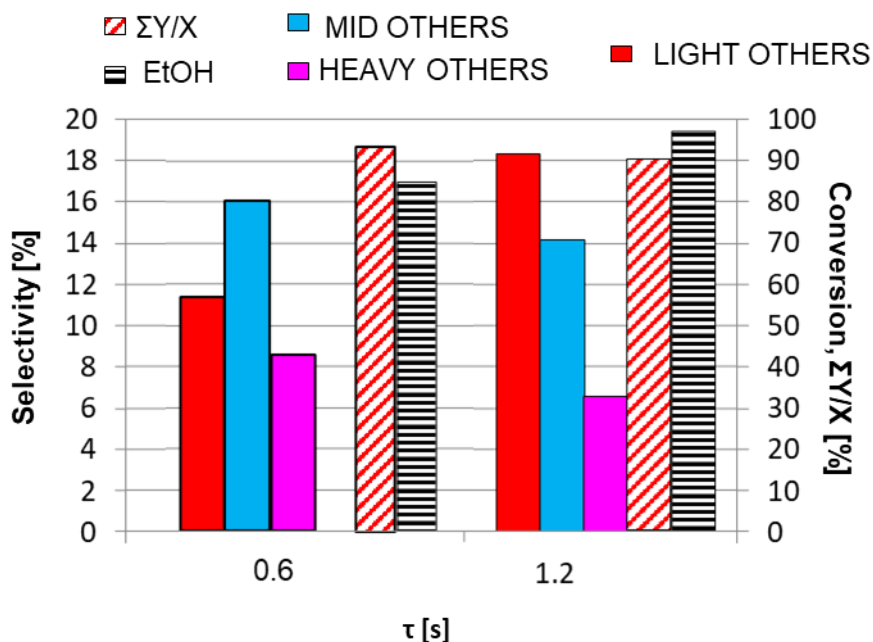
Figure 31   Effect of the contact time over the ethanol conversion, the carbon balance (ΣY/X) and the selectivity of the other products. Catalytic results obtained in the Ethanol conversion over Sr-HAP. Reaction conditions: EtOH **10** % v/v in He, T= 450°C, P= 1 atm, τ**= 0.6 - 1.2** s.

Furthermore, a general decreasing trend of the carbon balance with the time on stream can be noticed. It could be possible that part of the products could have been condensed into the lines connecting the reactor with the analytic system, affecting the overall catalytic quantification results. Since the heaviest products should be characterized by higher boiling point, an optimization of the reaction system has been performed, in order to better collect and analyse the heaviest part of the product mixture. Indeed, by adding a condenser into the line connecting the bottom of the down-flow reactor, before the on-line GC system, it could be possible to collect by condensation the heaviest part of the reaction products. Figure 32 depicts the reaction system modification, the condenser has been highlighted. In addition, for speeding up the condensation, the possibility of putting the condenser in an ice-bath has been considered.
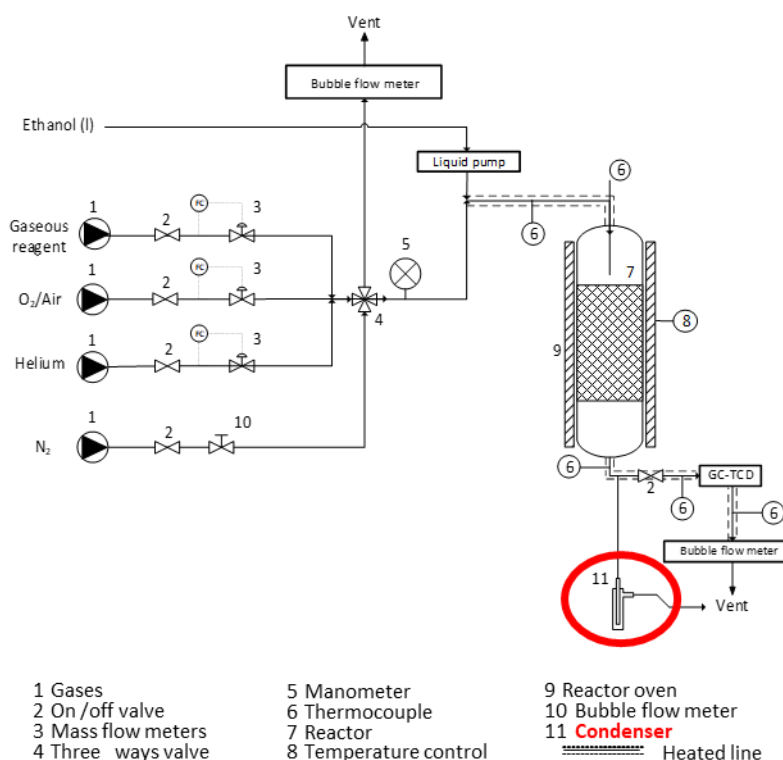
Figure 32   Reaction system modified, in red is highlighted the condenser.

4.1.2.4 Resume

The ion-exchanged hydroxyapatite catalysts have been tested for the ethanol gas-phase conversion at 450ºC, 1 atm and 0.6 s as contact time. In summary, both Fe-HAP and Cu-HAP, showed a greater catalytic activity compared to Ca-HAP, leading to higher conversion of ethanol. However, the increased acidity of the catalysts led to the preferentially formation of ethylene (and traces of butadiene) while the redox properties enhanced the formation of acetaldehyde but without promoting the desired condensation reactions. On the contrary, the Sr-HAP catalyst led to the formation of a wide distribution of compounds in the same reaction conditions, leading to formation to heavy products with longer carbon chain (up to C_{12}, Figure 23). Hence, the catalytic activity of this material has been investigated in depth.

In particular, with the aim of enhancing the production of compounds characterised by a longer carbon chain (i.e. $>C_6$), two different approaches have been taken into account. Firstly, the effect of increasing contact time, then the increasing ethanol feeding concentration have been evaluated. The best reaction conditions, in terms of selectivity of hydrocarbons mixture, have been located as follows: a feeding concentration of EtOH 10% v/v in He, 0.6 s as contact time and a reaction temperature of 450ºC. In such conditions, an ethanol conversion of ~85% has been obtained, with a carbon balance of ~92%. The cumulative selectivity of medium (average C_6-C_{10}) and heavy (average C_{10}-C_{14}) other products at those condition was 25%, while the one of higher Guerbet alcohols (C_6-

C_{12})~2%, C_4 compounds (alkene and aldehydes) ~9% and aromatics (C_7 –C_{10}) around 4%. By summing the selectivity of the products with a carbon chain length >C_6, an overall selectivity of ~31% has been obtained, corresponding to a ~26% of cumulative yield. The cumulative selectivity of lighter products (i.e., C_4-C_6) was 29% and can be calculated considering the selectivity of *n*-butanol (~10%), the one of C4 quantified products (i.e., olefins and aldehydes; ~9%) and the one of light other products (average C_3-C_6; 10%), corresponding to a cumulative yield of ~25%.

Thus, we managed to obtain a mixture of hydrocarbons of >C_4 carbon chain with a cumulative yield of 50% and ethanol conversion of 85% (i.e, 60% total selectivity). The main issues were the high selectivity of acetaldehyde, that was obtained as major product (i.e., 25% of selectivity) and the high percentage of total aromatic compounds produced (34%). Nevertheless, the obtained mixture had the composition suitable to be used as gasoline (C_4-C_{12}), in which an higher aromatic percentage is accepted (35%).[106]

Nevertheless, with the perspective to produce a more attractive hydrocarbon mixture with composition resembling the one of jet fuel, even though Sr-HAP was active and pretty stable in the reaction conditions, the composition of the products obtained was not optimal since the production of aromatic compounds was predominant (should be below 25% in Jet Fuel composition[106]). Indeed, by an off-line sampling and GC-MS analysis of the outlet gaseous stream it was noticed the presence of aromatics compounds in high amount. Table 4 reports a summary of the percentage of the aromatic compounds found in the outlet gaseous stream of the catalytic tests performed over Sr-HAP (i.e. by varying both the contact time and the inlet ethanol concentration). The amount of aromatic in the stream (reported in Table 4), were calculated through the peaks area obtained into the GC-MS chromatograms.

Table 4. *Percentage of aromatic compounds in the reaction product mixture, by means of the peaks area of the GC-MS chromatograms ($A_{AROMATIICI}/A_{TOTALE}*100$ [%]).*

τ [s]	% EtOH in He [v/v]		
	5	10	20
0.6	28%	34%	28%
1.2	52%	**45%**	-

4.1.3   CONCLUSIONS

In this work, a commercial Ca-HAP has been employed and then modified (by means on in-exchange method) to study the ethanol gas-phase conversion through the Guerbet route while trying to favouring consecutive condensation reactions and obtaining longer carbon chain compounds with

potential applications as bio-fuels. To do so, attempts to optimize both the reaction parameters and the catalyst characteristics have been carried out, observing a high dependence of the overall composition of the reaction products on the reaction temperature. A reasonable balance between catalytic activity and overall carbon balance has been achieved by working at 450ºC and 0.6 s as contact time.

Then, Ca-HAP has been modified through ion-exchange method. The transition metals (Cu and Fe) exchanged hydroxyapatites mainly performed as acid catalysts, yielding preferentially the dehydration product of ethanol, ethylene. On the other hand, Sr-HAP lead to the production of a complex reaction mixture containing compounds different in nature and carbon chain lengths. Indeed, the mechanism of the ethanol conversion producing the hydrocarbons of different nature observed is pretty complex, involving a net of parallel, consecutive and cross reactions.

Accordingly, the Sr-HAP catalyst has been chosen to gain insight in the formation of the heaviest products. It has been observed that the product distributions is affected from the contact time and the ethanol feeding concentration, finding the best condition by working with an EtOH concentration of 10% in He and a contact time of 0.6s. In such condition it was obtained a total yield of 50% of hydrocarbons with carbon length in the range C_4-C_{14} that could resemble the required composition of the conventional gasoline. Notwithstanding, in general the outlet streams of the product was characterized by a 30 to 45% of aromatic compounds, depending on the reaction conditions. In order to be suitable for jet-fuel, this value should be lower than 25%.

Nevertheless, the catalytic tests performed enabled to set the reaction system with the perspective of deepen the study of ethanol conversion into heavier hydrocarbon. Indeed, with the addition of a condenser in which collect the heavy products to be analysed off-line, let to better analyse the mixture composition, avoiding operational troubles.

Considering the high selectivity of acetaldehyde, always obtained as major product, and the beneficial effect observed of the decreased acidity/basicity ratio related to the Sr-exchanged HAP, it would be interesting to further modify the catalytic system in this regard.

Angelici et al. [148,271] observed that the state in which copper is present on the catalyst is important not only to catalyse the dehydrogenation step, but also to affect the acid/base properties of the catalyst and favouring the consecutive aldol-condensation step, which is supposed to become the rate limiting step after copper addition. The way in which copper is present on the surface is strictly related to the method employed to add it on the catalyst. Consequently, changing the way by which adding a redox element (i.e., a transition metal, Fe or Cu) could be helpful in regard to favouring both the formation and consecutive condensation of acetaldehyde. Herein, Fe and Cu have been added to HAP by ion-exchange method, it could be interesting to investigate their addition by other synthesis methods (e.g., incipient wetness impregnation, wet impregnation).

When HAP exposes fewer basic sites, the catalytic activity and selectivity toward *n*-butanol decreases [59], but at the same time, acid sites are necessary to stabilize intermediate species during the aldol condensation of acetaldehyde as well as catalyse dehydration reactions. [58] Indeed, it is well known that a multifunctional catalysts is needed in order to selectively catalyse the Guerbet reaction. By taking thins in mind, it could be interesting to further exploit the capacity of the crystal lattice of the HAP to undergo big distortion by incorporating ions, both cations an anions with different sizes[272], and try to synthetize other hydroxyapatite-based materials modified with diverse ions and evaluate its performance into the optimized reaction system, with particular regard to minimize the aromatic compounds formation, that could be attributable to acid-catalysed reactions[267]. Since the Sr-exchanged exhibited the most promising performance (i.e., C-C bonds formation) in our reaction system and it was the one characterized by the lowest acidity/basicity ratio (i.e., A/B ratio: 9.4, as reported in Table 2), it could be interesting to further modify the HAP by increasing its basicity (i.e. lowering the A/B ratio).

4.2 Ethanol transformation over zirconium oxide - based catalysts – ITQ-UPV

During the research period spent in the laboratiories of the of the "Istituto de Teqnologia Quimica" (ITQ) of the "Universitat Politecnica de Valencia" (UPV), part of the work focused on the synthesis and characterization of zirconia-based catalysts. It is well-known that pure zirconia (ZrO_2) at atmospheric pressure exhibits in three different polymorphs (i.e., monoclinic, cubic and tetragonal) and that the monoclinic one is the thermodynamically stable. Depending upon the preparation method, the final crystal structure of ZrO_2 varies and it affects its surface properties and related catalytic features. In the present work, various zirconia samples have been prepared following different procedures (i.e., precipitation and hydrothermal synthesis, variation of pH and nature of the base used, metal dopant addition) studying the effects of various synthetics parameters on the resulting zirconium oxide through several characterization techniques. Then, their catalytic activity in the ethanol gas-phase transformation have been evaluated into a bench scale continuous flow quartz reactor using as feeding a mixture of 5% Ethanol in N_2.

4.2.1   Nomenclature

Zirconium oxide samples have been synthetized by hydrothermal or precipitation method and with or without the addition of a metal dopant (Ti or Y), in order to have an overview on the influence of this synthetic parameters on the resulting properties of the material. Then, the structural, textural and morphological properties of the synthetized catalysts will be correlated to their activity for the ethanol gas-phase conversion.

In order to facilitate the identification of the synthetized materials, a specific nomenclature has been designed. In the following scheme, the utilized nomenclature is explained, finally, an example is given.

MB-pH-DZO

M: synthesis methodology, which can be **P**recipitation or **H**ydrothermal.

B: base used in the synthesis. Could be **S**odium hydroxide (5 M solution), **A**mmonium hydroxide solution (25%w), or solid **U**rea.

The **pH** value is always indicated with its related figure since it is assumed to be a crucial parameter during the synthesis.

D: dopant element, which can be **T** for Ti, and **Y** for yttrium.

ZO is common for all the samples and indicates the ZrO_2.

For example: *HS-13-5TZO* is related to a catalyst synthetized by **H**ydrothermal method, using **S**odium hydroxide as base to reach a pH of synthesis of **13**. The sample contains a 5% molar amount of **T**i and a 95% of Zr.i

4.2.2   Catalyst synthesis and characterization

TG/DSC thermal analysis has been used to analyse the zirconium hydroxide precursor in order to identify the right calcination temperature to obtain zirconium oxide. Then it has been used to investigate the presence of carbon deposits on the spent catalyst's surface after performing the catalytic tests.

The studied catalysts have been synthetized with two different methods, as explained in detail the previous section (Section 3.2.4.1):

- Hydrothermal synthesis
- Precipitation method

The precursor obtained with one of these methods has been filtered, washed, dried overnight at 100°C and then calcined at 500°C for 2h with a 10ºC/min ramp.

The crystallographic phase of the obtained oxide is one of the most important parameters to study for understanding the catalytic, structural, and textural properties of the synthetized catalyst. The analysed samples at XRD can be divided in three main categories, according to the polymorph formed:

- Pure monoclinic phase
- Pure tetragonal phase
- Mixed phases

Several synthesis parameters have been investigated to evaluate their effect on the formed zirconia phase. To compare the obtained crystallographic phases, the tetragonal phase fraction (%t) has been derived from the XRD analysis of each synthetized sample. It was calculated from the ratio of the peak intensities according to the following equation [247]:

$$\%t = \frac{It(101)}{It(101) + 1.6\,Im(\overline{1}11)} \times 100$$

4.2.2.1 Calcination temperature study

Basically, the precursors obtained through the two hydrothermal and precipitation methods have been filtered, washed and dried overnight at 100°C. The dried materials obtained methods have been firstly analysed to select the proper calcination temperature. The calcination temperature is a crucial parameter when we want to produce metal oxides, the polymorphism of this kind of material can lead to the formation of a different polymorph depending on the calcination temperature. As a reference, two samples have been analysed, one for each synthesis method employed.
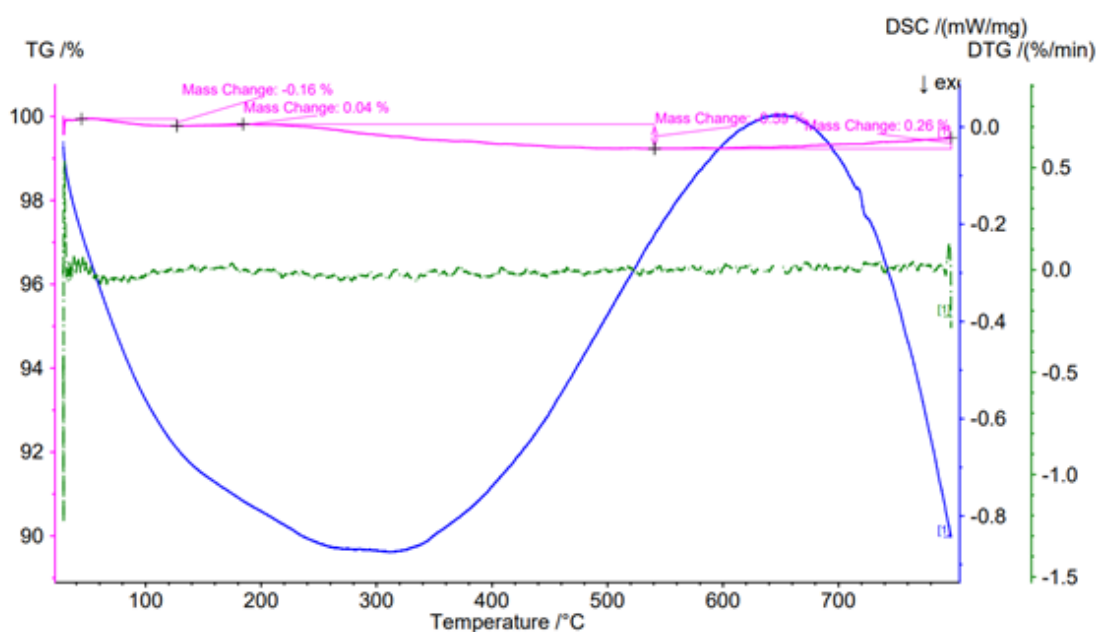
Figure 1 - TGA-DSC analysis performed over ZrO_2 sample before performing the final thermal treatment, synthetized via hydrothermal method with NaOH at pH = 13.

The first sample did not show a significant mass loss during the experiment. This data can suggest that a stable zirconia phase can be formed within the hydrothermal synthesis. To prove this hypothesis, an XRD analysis of the same sample has been carried out, it is reported in Figure 2.
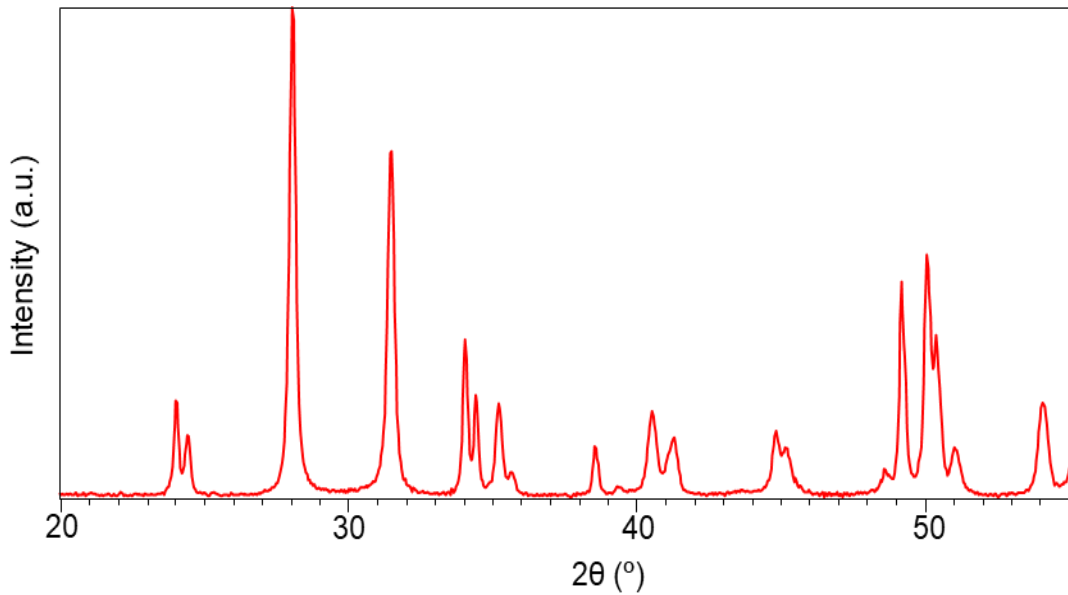
Figure 2 - XRD analysis performed over an uncalcined ZrO_2 sample, synthetized via hydrothermal method with NaOH at pH = 13.

The obtained diffractogram matches the one of Baddeleyite (monoclinic zirconia, Ref. code:00-024-1165), the most stable polimorph of zirconium oxide. This approach did not allow to select a proper calcination temperature since no mass loss were observed at TGA.

In the case of the zirconia sample prepared by precipitation, as in can be observed in Figure 3, the obtained material appeared amorphous. The TGA anaylisis performed over this sample is depicted in Figure 23, were some mass losses possibly related to phase transformation are observed.
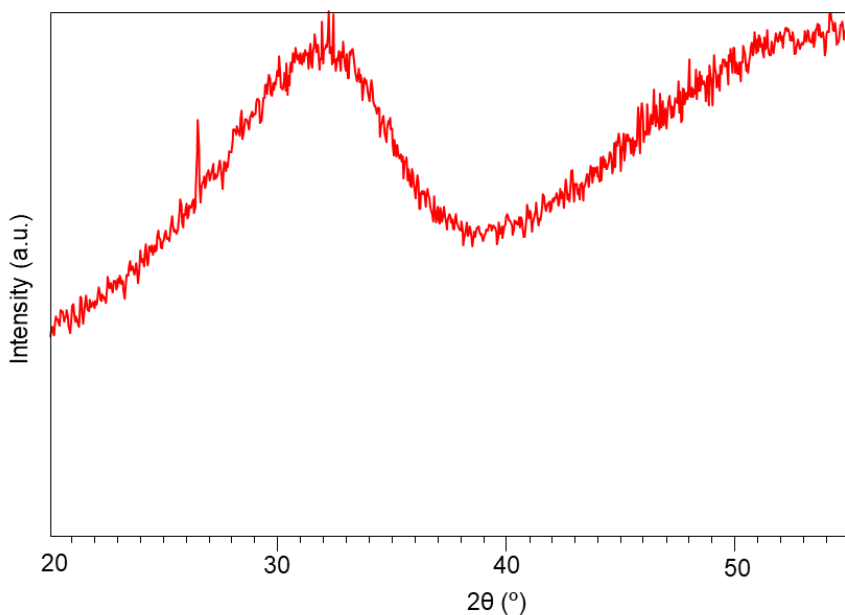
Figure 3 XRD analysis performed over an uncalcined ZrO_2 sample, synthetised via precipitation method with NH_4OH 25%w water solution at pH = 7,6.
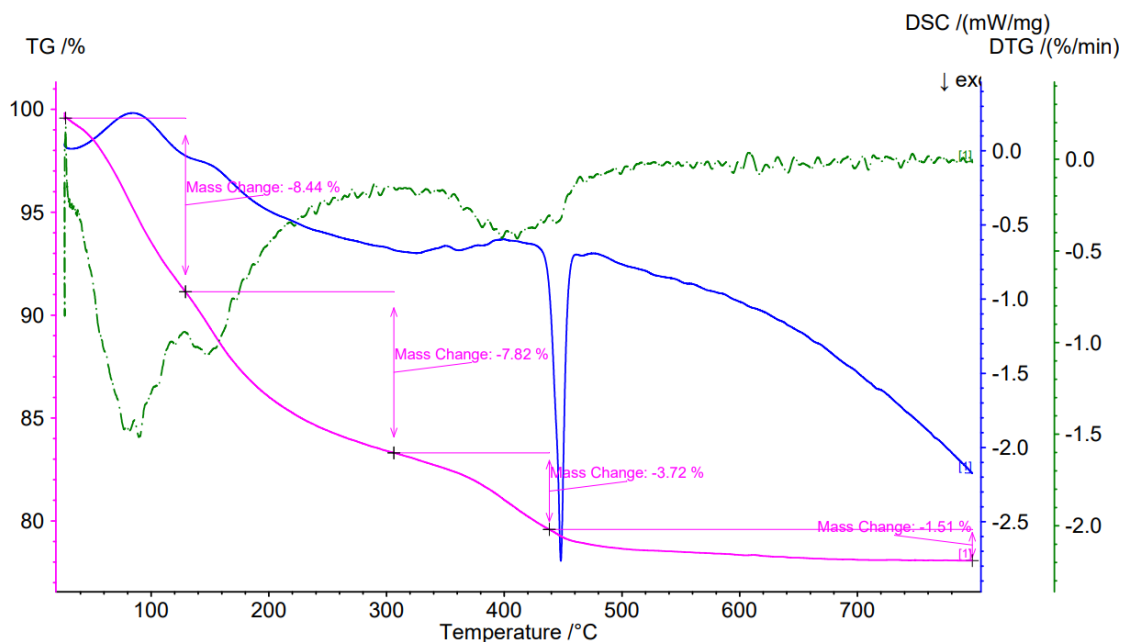
Figure 4   - TGA-DSC analysis performed over an uncalcined ZrO2 sample, synthetized via precipitation method with NH4OH 25%w water solution at pH = 7,6.

The TG profile depicted in Fig. 4 shows that the phase transition probably happens around 450°C since an endothermic peak observable at the DSC signal is present. The calcination temperature selected in this work for all the zirconia samples was 500°C.

4.2.2.2 Zirconia phase study- pH and synthesis method effects

The value of pH is one of the most important parameters when a metal oxide catalyst is synthetized, both the [H$^+$] and [OH$^-$] strongly affect the properties of the forming material[273]. In the synthesis performed to prepare the zirconia samples, the pH value was varied from 7,6 to 13 using 3 M NaOH, 25%w NH$_4$OH solution or urea. In Figure 5 are reported the XRD patterns obtained of the synthetized samples. In particular, the XRD patters of the samples obtained by hydrothermal method varying the pH (i.e., 7.5, 9.5, 10, 13) with NaOH (HS-7.5, HS-10 and HS-13) and with NH$_4$OH (HA-7,5 and HA-9.5) as well as the ones synthetized by precipitation method using NH$_4$OH (PA-7.5 and PA-9.5), urea (PU-8.5, PU-9.5 and PU-13) and NaOH (PS-13) are depicted. The samples matched with zirconia tetragonal t-ZrO$_2$ (Ref. code: 01-088-1007) or the zirconia monoclinic m-ZrO$_2$ (Ref. code:00-024-1165), depending on the synthesis method; most of them showed to be contain both phases. y. The presence of tetragonal phase along with monoclinic phase indicates the crystallographic rearrangement in ZrO2 due to the oxygen vacancies. [274] In Fig. 5 the reflections of the two phases employed to compute the tetragonal fraction are highlighted (i.e., $m(\bar{1}11)$ for the monoclinic phase and $t(101)$ for the tetragonal).
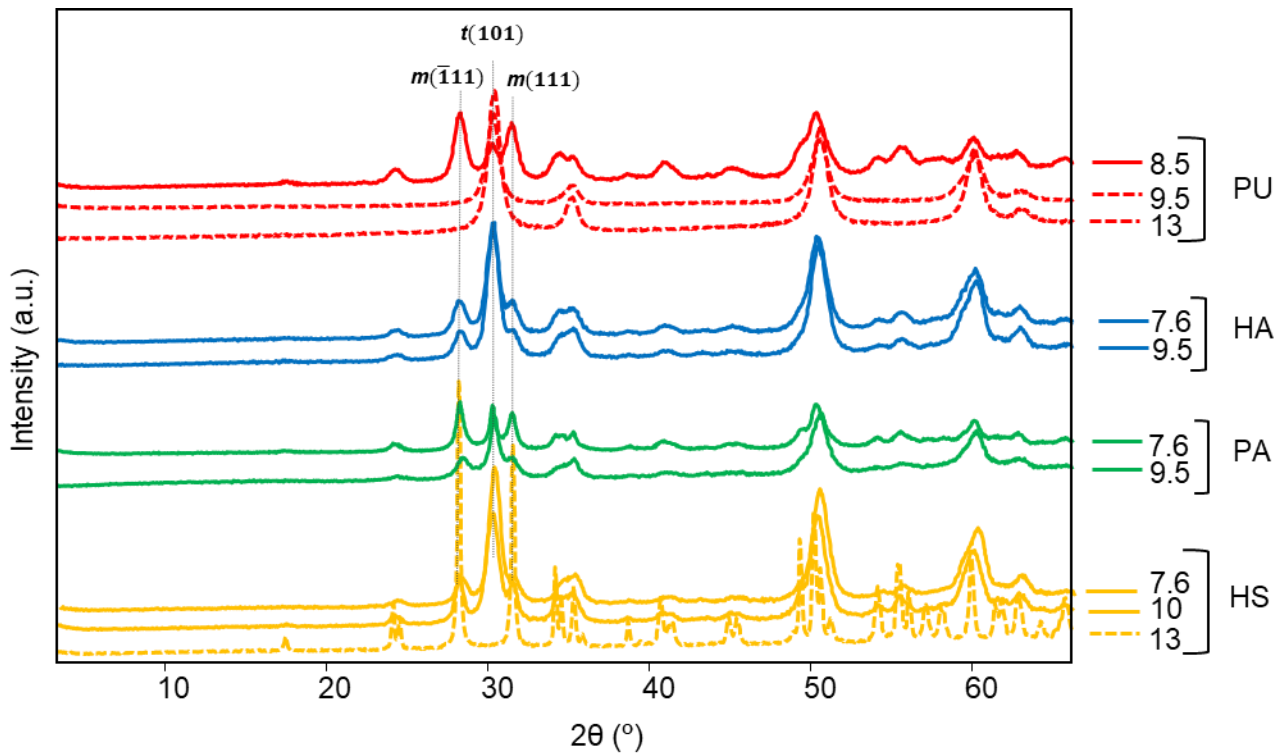
Figure 5 XRD patterns of the zirconia samples prepared by precipitation (P) or hydrothermal (H) methods, in the right the figures represents the pH values employed. HS: Hydrothermal synthesis using NaOH as base (yellow), HA: hydrothermal synthesis using NH4OH as base (blue), PA: precipitation using NH4OH as base (green), PU: precipitation using urea as base (red), and PS: precipitation using NaOH as base (X). The mixed phases are plotted with solid lines, the pure phases are plotted with dotted lines.

In the following graph reported in Figure 6, the pH influence on the tetragonal fraction (%) formation is showed related to the different synthesis methods and bases used.
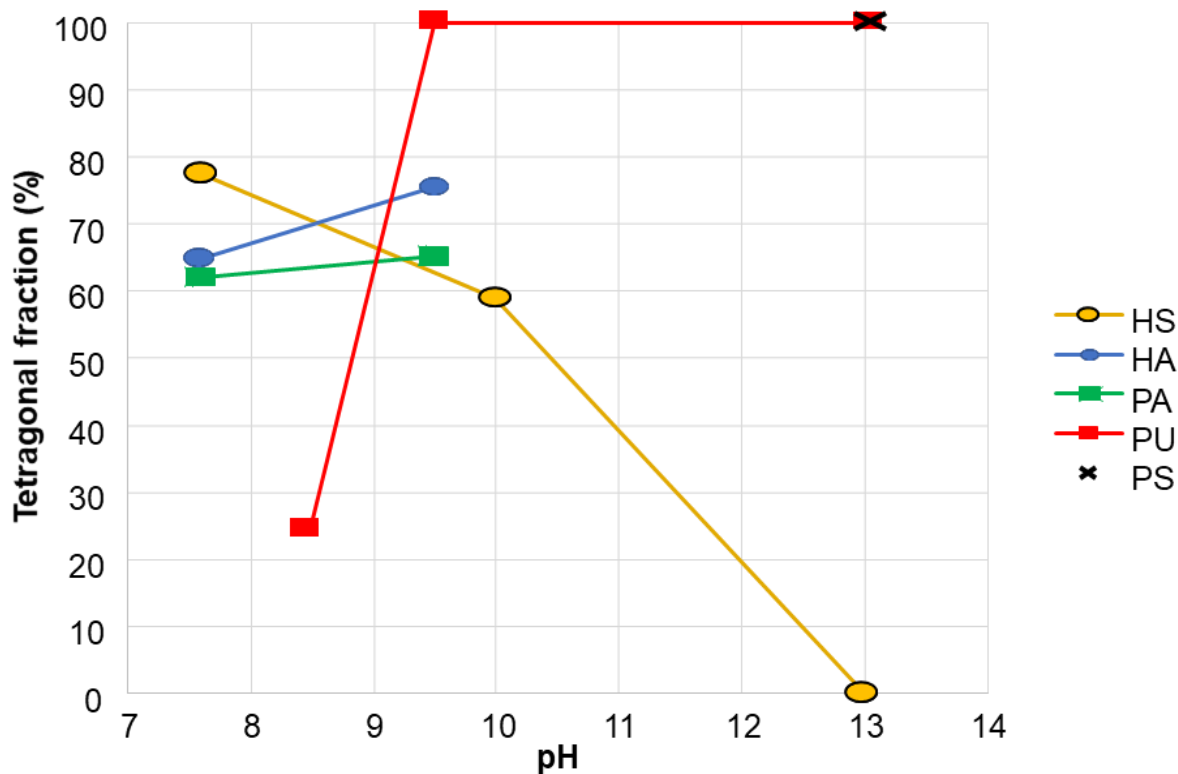
Figure 6   pH influence on ZrO2 samples tetragonal fraction. HS: Hydrothermal synthesis using NaOH as base (yellow), HA: hydrothermal synthesis using NH4OH as base (blue), PA: precipitation using NH4OH as base (green), PU: precipitation using urea as base (red), and PS: precipitation using NaOH as base (X).

As in can be observed into Figure 5 and Figure 6, the only case in which a pure monoclinic zirconia sample (0% tetragonal fraction) was formed is the HS-13-ZO, showed in yellow in the graph. The hydrothermal synthesis method usually favours an overall free energy decrease of the system since the samples is aging for a long time in its mother liquor. The formation of the most stable phase, the monoclinic one, can be explained according to this concept. By the way, with lower pH values, the monoclinic phase is no longer the predominant one in the formed solid. At a pH value of 7.6, the monoclinic phase obtained by hydrothermal treatment is even lower than the one obtained with the precipitation method. Using ammonium hydroxide as a base there are not relevant differences between the hydrothermal and the precipitation method, leading to the formation of mixed phases containing samples slightly more tetragonal than monoclinic. When urea was used as a basic agent, a pure tetragonal phase was formed at pH values of 13 and 9.5, while a mixed phase solid was obtained at a pH value of 8.5, with a tetragonal fraction presence of 25%. Finally, a precipitation synthesis with sodium hydroxide at a pH value of 13 was performed, obtaining a pure tetragonal sample. This data is the opposite respect to the corresponding one synthetized with the hydrothermal method. These data show that for pH values between 7 and 10 there is not a big difference between the hydrothermal method and the precipitation one in terms of phase formation. At a pH of 13 the

synthesis method strongly affects the phase formation; the precipitation and the hydrothermal method show diametrically opposite results in terms of phase formation.

4.2.2.3 Zirconia phase study- Dopant effect

To evaluate the effect of dopant addition in the zirconia structure, a 5% molar amount of the doping element (Ti and Y) has been added to the precursors solution as previously described in Section 3.2.4.1. Figure 7 and Figure 8 show the effect of dopant addition on the nature of zirconia phase when using two different synthesis methods and considering two different dopants, i.e. titanium or yttrium. Since while synthetizing zirconia via hydrothermal method at pH 13, pure monoclinic phase has been obtained, the dopant addition has been performed in those conditions in order to evaluate a possible tetragonal phase stabilization. Two methods have been employed to study the effect of the metal dopant effect: one via hydrothermal method at a pH value of 13 using sodium hydroxide as base and one by precipitation synthesis at a pH value of 7.6 using ammonium hydroxide as a base. Figure 7 reports the XRD patterns of the obtained samples, an increase of the tetragonal phase presence over the monoclinic can be noticed.
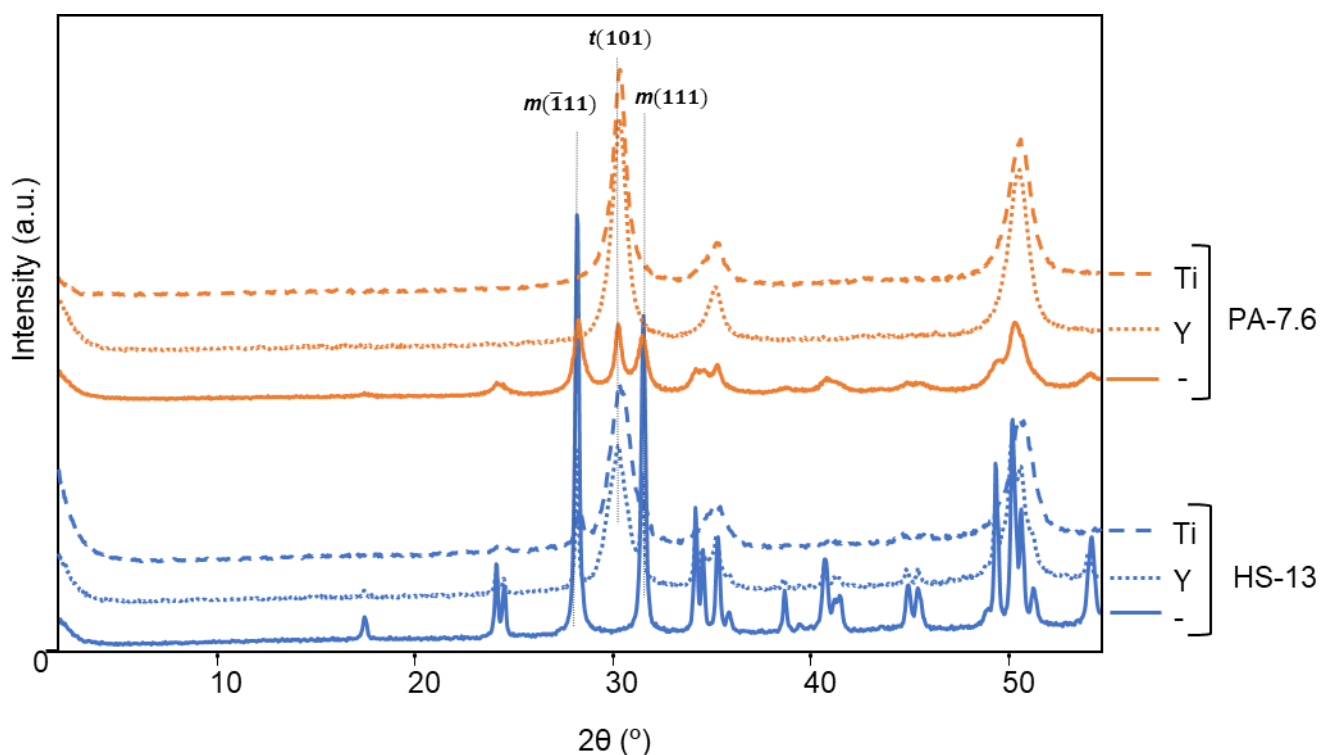
Figure 7 XRD patterns of the zirconia samples prepared by precipitation (PA) or hydrothermal (HS) methods, effect of the transition metal addition. HS-13: Hydrothermal synthesis using NaOH as base (at pH 13, doped with Ti or Y (blue lines). PA-7.6: hydrothermal synthesis using NH_4OH as base at pH 7.6, doped with Ti or Y. (orange).
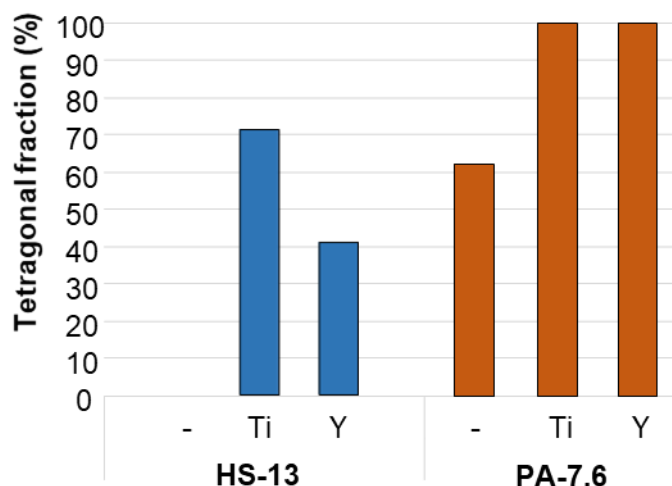
Figure 8   Dopant (Ti or Y) addition influence on the zirconia phase (tetragonal fraction %), on HS-13 (hydrothermal method at pH 13 with NaOH, blue) and PA-7,6 (precipitation at pH=7,6 with ammonium hydroxide, orange). H: hydrothermal, P: precipitation.

The precipitation serie, plotted in orange, showed that a dopant addition might favour the tetragonal phase formation. In particular, all the doped zirconias synthetized via precipitation method (PA-7,6), appeared purely tetragonal according to the XRD analysis (summarized in Fig. 8 and showed in Figure 7). As fasr as the hydrothermal synthesis (HS-13) is concernerd, it possible to draw some conclusions. With the absence of a dopant, no tetragonal phase formation was observed while after dopant addition, a remarkable increase of tetragonal phase has been observed. Accordingly, a dopant addition favoured the tetragonal phase stabilization; in particular when titanium is used, since high tetragonal fraction has been obtained even when the sythesis was performed by hydrothermal method (71%).

4.2.2.4 Textural analysis, nitrogen adsorption isotherms (BET)

BET surface area is a crucial parameter in heterogeneous catalysis. When a gas phase reaction on a solid catalyst occurs, just the surface atoms of the catalyst are involved in the reaction kinetics.[275] For this reason, a measurement of the surface area of the sample can give an important information about its activity in the studied process. The collected data wants to propose a correlation between the BET surface area and the zirconia phase obtained in the analysed sample. In the following graph (Fig. 9), the BET surface area is plotted against the tetragonal fraction (%t) obtained by XRD experiments; Table 1 resumes of the collected results.
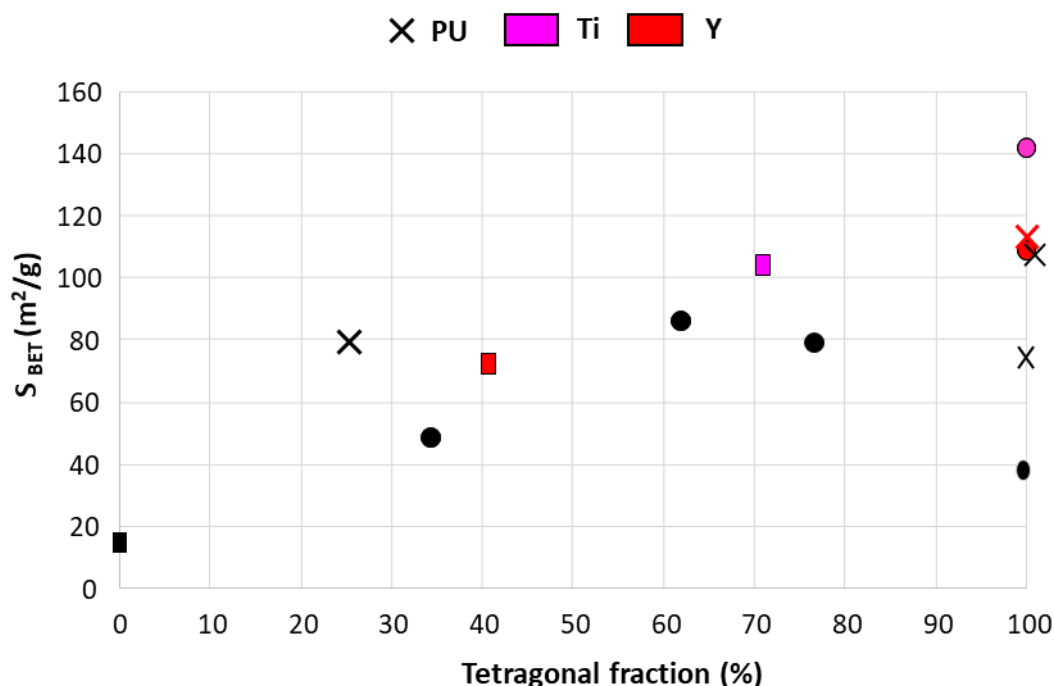
Figure 9   Tetragonal fraction influence on the BET surface area – □ samples prepared via precipitation method(●) or hydrothermal (□), with and without a metal dopant. X: precipitation with Urea; Black: pure zirconia sample; Purple: Ti; Red: Y;.

As stated before, the presence of a metal dopant into the zirconia structure stabilized the tetragonal phase. Here is possible to notice a correlation between the tetragonal fraction and the surface area. From a general point of view, the BET surface area seems to increase with the tetragonal fraction within the sample's structure. All the doped catalysts, which have a higher tetragonal fraction than their corresponding pure zirconia samples, appears to have a higher surface area. This is particularly true when precipitation method is used to synthetized the zirconia samples. The titanium doped zirconia sample synthetized via precipitation employing NH_4OH to produce a pH of 7.6 (PA-7,6-TZO) is the synthetized catalyst with the highest surface area, around 141 m^2/g. While the pure zirconia catalyst synthetized by hydrothermal method with NaOH at pH=13 (HS-13-ZO) presents the lower value of BET surface area (13 m^2/g). These data will be useful when the catalytic behaviour of the synthetized material will be studied.

Table 1. *BET surface data (S_{BET} [m^2/g]) and tetragonal fraction (%t) of the zirconia samples. Synthetized by hydrothermal (HT) or precipitation (Ppt) methods, employing different of pH values in the range:7.6-13, and by adding a transition metal as dopant (Ti or Y).*

Method	Base	pH	Dopant	%t	S_{BET} [m^2/g]
HT	NaOH	13	-	0	13
Ppt	Urea	8.5	-	25	80
Ppt	NH4OH	7.6	-	34	49
HT	NaOH	13	Y	41	71
Ppt	NH4OH	7.6	-	62	86
HT	NH4OH	7.6	-	65	71
Ppt	NH_4OH	9.5	-	65	80
HT	NaOH	13	Ti	71	104
HT	NH_4OH	9.5	-	75	81
HT	NaOH	7.6	-	77	69
Ppt	NaOH	13	-	100	37
Ppt	Urea	13	-	100	76
PPt	Urea	9.5	-	100	108
Ppt	NH4OH	7.6	Y	100	109
Ppt	Urea	8.5	Y	100	113
Ppt	NH4OH	7.6	Ti	100	142

4.2.2.5 Raman spectroscopy

Assignment of cubic and tetragonal structures, based solely on the X-ray diffraction analysis, can be misleading because the cubic and tetragonal structures have very similar lattice parameters (i.e, a_0 = 0.5124 nm for cubic and a_0 =0.5094 nm and c_0 = 0.5177 nm for tetragonal structures).[276] Figure 10 reports the XRD patterns and the Raman profiles of the three zirconia polymorphs, where it can be observed that the reflections of tetragonal and cubic phases overlaps.[274] While cubic structure presents only single peaks, the tetragonal one is characterized by of the presence of the splitting of the diffraction peaks. Accordingly, they could be distinguished. [276] Nevertheless, normally a significant line broadening obscures any clear distinction between the tetragonal and cubic polymorphs of ZrO_2.[274] The XRD diffractograms of the zirconia polymorphs are shown in Fig.10A.
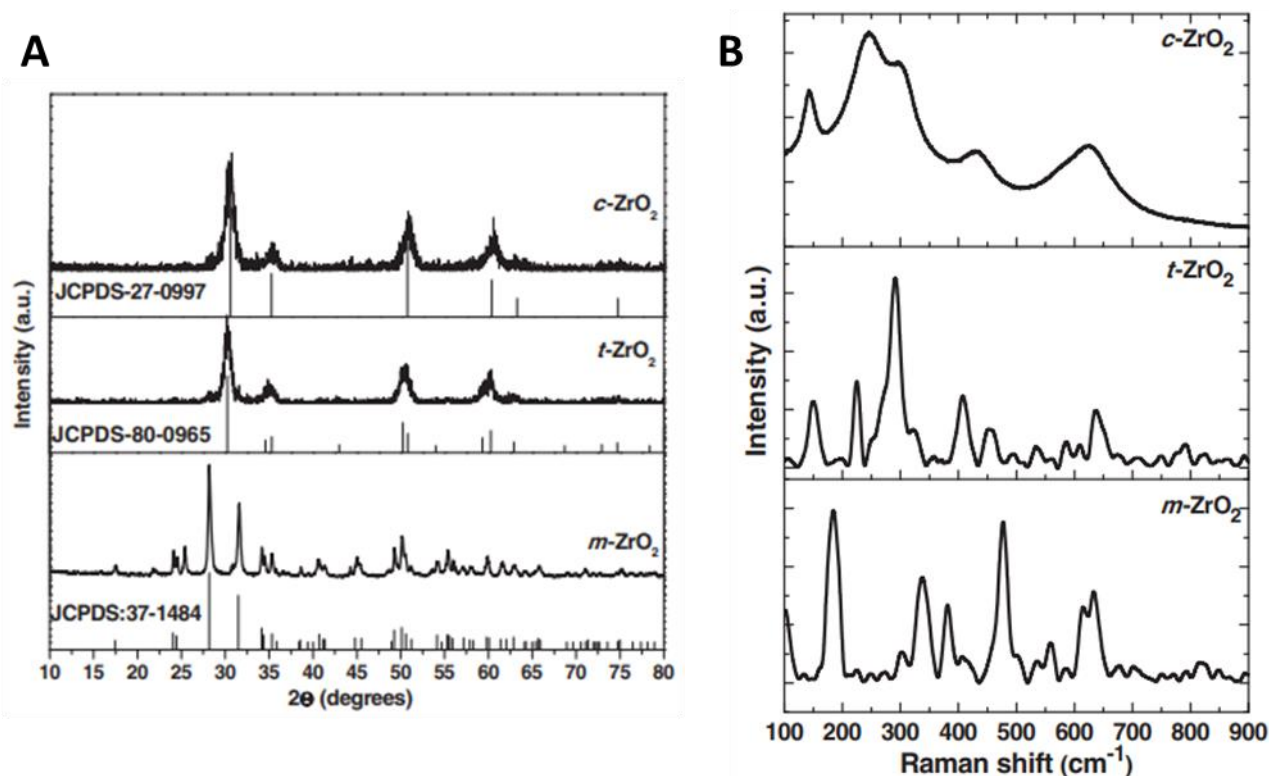
Figure 10   A) XRD Patterns of the zirconia polymorphs, B) Raman spectra of the zirconia polymorphs.[274]

In contrast, the monoclinic, tetragonal, and cubic zirconia structures can be readily distinguished from one another by Raman spectroscopy, as it can be observed in the representative spectra in Figure 10B. The monoclinic phase is characterized by the presence of a doublet a 181-190 cm⁻¹, while the tetragonal phase can be confirmed by the presence of peaks at 147 and 265 cm⁻¹. In addition, the spectrum of tetragonal phase presents relatively sharp peaks even at around 326, 474, 616 and 646 cm⁻¹ . The Raman spectrum for c-ZrO_2 is characterized by a narrow band at 145 cm⁻¹ and broad bands centred at 246, 301, 436, and 625 cm−1. The Raman peak at 149 cm⁻¹ is common for both the phases while cubic ZrO_2 presents a broad band between 530-670 cm⁻¹ and its spectra is poorly defined due to the distorted oxygen sublattice.[274,277]

In order to confirm the crystalline structure of the synthetized samples, some of them (i.e., PA-7.6-ZO, PA-7.6-TZO, PA-7.6-YZO, HS-10-ZO and HS-13-ZO) have been analysed by Raman spectroscopy, the results are reported in Figure 11.The Raman spectra obtained on the zirconia sample synthesised by hydrothermal method at pH=13 (HS-13-ZO sample, purple line) can be attributed to a monoclinic phase, in accordance with the data obtained from the XRD analysis.
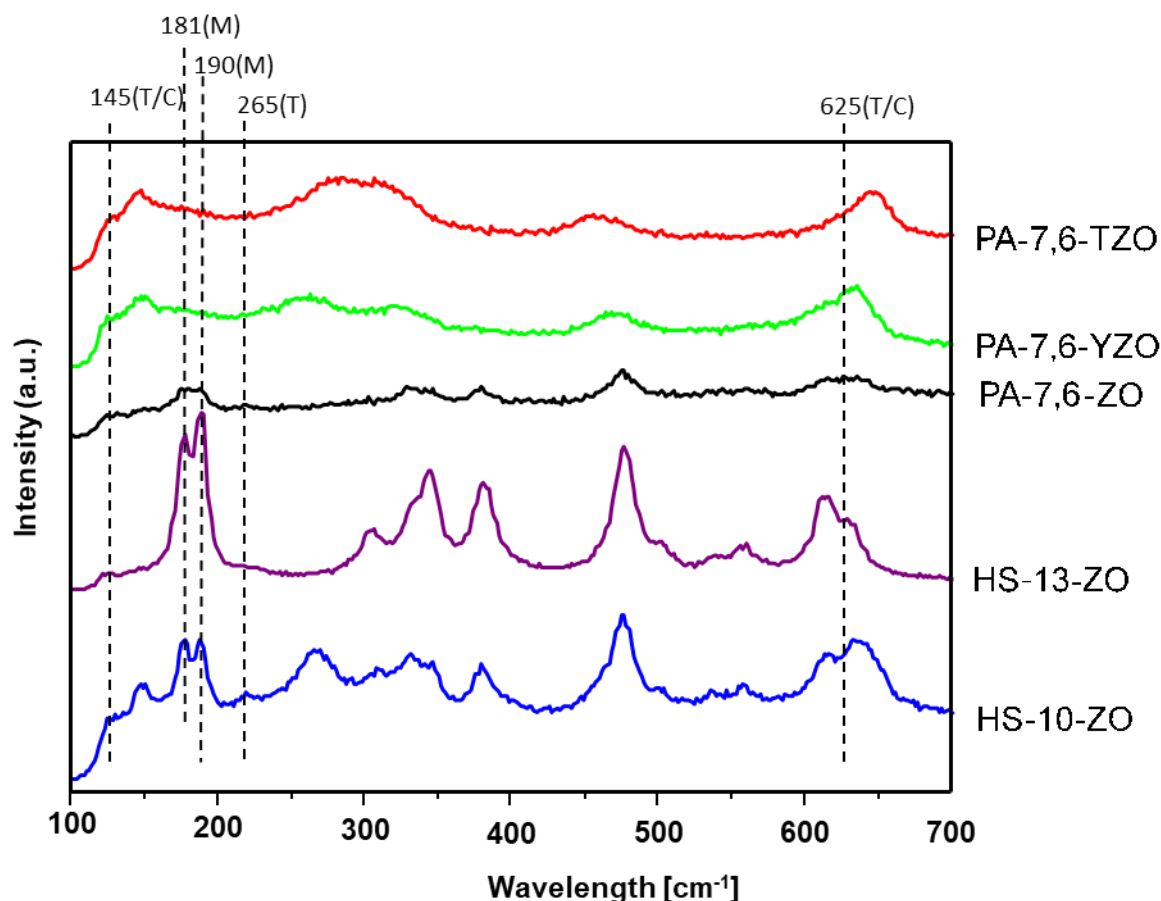
Figure 11 Raman spectra of the synthetized catalysts. **PA-7,6-YZO**: yttrium-doped zirconia synthetized by precipitation at pH 7.6 with NH₄OH; **HS-13-ZO**: zirconia synthetized by hydrothermal method at pH 13 with 5 M NaOH; **PA-7,6-TZO**: titanium-doped zirconia synthetized by precipitation at pH 7.6 with NH₄OH; **HS-10-ZO**: zirconia synthetized by hydrothermal method at pH 10 with 5 M NaOH; **PA-7,6-ZO**: zirconia synthetized by precipitation at pH 7.6 with NH₄OH.

The titanium and yttrium doped zirconia samples obtained by the precipitation method (PA-7,6-TZO, red line, PA-7,6-YZO, green line) which have been considered to be purely tetragonal from the XRD analysis, showed a Raman spectra characterized by broad peaks, suggesting that they are not purely tetragonal, while probably a mixture of tetragonal and cubic phases. The zirconia sample obtained via hydrothermal method at pH=10 (HS-10-ZO, blue line) and the precipitated one at pH=7.6 (PA-7,6-ZO, black line), showed a combination between the three polymorphs, even ithough the one obtained through HS-10-ZO showed a predominance of the monoclinic one, in accordanrce with the results obtained through XRD analysis.

Overall, the presence of the cubic phase has been observed, although it is not possible to accertain in which amount. Even though in this study the zirconia samples composition has been qualified considering only the metastable tetragonal phase, it is plausible that a combination of both tetragonal and cubic phases is incorporated in most of the samples. In order to distinguish between the

tetragonal and cubic structures of zirconia, other analysis are needed (i.e., synchrotron radiation source for X-ray diffraction). [276]

4.2.2.6 Sodium presence investigation in HS catalysts

Only one sample showed a pure monoclinic phase; that is the one synthetized by hydrothermal route at pH= 13 using NaOH as base (HS-13-ZO). To give an explanation to this data, it was proposed that the sodium cation present in the utilised base (i.e., sodium hydroxide) could have entered into the zirconia structure and affected the crystal lattice composition. To investigate its presence, two different characterization method have been used on two different catalysts. ICP and SEM-EDX were performed on pure monoclinic HS-13-ZO and another catalyst synthetized with the same method but with a lower value of pH (i.e. 10), HS-10-ZO. The main difference between these two catalysts is the tetragonal fraction in the solid, which increased from 0% in the sample synthetized at a pH value of 13, to 59% in the sample synthetized at pH=10, and so by using less NaOH. SEM-EDX analysis provided a picture of the analysed samples in which the two specimens showed the presence of Na. The sodium weight percentage was estimated to be between 0.8 and 2.2 % by SEM-EDX analysis and 3.1% by ICP analysis in sample HS-10-ZO. On the other hand, sample HS-13-ZO showed a sodium weight percentage between 1.2 and 1.8 % while according to ICP analysis it was around 2.6%.

Since sodium is present in both the samples while the tetragonal fraction of the two materials is largely different, it was assumed that sodium is not promoting the monoclinic phase formation in pure zirconia samples.

4.2.2.7 Temperature programmed desorption (TPD)

The active site nature is critical in heterogeneous catalysis, several techniques allow to study the interaction of the catalyst's surface with probe molecules in gas phase which give an idea about the number and the strength of active site for that kind of interaction. Since this work mainly focuses on acid catalysis, several temperature programmed desorption of ammonia (TPD-NH$_3$) analyses were carried out on the pure and doped zirconia samples. Generally, the solid acid sites can be classified according to their acid strength determined using the temperature of NH3 desorption into three types: weak (150–300 °C), moderate (300–450°C) and strong (450–650 °C) acid sites. [137] Recorded spectra may be further deconvoluted by a Gaussian peak fitting method into separate peaks to be then attributed to different strength acid sites. In Table2, the acidity of the samples, expressed as ammonia desorbed by weight of catalyst [μmolNH$_3$/g$_{CAT}$] or surface area of the catalyst [μmolNH$_3$/m$^2_{CAT}$] of adsorbed ammonia is showed together with the catalyst's specific surface area.

Table 2. *TPD adsorbed ammonia and specific surface area of the analysed catalysts   HS-13-ZO: zirconia synthetized by hydrothermal method at pH 13 with 5 M NaOH; HS-13-TZO: titanium-doped zirconia synthetized by hydrothermal method at pH 13 with 5 M NaOH; HS-13-YZO: yttrium-doped zirconia synthetized by hydrothermal method at pH 13 with 5 M NaOH; PA-7,6-ZO: zirconia synthetized by precipitation at pH 7.6 with NH4OH; PA-7,6-TZO: titanium-doped zirconia synthetized by precipitation at pH 7.6 with NH4OH; PU-8,5-ZO: zirconia synthetized by precipitation at pH 8,5 with urea.*

Catalyst Code	BET [m^2/g]	ACIDITY	
		[$\mu molNH_3/m^2_{CAT}$]	[$\mu molNH_3/g_{CAT}$]
HS-13-ZO	13	0.1	1.2
HS-13-TZO	104	0.2	22
HS-13-YZO	71	0.0	0
PA-7,6-ZO	76	1.5	116
PA-7,6-TZO	142	1.7	236
PU-8,5-ZO	80	1.4	114

The acidity of three pure zirconia samples is compared in Fig. 12A by plotting the trend of the ion current signal of the mass 15 m/Z detected with increasing temperature in the desorption phase of the analysis. The zirconia sample synthetized by hydrothermal synthesis at pH 13 with 5 M NaOH (HS-13-ZO) did not show great acidity, maybe because of its low surface area of 13 m^2/g as reported in Table 2. Both the samples prepared by precipitation, PA-7,6-ZO and PU-8,5-ZO, showed ammonia desorption in the temperature range from 100°C to 400°C, corresponding to weak and medium strength cadi sites. The NH_3 desorption profiles of these two samples appeared to be quite similar.
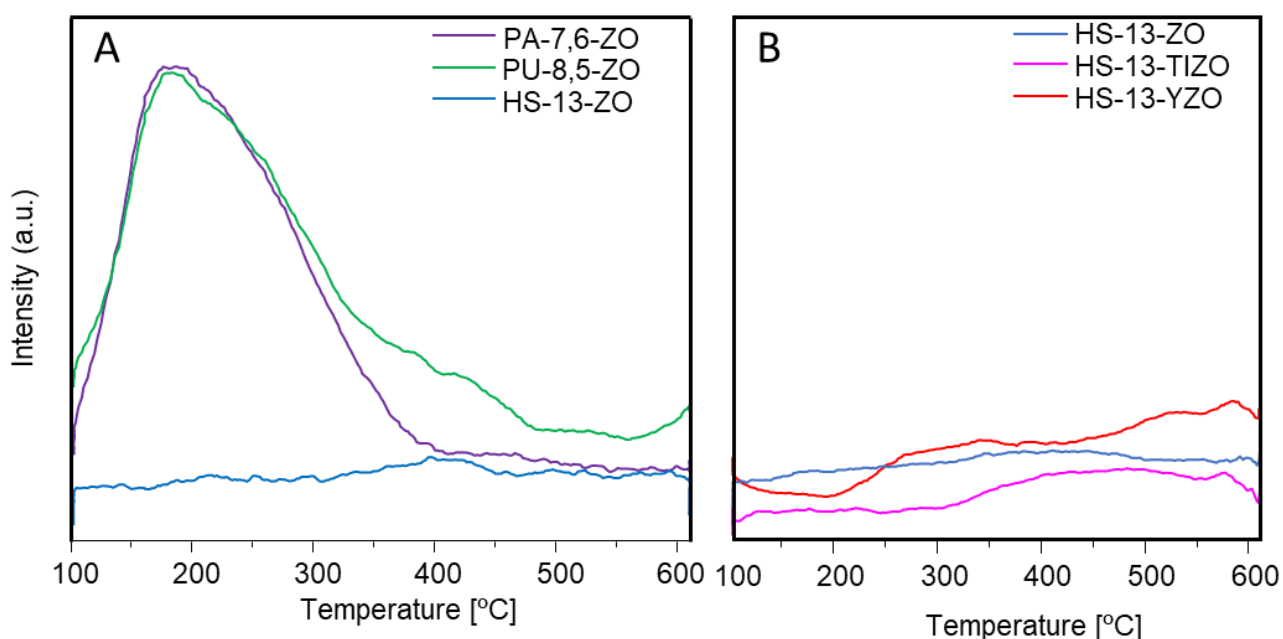
Figure 12 TPD-NH$_3$ over pure zirconia samples. A) Zirconia samples. HS-13-ZO: zirconia synthetized by hydrothermal method at pH 13 with 5 M NaOH; PA-7,6-ZO: zirconia synthetized by precipitation at pH 7.6 with NH$_4$OH; PU-8,5-ZO: zirconia synthetized by precipitation at pH 8,5 with urea. B) HT-Zirconia samples doped. HS-13-TZO: titanium-doped zirconia synthetized by hydrothermal method at pH 13 with 5 M NaOH; HS-13-YZO: yttrium-doped zirconia synthetized by hydrothermal method at pH 13 with 5 M NaOH.

The effect of a dopant addition on the acid properties of zirconia samples obtained by hydrothermal method is depicted in Fig. 12B The Ti-, Y- doped and the pure zirconia synthetized by hydrothermal method at pH 13 with 5 M NaOH did not show any peak related to ammonia desorption.

The effect of Ti doping addition to zirconia samples is shown in Fig. 13. Both the doped and the pure catalyst synthetized by hydrothermal method did not show ammonia desorption peaks. While when the two catalysts synthetized by precipitation method are compared, the effect of the titanium doping seemed to be important. The Ti-doped zirconia synthetized by precipitation appeared to have more and stronger acid sites respect to the pure one. In particular, it seems that some new and stronger acid sites were formed, its TPD-NH$_3$ desorption profile showed a broad desorption band in the temperature range 120-450°C, which indicates the presence of weak, medium-strength and strong acidic sites. In particular, in addition to the weak and medium strength acid sites observed in both the two sample synthetized by precipitation at pH 7,6, new stronger acid sites that desorbed at around 300ºC have been observed in the sample doped with titanium.
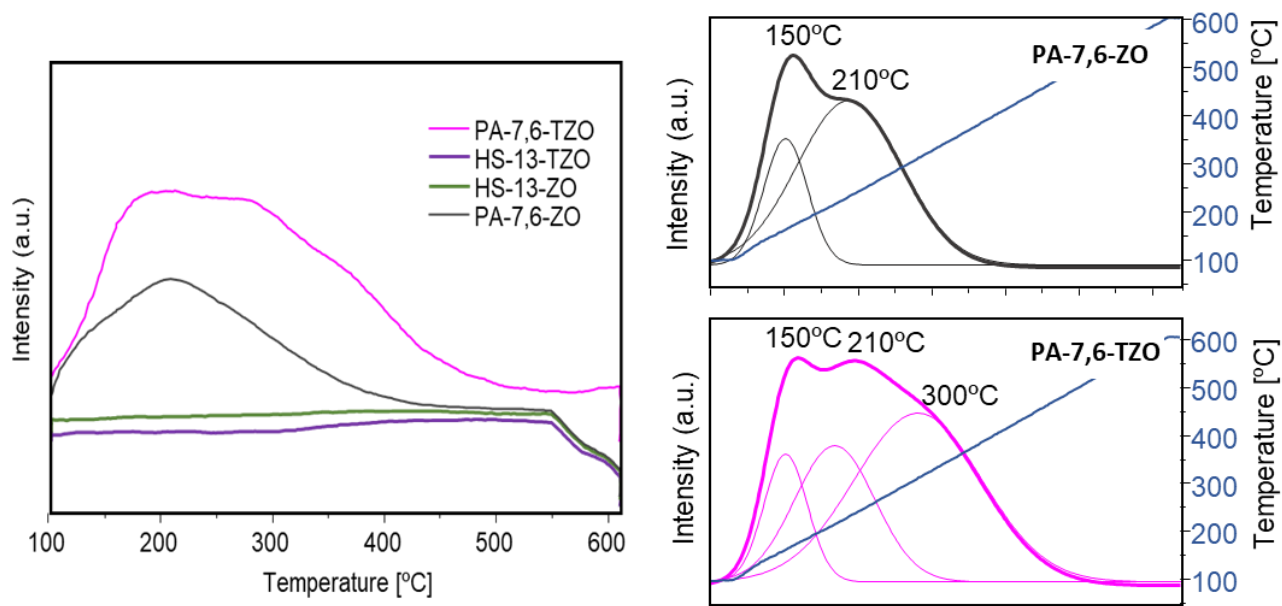
Figure 13   TPD-NH₃ over pure and Ti-doped zirconia samples. HS-13-ZO: zirconia synthetized by hydrothermal method at pH 13 with 5 M NaOH; HS-13-TZO: titanium-doped zirconia synthetized by hydrothermal method at pH 13 with 5 M NaOH; PA-7,6-ZO: zirconia synthetized by precipitation at pH 7.6 with NH₄OH; PA-7,6-TZO: titanium-doped zirconia synthetized by precipitation at pH 7.6 with NH₄OH.On the right, the signals of PA-7,6-ZO and PA-7,6-TZO deconvoluted.

4.2.3   Reactivity tests

Several catalytic tests have been performed to evaluate the catalytic activity of the synthetized samples in the gas-phase ethanol conversion. Before the reactivity tests, the synthetized catalysts have been shaped into 0,25-0,6 mm pellets. The pelletized catalyst has been loaded on the reactor's bed where the temperature was constantly controlled by a thermocouple. In this chapter, all the catalysts behaviour will be compared in order to give an overview on the effect of the main synthesis parameters such as the synthesis method, tetragonal fraction, and dopant presence. The pure and doped zirconia catalyst were tested at different temperatures and different contact times.

The catalytic tests on the supports have been performed in these operative conditions:

- $Feed = 5\%\ mol_{EtOH}\ in\ N_2$
- $P = 1\ atm$
- $T\ =\ 300 - 400\ °C$
- $\dot{V} = 21 - 22\ mL/min$ @ RT
- W/F= $0,78 - 1.93\ [\frac{g_{cat}}{mL_{tot}} \times s\ ]$

Most of the synthetized catalyst have been tested in ethanol transformation reaction. In this chapter, the reactivity results will be compared between the catalyst synthetized with the same method, with

different elemental composition. Three temperatures have been selected to study the catalytic performance at low, medium, and high conversion. The first reaction temperature was selected as 300°C, then 350 °C, and finally 400°C. In this chapter, several graphs are presented. All the synthetized catalysts will be compared in term of ethanol conversion (X) and different products selectivities (S_i) gathering them by the reaction temperature as well as the synthesis method. In Table 3, the tested catalysts are reported, as well as their BET surface area and their tetragonal fraction reference.

Table 3. *Zirconia samples tested into the reaction systems together with their characteristics (i.e., surface area S_{BET}, tetragonal fraction (%t) and acidity ($\mu mol NH_3/m^2_{CAT}$)). <u>Precipitation catalysts:</u> PA-7,6-ZO: zirconia synthetized by precipitation at pH 7.6 with NH_4OH; PA-7,6-TZO: titanium-doped zirconia synthetized by precipitation at pH 7.6 with NH_4OH; PA-7,6-YZO: yttrium-doped zirconia synthetized by precipitation at pH 7.6 with NH_4OH; PU-8,5-ZO: zirconia synthetized by precipitation at pH 8,5 with urea; PU-8,5-TZO: titanium-doped zirconia synthetized by precipitation at pH 8,5 with urea; PU-8,5-YZO: yttrium-doped zirconia synthetized by precipitation at pH 8,5 with urea. <u>Hydrothermal catalysts</u>: HS-13-ZO: zirconia synthetized by hydrothermal method at pH 13 with 5 M NaOH; HS-13-TZO: titanium-doped zirconia synthetized by hydrothermal method at pH 13 with 5 M NaOH; HS-13-YZO: yttrium-doped zirconia synthetized by hydrothermal method at pH 13 with 5 M NaOH.*

	Precipitation Catalysts			Hydrothermal catalysts			
Catalyst Code	S_{BET} [m^2/g]	t%	Acidity [$\mu mol_{NH_3}/m^2_{CAT}$]	Catalyst Code	S_{BET} [m^2/g]	t%	Acidity [$\mu mol_{NH_3}/m^2_{CAT}$]
PA-7,6-ZO	86	62	1.5	HS-13-ZO	13	0	0.1
PA-7,6-TZO	148	100	1.7	HS-13-TZO	104	71	0.2
PA-7,6-YZO	109	100		HS-13-YZO	71	41	0
PU-8,5-ZO	80	25	1.4				
PU-8,5-TZO	109	100					
PU-8,5-YZO	113	100					

4.2.3.1 Reaction temperature effect

4.2.3.1.1 Precipitation catalysts

In general, the presented values of ethanol conversion (X) and product yields (Y_i) are the mean value obtained by a series of five GC-online analysis obtained in 1.83 hours of time on stream. This was possible since the catalysts appeared stable in this time interval, showing constant values of the previously mentioned parameters. The catalyst stability will be described later in section 4.2.3.2.

Figure 14 depicts the catalytic performance of the zirconia samples obtained via precipitation method (Precipitation catalysts in Table 3) obtained while working at a reaction temperature of 300ºC.
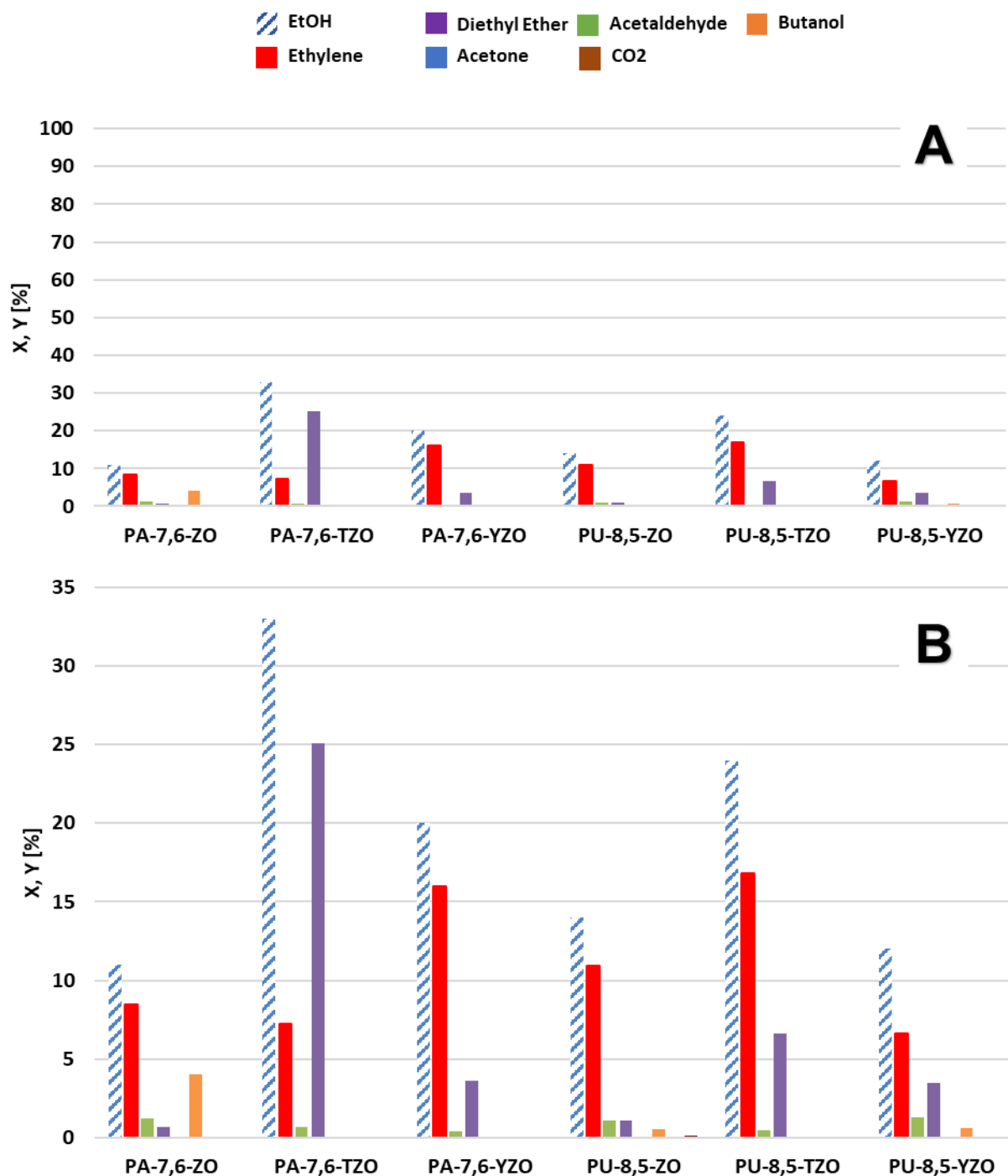
Figure 14   A) Ethanol conversion (X) and main products yields (Y) obtained from the catalytic tests performed over the catalysts obtained by precipitation. Reaction conditions: T: **300°C**; p: 1 atm; EtOH 5%mol in N_2, VTOT= 20 mL/min; W/F= 0,78 g·s/mL. B) The same results with narrowed y axis.

The titanium-doped zirconia obtained at pH 7.6 with NH_4OH (PA-7,6-TZO) shows diethyl ether as major product, the ethanol dehydration product[278]. All the other catalysts obtained via precipitation,

showed ethylene, the other dehydration product of ethanol, as major product. This difference can be explained with the nature of the acid active sites of the Ti-doped sample. As previously described in section 4.2.2.7, the Ti-doped zirconia obtained by precipitation at pH 7,6 with ammonium hydroxide (PA-7,6-TZO) presented stronger acid sites, which may favour diethyl ether formation respect to ethylene formation. In general, the doped samples led to an higher value of ethyl ether yields. In particular, the titanium-doped zirconia synthetized via precipitation at pH=7.6 (PA-7,6-TZO) led to the formation of ethyl ether with yield of 25% and exhibited the higher conversion of ethanol (33%) at 300°C. This higher value can be attributed to the high surface area of this catalyst which is the highest within the tested catalysts. Over pure zirconia catalyst PA-7,6-ZO, the Guerbet reaction product[279] of ethanol, *n*-butanol, was also observed while performing the reaction at relatively low conversion of ethanol, which was not observed over the doped catalyst that acted mainly as acid catalysts. However, the rest of the zirconia-based samples presented an ethanol conversion between 10% and 25%, in accordance with their lower surface areas (Table 3).

Figure 15 reports the results obtained at higher reaction temperature, namely 350ºC. Due to the endothermic nature of this reaction, higher temperatures lead the ethylene yield to increase.[278] The obtained products except from the already mentioned ethylene, diethyl ether and *n*-butanol are acetaldehyde and acetone. At 350°C (Fig. 15) the ethylene yield increased together with the achieved ethanol conversion. Sample PA-7,6-TZO was still the most active with an ethanol conversion of 88%, at this temperature, the main product obtained with this catalyst was ethylene, a decent amount of diethyl ether was produced (Y=19%) and small amounts of butadiene and acetaldehyde, the dehydrogenation product of ethanol, have been produced too. The other catalysts still presented ethylene as major product. The other side-products obtained were acetone and CO_2, which could be formed by the ethyl acetate ketonization reaction, the formation of which could come from Tischkenco-like disproportion of acetaldehyde.[82] Butadiene formation could occur through the mechanism proposed by Toussaint[280], based on the aldolic condensation of acetaldehyde, even if no intermediate products have been detected into the reaction mixture.
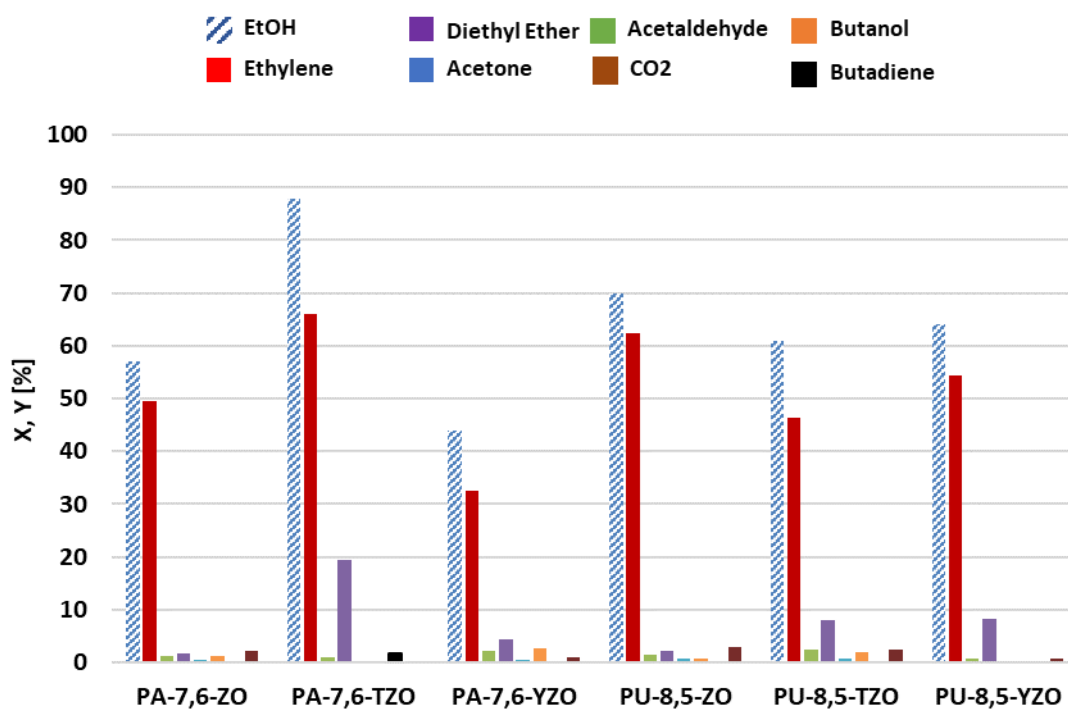
Figure 15   Ethanol conversion (X) and main products yields (Y) obtained from the catalytic tests performed over the catalysts obtained by precipitation. Reaction conditions: T: **350°C**; p: 1 atm; EtOH 5%mol in N2, VTOT= 20 mL/min; W/F= 0,78 g·s/mL.
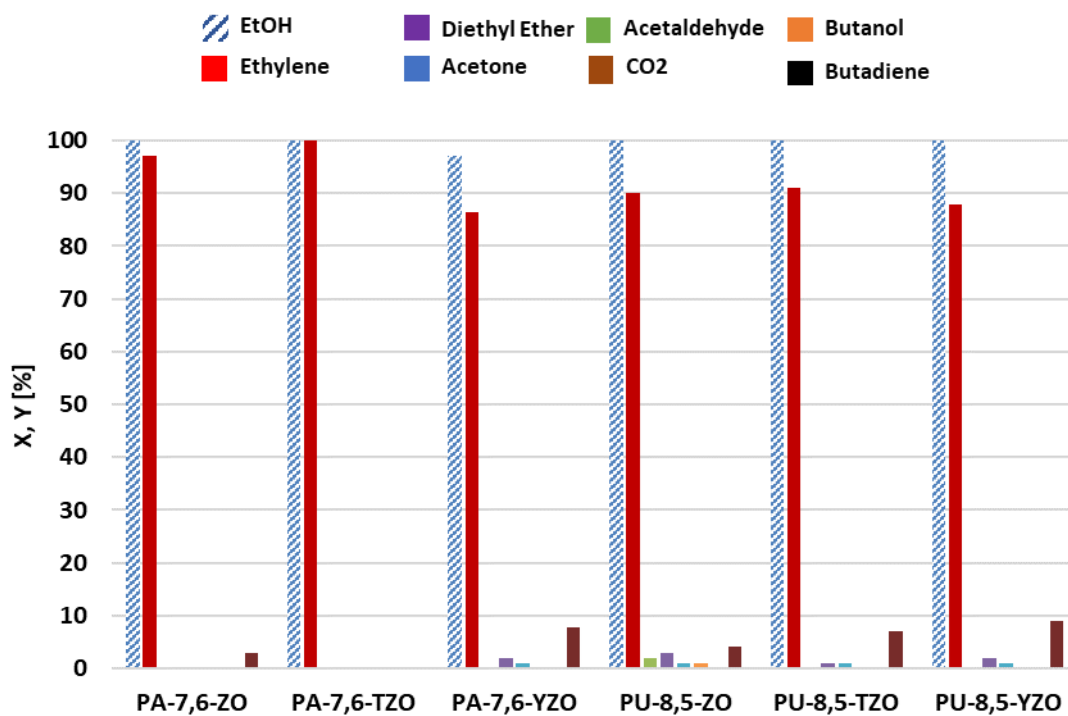
Figure 16   Ethanol conversion (X) and main products yields (Y) obtained from the catalytic tests performed over the catalysts obtained by precipitation. Reaction conditions: T: **400**°C; p: 1 atm; EtOH 5%mol in N2, VTOT= 20 mL/min. W/F= 0,78 g·s/mL.

When the temperature is raised to 400°C (Fig. 16), all the catalysts exhibited a conversion higher than 95% and similar catalytic activity. Ethylene is still the major product with yields always higher than 85%. For all the tested samples, the other products yields decreased except for acetone and CO_2 whose yields slightly increased.

4.2.3.1.2 Hydrothermal catalysts

The catalysts obtained by hydrothermal synthesis (see list in Table3) were tested also with the same reaction conditions to those used for catalysts prepared by precipitation, namely 1 atm, W/F= 0,78 g·s/mL. and reaction temperature range= 300-400ºC. Figure 17 shows the variation of ethanol conversion and products yields at 300°C and 350ºC. When the reaction temperature was 300ºC, the catalysts presented a very low catalytic activity, never exceeding 5% of ethanol conversion (Fig.17A). In this conditions, the main product formed where the dehydration product of ethanol, ethylene and the dehydrogenation one, acetaldehyde, as it can be better observed in Figure 17B.

As it can be observed in Fig. 17C, even at 350°C, the catalysts obtained via hydrothermal synthesis did not exhibit a high ethanol conversion. By rising the reaction temperature, ethylene has been preferentially formed, indeed all the three samples showed in Fig 18C-D, presented ethylene as major product.
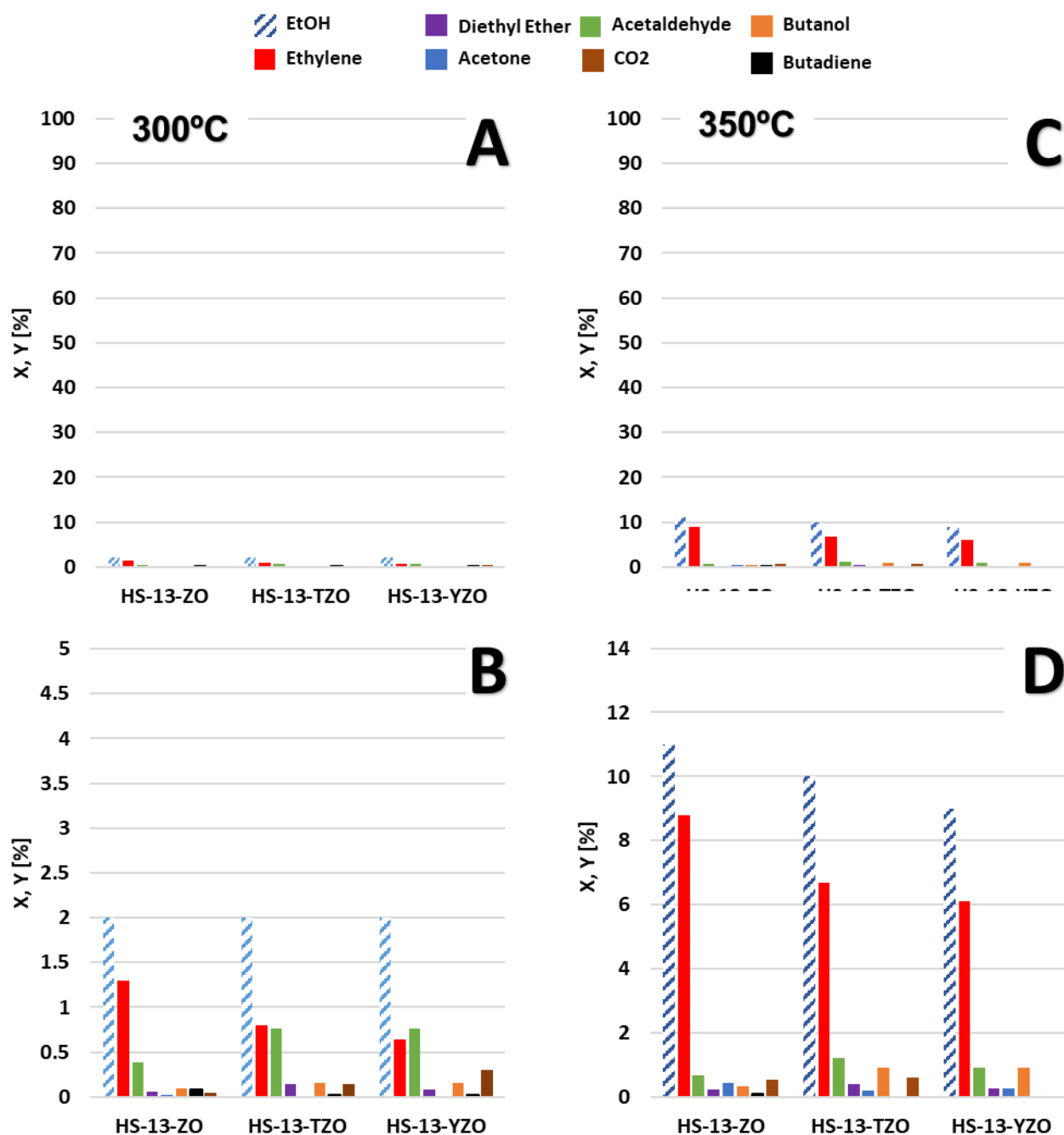
Figure 17   Ethanol conversion (X) and main products yields (Y) obtained from the catalytic tests performed over the catalysts obtained by hydrothermal synthesis. Reaction conditions: T**: 300-350°C**; p: 1 atm; EtOH 5%mol in N_2, V_{TOT}= 20 mL/min. W/F= 0,78 g·s/mL. A) Catalytic results obtained at 300ºC, B) Catalytic results obtained at 300ºC with narrowed y axis C) Catalytic results obtained at 350ºC, D) Catalytic results obtained at 350ºC with narrowed y axis

Higher conversion values were obtained when the catalysts were tested at 400°C converting almost half of the entering ethanol as can be seen in Fig. 18. The same graph shows that ethylene was still the major product of these series of catalysts in the given conditions.
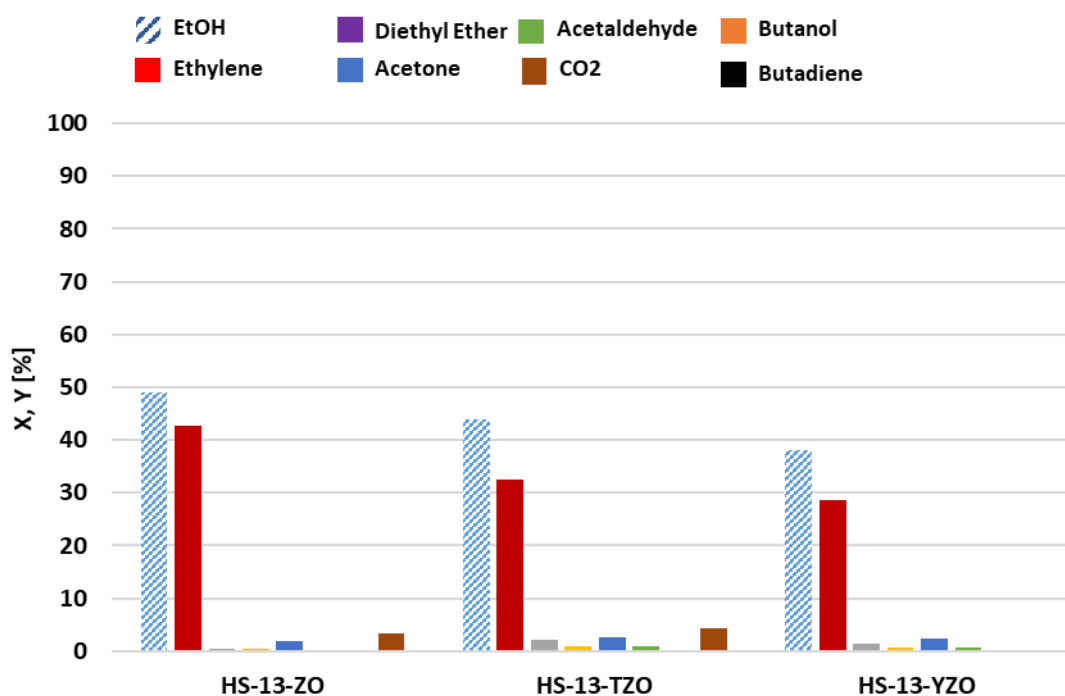
Figure 18 Ethanol conversion (X) and main products yields (Y) obtained from the catalytic tests performed over the catalysts obtained by hydrothermal synthesis. Reaction conditions: T: 400°C; p: 1 atm; EtOH 5%mol in N_2, V_{TOT}= 20 mL/min. W/F= 0,78 g·s/mL.

In summary, the catalysts obtained by precipitation have been in general more active respect to the ones synthetized via hydrothermal method in all the reaction temperature studied, namely 300°C, 350°C and 400°C. All the tested catalysts present ethylene as major product at all the tested temperatures. The titanium-doped zirconia catalyst obtained by precipitation at pH=7,6 appeared to be the most interesting among the tested ones, presenting higher ethanol conversion values respect to the other catalysts. Moreover, it presented diethyl ether as major product at 300°C, and a higher diethyl ether selectivity respect to the other catalysts at 350°C.

4.2.3.2 Stability tests over zirconia samples

Some of the tested zirconia samples have been chosen to investigate their stability over several hours of time on stream. In particular, the selected catalyst have been the zirconia catalyst synthetized by precipitation with ammonium hydroxide at pH=7,6 (PA-7,6-ZO), one sample containing Y, synthetized via precipitation with urea at pH=8,5 (PU-8,5-YZO) and one containing Ti (PA-7,6-TZO). The catalysts have been tested at T: 350°C; p: 1 atm; EtOH 5%mol in N_2, V_{TOT}= 20 mL/min and W/F= 0,78 g·s/mL. The selected time on stream was of 14.2 h. As depicted in Fig. 19, the zirconia catalyst synthetized by precipitation (PA-7,6-ZO) showed a decreasing in ethanol conversion by ~15%, from 87% to 72% after 14.2 h of time on stream, revealing a partial deactivation

of the catalyst. The products distribution looked constant since all the products yields decreased with the conversion during the time on stream.
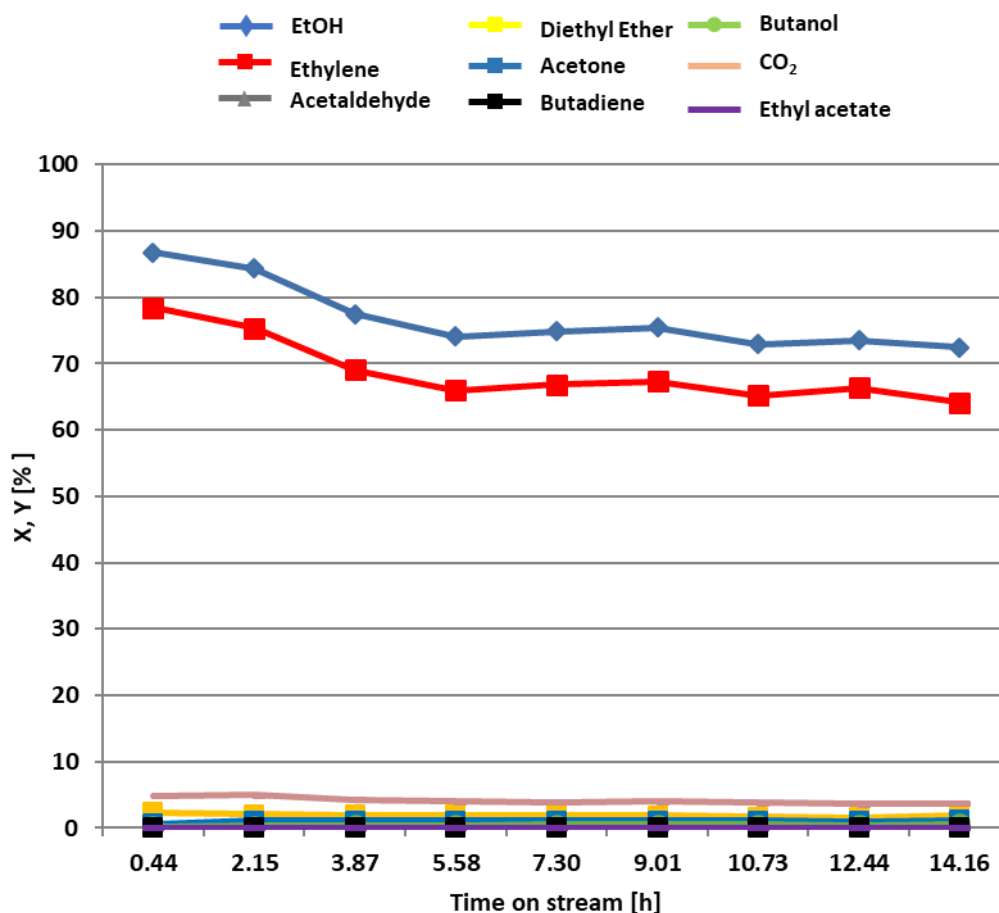
Figure 19   Ethanol conversion (X) and main products yields (Y) obtained from the catalytic tests performed over the zirconia catalysts obtained by precipitation with ammonium hydroxide at pH=7,6. (PA-7,6-ZO) Reaction conditions: T: 350°C; p: 1 atm; EtOH 5%mol in N_2, V_{TOT}= 20 mL/min. W/F= 0,78 g·s/mL.

Even the yttrium-doped zirconia samples (PU-8,5-YZO) showed a decreasing trend of ethanol conversion, dropping by around 12%, from 67% to 55% after 14.2 h, as shown in Fig. 20. All the products yields decreased with the time on stream, following the trend recorded for the ethanol conversion.
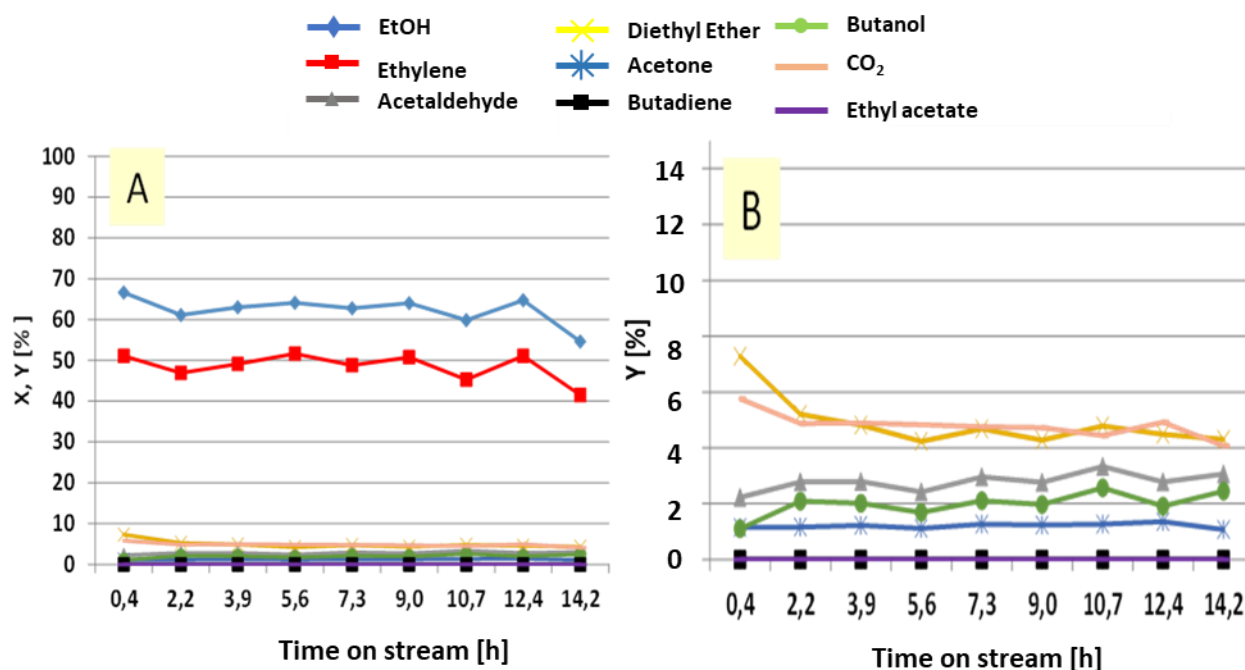
Figure 20 A) Ethanol conversion (X) and main products yields (Y) obtained from the catalytic tests performed over the yttrium-doped zirconia catalysts obtained by precipitation with urea at pH=8,5. (PU-8,5-YZO). Reaction conditions: T: 350°C; p: 1 atm; EtOH 5%mol in N2, V_{TOT}= 20 mL/min; W/F= 0,78 g·s/mL B) Yields to minority products.

Fig. 21 reports the conversion and yields as a function of the time on stream obtained over the titanium-doped zirconia catalyst synthetized by precipitation with ammonium hydroxide at pH 7,6 (PA-7,6-TZO). As can be observed the Figure , ethanol conversion appeared stable in the first 5.6 hours then decreased from 94% to 88% at 14.2 h. With this trend, ethylene yield decreased from 86% to 73% while diethyl ether yield increased from 5% to 12%. Suggesting that diethyl ether could be an intermediate product yielding ethylene, indeed as the catalyst partially deactivated and the ethanol conversion decreased, the ethyl ether yield concomitantly increased slightly. This result is in accordance with the literature.[281]
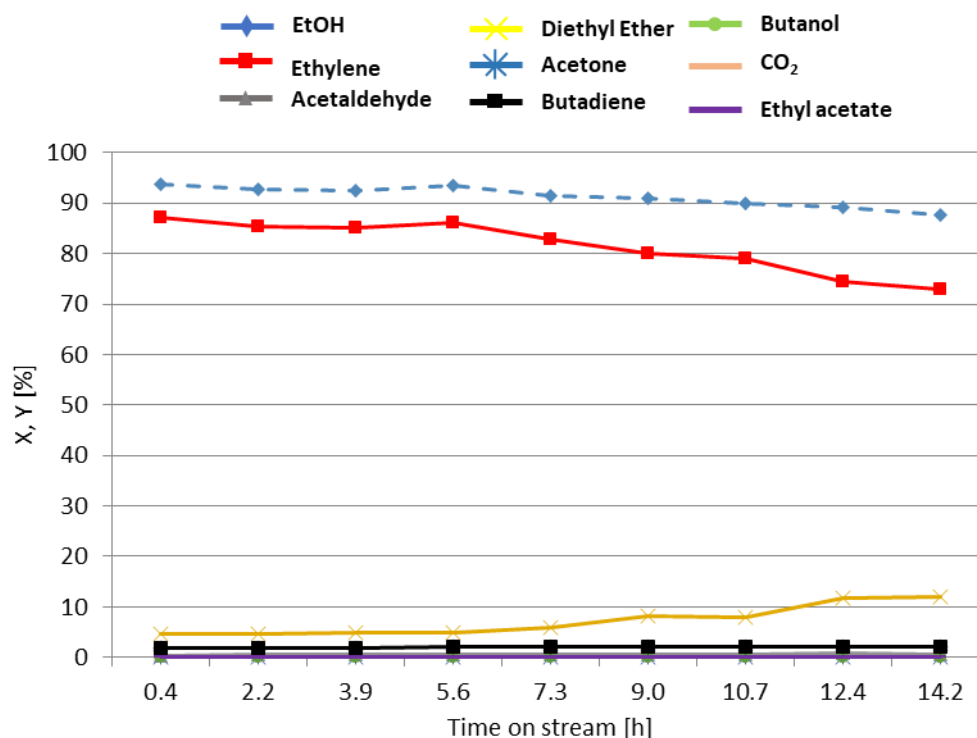
**Figure 21**) Ethanol conversion (X) and main products yields (Y) obtained from the catalytic tests performed over the titanium-doped zirconia catalysts obtained by precipitation with ammonium hydroxide at pH=7,6. (PA-7,6-TZO). Reaction conditions: T: 350°C; p: 1 atm; EtOH 5%mol in N_2, V_{TOT}= 20 mL/min. W/F= 0,78 g·s/mL.

4.2.3.3 Study of effect of the contact time

To evaluate the effect of the contact time on the products distribution, another catalytic test with a higher mass of catalyst was performed over the titanium-doped zirconia sample obtained by precipitation with ammonium hydroxide at pH=7,6 (PA-7,6-TZO). Indeed, catalyst has been tested at the following condition p: 1 atm; EtOH 5%mol in N_2, V_{TOT}= 20 mL/min, and 300ºC increasing the quantity of the catalyst charged in order to obtain a value of W/F = 1,93 g·s/mL. Figure 22A depicts the results obtained in the just mentioned conditions, comparing them with the ones at lower W/F (0.78 g·s/mL). The same procedure has been performed at higher temperature, namely 350ºC and the results are reported in Figure 22B. As can be seen in the figures, by enhancing the contact time, an increasing in the ethanol conversion was obtained, as expected. The products distribution changed as well, producing ethylene as the only product, with complete conversion of ethanol. By looking at Figure 22 both the effects of the contact time and the reaction temperature can be noticed, at least at the lowest contact time explored. Indeed, by working at W/F= 0,78 s·g/mL, an increase of the reaction temperature by 50ºC led to an abrupt increase of the ethanol conversion from 30% to ~90%. While the main product at low temperature was ethyl ether, with a yield of ~25% (and so a selectivity > 80%), when the reaction temperature was raised to 350ºC, the main product was again

ethylene, reaching a value of yield of ~68%. Regardless, at the higher contact time investigated, the same results have been obtained, complete conversion of ethanol producing ethylene as the only product.
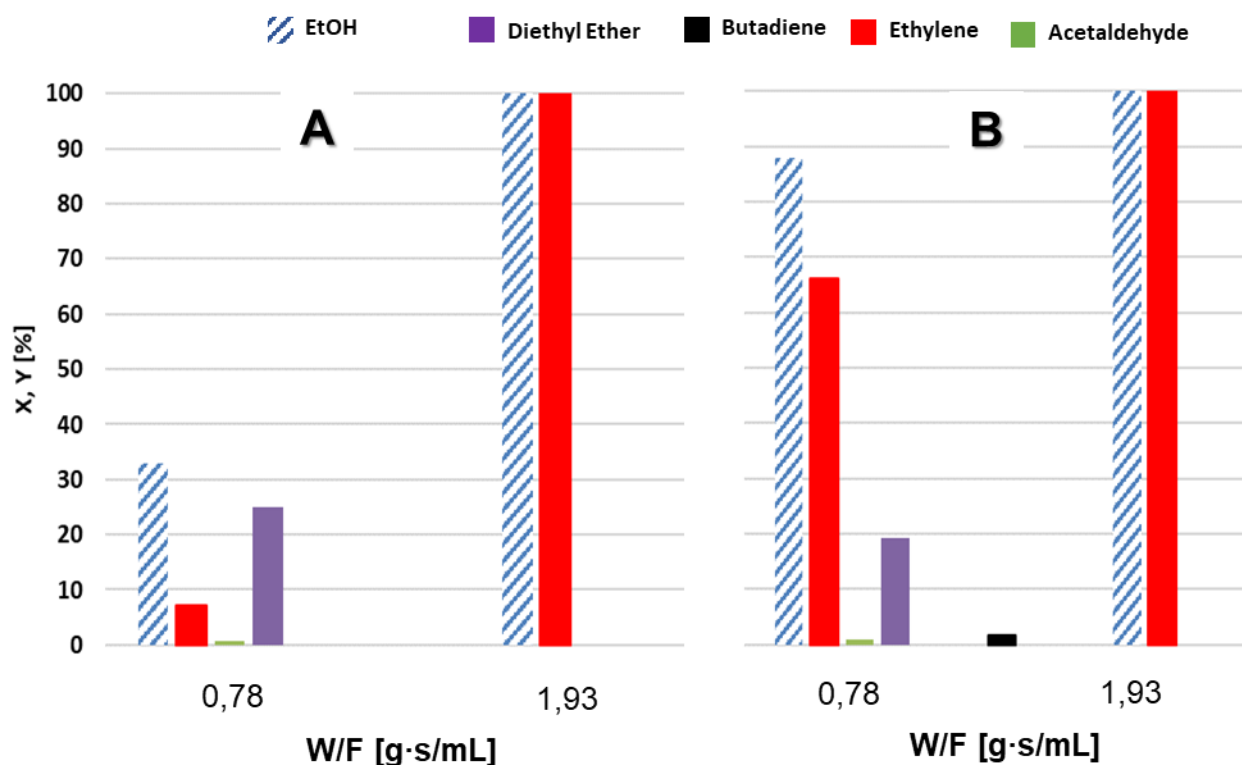
**Figure 22** Ethanol conversion (X) and main products yields (Y) obtained from the catalytic tests performed over the titanium-doped zirconia catalysts obtained by precipitation with ammonium hydroxide at pH=7,6. (PA-7,6-TZO). A) T_R= 300ºC; B) T_R= 350ºC. Reaction conditions: T: 300, 350°C; p: 1 atm; EtOH 5%mol in N_2, V_{TOT}= 20 mL/min. W/F= 0,78; 1,93 g·s/mL

4.2.4   Spent catalysts characterization

The TGA profiles of the analysis performed over the three catalysts which have been tested to evaluate their stability (PA-7,6-ZO, PA-7,6-TZO, and PU-8,5-YZO), are compared. TGA analysis was conducted to quantify the deposited carbon over the spent catalysts. In Figure 23A,B, C the TGA profiles illustrate the weight loss (%) as a function of temperature for the spent catalysts recovered after performing the stability tests at 350ºC, W/F= 0,78g·s/mL after 14,2 h on stream (see Figures 19-21). In detail, the spent catalysts weighing 45-50 mg were heated from ambient temperature to 800 °C at a heating rate of 10 ºC/min under air atmosphere, and the weight loss was recorded.
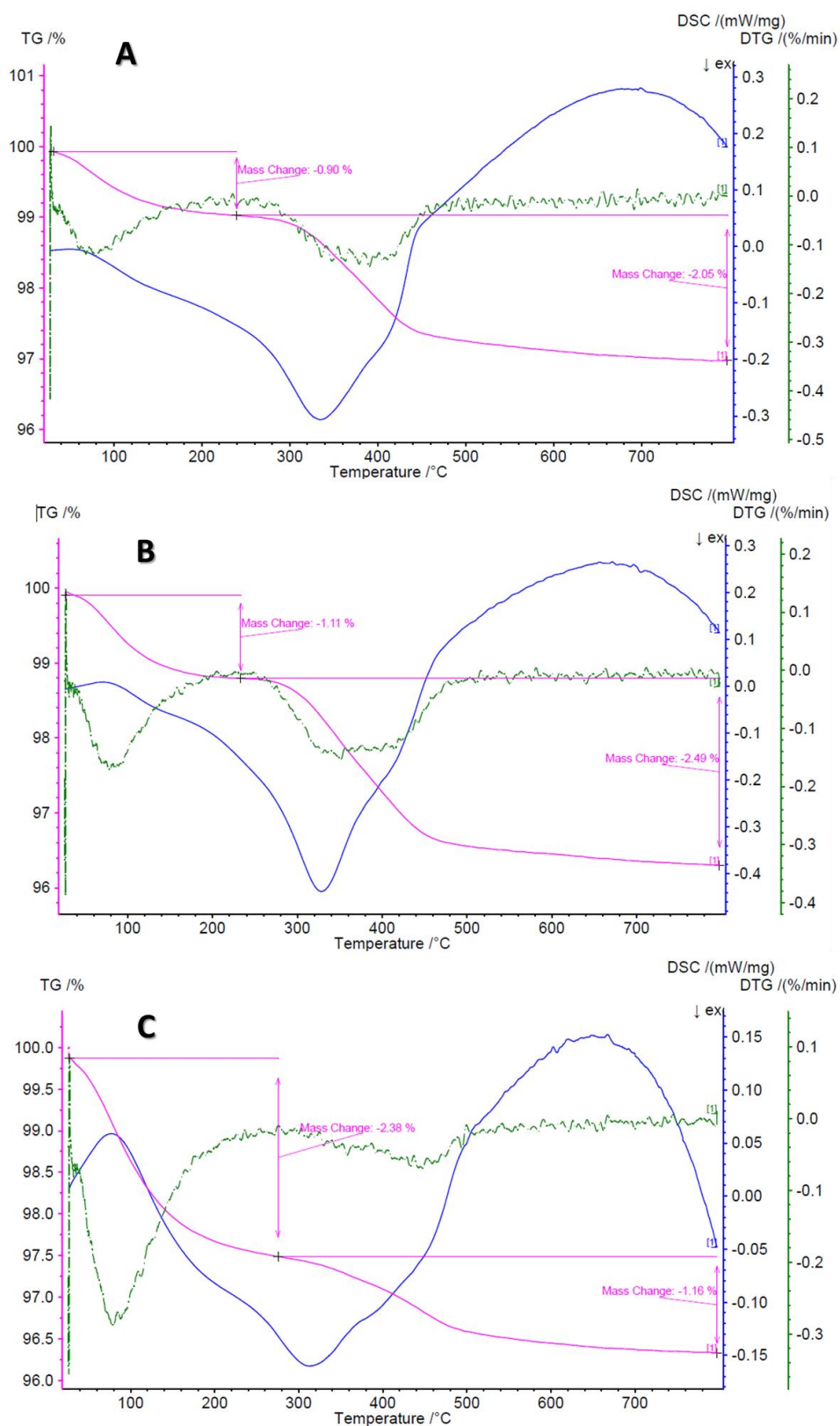
Figure 23   TGA/DSC profiles of spent zirconia catalyst tested at 350ºC for 14.2 h of time on stream. A) synthetized at pH=7,6 with 25%w NH₄OH solution (PA-7,6-ZO); B) The yttrium-doped zirconia sample synthetized at pH=8,5 with urea (PU-8,5-YZO); C) The titanium-doped zirconia sample synthetized at pH=7,6 with 25%w NH₄OH solution (PA-7,6-TZO).

The three TGA profiles are depicted in Fig 23. All of them presented two mass losses: the first one at around 100°C can be related to the loss of adsorbed water while the second one, around 400°C showed the combustion of carbon deposits. For all catalysts, the burning of carbon starts at the same temperatures around 300 °C. All the three catalysts showed similar total mass change at the TGA. Nevertheless, what can be noticed from Fig. 23C is that PA-7,6-TZO mass loss at 400°C consisted in just the 1,2% of the total mass, a lower amount compared to PA-7,6-ZO and PU-8,5-YZO which showed 2,0% and 2,5% respectively. This difference could have influenced the conversion loss of PA-7,6-TZO, which appeared to be lower respect to the other catalysts. Indeed, after 14.2h of time on stream, ethanol conversion lowered by 6% on this latter catalyst compared to the ~ 15% observed for the other two catalyst under consideration. However, the total mass change was similar between the three samples because PA-7,6-TZO presented a huge loss of adsorbed water at 100°C (-2,4%) which could be related to its higher surface area (148 m^2/g) compared to the other tested samples (PA-7,6-ZO and PU-8,5-YZO, 86 and 113 m^2/g respectively).

Table 4. *Ethanol conversion losses after 14.2 h of time on stream and TGA mass changes of different zirconia catalysts PA-7,6-ZO: zirconia synthetized by precipitation at pH 7.6 with NH_4OH; PA-7,6-TZO: titanium-doped zirconia synthetized by precipitation at pH 7.6 with NH_4OH; PU-8,5-YZO: yttrium-doped zirconia synthetized by precipitation at pH 8,5 with urea. X_{EtOH} loss after 14.2 h has been calculated as the difference between the ethanol conversion at the first analysed point with the online GC and the one obtained after 14.2 h.*

Catalyst code	ΔX_{EtOH} after 14.2 h	Δm [w%]
PA-7,6-ZO	-15%	-2.05%
PU-8,5-YZO	-12%	-2.49%
PA-7,6-TZO	-6%	-1.16%

4.2.5   CONCLUSIONS

Several zirconia samples have been synthetized by hydrothermal and precipitation methods. The catalysts have been characterised in order to investigate the influence of several synthetic parameters such as the method (i.e., precipitation or hydrothermal), the base used (i.e., NaOH, NH_4OH or Urea), and pH on the catalysts characteristics. Notably, mixed crystal phases have been obtained. However, particularly at higher pH, the catalyst preparation procedure played a crucial role over the nature of crystalline phase formation. Thus, by hydrothermal synthesis carried out at pH=13 it was obtained a sample of pure monoclinic zirconia. While, by precipitation method at the same pH value, tetragonal or cubic zirconia was formed.

Finally, the effect of the incorporation of a dopant (Y and Ti) on the nature of zirconia samples have been evaluated in both the synthetic methods employed. The main effect observed of the presence of a metal was an overall stabilization of the metastable tetragonal or cubic phases over the monoclinic one. Concomitantly, an increase of the BET surface are have been observed as well.

The synthetized zirconia-based catalysts have been tested in the gas-phase ethanol transformation in a range of temperatures from 300°C to 400°C. In general, the tested zirconia samples showed a clear acid behaviour, converting ethanol mainly into its dehydration products ethylene and diethyl ether, a well-known acid catalysed reaction. However, changes in conversion and selectivity were observed depending on the catalyst preparation procedure and/or the presence of a metal-dopant. Interestingly, the titanium-doped zirconia samples prepared by precipitation, that, according to TPD-NH_3 analysis, was the most acid between the ones analysed, allowed to obtain ethyl ether as main product while performing the reaction at relative low temperature (300ºC).

In the future, would be interesting to further modify those materials by adding a redox active site, such as a transition metal, in order to increase their hydrogenation/dehydrogenation properties. Indeed, acetaldehyde, the dehydrogenation product of ethanol, has been often identified as the key product for *n*-butanol and 1,3-butadiene formation starting from ethanol, both valuable compounds with many industrial applications.

4.3 Guerbet reaction over Sepiolite based catalysts – ITQ-UPV

The topic of the whole research has been the valorisation of ethanol through its gas-phase conversion over heterogeneous catalysts into added value derivatives. This includes *n*-butanol, which is an important chemical compound with many different uses such as additive in daily use products and intermediate to produce more valuable compounds, as well as a valid alternative to gasoline. Ethanol can be converted into *n*-butanol through the so-called Guerbet reaction, which comprises a complex reaction mechanism where a fine-tuning of the acid-base catalyst properties is thought to be a key aspect to optimize.

Sepiolite is a fibrous magnesia-silicate clay mineral, with the formula structure as $(Si_{12}Mg_8O_{30})(OH)_4(H_2O)_4 \bullet 8H_2O$. Its fibrous structure is formed by an array of parallel channels, consisting of a double layer of SiO_4 sandwiching an internal octahedral MgO_6 layer, it led to the formation of intracrystalline channels filled with coordinated water molecules and zeolitic water. The special crystal structure of sepiolite makes it have large specific areas and high surface activity and it has been applied widely in many areas including catalysis. It has been reported that sepiolite can undergo alkaline treatments for both increasing its ion-exchange capability and changing its acid/base characteristic.

In the present work, carried out in the laboratory of "Instituto de Tecnologia Química" (ITQ) of the "Universitat Politecnica de Valencia" (UPV), the natural clay Sepiolite has been treated in order to obtain a bi-functional acid-base catalyst and convert bio-ethanol into *n*-butanol through the Guerbet reaction. The catalysts so prepared have been characterized by several techniques and tested in a gas-phase bench scale continuous flow quartz reactor using as feeding a mixture of 5% Ethanol in N_2.

4.3.1   Catalysts characterization

4.3.1.1 X-ray diffraction (XRD) analysis

Catalysts crystal structure was determined by means of XRD of their powders; Figure 1 reports the XRD pattern of sepiolite samples, the raw and the calcined at 500 and 700ºC, respectively.

The XRD study (Fig. 1) shows that the main phase constituent of the raw material (SepNat) is a well crystallized sepiolite, as indicated by the characteristic narrow and intense diffraction peak at 2θ=7.3º. Indeed, the natural sepiolite XRD pattern match with the one of Sepiolite, Magnesium Silicate Hydroxide Hydrate (00-013-0595), $Mg_4Si_6O_{15}(OH)_2 \cdot 6H_2O$, and the sharp and strong peak at 2θ= 7.31° is characterized as (110) plane of sepiolite (S), with 1.21 nm d-value, which corresponds to the interlayer distance in the clay structure.

By heating the samples up to 500°C, it is totally eliminated the peak at 7.31º, indicating that the layered structure of catalyst collapsed with high temperature calcination and so the total degradation of sepiolite. In fact, the XRD pattern of calcined sepiolite (Sep@500) contains none of the reflections of the natural sample, showing the loss of all the initial reflections and revealing that the heating caused structural and textural changes associated with the dehydration and dehydroxylation processes.[218] Accordingly, both the sepiolite samples calcined at 500°C and 700ºC matched with the 00-026-1227 reference pattern related to the sepiolite anhydrate (SA), Magnesium Silicate Hydroxide, $Mg_8Si_{12}O_{30}(OH)_4$. Furthermore, the slight increase with calcination temperature of the peaks intensity at ~8.9°,~11.1º and 20.25°, corresponding to the planes (110), (120) and (031) respectively (Fig. 1), indicates the formation of sepiolite anhydrite.[218] Those data are in accordance with the ones reported in literature. [282] In addition, with increasing temperature, the presence of quartz peak at 26.7º can be observed.
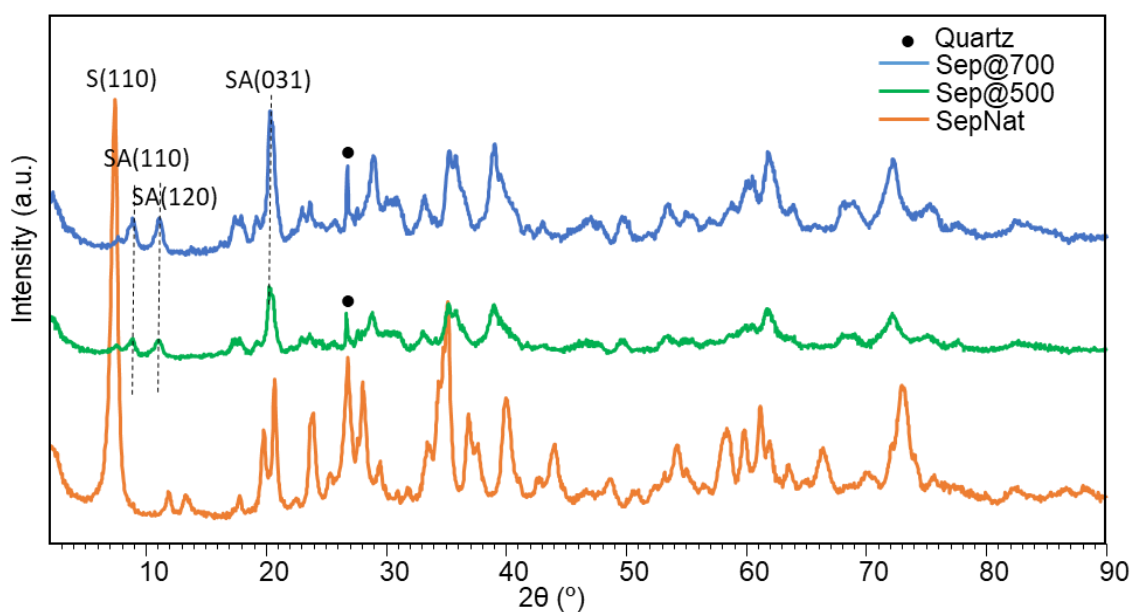
Figure 1 XRD patterns of sepiolite samples. Natural sepiolite (SepNat, orange line) and the two samples after calcination at 500ºC (Sep@500, green line) or 700ºC (Sep@700, blue line). Dot: quartz.

Table 1 summarizes the crystalline phases detected and the crystallite sizes, calculated by using Scherrer equation. To calculate the crystallite size of sepiolite samples, the crystallite of natural sepiolite corresponded to the 2θ= 7.3º while for the calcined ones, relating to the sepiolite anhydride, it was considered the reflection at 2θ= 20.25º.

Table 1. *Summary of information obtained from XRD analysis performed over the sepiolite samples, i.e. the natural one and those calcined at 500ºC and 700ºC. ª Calculated through Scherrer equation.*

Catalyst	Phase detected + Reference code	D [nm]^a
SepNat	Magnesium Silicate Hydroxide Hydrate (00-013-0595)	14.3
Sep@500	Magnesium Silicate Hydroxide (00-026-1227)	15.9
Sep@700	Magnesium Silicate Hydroxide (00-026-1227)	16

4.3.1.1.1 Alkali metals effect

Figure 2 and Figure 3 report the XRD patterns obtained for the alkali metals-impregnated samples. Generally, it can be observed a broadening (with reference to the sepiolite support itself) and reduced intensity of the peaks, suggesting significant chemical changes in the sepiolite crystallinity.
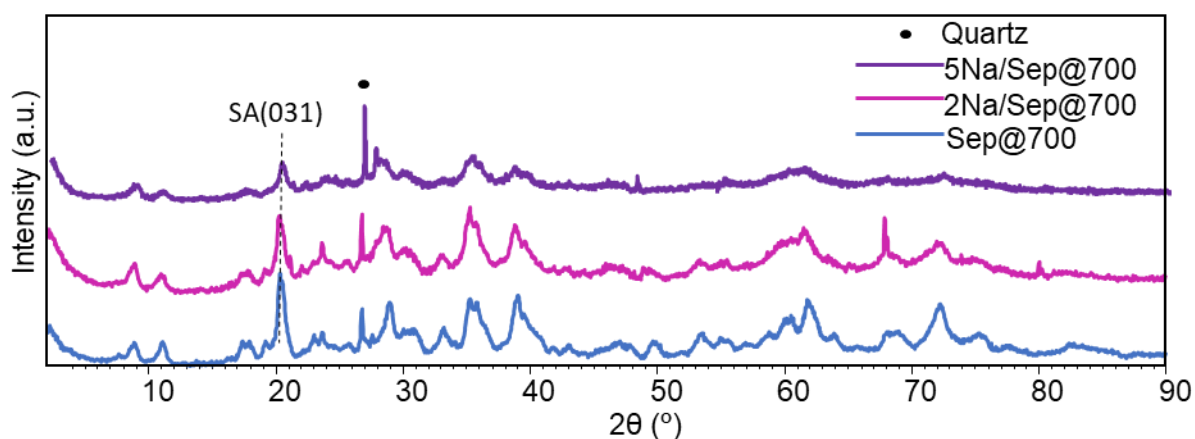
Figure 2 XRD patterns of sepiolite samples. Sepiolite calcined at 700ºC, Na/Sep@700 2 and 5 wt%.

The XRD diffractograms for samples of Na-impregnated sepiolite after calcination at 700ºC are shown in Figure 2. The samples are noted as XNa/Sep@700 where X denotes the weight percentage of metal loading. The diffraction patterns of the impregnated samples show similar pattern to that of the parent Magnesium Silicate Hydroxide, indicating that the framework structure has been retained after loaded with these percentages of sodium. However, diffractograms for sample containing 5wt% of Na shows partial amorphous phase suggesting that the framework of the support sepiolite have partially collapsed. Indeed, it can be observed a partial decrease of the crystallinity of the impregnated sample decreases with increasing Na amount.

The XRD diffractograms of the Na, K and Cs-impregnated sepiolite samples after calcination at 500ºC are shown in Figure 3. Even in this case, the diffraction patterns of the impregnated samples show similar pattern to that of the parent Magnesium Silicate Hydroxide, indicating that the framework structure has been retained after loaded with alkali metals. However, diffractograms for samples containing the higher amount of alkali metals showed partial amorphous phase suggesting that the framework of the support sepiolite had partially collapsed. Indeed, it can be observed a partial decrease of the crystallinity of the impregnated sample decreased with increasing alkali metals amount, as it is particularly evident from the decreased intensity of the reflection peak located at 2θ= 20.25º.
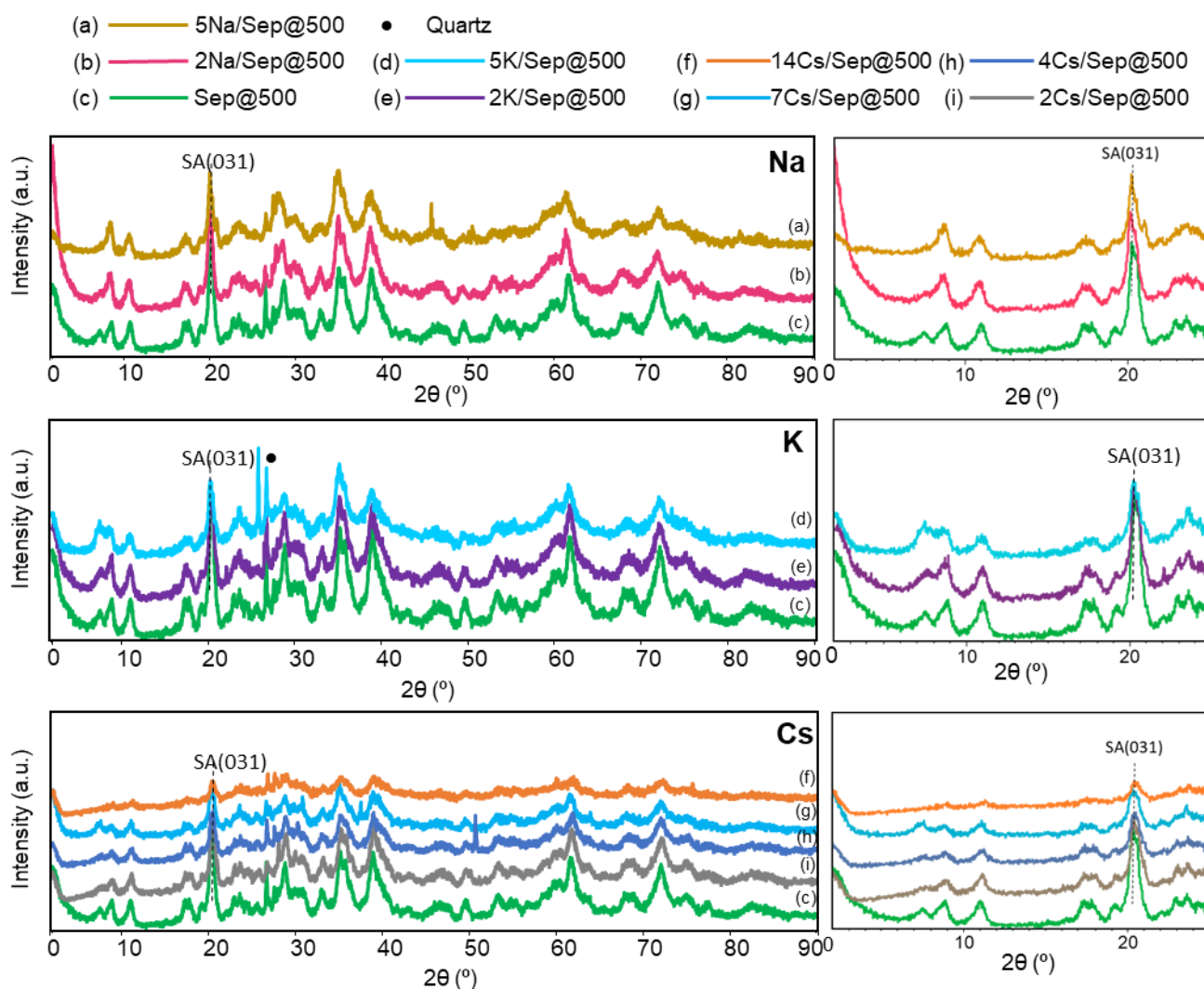
Figure 3. XRD patterns of sepiolite samples. a)5K/Sep@500, b)2K/Sep@500, c) Sep@500, d)5Na/Sep@500, e) 2Na/sep@500, f)14Cs/Sep@500, g) 7Cs/Sep@500, h) 4Cs/Sep@500, i) 2Cs/Sep@500.

In general, there is no indication of the presence of any crystalline phase such as any new alkali metal (Na, K, Cs) phase, other than the sepiolite dehydrate. Therefore, the alkali metal salt or oxides are well dispersed on the surface of the sepiolite calcined at 500ºC. Pure sepiolite gave sharper peaks than the alkali-metals-doped sepiolite catalysts, indicating that the pure sepiolite samples

consisted in larger crystallite sizes than the ones containing the alkali-metals. In addition, the intensity of XRD peak at 2θ = 8°,11º and 20.25º decreases with increasing metal loading, indicating the decrease in the crystallinity of sepiolite dehydrate framework structure. Figure 3 highlights the section of the XRD pattern in the 2θ range between 0-23 º. Table 2 summarized the XRD data of the sepiolite samples.

Table 2. *XRD data for the alkali-impregnated sepiolite samples, Calculated through Scherrer equation (a), and considering the peak at 20.25º as representative for the sepiolite anhydride (ref. 00-026-1227).*

Support	Metal	Metal loading [wt%]	D [nm]^a
Sep@700	-	-	16
	Na	2	13.8
		5	13.5
Sep@500	-	-	15.9
	Na	2	15.1
		5	12.7
	K	2	12.8
		5	13.3
	Cs	2	15.3
		4	15.0
		7	13.9
		14	12.6

4.3.1.1.2 Transition metal/sepiolite

4.3.1.1.2.1 Copper oxide impregnated sepiolite

To investigate the ethanol gas-phase Guerbet reaction over heterogeneous catalysts, a wide variety of basic oxides have been already employed. Between them, MgO appeared to be the most active and selective toward the Guerbet reaction and often it has been used as a reference catalyst. [60,283] In this work we decided as well to prepare a sample of magnesium oxide and employ it as reference catalyst. Hence, it has been synthetized by precipitation as explained in detail in Section 4.2.4.2. Successful synthesis was confirmed by XRD analysis performed over the calcined sample, as shown in Figure 4.

Copper was added to both MgO and the sepiolite (previously calcined at 500 or 700ºC), by wet impregnation as explained in Section 3.2.4.3.2. All samples after impregnation were calcined at 500ºC for 3 hours with a 2ºC/min heating ramp. Figure 4 reports the XRD patterns of MgO and the copper impregnated sample. Even if no copper oxide phases were detected, proving a good dispersion of copper over the magnesia support, a decrease of crystallinity of the MgO after impregnation can be noticed.
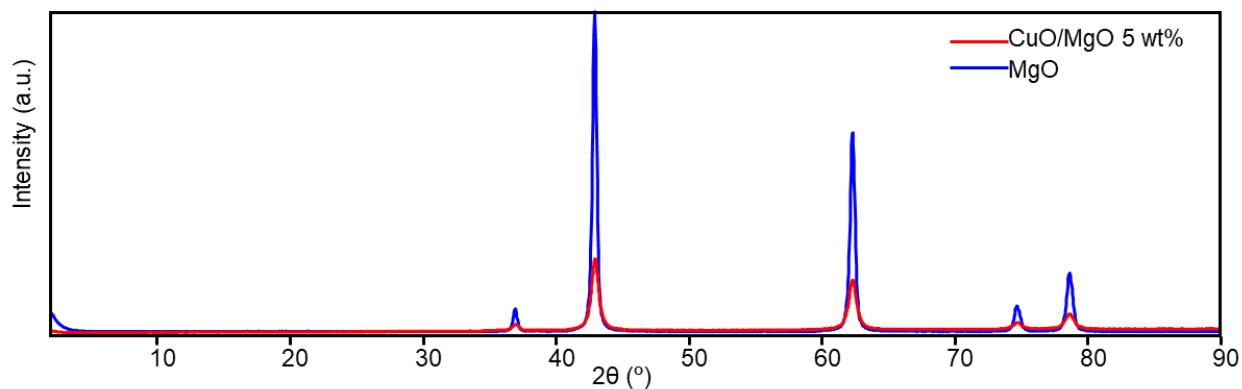
Figure 4   XRD of MgO and the copper oxide impregnate one (CuO/Sep@700 5 wt%).

Sepiolite sample calcined at 700ºC has been impregnated with 5 wt% of copper, and Fig. 5 shows the XRD patterns of the so-prepared samples. Upon CuO impregnation, the presence of the typical CuO (Tenorite, ref. 00-002-1040) patterns were observed at the Bragg angles, 2θ = 35.59º, 38.78º, 48.65º, 58.35º, 66.23º and 67.86º. The first three peaks, that are the most intense ones, coincided with the ones of the support sepiolite anhydride (00-026-1227) at 2θ: 35.35º and 38.81. Therefore, the presence of the copper oxide agglomerate can be confirmed by the three less intense peaks at 48,15º, 58.35º, and 66.22º that corresponds to the planes (-202), (202) and (022), respectively.
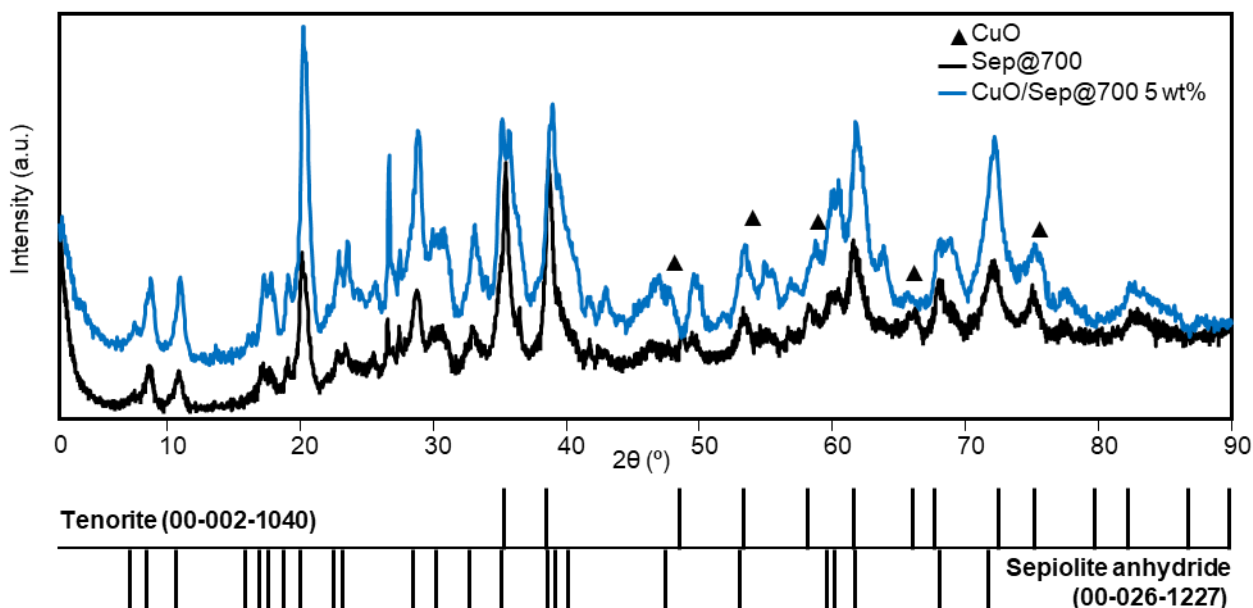
Figure 5   XRD of the natural sepiolite support calcined at 700ºC (Sep@700) and the copper oxide impregnate one (CuO/Sep@700 5 wt%).

Copper, with 5 and 10 wt% metal loading, has been added by wet impregnation over a calcined sepiolite, i.e. sepiolite calcined at 500ºC. Figure 6 depicts the XRD patterns obtained for those samples. Even in this case, aggregation of copper oxide can be observed by the presence of peaks at 2θ = 48.65º, 58.35º, 66.23º and 67.86º corresponding to planes of tenorite (-202), (202), (-311) and (022), respectively. Some sepiolite samples containing sodium have been impregnated with copper oxide, in particular the two sepiolite samples calcined at 500 and 700ºC and doped with 2wt%

of sodium have been impregnated with 5 or 10 wt% of CuO (i.e., CuO/2Na/Sep@700 5wt%, CuO/2Na/Sep@500 5 wt% and CuO/2Na/Sep@500 10 wt%). Likewise, the addition of copper over the sepiolite containing sodium led to similar results. The XRD analysis results of the concerned samples are depicted in Figure 7.
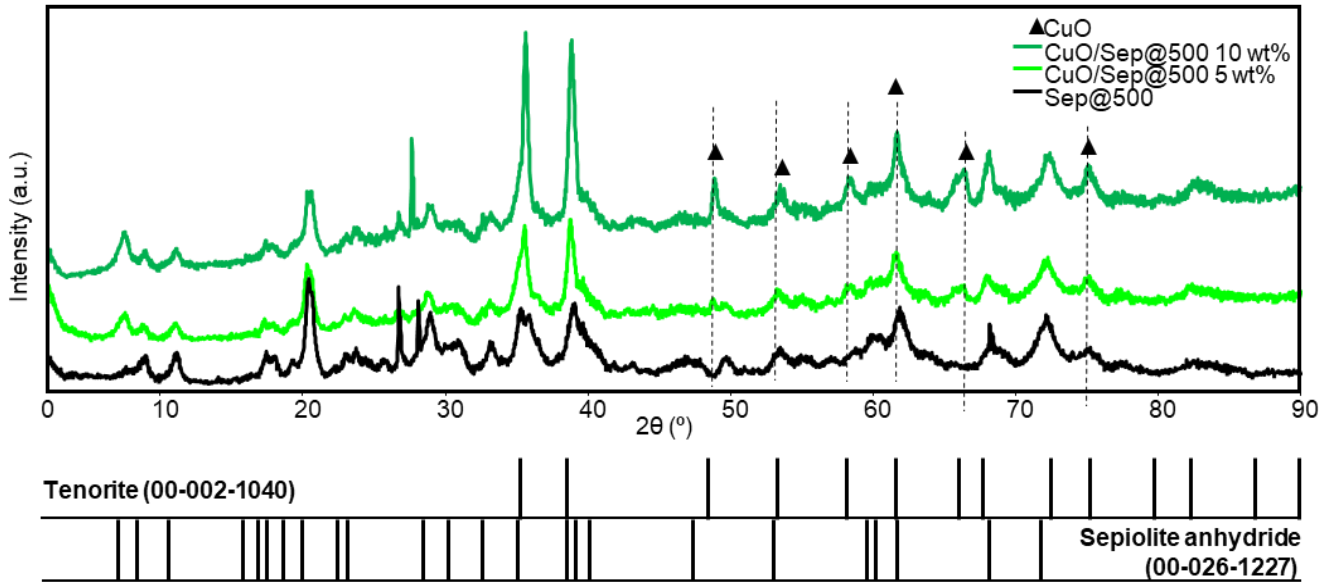
Figure 6   XRD of the natural sepiolite support calcined at 500ºC (Sep@500) and the copper oxide impregnate ones (CuO/Sep@500 5 wt%, CuO/Sep@500 10 wt%).
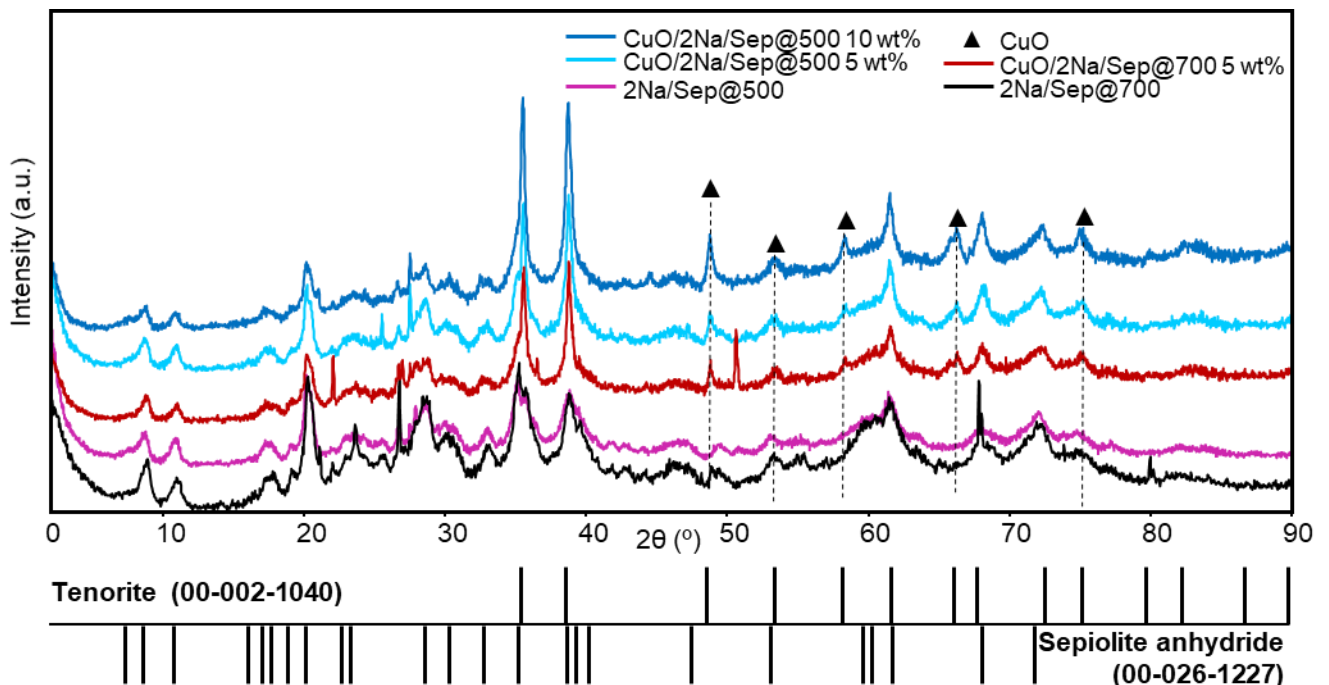
Figure 7   XRD of the 2 wt% Na-doped natural sepiolite samples calcined at 500ºC (2Na/Sep@500) and 700ºC (2Na/Sep@700) and the copper oxide impregnate ones with different metal loading (CuO/2Na/Sep@500 5 wt%, CuO/2Na/Sep@500 10 wt%, CuO/2Na/Sep@700 5 wt%).

4.3.1.1.2.2   *Nickel - oxide impregnated sepiolite*

A nickel-impregnated sample has been prepapared as explained in Section X. In particular, NiO has been supported on 2Na/Sep@500 with a metal loading of 5 wt%. The corresponding XRD pattern is presented in Fig.8 together with the one of the support (i.e 2Na/Sep@500). Even in this case, the XRD patterns of the NiO supported sample displays the set of observable reflections at corresponding to the sepiolite anhydride (00-026-1227) support. The appearance of nickel oxide (NiO, Ref.: 01-089-5881) can be noticed by the presence of the reflections lines at 2θ=43.29⁰ corresponding to the (400) plane and at 62.88⁰ corresponding to (440) plane.
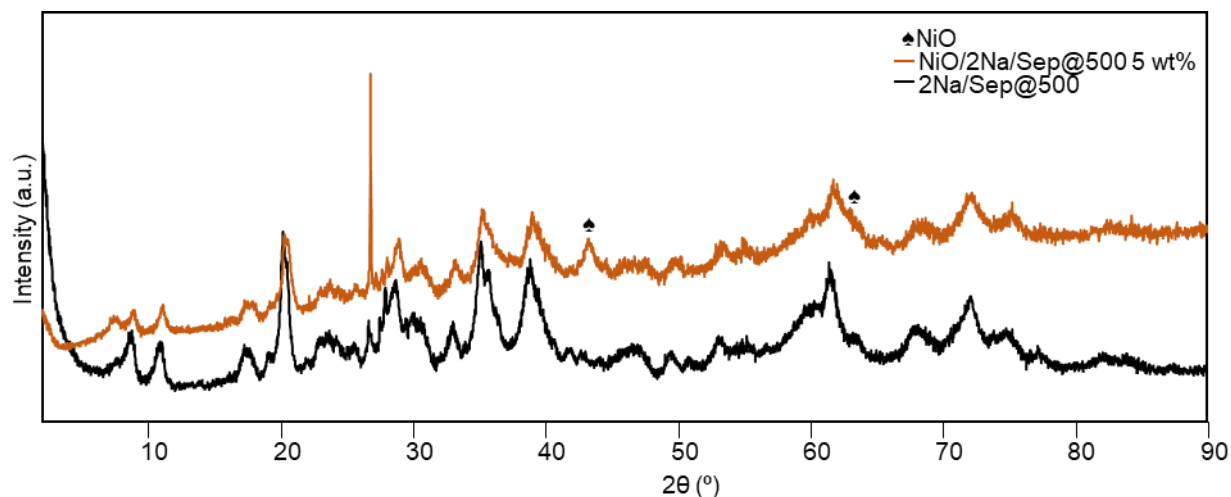
Figure 8   XRD of the 2 wt% Na-doped natural sepiolite samples calcined at 500ºC (2Na/Sep@500) and the nickel oxide impregnated one with 5 wt% of metal loading (NiO/2Na/Sep@500 5 wt%).

4.3.1.2 Thermogravimetric analysis (TGA)

TGA analysis confirmed the removal of water with increasing temperature. From the TGA analysis results, performed in the 25 – 800ºC temperature range, three mass losses can be observed (Figure 9):

I)   ~100ºC the loss of adsorbed water and zeolitic water (7,6%),

II)   ~300ºC the loss of hydration water (2,6%),

III)   ~500ºC the loss of coordination water (3,6%).[284]

These tree steps (with peaks at around 100, 300 and 500ºC) were accompanied with mass loss percentages of 7.6, 2.6, and 3.6%, respectively (Fig. 9), and correspond to: i) the loss of the weakly adsorbed water on the surface; ii) the loss of hydration water and; iii) the loss of coordination water. It can be noted that around 800ºC a fourth mass can be also observed which, in agreement to the literature, could be related to the loss of water through dehydroxylation, leading to the formation of enstatite ($MgSiO_3$).[218,285]

It is well known[218,219] that the sepiolite dehydration takes place in two steps: i) the first one around 300ºC produces sepiolite dihydrate $Mg_8Si_{12}O_{30}(OH)_4(H_2O)_2$, ii) the second one, by heating sepiolite

up until 550ºC, yields sepiolite anhydrate $Mg_8Si_{12}O_{30}(OH)_4$. It addition, between 600–700 °C occurs the chemical removal of the structural hydroxyls until structure collapse around 800ºC.[219]
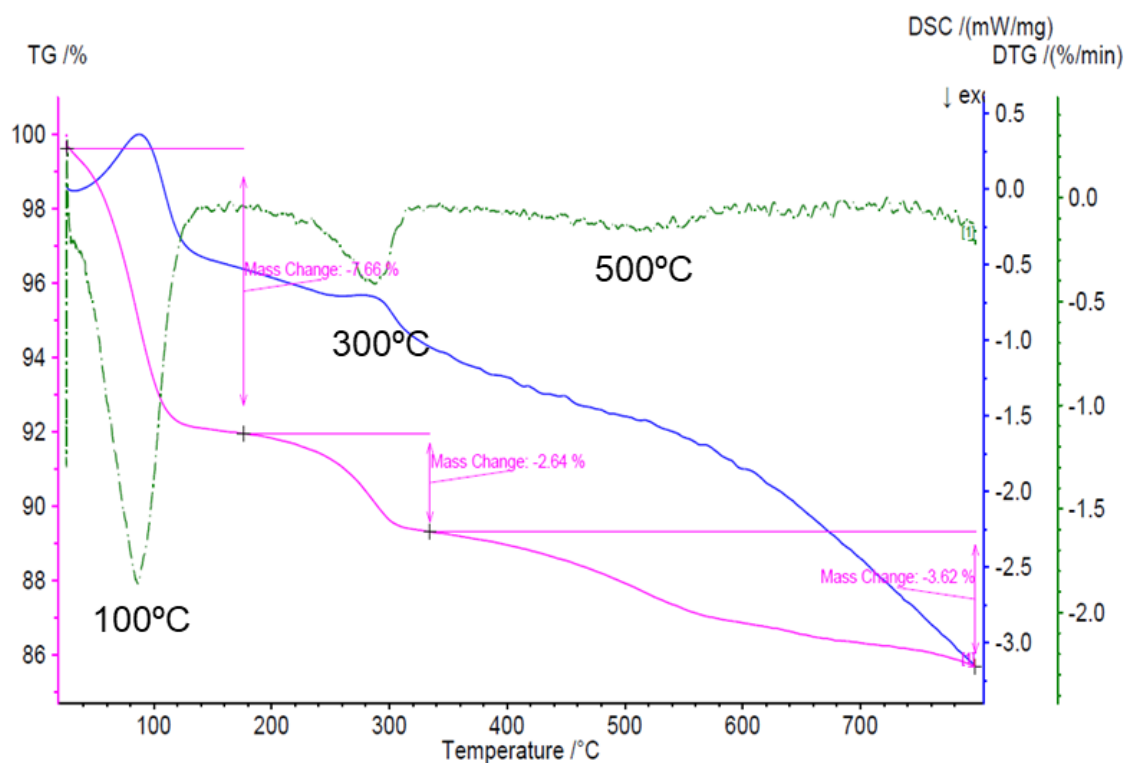
Figure 9 TGA analysis of natural sepiolite sample

4.3.1.3 Surface area, BET

BET surface areas of supports and catalysts were determined by N_2 physisorption isotherms. The texture parameters, such as the specific surface area, the pore volume and the pore size of MgO and the sepiolite samples, the calcined ones and the alkali metals impregnated samples, are listed in Table 3. Whereas some examples of calcined sepiolite are shown in Figure 10.
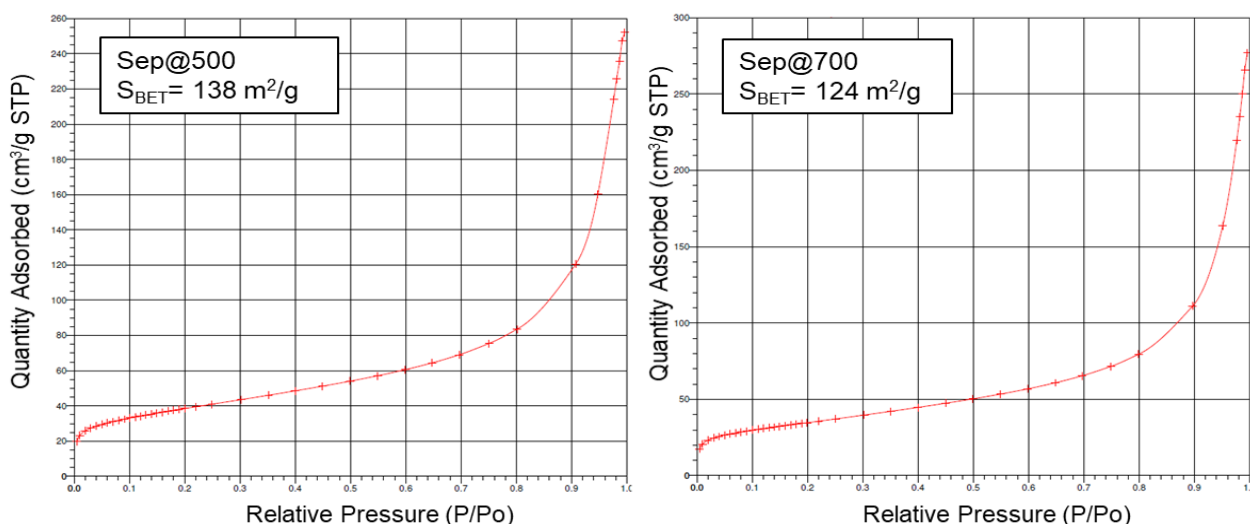
Figure 10 Representative adsorption isotherms and BET values for natural sepiolite calcinated at 500ºC (Sep@500) and at 700ºC (Sep@700).

The MgO sample had a relatively low surface area of 41 m²/g in agreement with literature values.[286,287] On the other hand, the sepiolite samples displayed an adsorption isotherm belonging to IUPAC type IV with H-3 hysteresis loop (Figure 10), typical of mesoporous adsorbents.[288] The BET surface area of the two samples calcined at 500 and 700ºC were 138 m²/g and 124 m²/g, respectively; showing a lower value of BET surface area at higher calcination temperature.

BET surface area (S_{BET}) results are in accordance with the XRD analysis. Thus, the incorporation of an alkali metal on the surface of sepiolite led to a partial degradation of the structure, confirmed by a decrease of the surface area with increasing metal loading (Table 3).

Table 3. *BET analysis results of the sepiolite-based catalysts and MgO, determined by nitrogen adsorption using BET technique (a) or Determined by BJH method (b).*

Support	Metal	Metal loading [%w/w]	S_{BET}^{a} [m²/g]	Pore[b] Volume [m³/g]	Pore[b] Average diameter [nm]
MgO	-	-	41	0.06	11.3
Sep@700			124	0.22	9.4
	Na	2	126	0.18	7.7
		5	102	0.15	8.0
Sep@500		-	138	0.21	8.7
	Na	2	124	0.20	9.0
		5	100	0.20	9.7
	K	2	119	0.19	9.0
		5	86	0.16	11.3
	Cs	2	130	0.17	7.9
		4	118	0.17	7.6
		7	110	0.15	8.1
		14	79	0.13	8.9

Figure 11 shows the results of the BET surface area analysis performed over the alkali metals-impregnated sepiolite samples, for both sepiolite supports calcined at 500ºC and 700ºC. It can be observed that the surface area, calculated by the BET method, decreased with increasing metal loading; this decrease may reflect micropore blockage. In general, the BET surface area of sepiolite was found to decrease as the alkali-metal loading increased (Table 3 and Figure 11). This could be attributed to the "dissolution" of part of the framework during impregnation and pore filling by the alkali oxides. [289]
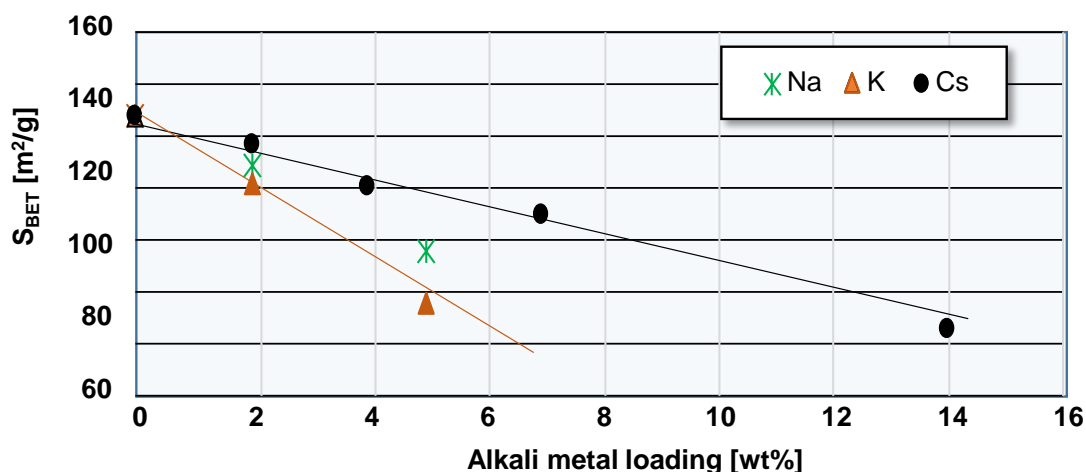
Figure 11   BET surface area as a function of alkali metal loading wt% over natural sepiolite calcined at 500 ºC

4.3.1.3.1 Transition metals supported on Sepiolite

Physical properties of sepiolite-supported copper catalysts, prepared by impregnation, are reported in Table 4. In general, the incorporation of metal oxides on the surface of sepiolite support leads to a small decrease of BET specific surface area. The increase of surface area of MgO impregnated sample is coupled to the partial loss of crystallinity of this support (probably related to changes of support during the impregnation step) as shown by the comparison of XRD pattern of pure MgO and CuO/MgO 5 wt% in Figure 4.

Table 4. *BET analysis results of the CuO impregnated samples sepiolite and MgO. [a] Determined by nitrogen adsorption using BET technique; [b] Determined by BJH method;*

Support	Alkali metal	CuO [wt%]	S_{BET} [a] $[m^2/g]$	Pore [b] Volume $[m^3/g]$	Pore [b] Average diameter [nm]
MgO	-	-	41	0.06	11
		5	78	0.28	15
Sep@500	-	-	138	0.21	8.7
		5	138	0.18	8.5
		10	135	0.14	8.5
	2Na	-	124	0.20	9.0
		5	101	0.18	9.8
		10	101	0.16	10.2
Sep@700	-	-	124	0.22	9.4
		5	110	0.19	9.1
	2Na	-	126	0.18	7.7
		5	91	0.15	9.0

The BET surface area of sepiolite calcined at 500ºC was about 138 m^2/g. After impregnation with copper, and calcination, there was a slight reduction of the surface area. However, when the sodium-impregnated sepiolite samples have been used as catalysts, the subsequent impregnation with copper led to a more significant reduction of the surface area, i.e., the surface and pores of the support were covered. We must notice that the BET surface areas of catalysts with 5 or 10 wt.% of CuO were similar, while the pore dimension of CuO doped catalyst particles decreased with increasing CuO loading (Table 4).

4.3.1.4 SEM-EDX analysis

Successful impregnation of the sepiolite support with alkali metals was confirmed by elemental analysis EDX, the analysis results are summarized in Table 5 and 6. Figure 12 reports the SEM images obtained over the sodium-doped sepiolite samples, while in Figure 13 are reported the SEM images of the potassium and caesium – doped sepiolite samples. In general, there were no substantial alterations in the materials morphology; the typical fibrous morphology of sepiolite structure is can be observed in SEM images.
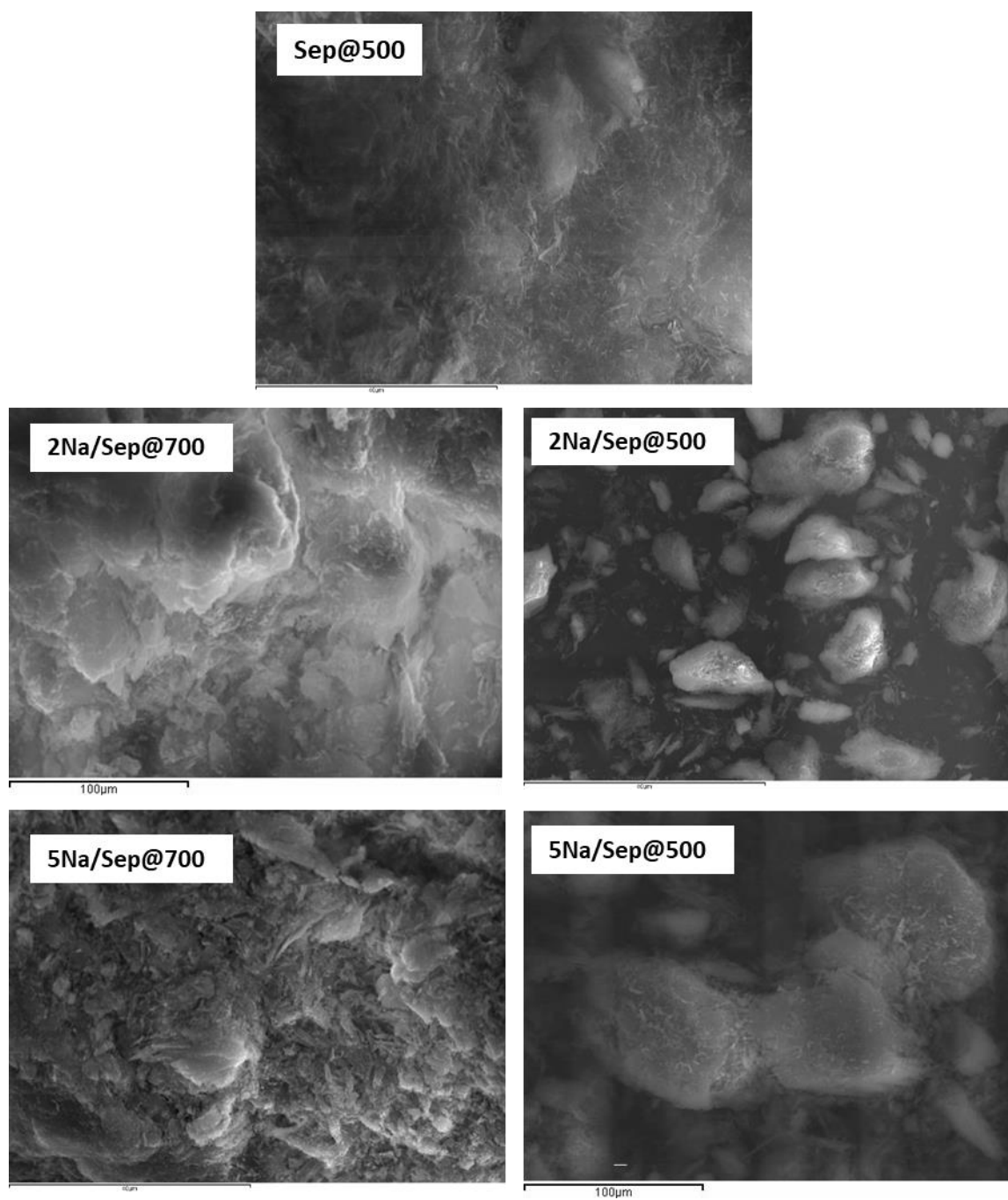
Figure 12   SEM micrographs of Na-impregnated sepiolite recorded at different magnifications
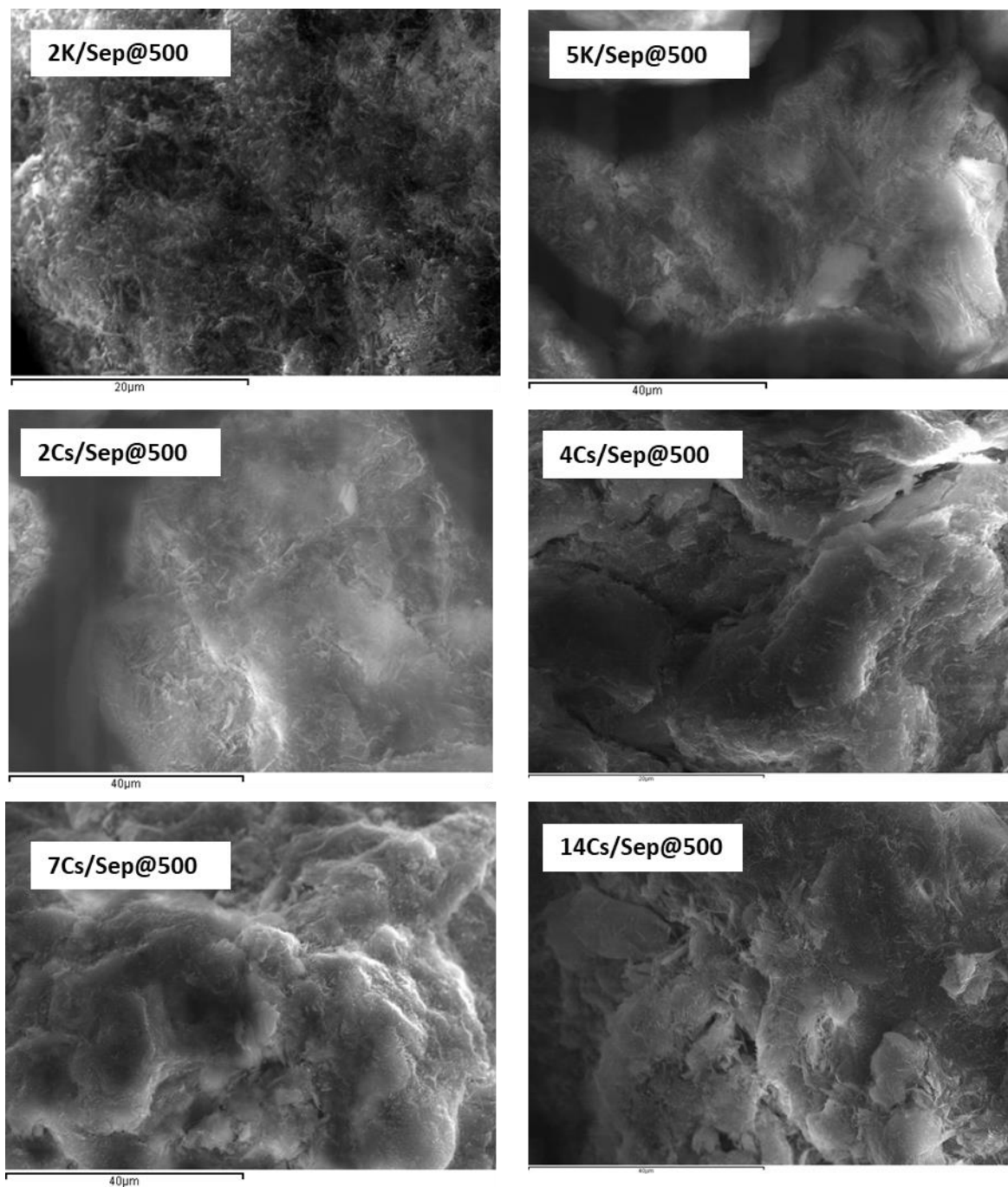
Figure 13   . SEM micrographs of K and Cs-impregnated sepiolite recorded at different magnifications.

As an example, Fig. 14 shows the typical SEM–EDX micrographs of sepiolite doped with Cs_2CO_3 with a theoretical cesium metal loading of 4 and 14wt% The intensities of the peaks associated with the Cs content of the sepiolite surface increased with increasing Cs loading in the EDX spectrum (Fig. 14 a and b). However, the intensities of the Si and Mg peaks decreased with increasing Cs content, as expected.
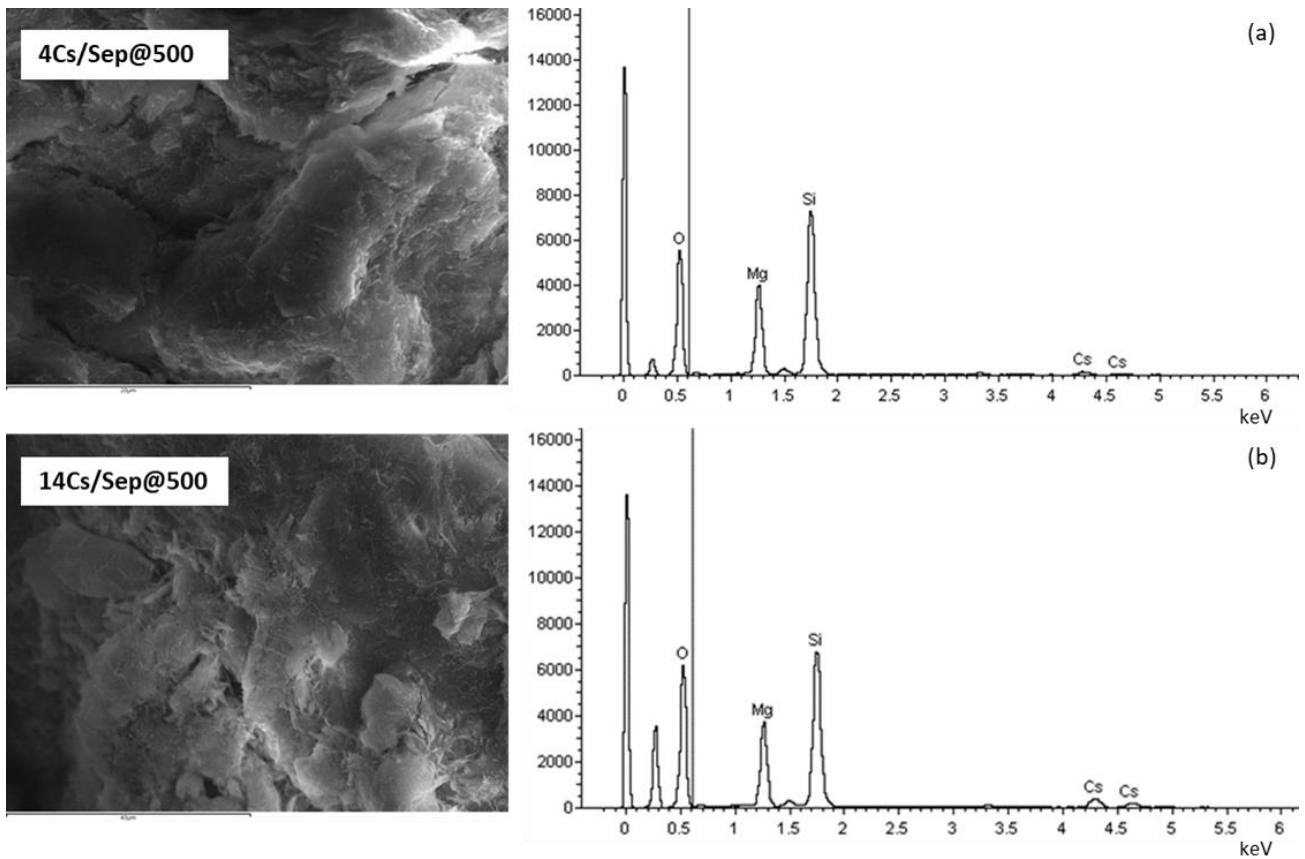
Figure 14   SEM photographs with EDS spectrum of (a) 4Cs/Sep@500; (b) 14Cs/Sep@500.

EDX analysis of the sepiolite and synthesized catalyst particles surface are also reported in Table 5. Each datum reported corresponds to the average value determined from six locations on the catalyst surface.

The EDX analysis showed that the Mg/Si atomic ratio in the solids after alkali-metal impregnation of sepiolite grew with respect to the value observed in the parent sample. From the literature[290] , this observed growing Mg/Si ratio has been attributed to the increasing desilication of sepiolite, with the amount of Mg retained by the solid remaining practically constant (Figure 15).
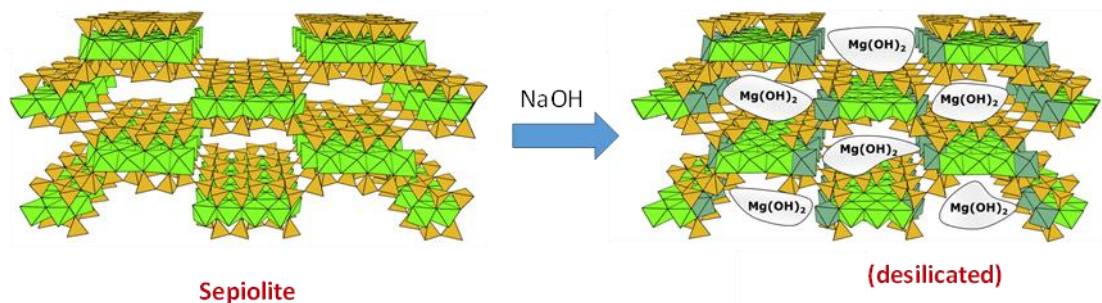
Figure 15   On the desilication of sepiolite. Adapted from ref.[290]

Table 5. *EDX analysis of the surfaces of sepiolite prior to and after the impregnation with alkali metals. [a] Atomic ratio in the solids between Mg/Si.*

	weight [%]											
		Sep@700		**Sep@500**								
Element	**Sepiolite**	**2Na**	**5Na**	**1.2Na**	**2Na**	**5Na**	**2K**	**5K**	**2Cs**	**4Cs**	**7Cs**	**14Cs**
O	44.9	54.8	50.2	63.0	52.8	56.2	51.1	50.9	54.0	47.0	49.8	45.1
Na	-	1.6	5.6	0.6	1.3	3.7	-	-	-	-	-	-
Mg	17.0	15.0	13.7	13.3	15.5	14.7	15.5	14.7	15.1	16.1	14.3	15.8
Si	38.2	28.6	30.5	23.2	30.5	25.4	31.2	28.8	29.4	31.7	26.6	30.0
K	-	-	-		-	-	2.2	5.6	-	-	-	-
Cs	-	-	-	-	-	-	-	-	1.6	5.2	7.8	9.2
Mg/Si [a]	0.51	0.60	0.52	0.57	0.59	0.67	0.57	0.59	0.59	0.59	0.62	0.61

Since an equal value of alkali metal amount expressed in weight % is related to a different moles amount of the alkali metals considered, in order to make a more equitable comparison, the metal loading was calculated even by molar ratio between the metal and the weight of the sepiolite (n_{MET}/w_{SEP}, mmol/g). The results of the EDX analysis are reported in Table 6.

Table 6. *EDX analysis of the surfaces of alkali-doped sepiolite catalysts.*

		Alkali metal loading				
Support	**Met**	**Nominal [wt%]**	**Measured [wt%]**	**Nominal n_{MET}/w_{SEP} [mmol/g]**	**Measured n_{MET}/w_{SEP} [mmol/g]**	**Measured [Atomic %]**
Sep@700	Na	2	1.6	0.87	0.7	1.4
		5	5.6	2.17	2.44	4.8
Sep@500	Na	2	1.3	0.87	0.56	1.1
		5	3.7	2.17	1.62	3.1
	K	2	2.2	0.51	0.56	1.1
		5	5.6	1.28	1.43	2.9
	Cs	2	1.6	0.15	0.12	0.2
		4	5.2	0.30	0.39	0.8
		7	7.8	0.53	0.59	1.2
		14	9.2	1.05	0.69	1.5

4.3.1.5 Temperature programmed desorption, TPD

From the literature emerge that a fine-tuning of both the nature and the amount of acid-base sites is crucial to obtain high *n*-butanol yield.[59,93,99,291] In this section the acid-base properties of the sepiolite

based catalysts have been studied by means of temperature desorption of probe molecules, NH_3 and CO_2, in order to evaluate the acidity and basicity of the samples, respectively.

4.3.1.5.1 Acidity study - TPD-NH₃

Temperature programmed desorption of ammonia (TPD-NH_3) experiments were performed to explore the surface acidity of the samples (Fig. 16-18 and Table 7-9). The NH_3-TPD profile and amount of NH_3 desorbed from the catalyst can be considered as the acid strength distribution and the number of acid sites on the catalyst, including both the Brønsted and Lewis acid sites, respectively.[263] Generally, the solid acid sites can be classified according to their acid strength determined using the temperature of NH3 desorption into three types: weak (150–300 °C), moderate (300–450°C) and strong (450–650 °C) acid sites. [137] Recorded spectra may be further deconvoluted by a Gaussian peak fitting method into separate peaks to be then attributed to different strength acid sites.

Four peaks with maximal temperatures at ~ 180ºC, ~ 260ºC, ~ 350ºC and 560ºC, corresponding to the weak, medium and strong acid sites[292] respectively have been observed. The results of TPD-NH_3 experiments performed over the two sepiolite supports, calcined at 500ªC (Sep@500) and 700ºC (Sep@700) are shown in Fig. 16. The sepiolite sample calcined at 500ºC appeared more acid than the one calcined at higher temperature. There can be noticed three different desorption peaks at 180, 260 and 350 ºC reflecting the presence of acid sites of weak and medium strength white the peak at 560ºC represent the presence of strong acid sites. Calcining the sepiolite sample at 700ºC led to an overall decrease of the desorption peaks and hence acidity, from 2 $\mu mol_{NH3}/m^2$ to 1.4 $\mu mol_{NH3}/m^2$ respectively.
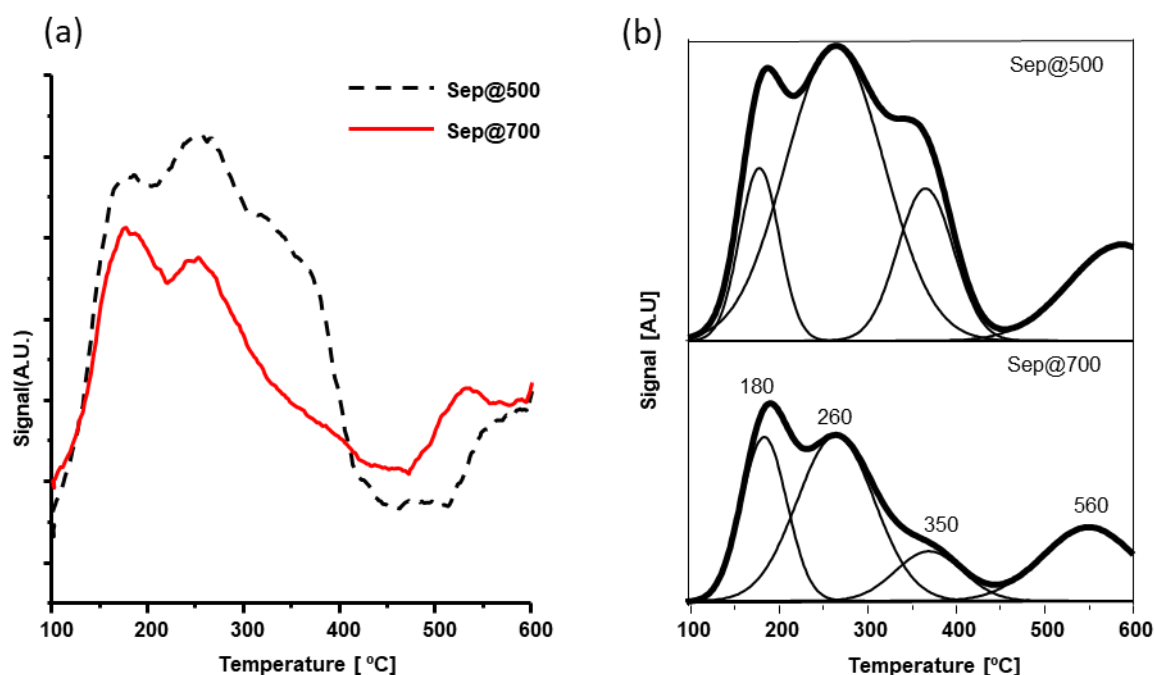
Figure 16   a) Profiles of temperature programmed desorption of ammonia for natural sepiolite calcined at 500 and 700ºC. b) TPD-NH_3 signal in deconvoluted peaks.

The results presented in Figure 17 reflect the acidity changes caused by Na-modification. As in unmodified sepiolite, the Na-sepiolite material contained some acidic sites but with a lower amount. The addition of percentage quantities of sodium to natural sepiolite catalysts progressively eliminates some acid sites as determined by the TPD of NH_3. Indeed, the samples impregnated with sodium exhibited a decreased NH_3 desorption amount, showing fewer fraction of acid sites. Pure sepiolite sample showed a higher fraction of acid sites with higher strength (Figure 17). In table 7, the results of the integration of TPD profiles are reported as moles of NH_3 both per unit weight and per unit surface of the catalyst. It can be observed a general decreasing trend of the quantity of NH_3 adsorbed with increasing sodium amount.
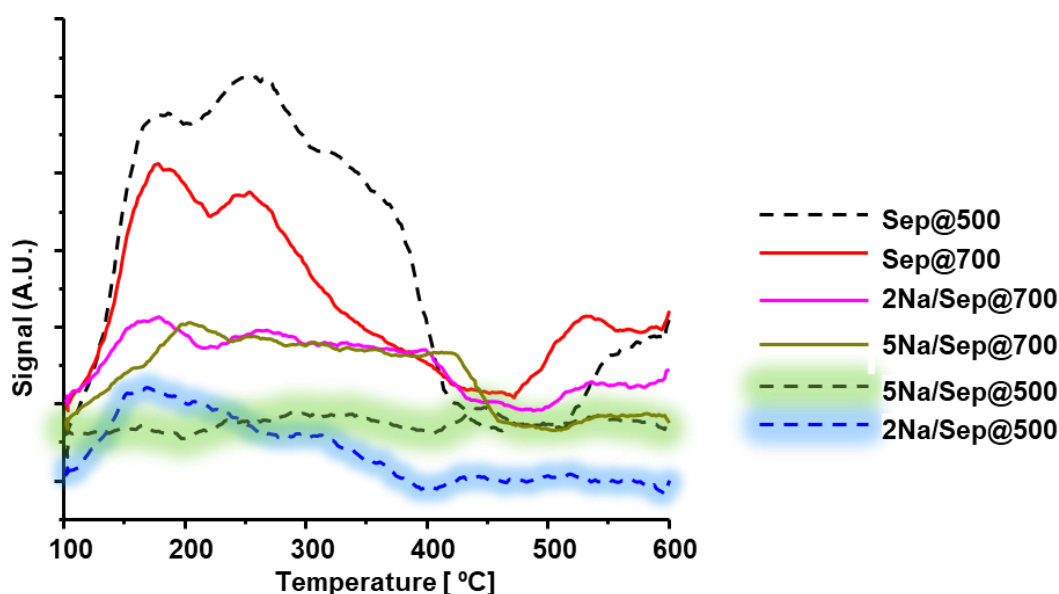
Figure 17   Profiles of temperature programmed desorption of ammonia for the natural sepiolite supports calcined at 500 and 700ºC and the sodium-doped ones, with 2 and 5 wt% of sodium loading.

Table 7. *Characterization results of the sepiolite supports calcined at 500 and 700ºC and the sodium impregnated samples with 2 and 5 wt% metal loading.[a] Determined by EDX analysis. [b] Determined by nitrogen adsorption using BET technique; [c] Determined by BJH method; [d]Determined by TPD-NH3 analysis.*

| Metal | Support | Metal loading | | S_{BET}[b] | Pore[c] | | ACIDITY[d] | |
		Nominal [wt%]	Measured n_{MET}/w_{SEP} [mmol/g][a]	[m^2/g]	Volume [m^3/g]	Average diameter [nm]	[$\mu mol_{NH3}/g_{CAT}$]	[$\mu mol_{NH3}/m^2$]
-	Sep@500	0	-	138	0.21	8.7	280	2.0
	Sep@700	0	-	124	0.22	9.4	175	1.4
Na	Sep@500	2	0.56	124	0.20	9.0	120	1.0
		5	1.62	100	0.20	9.7	54	0.5
	Sep@700	2	0.7	126	0.18	7.7	79	0.6
		5	2.44	102	0.15	8.0	32	0.3

Figure 18 reports the results of the TPD-NH$_3$ performed over the alkali-metals impregnated sepiolite samples.
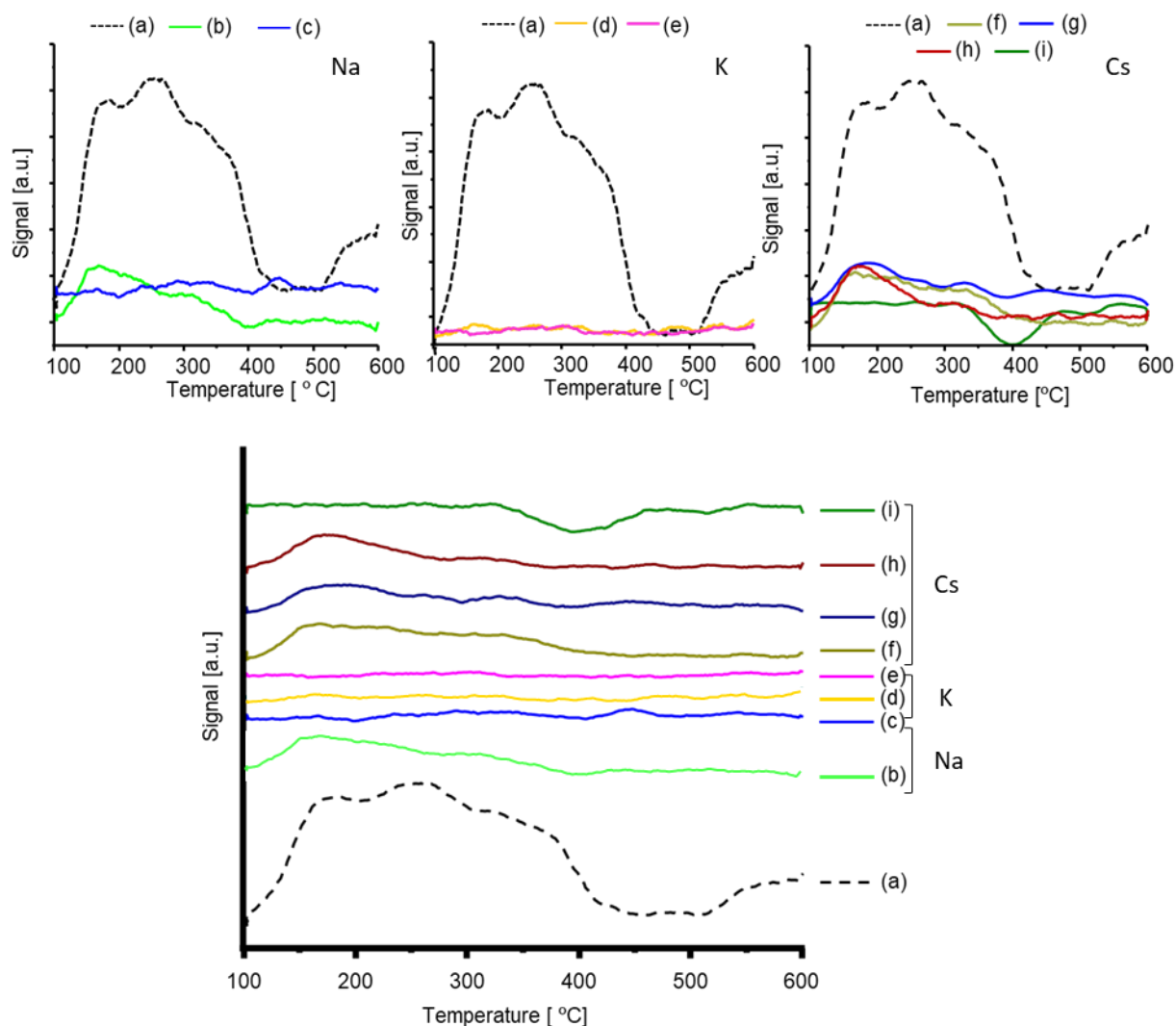
Figure 18   Profiles of temperature programmed desorption of ammonia for the natural sepiolite calcined at 500ºC (Sep@500), and the related alkali metal-doped sepiolite samples. **(Na)** a) Sep@500; b) 2Na/Sep@500; c) 5Na/Sep@500; **(K)** d) 2K/Sep@500; e) 2K/Sep@500; **(Cs)** f) 2Cs/Sep@500; g) 4Cs/Sep@500; h) 7Cs/Sep@500; i) 14Cs/Sep@500.

The incorporation of percentage of alkali-metals to natural sepiolite catalysts progressively eliminates acid sites as determined by the TPD of NH$_3$. Table 8 summarized the TPD-NH$_3$ analysis results performed over the alkali metals-doped sepiolite samples related to their surface areas.

Table 8. *Acidic characteristics of solids determined from TPD-NH3, expressed by μmol of NH3 adsorbed per grams of catalyst and per surface area of catalysts. [a] Determined by EDX analysis. [b] Determined by nitrogen adsorption using BET technique, [c] Determined by BJH method; [d] Determined by TPD-NH3 analysis.*

Support	Met	Alkali metal loading Nominal [wt%]	Measured n_{MET}/w_{SEP} [mmol/g][a]	S_{BET}[b] [m²/g]	Pore[c] Volume [m³/g]	Average diameter [nm]	ACIDITY[d] [μmol$_{NH3}$/g$_{CAT}$]	[μmol$_{NH3}$/m²]
Sep@700	-	-	-	124	0.2	9.4	175.1	1.4
	Na	2	0.7	126	0.2	7.7	79.1	0.6
		5	2.44	102	0.2	8.0	32.3	0.3
Sep@500	-	-	-	138	0.2	8.7	280.2	2.0
	Na	2	0.56	124	0.2	9.0	119.7	1.0
		5	1.62	100	0.2	9.7	53.5	0.5
	K	2	0.56	119	0.2	9.0	144	1.2
		5	1.43	86	0.2	11.3	47	0.5
	Cs	2	0.12	130	0.2	7.9	203.7	1.6
		4	0.39	118	0.2	7.6	148.3	1.3
		7	0.59	110	0.1	8.1	107.8	1.0
		14	0.69	79	0.1	8.9	25.7	0.3

In order to evaluate the effect of copper oxide impregnation over the acid characteristic of the surface resulting sepiolite-based catalysts, a TPD-NH$_3$ analysis have been performed over the sample impregnated with 5 wt% of copper oxide (CuO/Sep@700 5 wt%). Figure 19 reports the results obtained, compared to the corresponding sepiolite support calcined at 700ºC, and it can be observed that copper addition led to a slight decrease of overall acidity. Comparing to the sepiolite support that adsorbed 1.4 μmol$_{NH3}$/m², the CuO/Sep@700 5 wt% adsorbed 1.4 μmol$_{NH3}$/m² (Table 9).
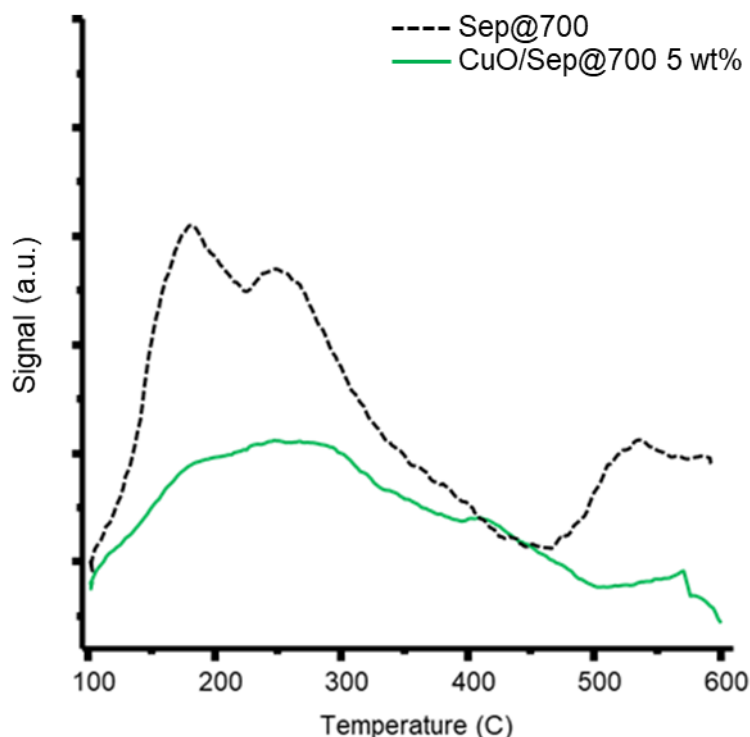
Figure 19   Profiles of temperature programmed desorption of ammonia for the natural sepiolite calcinated at 700ºC (Sep@700), and the 5 wt% copper oxide-impregnated sepiolite sample (CuO/Sep@700 5 wt%).

Table 9. *Acidity from temperature programmed desorption of TPD-NH3, expressed by µmol of NH3 adsorbed per grams of catalyst and per surface area in comparison between the sepiolite support and the 5 wt% CuO-impregnated sepiolite sample. [a] Determined by nitrogen adsorption using BET technique; [b] Determined by TPD-NH3 analysis.*

	S_{BET} [a] $[m^2/g]$	ACIDITY[b]	
		$[\mu mol_{NH3}/g_{CAT}]$	$[\mu mol_{NH3}/m^2]$
Sep@700	124	175.1	1.4
CuO/Sep@700 5 wt%	110	139.9	1.3

4.3.1.5.2 Basicity study – TPD-CO₂

To study the basicity of the sepiolite samples, some temperature-programmed desorption of CO_2 have been performed. The desorption profiles were deconvoluted using Gaussian curves in order to separate the weak, medium and strong basic sites. The weak strength sites are related to curves that show a maximum at temperature lower than 170ºC, the ones between 170 and 270ºC are assigned to medium strength basic sites, and finally, the ones above 270 ∘C are strong basic sites.[99] Table 10 reports the quantification of the basicity in terms of CO_2 desorbed per grams and surface area of the samples. In addition, basicity/acidity ratio in highlighted since from literature [293] is reported that *n*-butanol selectivity is strictly connected with the ratio between acid and basic centres of the

catalyst surface. More in detail, the highest *n*-butanol yields were associated to low ratio between acid and basic centres.

Figure 20 depicts the TPD-CO_2 profiles of the natural sepiolite samples calcinated at 500ºC (Sep@500) and at 700ºC (Sep@700). Both samples exhibited basic behaviour and their TPD-profiles showed several peaks related to basic sites of different strength. In particular, sepiolite calcined at 500ºC exhibited one weak basic sites related to the peaks at 120ºC, then two medium strength basic sites at 220 and 330ºC and another strong basic sites at 420ºC. Calcining the sepiolite at higher temperature led to the disposal of the medium strength basic sites at 220ºC and to a lower value of overall basicity from 1.8 to 1.2 [μmolCO_2/m^2]. In addition, the basic/acid sites ratio decreased from 0.92 to 0.83 while calcining sepiolite at 500ºC and 700ºC, respectively. Mora et al.[282] studied the effect of thermal treatment on sepiolite structure by means of IR analysis, finding a progressive removal of OH groups (of zeolitic water, Mg-OH groups and water octahedrally coordinated to magnesium) with increasing calcination temperature until 800ºC, at which the layered structure of sepiolite collapsed and a new phase formed (estantite). Since exposed hydroxyl groups potentially can act both as Brønsted acid sites and basic sites[294], their changes in quantity during thermal treatment can be the cause of the acidity/basicity changes with increasing calcination temperature.
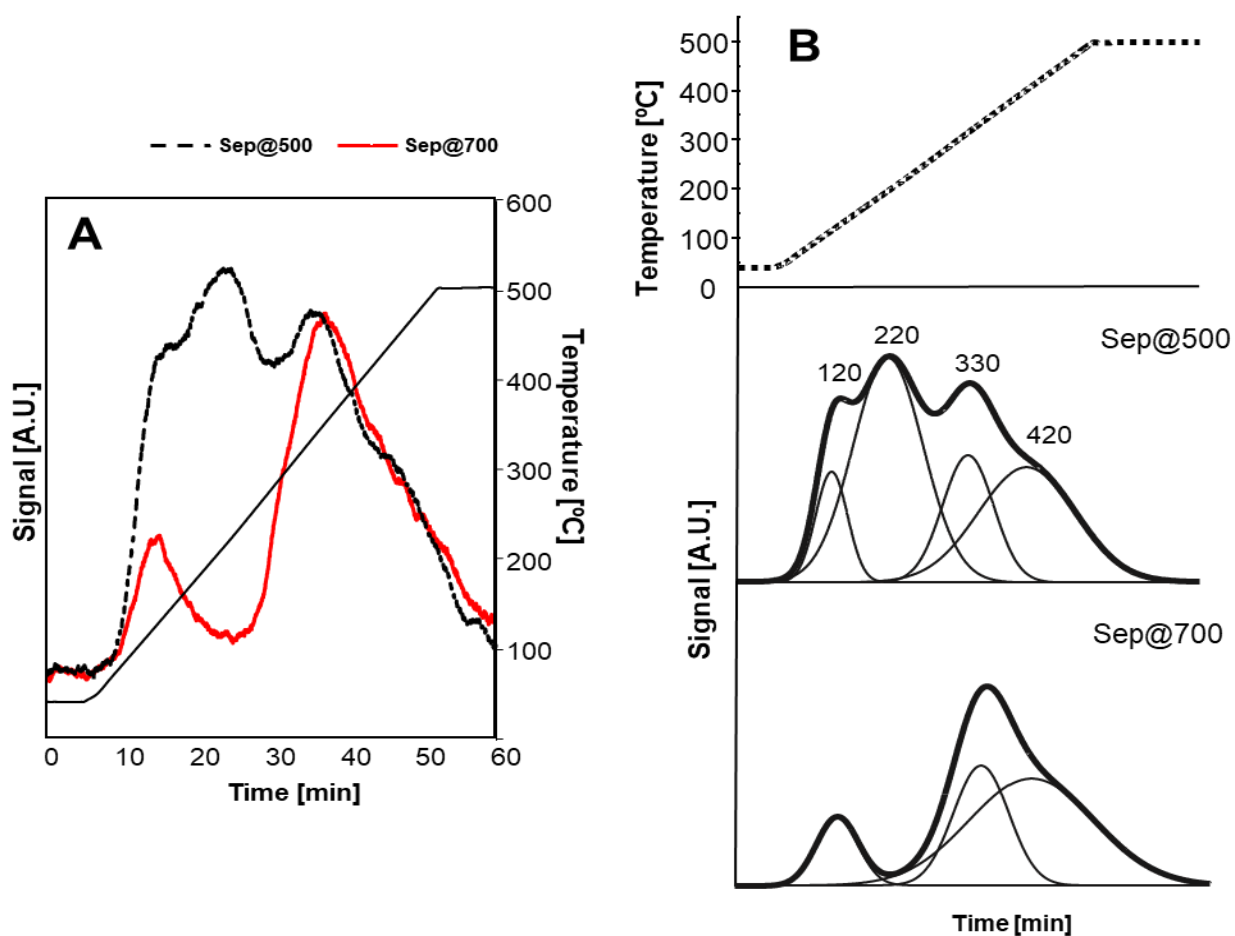
Figure 20   TPD - CO_2 profiles of the sepiolite catalysts calcined at 500ºC (Sep@500) and at 700ºC (Sep@700). (B): The profiles deconvoluted.

Table 10 resumes the TPD-CO$_2$ analysis results obtained over the alkali-doped sepiolite samples, together with the acidity results. The *n*-butanol selectivity from the ethanol Guerbet conversion has been found strictly related to the acid/ base properties of the catalyst, in particular to their relation. [164,295] Accordingly, the acidity/basicity ratio (A/B ratio) has been computed. A prevalent unexpected decrease of the overall basicity after alkali/metal addition has been observed. Nevertheless, a general decrease of the A/B ratio can be noticed with the presence of the alkali metals, linearly related with the extent of the quantity added. As a consequence, a general increase of the overall basicity can be observed with increasing alkali metal loading.

Figure 21A depicts the TPD-CO$_2$ profiles of the Na, K and Cs-doped sepiolite samples containing ca. 0.6 n_{MET}/w_{SEP} [mmol/g] measured (i.e. nominal 2, 2, and 7 wt%, respectively). It is possible to observe that each alkali metal had a different effect on the nature of the basic sites of the sepiolite samples. The potassium addition led to a slight increase of basicity, as can be noted in Table 10. A higher amount of potassium (i.e., 5 wt%) led mainly to an increase of the weakest basic sites (i.e., desorption peak at 120ºC) and to the disappearance of the strongest one. Regarding the cesium impregnated, the basicity increased with increasing Cs amount. Also, even the nature if the basic sites seemed affected by Cs amount. Indeed, with a metal loading of 7wt%, weak (120ºC) and strong (420ºC) are observed. By contrast, the main effect of increasing Cs amount was the enhancement of the density of medium basic sites (220ºC). Overall, a general effect observed is an unexpected decrease of the basic sites number after alkali metal addition and a change of the nature of the basic sites depending on the nature and amount of the alkali metal added. Nevertheless, with increasing metal loading, the basic sites increased, mostly the weak and basic ones at the expense of the strongest ones.
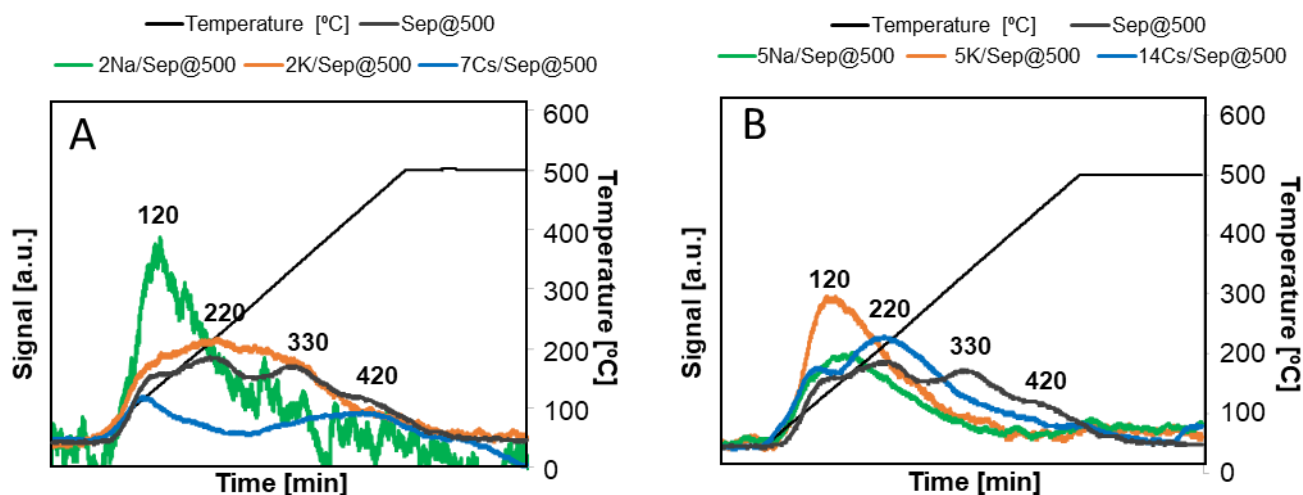
Figure 21 TPD-CO$_2$ desorption profiles of the alkali-metals impregnated sepiolite catalysts. A) 2Na, 2K and 7Cs /Sep@500; B) 5N, 5K and 14 Cs /Sep@500.

Table 10. *Acidity and basicity from temperature programmed desorption of TPD-NH3 and TPD-CO2, expressed by µmol of NH3 or CO2 adsorbed per grams of catalyst and per surface area of the sepiolite catalysts. . [a] Determined by EDX analysis [b] Determined by nitrogen adsorption using BET technique; [c] Determined by TPD-NH3 analysis, [d] Determined by TPD-CO2 analysis, [e] Acidity/Basicity ratio. [e] Basicity/Acidity ratio.*

Support	Met	Alkali amount		S_{BET} [b] $[m^2/g]$	ACIDITY [c]		BASICITY [d]		A/B ratio [e]	B/A ratio [f]
		Nominal [wt%]	Measured n_{MET}/w_{SEP} [mmol/g] [a]		$[\mu mol_{NH3}/g_{CAT}]$	$[\mu mol_{NH3}/m^2]$	$[\mu mol_{CO2}/g_{CAT}]$	$[\mu mol_{CO2}/m^2]$		
Sep@700	-	0	0	124	175.1	1.4	143.6	1.2	1.69	**0.83**
	Na	2	0.7	126	79.1	0.6	149.2	1.2	0.30	**1.98**
		5	2.44	102	32.3	0.3	134.1	1.3	0.07	**4.37**
Sep@500	-	0	0	138	280.2	2	251.6	1.8	2.19	**0.92**
	Na	2	**0.56**	124	119.7	1	168.9	1.4	0.73	**1.37**
		5	1.62	100	53.5	0.5	118.9	1.2	0.21	**2.38**
	K	2	**0.56**	119	144	1.2	268.3	2.3	0.64	**1.88**
		5	1.43	86	47	0.5	142.1	1.7	0.15	**3.31**
	Cs	2	0.12	130	203.7	1.6	44.9	0.3	7.38	**0.22**
		4	0.39	118	148.3	1.3	120.3	1.0	1.66	**0.78**
		7	**0.59**	110	107.8	1	180.9	1.6	0.61	**1.64**
		14	0.69	79	25.7	0.3	154.1	2.0	0.05	**6.53**

The characterization results of the alkali-doped sepiolite samples are summarized in Table 11. The results showed that the most pronounced effect of alkali metals addition on the texture of sepiolite consisted in a fall of the specific surface area. This could be occurred maybe due to a reduction of microporosity of the sample, as can be found in literature for NaOH treated sepiolite. [290] A. Walczyk, et al. [290] related the fall of specific surface area to the fall of micropore surface and volume by an order of magnitude explaining that with the formation and precipitation of $Mg(OH)_2$ from the external Mg^{2+} ions exchanged with sodium ones that have been retained into the structural micropores. Dimensions of sepiolite micropores precluded formation of long range ordering in the precipitated clusters of magnesium hydroxide, hence no relevant reflections appeared in the XRD patterns of alkali activated solids.

It is known that base strength increases with the radius of alkali cations[296]. However, with the same amount of alkali metal added over sepiolite (i.e., ca. 0.6 $mmol_{MET}/g_{SEP}$), neither the acidity nor the basicity followed a linear trend with increasing alkali metal radius. No other phases or species have been detected through XRD analysis, meaning that they could well dispersed over the catalyst surface. Thus, other characterization techniques should be needed to better understand the active sites structures (e.g. XPS, X-ray Absorption Fine Structure XAFS). Nevertheless, linear decrease of the A/B ratio of the sapiolite samples can be noticed with increasing alkali-metal loading.

Table 11. *Textural parameters and characterization results summarized: S_{BET}, V_{PORE}, D_{PORE}, acidity from temperature programmed desorption of TPD-NH3, for the alkali-sepiolite samples. [a] Determined by EDX analysis; [b] Calculated through Scherrer equation, considering the peak at 20.25° for the sepiolite anhydride (ref. 00-026-1227).[c] Determined by nitrogen adsorption using BET technique; [d] Determined by BJH method; [e] Determined by TPD-NH3 analysis. ; [f] Determined by TPD-CO2 analysis; [g] Acidity/basicity ratio; [f] Basicity/acidity ratio.*

Support	Met	Alkali metal loading					D[b]	S_{BET}[c]	Pore[d]		ACIDITY[e]		BASICITY[f]		A/B ratio[g]	B/A Ratio[h]
		Nominal [wt%]	Measured [wt%][a]	Nominal n_{MET}/w_{SEP} [mmol/g]	Measured n_{MET}/w_{SEP} [mmol/g][a]	Measured [Atomic %][a]	[nm]	[m²/g]	Volume [m3/g]	Average diameter [nm]	[$\mu mol_{NH3}/g_{CAT}$]	[$\mu mol_{NH3}/m^2$]	[$\mu mol_{CO2}/g_{CAT}$]	[$\mu mol_{CO2}/m^2$]		
Sep@700	-	0	-	-	-	-	16	124	0.2	9.4	175.1	1.4	143.6	1.2	1.69	0.83
	Na	2	1.6	0.87	0.7	1.1	22.2	124	0.2	9.0	119.7	1	149.2	1.2	0.30	1.98
		5	5.6	2.17	2.44	3.1	17.1	100	0.2	9.7	53.5	0.5	134.1	1.3	0.07	4.37
Sep@500	-	0	-	-	-	-	14.7	138	0.2	8.7	280.2	2	251.6	1.8	2.19	0.92
	Na	2	1.3	0.87	0.56	1.4	13.8	126	0.2	7.7	79.1	0.6	168.9	1.4	0.73	1.37
		5	3.7	2.17	1.62	4.8	13.4	102	0.2	8.0	32.3	0.3	118.9	1.2	0.21	2.38
	K	2	2.2	0.51	0.56	1.1	14.7	119	0.2	9.0	144	1.2	268.3	2.3	0.64	1.88
		5	5.6	1.28	1.43	2.9	14.7	86	0.2	11.3	47	0.5	142.1	1.7	0.15	3.31
	Cs	2	1.6	0.15	0.12	0.2	20.5	130	0.2	7.9	203.7	1.6	44.9	0.3	7.38	0.22
		4	5.2	0.30	0.39	0.8	14.7	118	0.2	7.6	148.3	1.3	120.3	1.0	1.66	0.78
		7	7.8	0.53	0.59	1.2	14.7	110	0.1	8.1	107.8	1	180.9	1.6	0.61	1.64
		14	9.2	1.05	0.69	1.5	20.5	79	0.1	8.9	25.7	0.3	154.1	2.0	0.05	6.53

4.3.2   Catalytic tests

The synthetized MgO was used as reference to compare the catalytic results obtained in the same condition over the sepiolite based catalysts.

All the catalyst samples have been tested into the gas-flow reaction system well explained in the Section 3.2.2, in order to study their catalytic activity in the gas-flow ethanol conversion by feeding a gaseous mixture of EtOH 5 v/v% in N_2.

A typical reaction was performed as follows: the reactor charged with the catalyst was pre-heated at 120°C, at this temperature the vaporized ethanol was fed and analysed with the on-line GC in order to evaluate the exact starting concentration of the reagent. After that, the temperature of the furnace was set to the desired reaction temperature and when reached, the reaction started. For each reaction, fresh new catalyst was loaded inside the reactor.

Several blank tests were performed by feeding ethanol into the reactor, in the absence of the catalytic bed, in the range of the desired temperatures (250 - 450°C), and no EtOH conversion have been detected into the temperature range evaluated.

Initially, the catalytic activity of the sepiolite supports have been studied in the reaction condition of 450°C and atmospheric pressure, with a weight hourly space velocity (WHSV) of 1 g/(g_{CAT}·h) (weight of ethanol fed per hour per unit weight of catalyst loaded in the reactor). Both sepiolite samples, calcinated at 500°C and 700°C have been tested.

The results of the reaction are shown in Fig. 22, where the results obtained with MgO catalyst at 450°C are shown comparatively. It can be noted that the sepiolite samples, Sep@500 and Sep@700, are more active leading to a higher value of ethanol conversion compared to the MgO, 80%, 55% and 35%, respectively. Regardless, the thermally treated sepiolite samples mainly performed as acid catalysts leading to the formation of the dehydration products of ethanol, namely ethyl ether and ethylene. In addition, the sepiolite sample calcined at 700°C was less active than the one treated at 500°C, the lower activity can be related to the lower value of surface area (see Table 11).
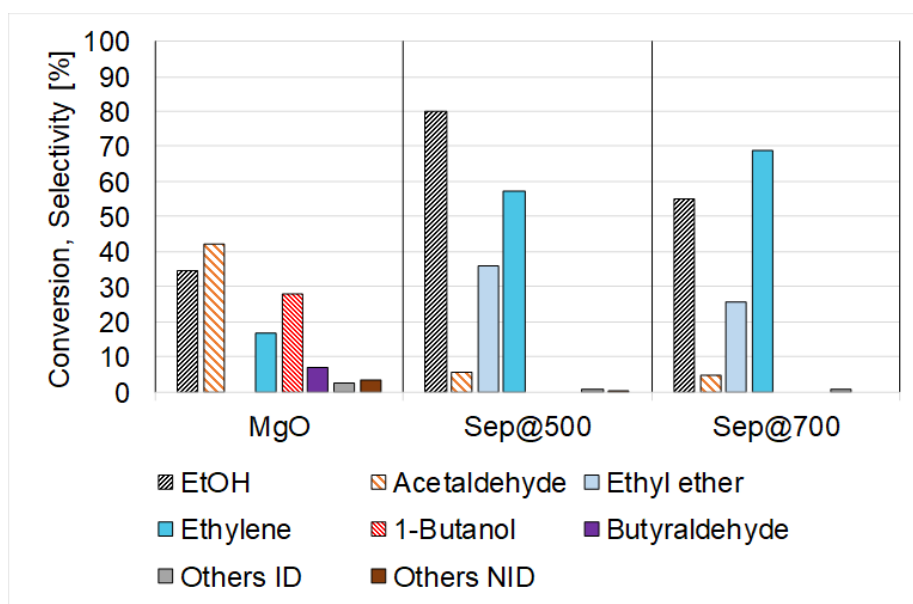
Figure 22 Catalytic results obtained, in terms of ethanol conversion and products selectivity, for the Ethanol gas-phase conversion over MgO and natural Sepiolite calcinated at 500ºC and 700ºC. Others ID: acetone,CO_2, ethane. Reaction conditions: EtOH 5% v/v in N_2, T= 450°C, P= 1 atm, WHSV= 1 g/(g$_{CAT}$·h).

Table 12. *Products distributions from EtOH gas-phase conversion over MgO and natural Sepiolite calcinated at 500ºC and 700ºC. Others ID: acetone, ethane, CO_2. Reaction conditions: EtOH 5% v/v in N2, T= 450°C, P= 1 atm, WHSV= 1 g/(g$_{CAT}$·h).*

		Selectivity [%]						
Catalyst	*X EtOH [%]*	*AA*	*DEE*	*Ethylene*	*BuOH*	*BuA*	*Others ID*	*Others NID*
MgO	35	42		17	28	7	2	3
Sep@500	80	6	36	57	0	0	1	0
Sep@700	55	5	26	69	0	0	1	0

		Yield [%]						
Catalyst	*X EtOH [%]*	*AA*	*DEE*	*Ethylene*	*BuOH*	*BuA*	*Others ID*	*Others NID*
MgO	35	15	0	6	10	2	1	1
Sep@500	80	5	29	46	0	0	1	0
Sep@700	55	3	14	38	0	0	0	0

4.3.2.1 Sodium doped Sepiolite

4.3.2.1.1 Influence of Sodium loading

One possible way to decrease the dehydration rate of ethanol over sepiolite is to selectively remove, block or deactivate the acid sites responsible for dehydration by adding small amounts of alkali metal. Indeed, sodium-impregnated samples, with 2 and 5 wt% of metal loading, have been prepared (Section 3.2.4) and tested in the same reaction conditions used with the sepiolite supports, namely 450ºC and atmospheric pressure and WHSV of 1 g/(g$_{CAT}$·h).

The catalytic results are summarized in Figure 23 and Table 13, reporting the catalytic results in terms of conversion of ethanol and selectivity of the main products, namely ethylene, ethyl ether, acetaldehyde, *n*-butanol and butyraldehyde. The results have been reported in relation with the sodium amount and gathered by means of the sepiolite supports calcined at different temperature, 500ºC (Sep@500) and 700ºC (Sep@700).
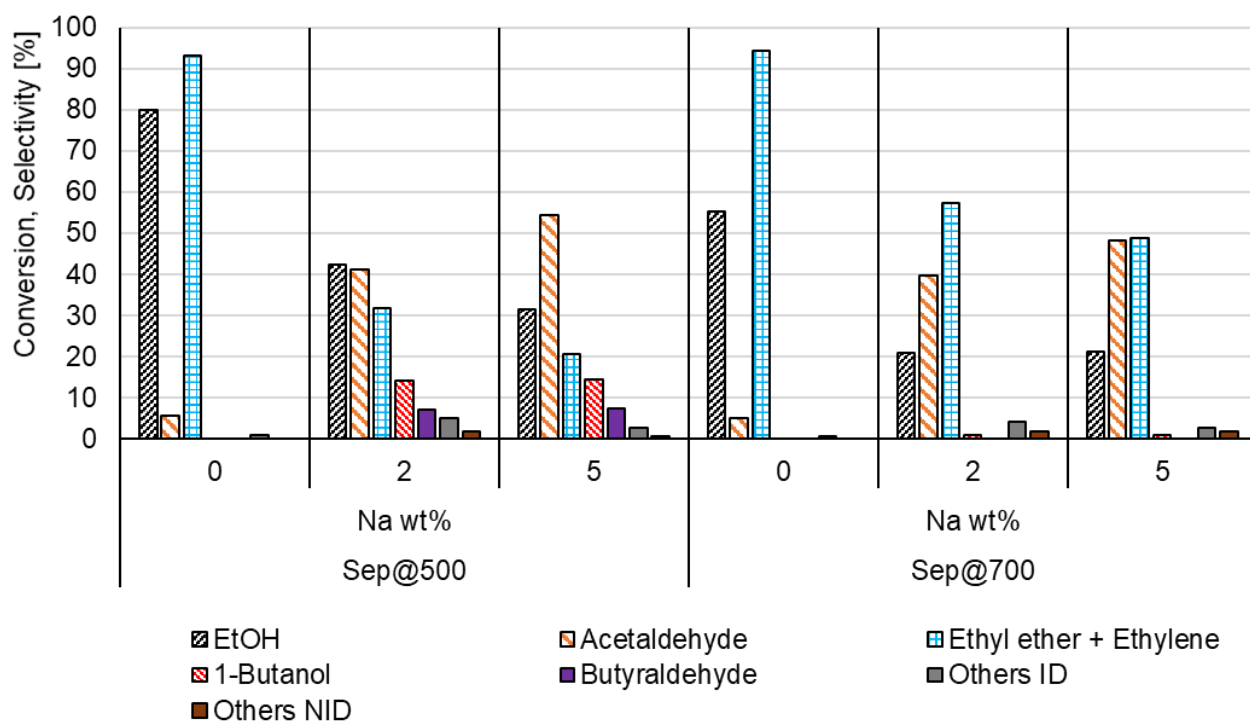
Figure 23   Catalytic results obtained, in terms of ethanol conversion and products selectivity, for the Ethanol gas-phase conversion over the Sepiolite supports calcinated at 500ºC and 700ºC samples, and the sodium impregnated ones with 2 and 5 wt% of metal loading. Others ID: acetone, 2-pentanone, CO$_2$, ethane. Reaction conditions: EtOH 5% v/v in N$_2$, T= 450°C, P= 1 atm, WHSV= 1 g/(g$_{CAT}$·h).

Table 13. *Products distributions from EtOH gas-phase conversion over conversion over the Sepiolite supports calcinated at 500ºC and 700ºC samples, and the sodium impregnated ones with 2 and 5 wt% of metal loading. Others ID: acetone, 2-pentanone, CO2, ethane. Reaction conditions: EtOH 5% v/v in N2, T= 450°C, P= 1 atm, WHSV= 1 g/(g_{CAT}·h).*

	Na wt%	X EtOH [%]	AA	Ethylene	DEE	BuOH	BuAA	Others ID	Others NID
				Selectivity [%]					
Sep@500	0	80	6	57	36	0	0	1	
	2	42	41	19	13	14	7	5	2
	5	31	54	13	8	14	7	3	1
Sep@700	0	55	5	69	26	0	0	1	
	2	21	40	38	13	1	0	4	2
	5	21	48	35	6	1	0	3	2
				Yield [%]					
Sep@500	0	80	5	46	29	0	0	1	0
	2	42	17	8	6	6	3	2	1
	5	31	17	4	3	4	2	1	0
Sep@700	0	55	3	38	14	0	0	0	0
	2	21	8	8	3	0	0	1	0
	5	21	10	7	1	0	0	1	0

As in it can be noted from the catalytic results reported in the figure, the introduction of sodium ions Na⁺ into the sepiolite catalyst resulted in a generalized reduction in activity, leading to lower values of ethanol conversion. Subsequently and simultaneously, the selectivity of ethanol dehydration products, ethylene and ethyl ether, decreased while the dehydrogenation reaction product of ethanol, acetaldehyde, increased. This can be related to the change of acid-base properties of the catalysts, as measured by TPD-NH₃ analysis (Table 10), where it has been observed a decrease of the acidity with increasing alkali-metal loading. The addition of the alkali metal led to the formation of new basic sites the presence of which can be related to the formation of the dehydrogenation product of ethanol, acetaldehyde.

Interestingly, over the Sep@700 supported samples in addiction of being less active, the extent of the decreasing of acid reaction products was lower than the one obtained over the Sep@500 supported samples. The overall selectivity of ethyl ether and ethylene decreased from ~95% for the support alone to ~ 50% with 5wt% of sodium for the sepiolite calcined at 700ºC, while it decreased from ~95% to ~20% for the one supported over sepiolite calcined at 500ºC.

Particularly noteworthy is that the Sep@500 supported catalysts led to the formation of the Guerbet reaction product of ethanol, *n*-butanol. Indeed, the 2Na/Sep@500 catalyst in the above mentioned reaction conditions allowed to obtain *n*-butanol with a selectivity of 14%. An increase of the alkali metal loading did not lead to an increase of *n*-butanol selectivity, obtaining even in this case a selectivity of about 14%. The catalytic results are in accordance with the BET and TPD-NH₃ results. (see Table 11). Indeed, the lower activity can be related to the lower BET surface area with increasing metal loading and at the same time. The lower amount of acid sites detected by TPD

analysis is in accordance with the lower amount of acid reaction products. A lowered acidity can be the reason of the formation of *n*-butanol, that requires a right balance between acid and basic sites.[293]

4.3.2.1.2 Contact time effet

In order to evaluate how the 2Na/Sep@700 catalyst worked at higher ethanol conversion, over the latter it was explored the effects of WHSVs variation on products distribution in the range 1, 0.5 and 0.33 g/(g$_{CAT}$·h), by keeping the reaction temperature at 450°C. The catalytic results are reported in Figure 24 and Table 14 as a function of 1/WHSV (g$_{CAT}$/g·h).

Table 14. *Catalytic results obtained, in terms of ethanol conversion (X%) and products selectivity and yield, for the ethanol gas-phase conversion over **2Na/Sep@700**. Others ID: ethane, 1,3-butadiene. Reaction conditions: EtOH 5% v/v in N$_2$, T= 450°C, P= 1 atm, WHSV= 1, 0.5 and 0.33 g/(g$_{CAT}$·h).*

1/WHSV [h]	X EtOH [%]	Selectivity [%]						
		AA	Ethylene	DEE	BuOH	BuA	Others ID	Others NID
1	21	40	38	19	1	0	4	2
2	30	33	42	21	1	0	2	0
3	46	31	40	24	2	1	3	1

| 1/WHSV [h]	X EtOH [%]	Yield [%]						
		AA	Ethylene	DEE	BuOH	BuA	Others ID	Others NID
1	21	8	8	4	0.2	0	1	0.4
2	30	10	13	6	0.4	0	1	0
3	46	14	19	11	1	0.2	1	0.2
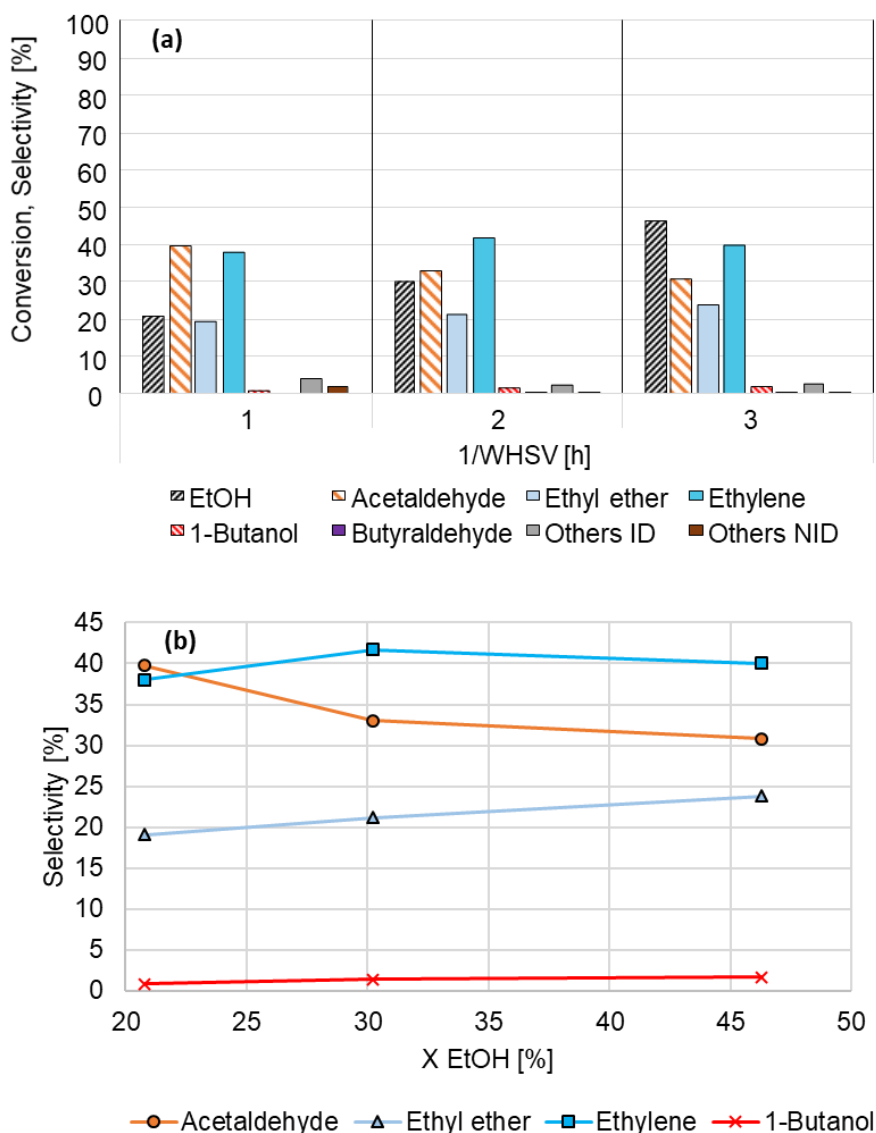
Figure 24   Catalytic results obtained, in terms of ethanol conversion and products selectivity, for the Ethanol gas-phase conversion over **2Na/Sep@700**. (a) EtOH conversion (X) and products selectivity in function of 1/WHSV. (b) Variation of selectivity of main products as a function of EtOH conversion. Others ID: ethane, 1,3-butadiene. Reaction conditions: EtOH 5% v/v in N_2, T= 450°C, P= 1 atm, WHSV= 1, 0.5 and 0.33 g/(g_{CAT}·h).

In general, decreasing the WHSV (defined as the mass flow rate of ethanol divided by the weight of catalyst) and so increasing the contact time between the catalyst and the reagents, led to an increase in both ethanol conversion and selectivity of its dehydrogenation products, ethylene and ethyl ether (Figure 24); with concomitant decrease of acetaldehyde selectivity. A slight increase of *n*-butanol selectivity (from 1 to 2 %) was observed.

A test with lower WHSV (0.5 g/(g_{CAT}·h)) by doubling the catalyst amount has been performed even over the 5Na/Sep@500. Figure 25 and Table 15 report the results obtained over the sodium impregnated samples including the test performed at higher contact time in order to evaluate its activity at higher ethanol conversion.
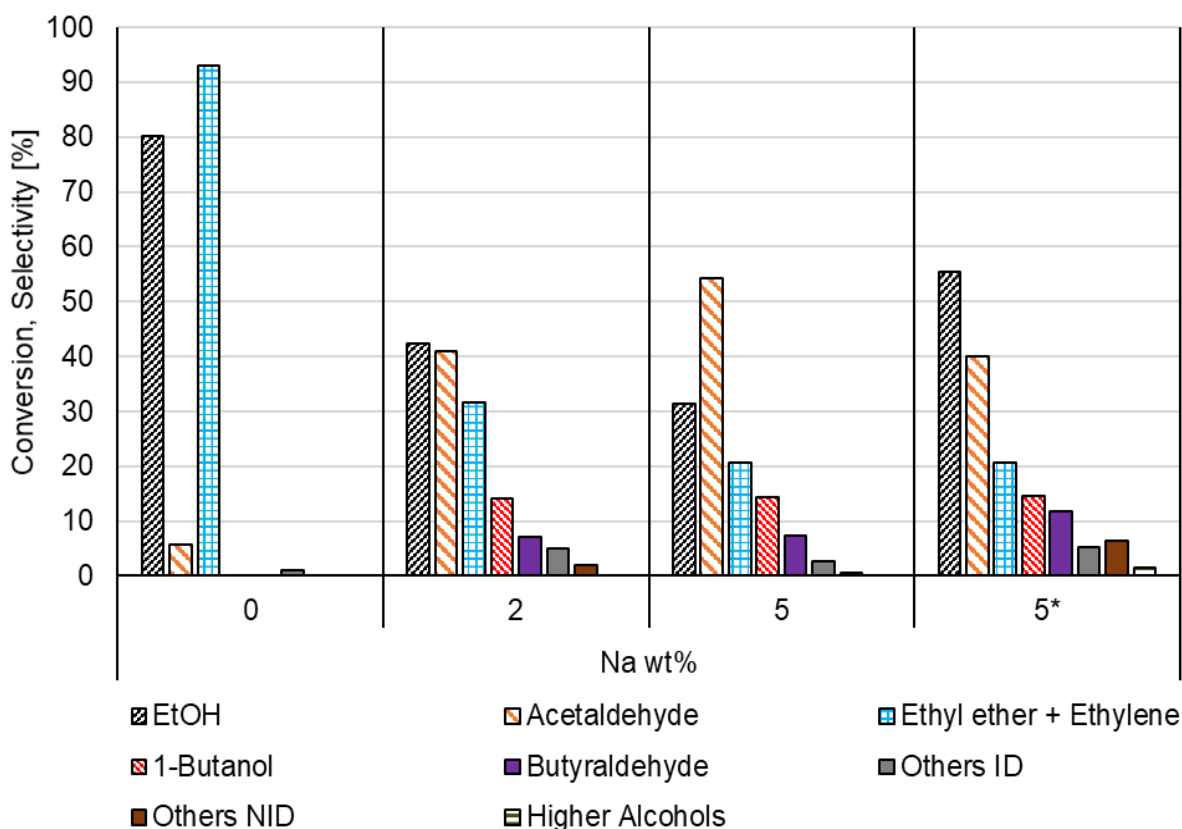
Figure 25 Catalytic results obtained in the Ethanol conversion over the Sepiolite supports calcinated at 500ºC and the sodium impregnated ones with 2 and 5 wt% of metal loading. Others ID: acetone, 2-pentanone, CO_2, ethane. Guerbet alcohols: 2-ethyl-butanol, 1-hexanol, 2-ethyl-hexanol, 1-octanol. Reaction conditions: EtOH 5% v/v in N_2, T= 450°C, P= 1 atm; WHSV= 1 g/(g_{CAT}·h). *WHSV= 0.5 g/(g_{CAT}·h).

Table 15. *Catalytic results obtained, in terms of ethanol conversion (X%) and products selectivity and yield, for the ethanol gas-phase conversion over **2Na/Sep@700**. Others ID: ethane, 1,3-butadiene. Reaction conditions: EtOH 5% v/v in N_2, T= 450°C, P= 1 atm, WHSV= 1, 0.5 and 0.33 g/(g_{CAT}·h).*

| WHSV [g/(g_{CAT}·h)] | Na wt% | X EtOH [%] | Selectivity [%] | | | | | | | |
			AA	Ethylene	DEE	BuOH	BuA	Others ID	Others NID	Higher Alcohols
1	0	80	6	57	36	0	0	1	0	0
1	2	42	41	19	13	14	7	5	2	0
1	5	31	54	13	8	14	7	3	1	0
0.5	5*	55	40	14	7	15	12	5	6	1

| WHSV [g/(g_{CAT}·h)] | Na wt% | X EtOH [%] | Yield [%] | | | | | | | |
			AA	Ethylene	DEE	BuOH	BuA	Others ID	Others NID	Higher Alcohols
1	0	80	5	46	29	0	0	1	0	0
1	2	42	17	8	6	6	3	2	1	0
1	5	31	17	4	3	4	2	1	0	0
0.5	5*	55	22	8	4	8	6	3	3	1

A rise in contact time led to an increase of ethanol conversion, as expected, but did not affected the selectivity of *n*-butanol, that remained around 14%. It can be observed a decrease of selectivity of

acetaldehyde and a concomitant increase of the selectivity of higher Guerbet alcohols as well as the other identified (Other ID) and unidentified (Other NID) products. It can be suggested that the selectivity of *n*-butanol remained stable since it has been converted to its dehydrogenation product, butyraldehyde, whose selectivity increased from 7 to 12%, and to higher alcohols through the Guerbet route acting as intermediate product, indeed their presence has been detected at higher contact time. The same suggestion can be proposed for the lower selectivity of acetaldehyde that acted as intermediate product for side reactions that led to the formation of acetone and 2-pentanone. Ketones can be formed through consecutive Tishchenko disproportion reaction[297] of acetaldehyde forming the ester (ethyl acetate, not detected) and consecutive ester ketonization reactions[105], producing water and CO_2 as by-products. The reaction mechanism from which ketones can be formed starting from ethanol is depicted in Scheme 1.
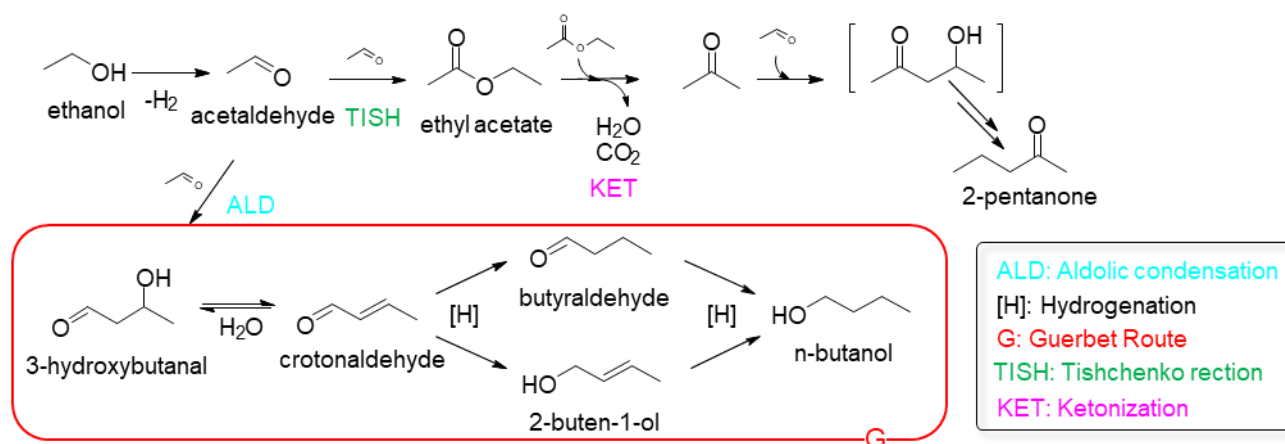
Scheme 1. Reaction mechanism proposed over the Na-sepiolite catalytic system.

4.3.2.2 Transition metals supported Sepiolite

The dehydrogenation reaction from ethanol to acetaldehyde, that is the generally accepted first step of the Guerbet reaction path which leads to the formation of *n*-butanol, is often identified as the rate limiting step, in particular when operating at low temperatures.[298] Catalytic systems without transition metals require higher temperature for alcohol coupling due to higher activation energy of dehydrogenation.[67,299,300]

In order to enhance the production of acetaldehyde, frequently reported as a key intermediate products into the Guerbet mechanism (accordingly to Scheme 1) as well as the subsequent hydrogenation steps of the coupled intermediates that characterize this mechanism, some sepiolite catalyst samples have been prepared by the addiction of a transition metal, namely copper and nickel. The synthesis method by means of wet impregnation has been explained in section 3.2.4.

4.3.2.2.1 Copper

Firstly, the two sepiolite supports calcinated at 500ºC and 700ºC (Sep@500 and Sep@700) have been impregnated with copper oxide with 5 wt% of metal loading (CuO/Sep@500 5wt% and CuO/Sep@700 5 wt%). Then, even the sodium impregnated sepiolite samples with 2 wt% of Na, both calcinated at 500ºC and 700ºC, have been impregnated with the same copper amount (CuO/2Na/Sep@500 5wt% and CuO/2Na/Sep@700 5 wt%).

Catalytic results, in terms of products distribution and ethanol conversion, obtained in the reactions performed at 450ºC, atmospheric pressure and WHSV of 1 g/(g$_{CAT}$·h) over the prepared catalysts are reported in Figure 26 and Table16.

Regarding the Sep@700, the addition of copper raised the ethanol conversion, showing higher activity and leading to lower production of the dehydration products of ethanol with concomitant increase of acetaldehyde formation. In particular, when copper is added over the sepiolite impregnated with sodium (i.e., CuO/2Na/Sep@700 5 wt%), a selectivity of acetaldehyde of 60% has been reached. Moreover, even a slight formation of *n*-butanol can be observed over the same catalytic system. As it can be observed in Figure 26, a general effect of the addition of copper has been the decrease of both ethanol conversion and ethylene selectivity with a concomitant increase of acetaldehyde selectivity, as expected. The decrease of the dehydration products of ethanol reflects the decrease of the overall acidity measured by TPD-NH$_3$ analysis as shown in Section 4.3.1.5. This result is in accordance with Angelici et at. [271] who explained the drop in ethylene and ethyl ether production by the poisoning activity of copper in regards of the most acidic sites of the support (i.e., SiO$_2$-MgO).
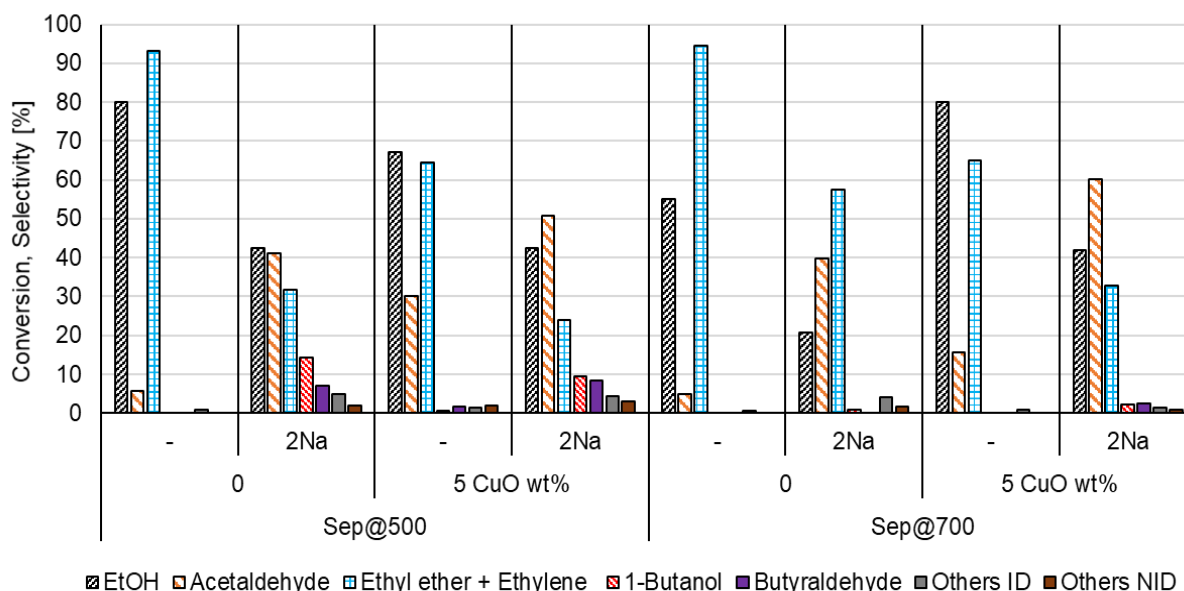
Figure 26   Catalytic results obtained in the Ethanol conversion over the Sepiolite supports calcinated at 500ºC and 700ºC (Sep@500, Sep@700), the sodium impregnated ones with 2wt% of metal loading (2Na/Sep@500, 2Na/Sep@700) and the copper impregnated ones with 5wt% of CuO metal loading. Others ID: acetone, 2-pentanone, CO$_2$, ethane, 1,3-butadiene. Reaction conditions: EtOH 5% v/v in N$_2$, T= 450°C, P= 1 atm; WHSV= 1 g/(g$_{CAT}$·h).

Table 16. *Catalytic results obtained, in terms of ethanol conversion (X%) and products selectivity and yield, for the ethanol gas-phase conversion over the Sepiolite supports calcinated at 500ºC and 700ºC (Sep@500, Sep@700), the sodium-impregnated ones with 2wt% of metal loading (2Na/Sep@500, 2Na/Sep@700) and the copper impregnated ones with 5wt% of CuO metal loading. Others ID: acetone, 2-pentanone, CO_2, ethane, 1,3-butadiene. Reaction conditions: EtOH 5% v/v in N_2, T= 450ºC, P= 1 atm; WHSV= 1 g/($g_{CAT}·h$).*

				Selectivity [%]						
Support	CuO amount [wt%]	Na Amount [wt%]	X EtOH [%]	AA	Ethylene	DEE	BuOH	BuA	Others ID	Others NID
Sep@500	-	-	80	6	57	36	0	0	1	
	5	-	67	30	37	27	1	2	1	2
	-	2	42	41	19	13	14	7	5	2
	5	2	43	51	15	9	10	8	4	3
Sep@700	-	-	55	5	69	26	0	0	1	
	5	-	80	16	52	29	0	0	1	0
	-	2	21	40	38	13	1	0	4	0
	5	2	42	60	22	11	2	2	1	1

				Yield [%]						
Support	CuO amount [wt%]	Na Amount [wt%]	X EtOH [%]	AA	Ethylene	DEE	BuOH	BuA	Others ID	Others NID
Sep@500	-	-	80	5	46	29	0	0.0	0.8	0.0
	5	-	67	20	25	18	1	1.2	0.9	1.3
	-	2	42	17	8	6	6	3.0	2.1	0.8
	5	2	43	22	7	4	4	3.6	1.9	1.3
Sep@700	-	-	55	3	38	14	0	0.0	0.4	0.0
	5	-	80	12	42	23	0	0.0	0.8	0.0
	-	2	21	8	8	3	0	0.0	0.8	0.0
	5	2	42	25	9	5	1	1.0	0.6	0.4

Even if the selectivity of acetaldehyde increased with copper addition, this did not lead to an increase of *n*-butanol formation, the selectivity of which instead decreased after copper addition, in all cases examined. For example, *n*-butanol selectivity obtained over 2Na/Sep@500 was 14% while after copper addition it decreased to 10%. Meanwhile, the selectivity of butyraldehyde (BuA) slightly increased from 7 to 8 %, the formation of which could be explained both by the hydrogenation of crotonaldehyde, an intermediate product of the aldol condensation route, but even by *n*-butanol dehydrogenation. Indeed, a concomitant decrease of *n*-butanol selectivity can be observed (from 14 to 10%). This could suggest that *n*-butanol formation over sepiolite could happen through a different pathway that did not involve acetaldehyde and its condensation, in contrast to the most accepted one based on aldol condensation. Indeed, *n*-butanol could be formed through the direct route, by dimerization of ethanol, for which redox catalyst properties are not required.[283]

The presence of copper in the catalytic system did not favoured *n*-butanol formation. In seems that copper only acted as dehydrogenation promoter, favouring acetaldehyde (and butyraldehyde) formation. In the literature is reported that copper addition to a SiO_2-MgO system resulted in a change of the rate limiting step, causing the consecutive aldol condensation of acetaldehyde to become the rate-determining one in ethanol conversion into butadiene.[148] Angelici et al. added copper to a SiO_2-MgO material in order to promote butadiene formation from ethanol (Ostromislensky and Lebedev process).[148,271] They stated that Cu addition had the double effect of promoting the dehydrogenation of ethanol toward acetaldehyde and of modifying the acidic/basic

properties of the support, enhancing butadiene formation. Indeed, the most accepted mechanism for butadiene formation from ethanol requires a multifunctional catalyst containing both redox and acid/base active sites in order to catalyse butadiene formation from ethanol. The so-called Toussaint's aldol condensation mechanism[301] by which butadiene should be formed, consists in a parallel reaction to the Guerbet one, with acetaldehyde as key intermediate.[302] The mechanism, depicted in Scheme 2, rely on of five steps: dehydrogenation of ethanol to acetaldehyde, aldol condensation or aldolization of acetaldehyde to 3-hydroxybutanal, then dehydrated to crotonaldehyde, reduction of crotonaldehyde to crotyl alcohol, dehydration of crotyl alcohol to butadiene. The intermolecular hydrogen transfer between ethanol and crotonaldehyde is believed to occur via a Meerwein–Pondorf–Verley mechanism (MPV), with ethanol acting as H-donor, which requires the participation of acid and basic sites. [145] Butadiene formation has not been observed over the CuO/Sep@500 5 wt% catalyst. Nevertheless, the concomitant presence of both alkali metal and copper led to the formation of butadiene (i.e. selectivity of 2%, grouped into the "others ID" products). Thus, the presence of sodium into the catalytic system could furnish the basicity required to catalyse that step. Regardless, neither the presence of crotonaldehyde nor the one of crotyl alcohol has been detected during the catalytic tests. Besides, the "direct route" in which acetaldehyde and ethanol condensate yielding alkenols that produce butadiene by consecutive dehydration, has been suggested from the literature. [303] Even in this case, basicity is required to catalyse the condensation step.
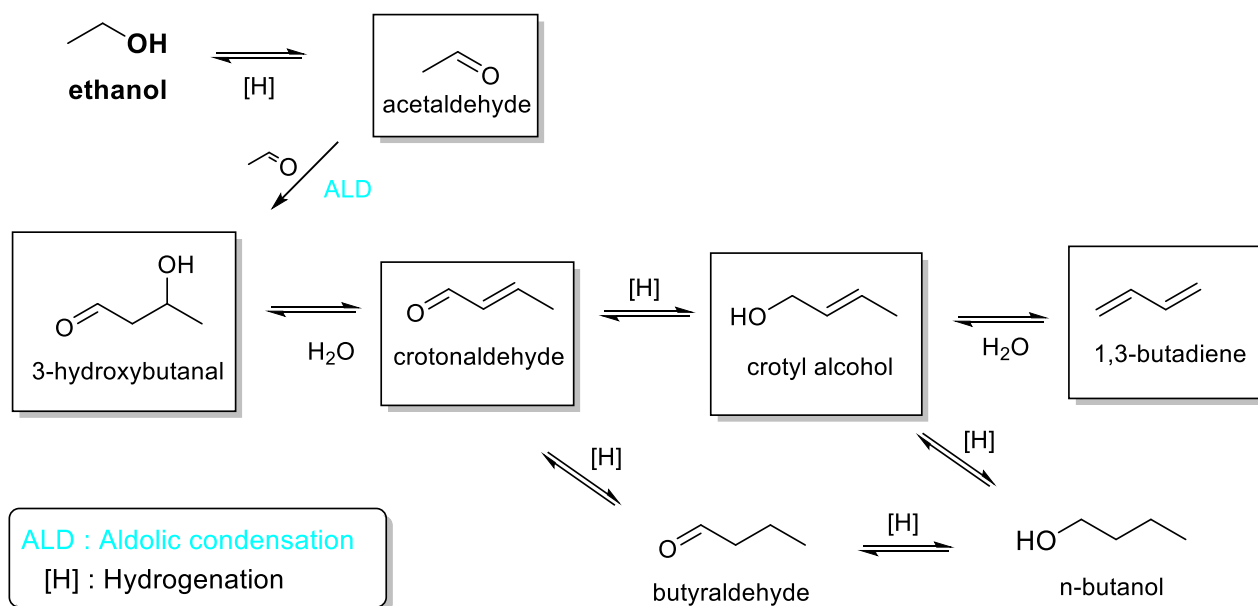
Scheme 2. Ethanol conversion to 1,3-butadiene (Toussaint pathway) and to *n*-butanol (Guerbet route).

4.3.2.2.1.1   *Catalytic results over the time on stream*

Figure 27 reports the catalytic results in terms of ethanol conversion and products selectivity as a function of the time on stream (h), obtained for the reactions performed for 2.2 hours, at 450ºC, atmospheric pressure and WHSV of1 h^{-1}. As it can be noticed, ethanol conversion decreased with the time on stream, suggesting that the catalysts partially deactivated during the reaction. Regarding

the catalyst CuO/Sep@500 5 wt%, with decreasing conversion (i.e., from 83 to 60%), the selectivity of the acidic products DEE and ethylene increased (i.e., from 47.5 to 70%) while the one of acetaldehyde decreased (i.e., from 33 to 27%). This could suggest that with partial deactivation of the catalyst is related to the change of active sites responsible for ethanol dehydrogenation.

Nevertheless, with regard to the CuO/2Na/Sep@500 5 wt%, ethanol conversion decreased from 55 to 40% with the time on stream. Concomitantly, the selectivity of the ethanol-Guerbet product (i.e., *n*-butanol) slightly increased and the one of its dehydrogenation product (i.e., butyraldehyde) decreased. Only a slight decrease of acetaldehyde and concomitant increase of dehydration products (i.e., DEE and ethylene) can be observed, of around 2%, resembling the behaviour observed of the catalyst devoid of alkali metal.
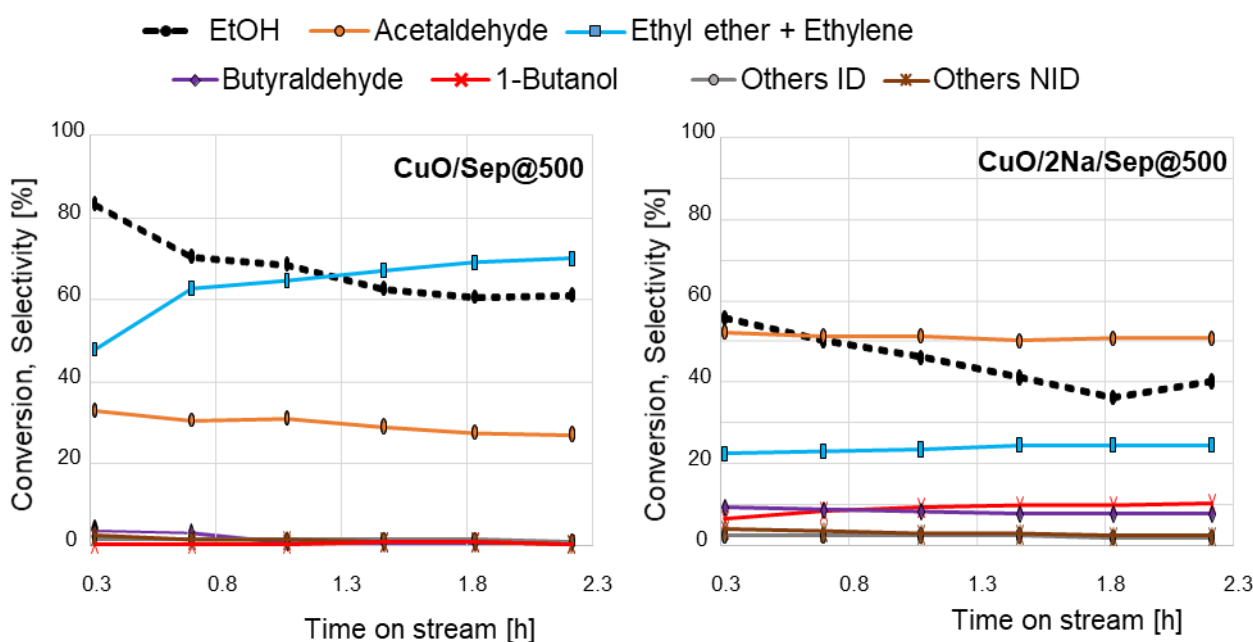
Figure 27   Catalytic results obtained in the Ethanol gas-phase conversion over the CuO/Sep@500-5wt% and the CuO/2Na/Sep@500-5wt% catalyst in terms of conversion of ethanol and main products selectivity as a function of the time on stream,(h). Others ID (acetone, 2-pentanone, CO_2, ethane).Reaction conditions: EtOH 5% v/v in N_2, T=450°C, P= 1 atm, WHSV= 1 g_{EtOH}/(gcat·h).

4.3.2.2.1.2   Diffuse-reflectance UV-visible (DR-UV-vis) spectrometry

To shed some light on the nature of the copper species, supported catalysts with 5 wt% of metal loading were studied by means of diffuse-reflectance UV/Vis (DR-UV-vis) spectroscopy, in particular the CuO/Sep@500-5wt% and the CuO/2Na/Sep@500-5wt%. In order to evaluate the copper state after reaction, the same analysis has been performed even over the spent catalysts. Figure 28 reports the results obtained.
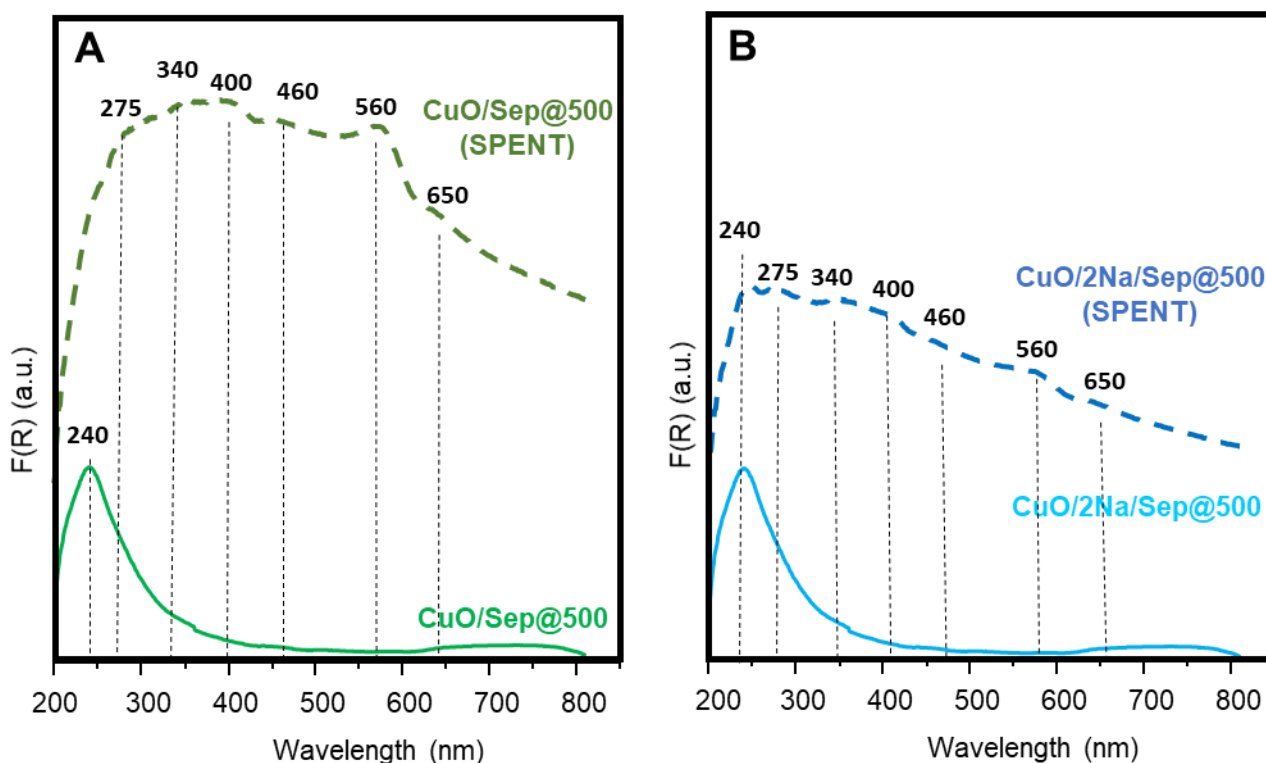
Figure 28   Diffuse-reflectance UV/Vis spectra of fresh and spent catalyst after reaction performed at 450ºC, atmospheric pressure and WHSV of 1 h^{-1}, EtOH in N$_2$ 5% v/v. A): CuO/Sep@500 5 wt%; B) CuO/2Na/Sep@500 5 wt%.

Both the fresh catalysts analysed exhibited a similar spectra, characterized by two absorption bands. The sharp one at ca. 240 nm can be assigned the ligand-to-metal charge-transfer (LMCT) from a molecular orbital primarily on O^{2-} to an orbital mainly on an isolated Cu^{2+} in octahedral coordination.[304] This CT is characteristic of highly dispersed (isolated) Cu^{2+}−O^{2-} in octahedral coordination of CuO oligomers (O^{2-}Cu^{2+} → O$^-$Cu$^+$ LMCT transition), showing the presence of isolated CuO species. [271] The other band in the spectral range 600-800 nm is a relatively broad asymmetrical peak related to Cu(II) ligand field d-d transitions, in line with the reported for the bulk CuO. [305,306] They are also indicative of Cu(II) species in a (distorted) octahedral field. Similar spectra have been reported for different Cu-zeolites, and have been discussed in terms of hydrated Cu(II) ions. [304,305]

The spectra of the spent catalysts obtained were quite different from the fresh ones, indicating the presence of carbonaceous materials deposits[271,307–309] as well as a structural changes presumably via a redistribution of the Cu(II) sites. [271] After reaction, in the spectra appeared bands at ca. 275, 340, 400, 460, 560 (6) and 650 (7) nm. From the literature[309], some of those signals has been assigned to carbonaceous deposits, mainly located inside the porous structure when the methanol-to-olefin reaction over zeolite catalyst is performed.[308,309] Nevertheless, in addition to the formation of absorption bands, an increase in absorbance over the whole range of wavenumbers can be observed, which could be related to formation of larger carbonaceous deposit on the surface of the catalyst.[307] The bands at 275 can be assigned to benzene, toluene and xylenes; the band at ca. 400 nm - to mononuclear aromatics with 4, 5 and 6 methyl groups; the broad bands at ca. 460 - to a

group of binuclear aromatics with different degrees of methylation; the bands at ca. 650 nm - to aromatics with ≥3 nuclei.

In addition, the variations in the absorption bands between fresh and spent catalysts may be explained by the redox cycle undergone by Cu during the reaction. The broad bands in the range 200-800 nm presented in the spectra could suggest the appearance of cluster-like species of CuO, Cu(0) nanoparticles, as well as large size CuOx. [310] [a]According to the literature[311], the signals at ca. 360, 430, 550 nm and the wide absorption in 630–660 range observed could belong to O–Cu–O (360) and Cu–O–Cu (430) complexes (charge transfer bands), plasmon resonance bands of Cu_n nanoparticles (550) and to electron d–d transitions in Cu(II) in distorted octahedral field surrounded by oxygen in CuO particles(5), respectively. Moreover, Angelici et al.[271] attributed the same d−d transitions to peaks observed at 700−800 nm. Thus, the band at 650 nm could be assigned to copper oxide nanoparticles of large size.[310] The peak observed at 560 nm could be related the presence of plasmon resonance bands of Cu_n particles, suggesting that the catalytic reaction, accompanied by oxidation-reduction cycle of Cu, favoured the formation of copper metal particles. [311]

From the literature[271], the partial deactivation observed over similar catalytic system for the ethanol conversion into butadiene, has been mainly attributed to the carbonaceous deposition over the catalyst surface, blocking active sites. The presence of carbonaceous compounds could be confirmed by the DR-UV analysis here displayed. Interestingly, carbonaceous deposits formation appeared more prominent over the catalyst devoid of sodium, showing more intense absorption bands. Indeed, the presence of sodium, which lead to lowering the acidity of the catalyst and to an overall higher B/A ratio, Table11) may be the cause of the lower ethylene formation, which is probably the intermediate product for carbonaceous compound formation[267,312,313], allowing the catalyst to catalyse the successive condensation reaction required for butadiene formation.

4.3.2.2.1.3   Copper metal loading effect

In order to evaluate the copper amount effect, some samples have been prepared by doubling the amount of copper oxide. Specifically, copper has been added with a 10 wt% of metal loading over the sepiolite calcined at 500ºC support and over the one containing 2 wt% of sodium, namely CuO/Sep@500 10 wt% and CuO/2Na/Sep@500 wt%. The catalytic results are depicted in Figure 29 and Table 17.

Table 17. *Catalytic results obtained, in terms of ethanol conversion (X%) and products selectivity and yield, for the ethanol gas-phase conversion over the Sepiolite support calcinated at 500ºC (Sep@500), the sodium impregnated one with 2wt% of metal loading (2Na/Sep@500) and the copper impregnated ones with 5wt% and 10 wt% of Cu metal loading. Others ID: acetone, 2-pentanone, CO_2, ethane. Reaction conditions: EtOH 5% v/v in N_2, T= 450ºC, P= 1 atm; WHSV= 1 g/(g_{CAT}·h).*

| Support | CuO [wt%] | X EtOH [%] | Selectivity [%] | | | | | | | |
			AA	Ethylene	DEE	BuOH	BuA	BD	Others ID	Others NID
Sep@500	0	80	6	57	36	0	0	0	1	
	5	67	30	37	27	1	2	0	1	2
	10	82	40	30	19	0	2	2	2	4
2Na/Sep@500	0	42	41	19	13	14	7	2	2.9	2
	5	43	51	15	9	10	8	2	2	3
	10	53	53	14	8.4	8	8	2.6	2	4

| Support | CuO [wt%] | X EtOH [%] | Yield [%] | | | | | | | |
			AA	Ethylene	DEE	BuOH	BuA	BD	Others ID	Others NID
Sep@500	0	80	5	46	29	0	0	0	1	0
	5	67	20	25	18	0	1	0	1	1
	10	82	33	25	16	0	1	2	1	4
2Na/Sep@500	0	42	17	8	6	6	3	1	1	1
	5	43	22	7	4	4	4	1	1	1
	10	53	28	7	4	4	4	1	1	2

By increasing the copper amount, higher value of both ethanol conversion and acetaldehyde selectivity have been obtained; simultaneously a decreasing trend of dehydration products (ethylene and diethyl ether) selectivity with copper oxide amount can be observed. Considering the sepiolite support alone, Sep@500, a higher amount of copper led to higher activity. Indeed, ethanol conversion increased from 67% to 82% while increasing the copper amount from 5 to 10 wt% of CuO metal loading. In addition, it can be observed the presence of 1,3-butadiene, gathered into the "Other ID" products in Figure 29, with an higher amount of copper. On the other hand, the presence of a 2 wt% of sodium into the catalytic system led to a small formation of ketones, acetone and 2-pentanone, with the concomitant formation of the side product CO_2, as side products, gathered into "Other ID" in table 17. The presence of sodium generally led to lower the activity of the catalyst but appeared necessary to catalyse *n*-butanol formation. It seems that the presence of copper only favoured the dehydrogenation reaction of ethanol without playing any helpful role in *n*-butanol formation.
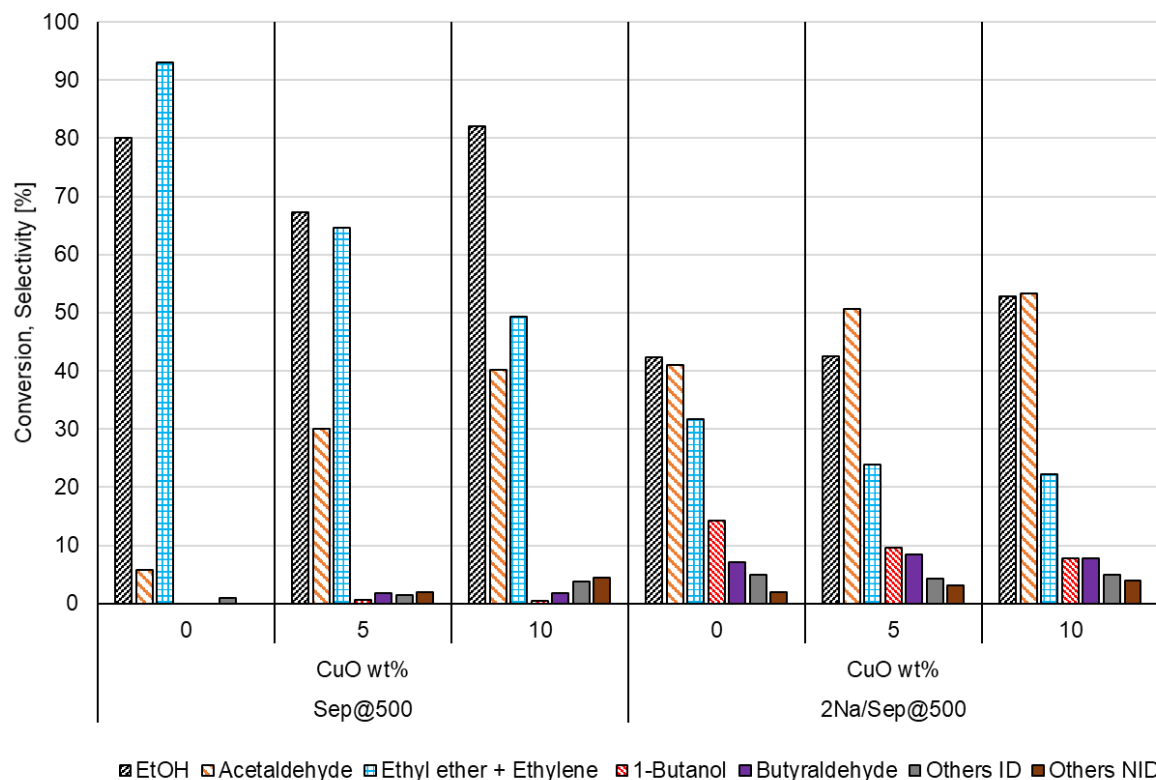
Figure 29 Catalytic results obtained in the Ethanol conversion over the Sepiolite support calcinated at 500ºC (Sep@500), the sodium impregnated one with 2wt% of metal loading (2Na/Sep@500) and the copper impregnated ones with 5wt% and 10 wt% of Cu metal loading. Others ID: acetone, 2-pentanone, CO_2, 1,3-butadiene, ethane. Reaction conditions: EtOH 5% v/v in N_2, T= 450ºC, P= 1 atm; WHSV= 1 g/(g_{CAT}·h).

4.3.2.2.1.4 Copper reduction effect

For the purpose of evaluate the effect of the presence of copper in the metallic phase in the ethanol gas-phase conversion, some reactions have been performed over catalyst that had undergone a previous thermal treatment hydrogen flow in order to reduce the copper. In particular, the catalyst consisting of 5wt% CuO over 2Na/Sep@500 and, for the sake of comparison, the one supported on MgO, have previously reduced in order to obtain the metallic copper and then tested. To do so, the catalyst have been put into a vertical reactor fed by a 40mL/min hydrogen flow for three hours at 350ºC in order to reduce the catalyst. After hydrogen treatment, the catalysts have been tested into the reaction system in the typical reaction condition of 450ºC and atmospheric pressure and WHSV of 1 g/(gcat·h). The results are reported in Figure 30 and table 18.

Table 18.   *Catalytic results obtained, in terms of ethanol conversion (X%) and products selectivity and yield, for the ethanol gas-phase conversion over the MgO and 2Na/Sep@500 catalysts impregnated with 5 wt% of CuO and reduced to Cu after treatment at 350ºC for 3h under hydrogen flow (40mL/min H_2). Others ID: acetone, 2-pentanone, CO_2, 1,3-butadiene, ethane. Guerbet alcohols: 2-ethyl-butanol, 1-hexanol, 2-ethyl-hexanol, 1-octanol. Reaction conditions: EtOH 5% v/v in N_2, T= 450°C, P= 1 atm; WHSV= 1 g/(g_{CAT}·h).*

| Support | 5 wt% | X EtOH [%] | Selectivity [%] | | | | | | | |
			AA	Ethylene	DEE	BuOH	BuA	Others ID	Others NID	Higher Alcohols
MgO	CuO	26	58	21	1	9	4	2	0	0
	Cu	41	43	25	5	23	8	2	11	3
2Na/Sep@500	CuO	43	51	15	9	10	8	4	3	
	Cu	46	52	8	14	10	9	5	3	

| Support | 5 wt% | X EtOH [%] | Yield [%] | | | | | | | |
			AA	Ethylene	DEE	BuOH	BuA	Others ID	Others NID	Higher Alcohols
MgO	CuO	26	15	5	0	2	1	0	0	0
	Cu	41	17	10	2	9	3	1	4	1
2Na/Sep@500	CuO	43	22	7	4	4	4	2	1	0
	Cu	46	24	4	6	4	4	2	1	0
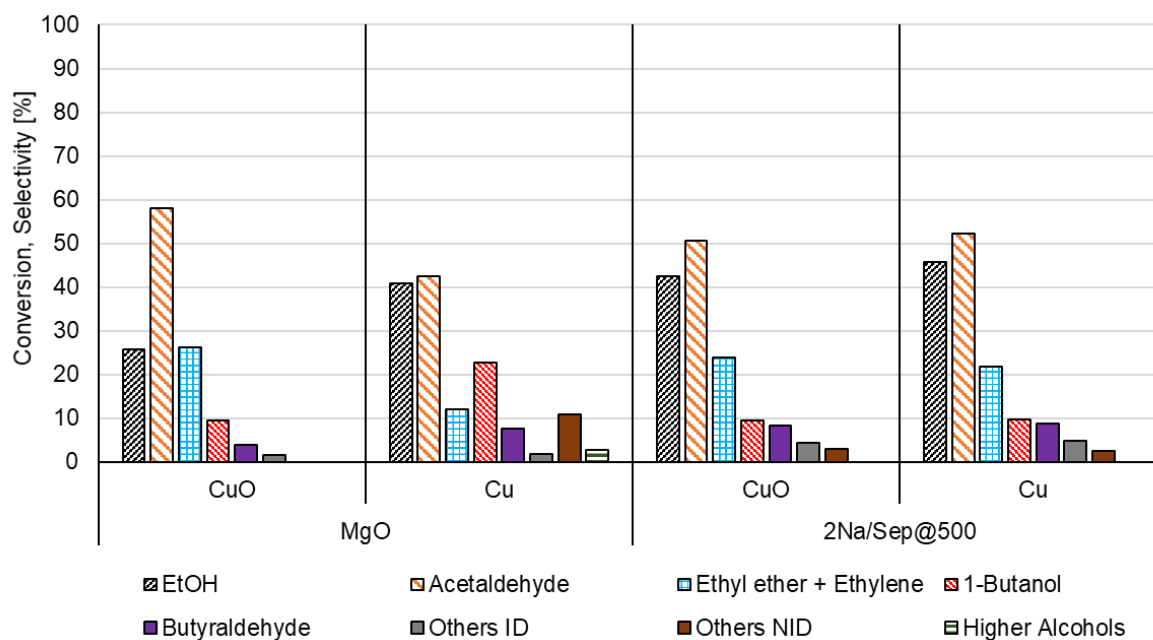
Figure 30   Catalytic results obtained in the Ethanol conversion over the MgO and 2Na/Sep@500 catalysts impregnated with 5 wt% of CuO and reduced to Cu after treatment at 350ºC for 3h under hydrogen flow (40mL/min H_2). Others ID: acetone, 2-pentanone, CO_2, 1,3-butadiene, ethane. Guerbet alcohols: 2-ethyl-butanol, 1-hexanol, 2-ethyl-hexanol, 1-octanol. Reaction conditions: EtOH 5% v/v in N_2, T= 450°C, P= 1 atm; WHSV= 1 g/(g_{CAT}·h).

As far as MgO is concerned, the copper reduction led to an increase of both ethanol conversion and *n*-butanol selectivity, from 26 to 41% and from 9 to 23% respectively. The most accepted reaction mechanism for the Guerbet route encompasses two dehydrogenation steps, namely the first one of the reagent alcohol yielding the corresponding aldehyde and then the reduction of the α,β-

unsaturated aldehyde (deriving from the aldol-condensation step) yielding the higher Guerbet alcohol. The presence of the metallic copper can play a crucial role into the dehydrogenation steps resulting in increased formation of *n*-butanol and even higher alcohols (selectivity of 3%).

By contrast, the reduction of copper when impregnated over the 2Na/Sep@500 sample did not lead to any repercussion on the catalytic results, only a slight increase of ethanol conversion and acetaldehyde selectivity can be noted. However, since the reduced catalyst after H_2 treatment was directly placed into the reaction system and then kept under inert gas flow (30 mL/min of N_2) in order to avoid the re-oxidation of copper into its oxide form, it was not possible to ascertain the successful reduction of the catalyst. Therefore, a probable explanation for the resembling catalytic results could be an ineffective reduction treatment of the catalyst.

4.3.2.2.2 Nickel

In order to evaluate the effect of a different transition metal, a sample impregnated with nickel, has been prepared. In particular, a 5 wt% of nickel oxide NiO has been prepared through wet impregnation method (Section 3.2.4) of the 2Na/Sep@500. After preparation, the catalyst has been tested in the ethanol gas-phase conversion with the reaction conditions as follows: 450ºC, atmospheric pressure and WHSV of 1 g/(g_{CAT}·h). In this case, the reaction temperature used has been decreased to 400 and 350ºC. Figure 31 reports the catalytic results obtained in terms of ethanol conversion and selectivity of the main products obtained. As it is possible to observe, while performing the reaction at the higher temperature, 450ºC, the NiO/2Na/Sep@500 5 wt% catalyst led to the formation of CO and CO_2. Carbon monoxide can derive from acetaldehyde or ethanol cracking decomposition.[136,314]
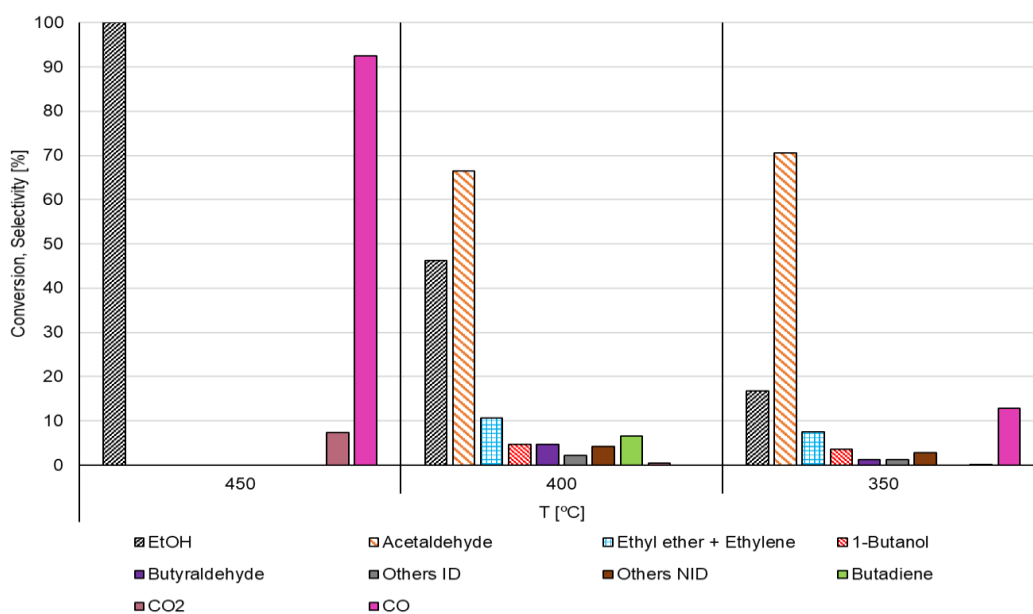
Figure 31   Catalytic results obtained in the Ethanol conversion over NiO/2Na/Sep@500. Others ID: acetone, 2-pentanone,ethyl acetate. Reaction conditions: EtOH 5% v/v in N_2, T=350, 400, 450°C, P= 1 atm, τ= 0.24 s; WHSV= 1 g/(gcat·h).

In order to compare the results obtained over the two different transition metals impregnate catalysts tested (i.e., CuO/2Na/Sep@500 5 wt% and NiO/2Na/Sep@500 5 wt%) the results obtained over the nickel-supported sample that have been considered were the one obtained at 400ºC. The results are compared in Figure 32: Generally, it is possible to appreciate the decreasing of ethanol conversion after impregnation with transition metal oxides. When pure sepiolite was used as catalyst support, the main products remained the dehydration products of ethanol, ethylene and ethyl ether, passing from a cumulative selectivity of 93% (57 and 36% respectively) to 65% (37 and 27%, respectively) when the CuO 5 wt% impregnated one was used. The slight decrease of the dehydration products of ethanol was balanced by an increase of its dehydrogenation product, acetaldehyde. Probably the addition of a transition metal over the catalyst covered part of the acid sites favouring the formation of the dehydrogenation product of ethanol.

On the other hand, when the sodium-doped sepiolite was used as support, the main product obtained after transition metal impregnation was acetaldehyde. Indeed, acetaldehyde selectivity passed from 41% over the 2Na/Sep@500 to 51 and 66 % over CuO/2Na/Sep@500 5 wt% and the NiO/2Na/Sep@500 5 wt%, respectively. Interestingly, when the sodium-doped sepiolite was used as support, even butadiene, the Lebedev reaction product of ethanol, has been detected (see Scheme 2). Moreover, after impregnation with nickel, butadiene selectivity increased from 2% over the 2Na/Sep@500 to 7% over the NiO/2Na@500 5 wt% catalyst.
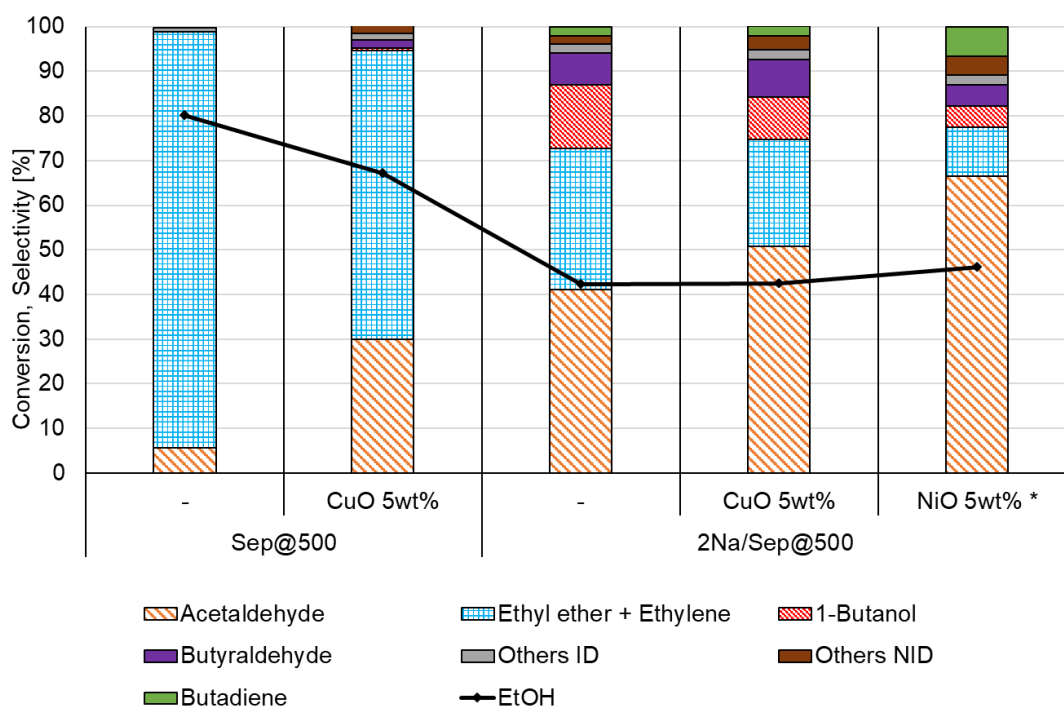
Figure 32   Catalytic results obtained in the Ethanol conversion over the Sep@500 and 2Na/Sep@500 supports in comparison with the CuO and NiO 5wt% impregnated samples. Others ID: acetone, 2-pentanone, CO_2, ethyl acetate. Reaction conditions: EtOH 5% v/v in N_2, T= 450°C (*400ºC), P= 1 atm; WHSV= 1 g/(g_{CAT}·h).

Table 19. *Catalytic results obtained, in terms of ethanol conversion (X%) and products selectivity and yield, for the ethanol gas-phase conversion over the Sep@500 and 2Na/Sep@500 supports in comparison with the CuO and NiO 5 wt% impregnated samples. Others ID: acetone, 2-pentanone, CO_2, ethyl acetate. Reaction conditions: EtOH 5% v/v in N2, T= 450°C, P= 1 atm; WHSV= 1 g/(g$_{CAT}$·h).*

| Support | Transition metal [5 wt%] | X EtOH [%] | Selectivity [%] | | | | | | | |
			AA	Ethylene	DEE	BuOH	BuA	BD	Others ID	Others NID
Sep@500	-	80	6	57	36	0	0	0	1	0
	CuO	67	30	37	27	1	2	0	1	2
2Na/Sep@500	-	42	41	19	13	14	7	2	2	2
	CuO	43	51	15	9	10	8	2	2	3
	NiO*	46	66	5	6	5	5	7	2	4

| Support | Transition metal [5 wt%] | X EtOH [%] | Yield [%] | | | | | | | |
			AA	Ethylene	DEE	BuOH	BuA	BD	Others ID	Others NID
Sep@500	-	80	5	46	29	0	0	0	1	0
	CuO	67	20	25	18	0	1	0	1	1
2Na/Sep@500	-	42	17	8	6	6	3	1	1	1
	CuO	43	22	7	4	4	4	1	1	1
	NiO*	46	31	2	3	2	2	3	1	2

4.3.2.3 Alkali metals doped sepiolite

The highest selectivity of *n*-butanol (14%) was obtained over the catalyst consisting in sepiolite calcinated at 500ºC impregnated with 2wt% of sodium. So the presence of an alkali metal showed to be crucial for favouring the *n*-butanol formation pathway. Its presence led to an overall decrease of the sepiolite acidity probably generating the right acidity/basicity ratio required to induce *n*-butanol formation. It was reported that base strength increases with the radius of alkali cations. [296] In order to evaluate the effect of bigger and more electropositive alkali metals, other sepiolite samples have been prepared adding potassium and cesium by incipient wetness impregnation. The synthesis method has been explained in section 3.2.4.

4.3.2.3.1 K-doped sepiolite

Two samples impregnated with 2 and 5 wt% of potassium have been synthetized by incipient wet impregnation and then have been tested in to the reaction system for the ethanol gas phase conversion at 450ºC, atmospheric pressure and WHSV of 1 g/(gcat·h). The catalytic results are reported in Figure 33 and Table 20.
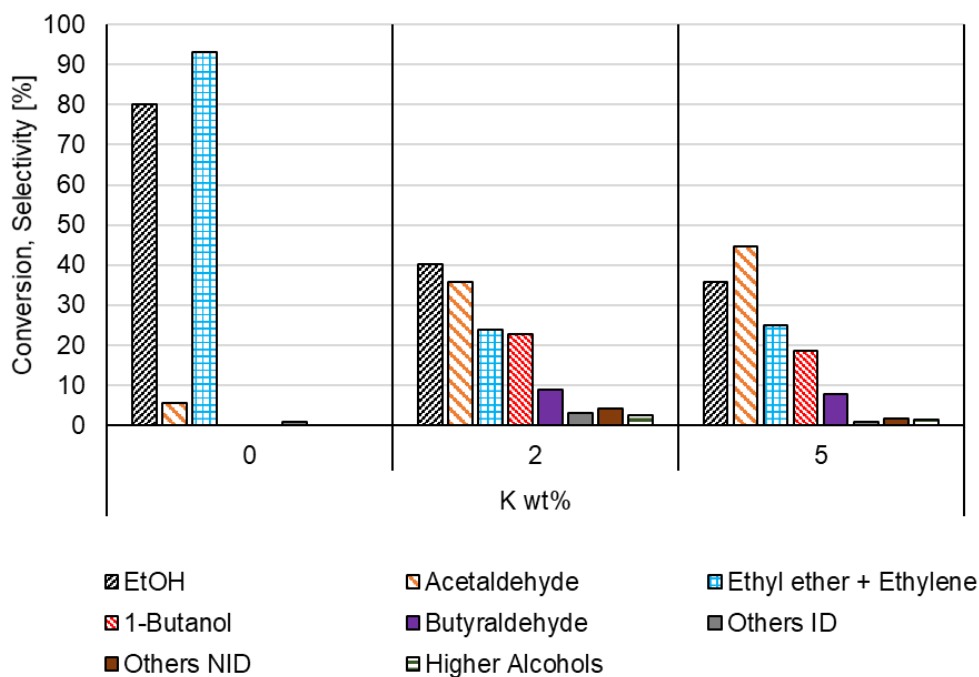
Figure 33 Catalytic results obtained in the Ethanol conversion over the Sep@500 support and the impregnated samples with 2 and 5 wt% of K. Others ID: acetone, 2-pentanone, CO_2, ethyl acetate. Higher alcohols: 2-ethyl-butanol, 1-hexanol, 2-ethyl-hexanol, 1-octanol. Reaction conditions: EtOH 5% v/v in N_2, T=450°C, P= 1 atm, WHSV= 1 g/(g$_{CAT}$·h).

Table 20. *Catalytic results obtained, in terms of ethanol conversion (X%) and products selectivity and yield, for the ethanol gas-phase conversion over the Sep@500 support and the impregnated samples with 2 and 5 wt% of K. Others ID: acetone, 2-pentanone, CO_2, ethyl acetate. Higher alcohols: 2-ethyl-butanol, 1-hexanol, 2-ethyl-hexanol, 1-octanol. Reaction conditions: EtOH 5% v/v in N_2, T=450°C, P= 1 atm, WHSV= 1 g/(g$_{CAT}$·h).*

| K wt% | X EtOH [%] | Selectivity [%] | | | | | | | |
		AA	Ethylene	DEE	BuOH	BuA	Others ID	Others NID	Higher Alcohols
0	80	6	57	36	0	0	1	0	0
2	40	36	12	12	23	9	3	4	2
5	36	45	15	10	19	8	1	2	1

| K wt% | X EtOH [%] | Yield [%] | | | | | | | |
		AA	Ethylene	DEE	BuOH	BuA	Others ID	Others NID	Higher Alcohols
0	80	5	46	29	0	0	1	0	0
2	40	14	5	5	9	4	1	2	1
5	36	16	5	4	7	3	0	1	0

By impregnating sepiolite calcined at 500ºC with potassium, it was possible to obtain *n*-butanol with higher selectivity comparing the results obtained over the sodium impregnated samples. Indeed, over the 2K/Sep@500 catalyst, *n*-butanol has been obtained with a 23% of selectivity, ~10% more than the analogous sample impregnated with sodium, i.e. 14% (see Figure 23 and Table 13). Interestingly, over that catalyst even higher alcohols (i.e., 2-ethyl-butanol, 1-hexanol, 2-ethyl-hexanol, 1-octanol) started to be produced. The formation of higher alcohols comes from consecutive

Guerbet reaction from *n*-butanol condensing with it-self (2-ethyl hexanol), with ethanol (1-hexanol, 2-ethyl butanol) and from condensation of hexanol with ethanol (1 octanol). (Scheme 3).

Scheme 3. Higher Guerbet alcohols formation (via aldol-condensation pathway).

Over the just mentioned potassium-doped catalyst, a stability test have been performed by feeding the EtOH 5 v/v% in N_2 gaseous mixture into the reaction system for ca. 4 hours, in Figure 34 are depicted the catalytic results as a function of the time on stream (h).

Figure 34 Catalytic results obtained in the Ethanol gas-phase conversion over the 2K/Sep@500 in terms of conversion of ethanol and main products selectivity as a function of the time on stream, TON (h). Others ID: acetone, 2-pentanone, CO_2, ethyl acetate. Higher alcohols: 2-ethyl-butanol, 1-hexanol, 2-ethyl-hexanol, 1-octanol. Reaction conditions: EtOH 5% v/v in N_2, T=450°C, P= 1 atm, WHSV= 1 g/(g$_{CAT}$·h).

From Figure 34 it can be noted a slight stable activity of the catalyst over the ToN, ethanol conversion fluctuated around 40%. With the time on stream, acetaldehyde selectivity increased a bit from ~34% to 37% while ethylene selectivity decreased from 27 to ~23%. This could be related to a partial deactivation of the catalyst of both basic and acid sites, probably due to the formation of carbonaceous compounds (coke) partially covering the catalyst surface. *n*-butanol selectivity was not affected by the time on stream, staying constant at 23% with all the time on stream under consideration.

Interestingly, even in the case of potassium doped sepiolite, a higher amount of potassium over the catalyst was not beneficial for *n*-butanol production neither catalytic activity. Indeed, by increasing the K metal loading from 2 to 5 wt%, *n*-butanol selectivity decreased from 23 to 19% as well as ethanol conversion, from 40 to 36%. The fact that they both decreased by the same extent could suggests that *n*-butanol is a primary kinetic product. Nevertheless, with increasing potassium amount, acetaldehyde formation increased reaching a selectivity value of 45%.

4.3.2.3.2 Cs-doped sepiolite

The same metal loading expressed by weight of different alkali metals corresponds to a different molar amount. Therefore, in order to do a better comparison between the alkali-doped samples, the alkali-metal molar ratios over the weight of sepiolite n_{MET}/w_{SEP} [mmol$_{METAL}$/g$_{SEPIOLITE}$] has been

computed. In addition, after SEM-EDX analysis, even the concrete alkali amount impregnated over the sepiolite has been measured (Table 21). Due to the higher molar mass of Cesium (i.e., M(Na):22.99 g/mol; M(K):39.10 g/mol and M(Cs):132.91 g/mol), some samples with higher metal loading (wt%) but with comparable n_{MET}/w_{SEP} ratio values have been synthetized.

Table 21. *EDX analysis of the surfaces of alkali-doped sepiolite catalysts.*

| Support | Met | Alkali metal loading | | | | |
		Nominal [wt%]	Measured [wt%]	Nominal n_{MET}/w_{SEP} [mmol/g]	Measured n_{MET}/w_{SEP} [mmol/g]	Measured [Atomic %]
Sep@500	Na	2	1.3	0.87	0.56	1.1
		5	3.7	2.17	1.62	3.1
	K	2	2.2	0.51	0.56	1.1
		5	5.6	1.28	1.43	2.9
	Cs	2	1.6	0.15	0.12	0.2
		4	5.2	0.30	0.39	0.8
		7	7.8	0.53	0.59	1.2
		14	9.2	1.05	0.69	1.5

Figure 35 and Table 22 report the catalyitc results obtained over the Cs-doped catalysts for the ethanol gas-phase conversion of ethanol performed at 450ºC, 1 atm and WHSV= 1 g/(g_{CAT}·h).
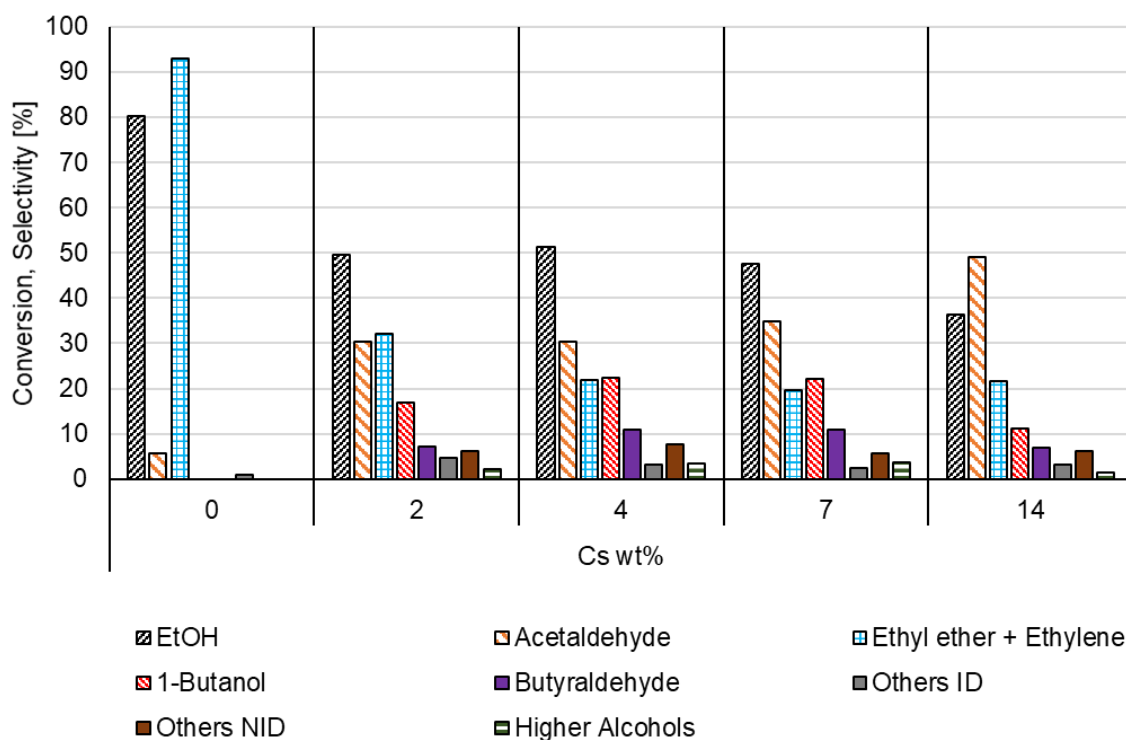
Figure 35 Catalytic results obtained in the Ethanol conversion over the Sep@500 support and the impregnated samples with 2, 4, 7 and 14 wt% of Cs. Others ID: acetone, 2-pentanone, CO_2, ethyl acetate. Higher alcohols: 2-ethyl-butanol, 1-hexanol, 2-ethyl-hexanol, 1-octanol. Reaction conditions: EtOH 5% v/v in N2, T= 450°C, P= 1 atm, WHSV= 1 g/(g_{CAT}·h).

Table 22. *Catalytic results obtained, in terms of ethanol conversion (X %) and products selectivity and yield, for the ethanol gas-phase conversion over the Sep@500 support and the impregnated samples with 2, 4, 7 and 14 wt% of Cs. Others ID: acetone, 2-pentanone, CO_2, ethyl acetate. Higher alcohols: 2-ethyl-butanol, 1-hexanol, 2-ethyl-hexanol, 1-octanol. Reaction conditions: EtOH 5% v/v in N2, T= 450°C, P= 1 atm, WHSV= 1 g/(g_{CAT}·h).*

| Cs wt% | X EtOH [%] | Selectivity [%] | | | | | | | |
		AA	Ethylene	DEE	BuOH	BuA	Others ID	Others NID	Higher Alcohols
0	80	6	57	36	0	0	1	0	0
2	50	30	12	20	17	7	5	6	2
4	51	30	9	13	22	11	3	8	4
7	47	35	10	10	22	11	3	6	4
14	36	49	17.6	4.1	11	7	3	6	2

| Cs wt% | X EtOH [%] | Yield [%] | | | | | | | |
		AA	Ethylene	DEE	BuOH	BuA	Others ID	Others NID	Higher Alcohols
0	80	5	46	29	0	0	1	0	0
2	50	24	10	16	14	6	4	5	2
4	51	16	4	7	12	6	2	4	2
7	47	17	5	5	10	5	1	3	2
14	36	18	6	1	4	3	1	2	1

From the results reported in Figure 35 and Table 22 it can be noticed the effect of the cesium amount over the catalytic activity and product distribution. Indeed, with increasing cesium amount, ethanol conversion decreased, as well as ethylene and DDE selectivity, probably due to the increasing amount of cesium that had neutralized part of the active acid sites of sepiolite, as observed by TPD-NH$_3$ analysis (Section 4.3.1.5). While *n*-butanol selectivity (together with BuA and higher alcohols) showed a maximum over the 4Cs/Sep@500 and 7Cs/Sep@500, acetaldehyde selectivity showed an increasing trend with increasing cesium loading.

4.3.2.3.3 Effect of the alkali-metals loading

Figure 36 summarizes the catalytic results obtained over the alkali-doped (Na, K, Cs) sepiolite samples prepared with different metal loading (2, 5, 7 wt%). In particular, the trends of ethanol conversion (X%) and main products selectivity (S%) are depicted as a function of the nominal molar metal loading, expressed as moles of the metals (mmol) divided by the weight of the sepiolite (g), mmol$_{MET}$/g$_{SEP}$.
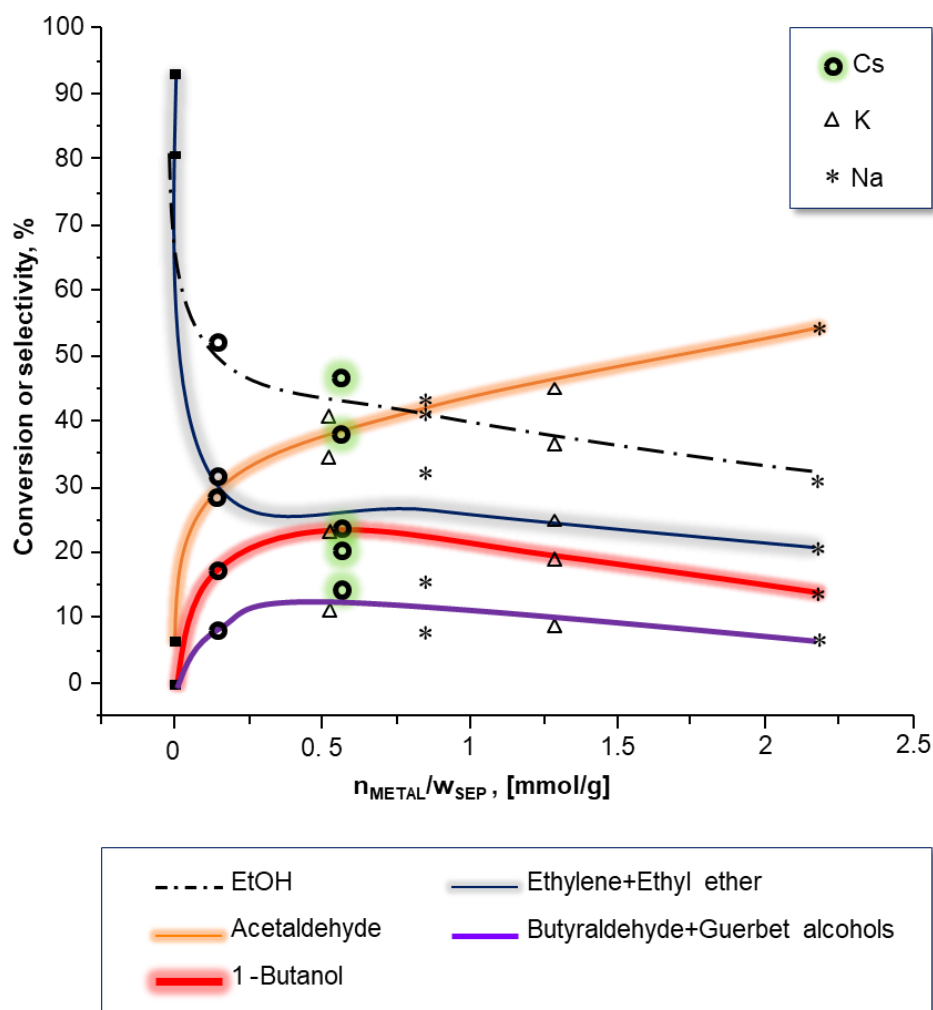
Figure 36 Influence of alkali metal loading (mmol$_{MET}$/g$_{SEP}$) on the conversion of ethanol and the selectivity of the main reaction products. Natural Sepiolite calcined at 500ºC; ▲: K/Sep@500 (2, 5 wt%, 0.51 and 1.28 mmol$_{MET}$/g$_{SEP}$); *: Na/Sep@500 (2,5 wt%, 0.87 and 2.17 mmol$_{MET}$/g$_{SEP}$); ○: Cs/Sep@500 catalysts (2, 7 wt%, 0.15 and 0.53 mmol$_{MET}$/g$_{SEP}$). Guerbet alcohols: 2-ethyl-butanol, 1-hexanol, 2-ethyl-hexanol, 1-octanol. Reaction conditions: EtOH 5% v/v in N$_2$, Temperature= 450 °C; WHSV= 1 g/(g$_{CAT}$·h).

In general, it is possible to observe that with increasing metal loading, the activity decreases as the ethanol conversion decreased. The dehydrogenation of ethanol seemed favoured by a higher alkali metal amount since acetaldehyde selectivity increased. While the selectivity of the dehydration products of ethanol, ethylene and ethyl ether, decreased with increasing metal loading, the ones of *n*-butanol, butyraldehyde and higher alcohols showed a maximum around 0.6 mmol$_{MET}$/g$_{SEP}$ and then, with a higher metal loading, decreased.

In Figure 37 the catalytic results obtained over the different alkali-impregnated sepiolite are shown in terms of ethanol conversion and the main products selectivity, as previously showed. Here, the catalytic results are reported in relation to the measured alkali metals amount by SEM-EDX analysis.
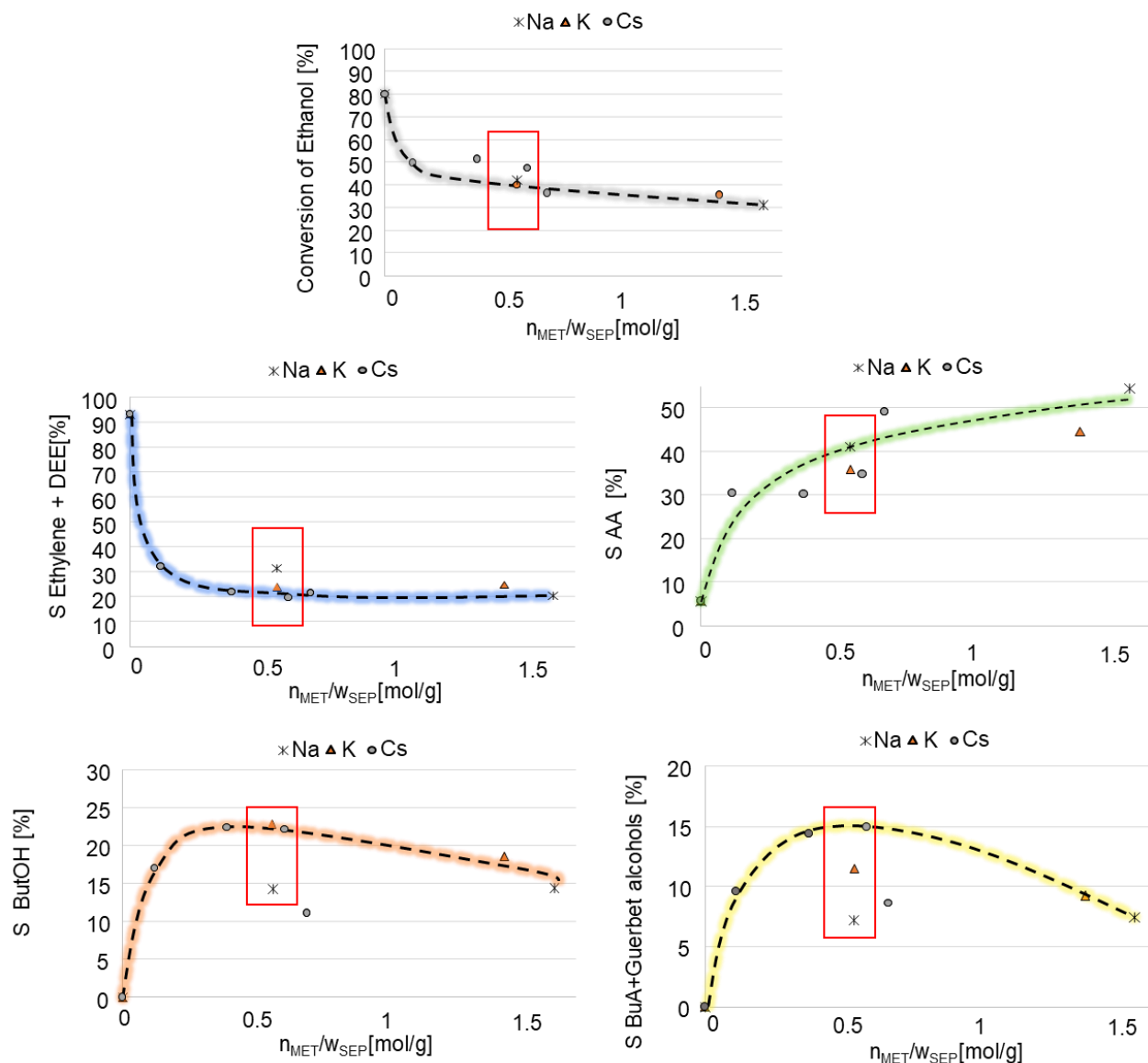
Figure 37 Influence of alkali metal loading (mmol$_{MET}$/g$_{SEP}$) on the conversion of the ethanol and the selectivity to the main reaction products. AA: acetaldehyde; BuA: butyraldehyde; Guerbet alcohols: 2-ethyl-butanol, 1-hexanol, 2-ethyl-hexanol, 1-octanol. Reaction conditions: EtOH 5% v/v in N$_2$, Temperature= 450 °C; W/F= 0.3 g$_{CAT}$/(mL/s) and WHSV= 1 g/(g$_{CAT}$·h).

From Fig.37 it possible to observe a trend of the ethanol conversion and products distributions with the molar amount of the alkali metals over sepiolite support. Ethanol conversion and its dehydration products, ethylene and ethyl ether, decreased with increasing alkali-metal amount, showing a linear relation between activity and acidity. On the other hand, acetaldehyde selectivity increased. The trends of *n*-butanol selectivity as well as the one of butyraldehyde and higher alcohols, is affected by, not only the nature of the metal impregnated to the support, but even its quantity. Indeed, both *n*-butanol and the consecutive Guerbet higher alcohols presented a maximum value of selectivity in relation with the alkali metal loading, namely around ~0.6 mmol$_{MET}$/g$_{SEP}$. The maximum value of *n*-butanol selectivity obtained was around 22% over the 2K/Sep@500 and 7Cs/Sep@500 catalysts that contained the same molar amount of alkali metal, namely ~0,6 mmol$_{MET}$ /g$_{SEP}$. It is worth noting

that the acidity/basicity ratio (A/B ratio) measured by TPD analysis for both catalysts was quite similar, 0.64 and 0.61, respectively (see section X).

Zooming in the catalytic results obtained over the catalysts containing the EDX-measured ca. 0.6 $mmol_{MET}/g_{SEP}$ (i.e., 2Na/Sep@500, 2K/Sep@500 and 7Cs/Sep@500), it is possible to point out the effect of the nature of the metal over the products distributions. Fig. 38 highlights the effect of the nature of the alkali metal over the EtOH conversion (X%) and the main products selectivity (S%) of the nature of the metal, considering the conditions in which the highest BuOH selectivity has been reached (i.e., ca. 0.6 $mmol_{MET}/g_{SEP}$). As far as the dehydration products formation is concerned, bigger alkali metal led to lower production of them in accordance with the lower acidity of the catalyst. In addition, it can be noted that cesium containing sample favoured the formation of higher alcohols and butyraldehyde. Nevertheless, the best results in terms of activity (X EtOH: 47%) and n-butanol selectivity (S BuOH: 22%), and so in terms of n-butanol yield, have been obtained over the 7Cs/Sep@500.
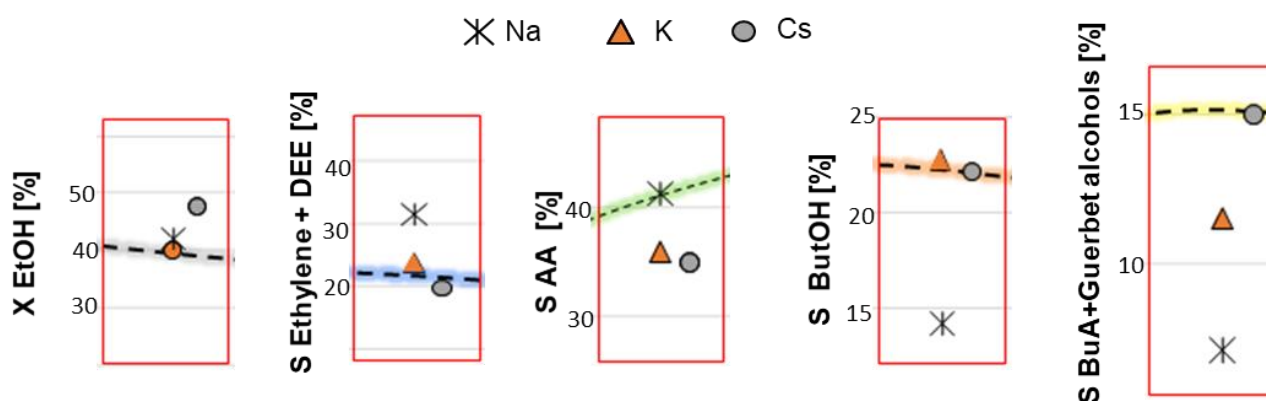
Figure 38   Conversion of the ethanol (X %) and the selectivity (S %) to the main reaction products over the alkali-metal doped catalyst with ~**0.6 mmol_MET/g_SEP** of molar metal loading (n_{MET}/w_{SEP}). AA: acetaldehyde; BuOH: butanol; BuA: butyraldehyde; Guerbet alcohols: 2-ethyl-butanol, 1-hexanol, 2-ethyl-hexanol, 1-octanol. Reaction conditions: EtOH 5% v/v in N_2, Temperature= 450 °C; W/F= 0.3 g_{CAT}/(mL/s) and WHSV= 1 g/(g_{CAT}·h).

The ethanol conversion and the selectivities of the main products for the gas-phase Guerbet reaction of ethanol over sepiolite-based catalysts calcined at 500ºC (Sep@500) are resumed in Figure 39. For the sake of comparison, the catalytic results obtained over MgO and the sepiolite support, in the same reaction conditions, i.e. 450ºC, 1 atm and WHSV= 1 g/(g_{CAT}·h), are reported as well.

	EtOH	Acetaldehyde	Ethyl ether	Ethylene	1-Butanol
MgO	35	42		17	28
Sep@500	80	6	36	58	0
2Na/Sep@500	42	41	13	19	14
2K/Sep@500	40	36	12	12	23
7Cs/Sep@500	47	35	10	10	22
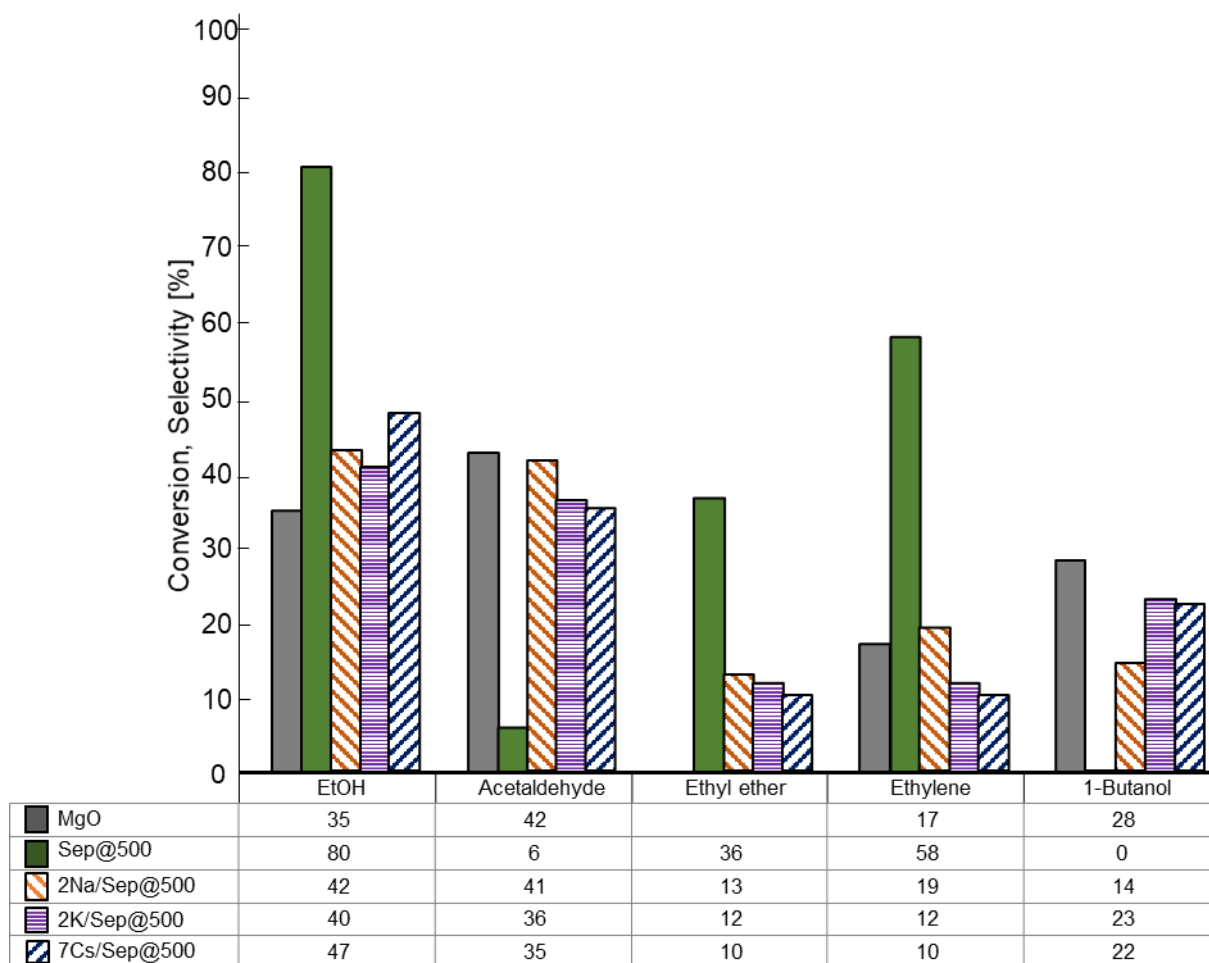
Figure 39   Comparison of the catalytic results, in terms of EtOH conversion and products selectivity, for the gas-phase ethanol conversion over MgO and natural sepiolite calcinated at 500ºC based catalysts. Reaction conditions: EtOH 5% v/v in N2, Temperature= 450 °C; WHSV= 1 g/(g$_{CAT}$·h).

4.3.2.4 7Cs/Sepiolite, optimization of experimental conditions

In order to monitor the conversions and selectivities, a typical way is to vary the reaction temperature or the contact time between the catalyst and the reagents. The main aim of the optimization study was to maximize the ethanol conversion while getting higher *n*-butanol and higher Guerbet alcohols selectivity, and thus higher yields. Therefore, the ethanol gas-phase conversion was performed at different WHSVs and reaction temperatures accordingly to find the optimal conditions.

After a first catalysts screening, focusing on favouring the Guerbet reaction pathway, the best performances in terms of ethanol conversion (47%) and *n*-butanol selectivity (22%) have been obtained over the catalyst Cs/Sep@500 7 wt%. Accordingly, this catalyst has been chosen to investigate the effects of the main reaction parameters, namely the reaction temperature and the contact time on ethanol conversion and products distributions.

4.3.2.4.1 Effect of temperature and space time on ethanol gas-phase conversion

In order to study the effect of the reaction temperature for the ethanol gas-phase conversion over 7Cs/Sep@500, the temperature was varied in the range of 300–450 °C by keeping WHSV (weight hourly space velocity) and the contact time, W/F, constant under otherwise similar conditions. On the other hand, the effect of the WHSV in the range = 1.7, 1, 0.3, 0.17, 0.11 $g_{EtOH}/(g_{CAT}\cdot h)$ has been investigated by keeping the other reaction parameters constant.

4.3.2.4.1.1   Temperature effect at WHSV=1 h^{-1}

Firstly, the effect of the reaction temperature on the ethanol conversion have been investigated at 0.4 $g_{CAT}/mL\cdot s$ as W/F (WHSV = 1 $g_{EtOH}/(g_{CAT}\cdot h)$). In particular, the reaction has been performed at 350, 400 and 450ºC by keeping the other reaction parameters constant. Figure 40 and Table 23 report the results obtained in terms of ethanol conversion (X%) and main products selectivity (S%).
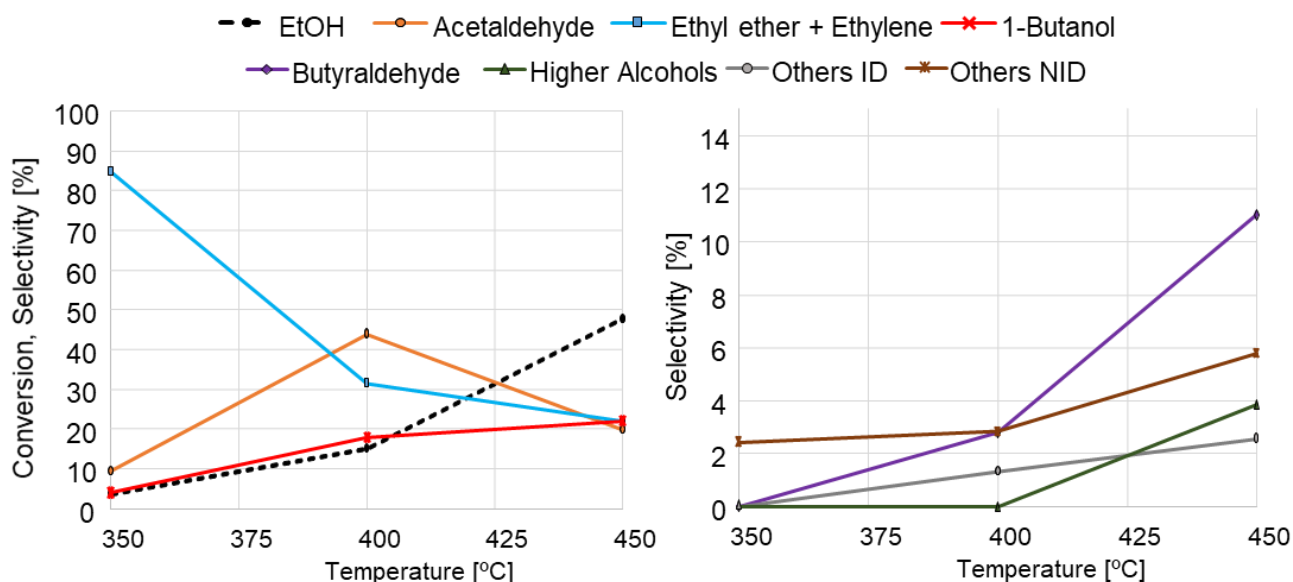
Figure 40   Influence of the temperature on the ethanol conversion and products selectivities over the 7Cs/Sep@500 catalyst. Higher alcohols: 2-ethyl-butanol, 1-hexanol, 2-ethyl-hexanol, 1-octanol. Others ID: acetone, 2-pentanone, CO_2, ethyl acetate. Reaction conditions: EtOH 5% v/v in N_2, T=350, 400, 450°C, P= 1 atm, W/F= 0.4 $g_{CAT}/mL\cdot s$; WHSV= 1 $g_{EtOH}/(g_{CAT}\cdot h)$.

Table 23. *Influence of the temperature on the ethanol conversion and products selectivities over the 7Cs/Sep@500 catalyst. Higher alcohols: 2-ethyl-butanol, 1-hexanol, 2-ethyl-hexanol, 1-octanol. Others ID: acetone, 2-pentanone, CO_2, ethyl acetate. Reaction conditions: EtOH 5% v/v in N_2, T=350, 400, 450°C, P= 1 atm, W/F= 0.4 g_{CAT}/mL·s; WHSV= 1 g_{EtOH}/(g_{CAT}·h).*

T [°C]	X EtOH [%]	Selectivity [%]							
		AA	Ethylene	DEE	BuOH	BuA	Others ID	Others NID	Higher Alcohols
350	4	9	10	75	4	0	0	2	0
400	15	44	13	18	18	3	1	3	0
450	47	20	10	10	22	11	3	6	4
Cs wt%	X EtOH [%]	Yield [%]							
		AA	Ethylene	DEE	BuOH	BuA	Others ID	Others NID	Higher Alcohols
350	4	0.3	0.4	2.7	0.1	0.0	0.0	0.1	0.0
400	15	6.5	1.9	2.7	2.7	0.4	0.2	0.4	0.0
450	47	9.4	4.6	4.8	10.5	5.2	1.2	2.7	1.8

As expected, ethanol conversion increased with increasing temperature. While working at 350°C, with an ethanol conversion of 4% a high value of ethyl ether selectivity was obtained (75%) the formation of which is known to be favoured at lower temperature, being its reaction formation exothermic.[138] Interestingly, at higher temperature, acetaldehyde selectivity decreased from 44% at 400°C to 20 % at 450°C. Concomitantly, *n*-butanol selectivity increased a bit from 18 to 22% as well as butyraldehyde selectivity from 3 to 11% and higher alcohols (4%). Even the selectivity of the other products, Other ID and Other NID increased with increasing temperature. The main composition of the Others NID products should be heavier products of consecutive reactions, being related to peaks obtained into the GC-online chromatogram with at high retention times. Nevertheless, the decreasing of acetaldehyde selectivity with reaction temperature and concomitant increase of *n*-butanol selectivity as well as the one of the other products suggest the acetaldehyde acted as intermediate product converting in consecutive products, e.g. *n*-butanol, acetone, 2-pentanone (grouped in "Other ID").

4.3.2.4.1.2   *WHSVs effect* at *450°C*

At the highest temperature used in the previous trials (450°C) it was studied the effect of increasing contact time W/F or decreasing WHSV. In particular, the reactions have been performed with W/F: 0.4, 1 and 3 g_{CAT}/mL·s or WHSV= 0.9, 0.3, 0.11 g_{EtOH}/(gcat·h); the results are reported in Figure 41 and Table 24.
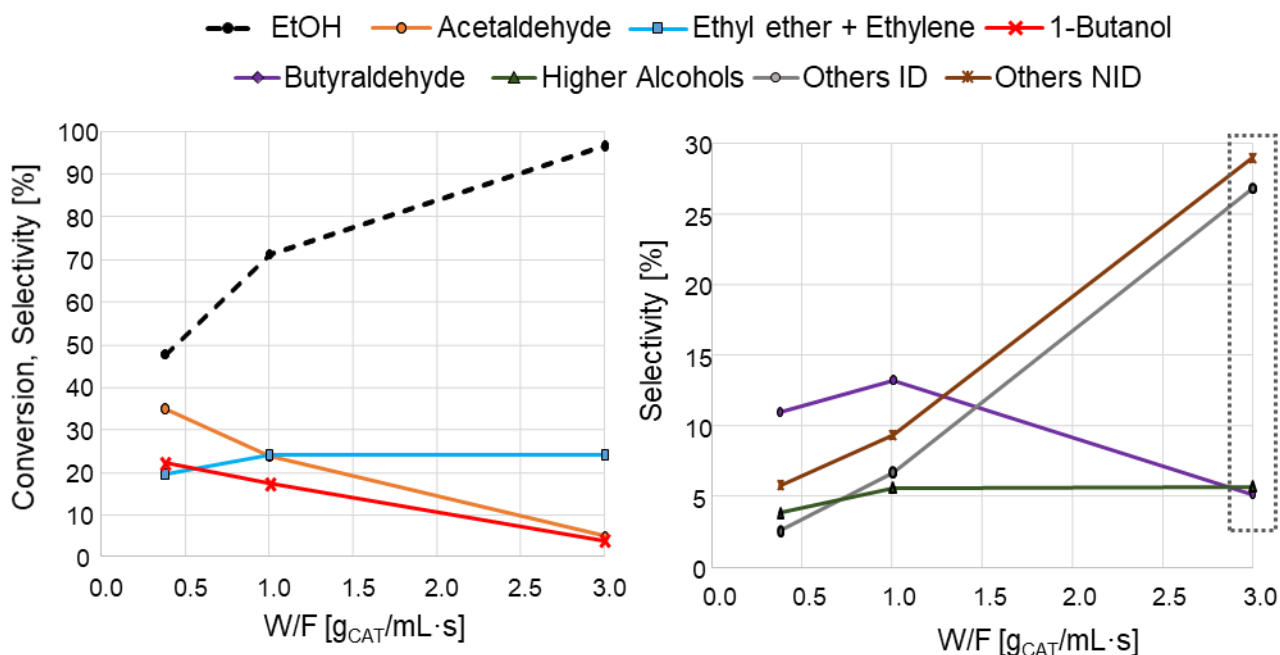
Figure 41 Influence of the contact time (W/F, g$_{CAT}$/mL·s) on the ethanol conversion and products selectivities over the 7Cs/Sep@500 catalyst. Higher alcohols: 2-ethyl-butanol, 1-hexanol, 2-ethyl-hexanol, 1-octanol. Others ID: acetone, 2-pentanone, CO$_2$, 1,3-butadiene, ethane. Reaction conditions: EtOH 5% v/v in N$_2$, T=**450ºC**, P= 1 atm, W/F: 0.4, 1, 3 g$_{CAT}$/mL·s; WHSV= 0.9, 0.3, 0.11 g$_{EtOH}$/(g$_{CAT}$·h).

**Table 24.** Influence of the contact time (W/F, g$_{CAT}$/mL·s) on the ethanol conversion and products selectivities over the 7Cs/Sep@500 catalyst. Higher alcohols: 2-ethyl-butanol, 1-hexanol, 2-ethyl-hexanol, 1-octanol. Others ID: acetone, 2-pentanone, CO$_2$, 1,3-butadiene, ethane. Reaction conditions: EtOH 5% v/v in N$_2$, T=**450ºC**, P= 1 atm, W/F: 0.4, 1, 3 g$_{CAT}$/mL*s; WHSV= 0.9, 0.3, 0.11 g$_{EtOH}$/(g$_{CAT}$·h).

| W/F [g$_{CAT}$/mL·s] | X EtOH [%] | **Selectivity [%]** | | | | | | | |
		AA	Ethylene	DEE	BuOH	BuA	Others ID	Others NID	Higher Alcohols
0.4	47.5	34.9	9.7	10.1	22.1	11.0	2.6	5.8	3.8
1.0	71.3	23.6	16.0	8.2	17.2	13.3	6.7	9.4	5.6
3.0	96.7	5.1	14.2	9.8	4.1	5.2	26.8	29.0	5.7

| W/F [g$_{CAT}$/mL·s] | X EtOH [%] | **Yield [%]** | | | | | | | |
		AA	Ethylene	DEE	BuOH	BuA	Others ID	Others NID	Higher Alcohols
0.4	47.5	17	5	5	10	5	1	3	2
1.0	71.3	17	11	6	12	9	5	7	4
3.0	96.7	5	14	9	4	5	26	28	6

With increasing contact time, ethanol conversion increased as expected, from 47.5 to 96.7%. On the other hand, it is possible to notice a decreasing trend for the selectivity of acetaldehyde, *n*-butanol and butyraldehyde, from 34.9% to 5.1%, 22.1 to 4.1 and 11 to 5.2% respectively, with increasing contact time from 0.4 to 3 g$_{CAT}$/mL·s. At the same time, while the selectivity of higher alcohols

remained constant with increasing contact time, by contrast, an abrupt increase of selectivity of both ID (i.e., acetone, 2-pentanone, CO_2, butadiene and ethane) and NID others products can be observed, from 2.6 to 26.8% and from 5.8 to 29%, confirming their nature as consecutive products that could come from the conversion of acetaldehyde or *n*-butanol. Figure 42 depicts the trends of the just mentioned products selectivity with increasing contact time. The values of the selectivity obtained at the highest value of W/F examined, 3 g_{CAT}/mL·s, are framed. Interestingly, the selectivity of 1-3-butadiene obtained at the highest contact time was as high as 14.6%. In addition, even ketones selectivity increased with increasing contact time. The formation of both those side-products involves acetaldehyde as intermediate product (see Scheme 1 and Scheme 2).
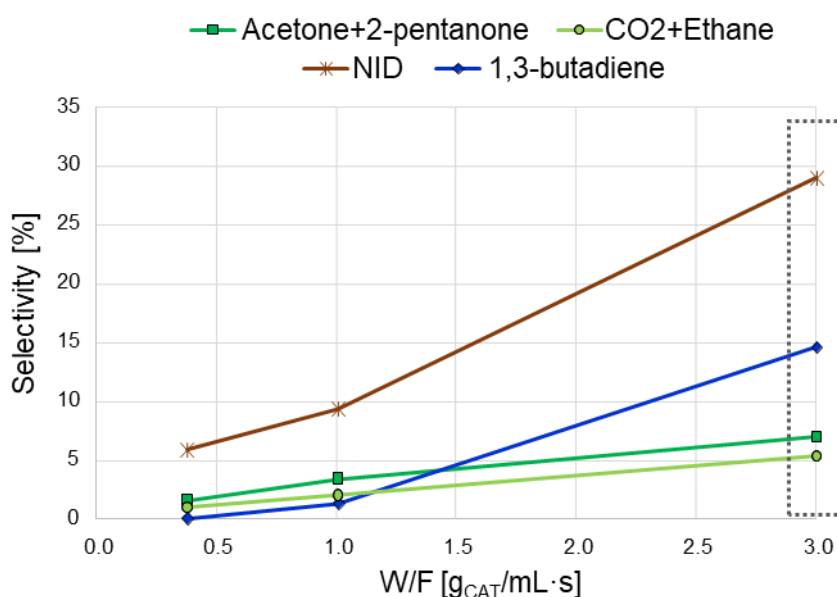
Figure 42 Influence of the contact time (W/F, g_{CAT}/mL·s) on side products selectivities over the 7Cs/Sep@500 catalyst. Reaction conditions: EtOH 5% v/v in N_2, T=450ºC, P= 1 atm, W/F: 0.4, 1, 3 g_{CAT}/mL·s; WHSV= 0.9, 0.3, 0.11 g_{EtOH}/(gcat·h).

Table 25. *Influence of the contact time (W/F, g_{CAT}/mL·s) on side products selectivities over the 7Cs/Sep@500 catalyst. Reaction conditions: EtOH 5% v/v in N_2, T=**450ºC**, P= 1 atm, W/F: 0.4, 1, 3 g_{CAT}/mL·s; WHSV= 0.9, 0.3, 0.11 g_{EtOH}/(gcat·h).*

W/F [g_{CAT}/mL·s]	Selectivity [%]					
	Others NID	Acetone	2-Pentanone	BD	CO2	Ethane
0.4	5.8	0.7	0.9	0.0	0.3	0.7
1.0	9.4	1.5	1.8	1.4	0.8	1.2
3.0	29.0	2.9	4.1	14.6	2.6	2.7
W/F [g_{CAT}/mL·s]	Yield [%]					
	Others NID	Acetone	2-Pentanone	BD	CO2	Ethane
0.4	2.7	0.3	0.4	0.0	0.1	0.3
1.0	6.7	1.1	1.3	1.0	0.5	0.9
3.0	28.1	2.8	3.9	14.1	2.5	2.6

Since with the highest contact time, 3 g_{CAT}/mL·s, ethanol conversion was almost completed (97%) and the unknown products (Others NID) where produced in high quantity (with an overall selectivity of 29%), an attempt to better identify the nature of those products was performed by collecting them by condensation and then injecting a sample into the GC-MS system. In detail, the out-flowing line of the reaction system has been connected with a condenser, put into an ice-bath, situated in a point before sending the reaction mixture to the vent. In this way, the heavier products have been accumulated by condensation. The collected liquid mixture so obtained was diluted with acetonitrile and injected into a GC-MS system. The qualitative analysis led to notice the nature of some of the NID, i.e. a mixture of aromatics and ketones organic compounds. Interestingly, between the major compounds detected (in relation of the peaks areas obtained), higher ketones have been detected (i.e., 4-nonanone and 4-undecanone). Those results suggest that in such harsh condition with high temperature (450ºC) and contact time (W/F=3 g_{CAT}/mL·s), the ethanol conversion over the catalyst 7Cs/Sep@500 led to the formation of heavier products following mainly two reaction paths: the ketonization and aromatization. The latter could come from: i) ethylene aromatization[267]; ii) radical or Diels-Alder type reactions between conjugated dienes compounds (such as butadiene) and a dienophile (such as ethylene) and subsequent dehydrogenation of the cyclic compounds[270,315].

In accordance with the literature, at higher ethanol conversion it is difficult to control the Guerbet products selectivity. Indeed, the produced primary alcohols undergoes further condensation to produce heavier alcohols and other heavier byproducts.[316] Nevertheless, these heavier products/alcohols mixtures can be used as fuel additives, solvents or plasticizers, after some separation steps, if needed. [61]

4.3.2.4.1.3   *Temperature effect at WHSV=0.3 h⁻¹*

Since by performing the reaction at 450ºC with a contact time of 1 g_{CAT}/mL·s (WHSV=0.3 h⁻¹) the highest yield of *n*-butanol have been obtained (12%), a study of the effect of temperature reaction in the range 300-450ºC has been performed by keeping the contact time constant at that value. The results, in terms of ethanol conversion and product selectivity are depicted in Figure 43 and Table26.
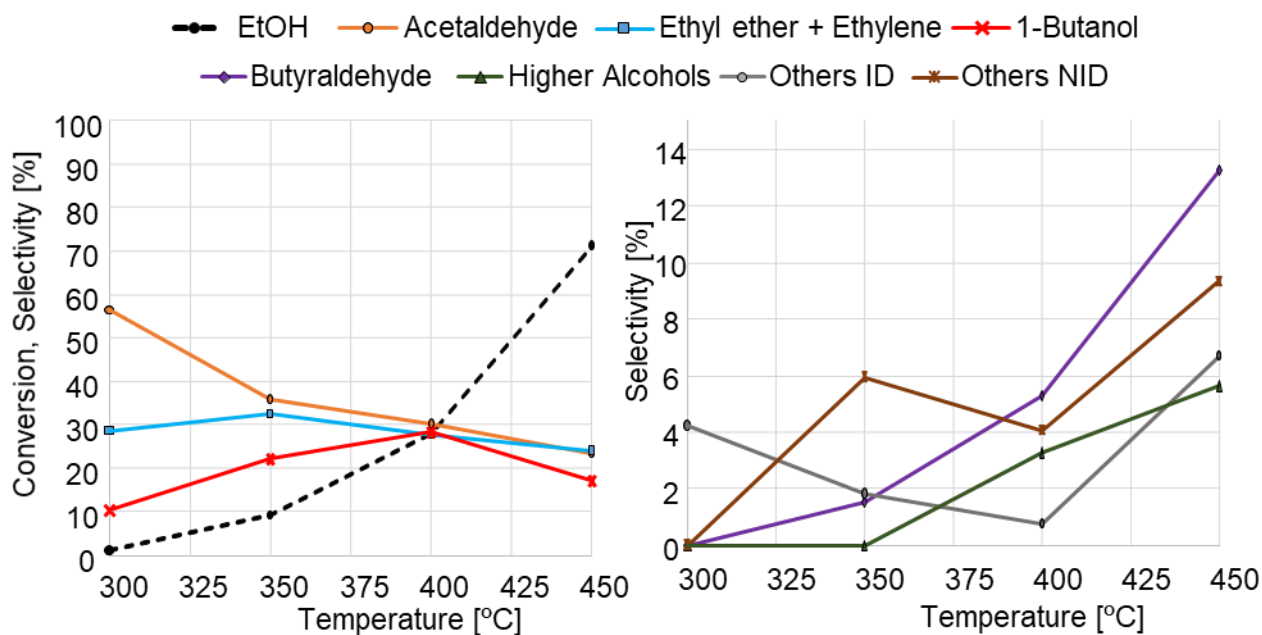
Figure 43 Influence of the temperature on the ethanol conversion and products selectivities over the 7Cs/Sep@500 catalyst. Higher alcohols: 2-ethyl-butanol, 1-hexanol, 2-ethyl-hexanol, 1-octanol. Others ID: acetone, 2-pentanone, CO_2, ethyl acetate. Reaction conditions: EtOH 5% v/v in N_2, T=300, 350, 400, 450°C, P= 1 atm, W/F= 1 g_{CAT}/mL·s; WHSV= 0.3 g_{EtOH}/(gcat·h).

Table 26. *Influence of the temperature on the ethanol conversion and products selectivities over the 7Cs/Sep@500 catalyst. Higher alcohols: 2-ethyl-butanol, 1-hexanol, 2-ethyl-hexanol, 1-octanol. Others ID: acetone, 2-pentanone, CO_2, ethyl acetate. Reaction conditions: EtOH 5% v/v in N_2, T=300, 350, 400, 450°C, P= 1 atm, W/F= 1 g_{CAT}/mL·s; WHSV= 0.3 g_{EtOH}/(gcat·h).*

T [ºC]	X EtOH [%]	Selectivity [%]							
		AA	Ethylene	DEE	BuOH	BuA	Others ID	Others NID	Higher Alcohols
300	1	57	7	22	10	0	4	0	0
350	9	36	11	22	22	2	2	6	0
400	28	30	12	16	28	5	1	4	3
450	71	24	16	8	17	13	7	9	6
T [ºC]	X EtOH [%]	Yield [%]							
		AA	Ethylene	DEE	BuOH	BuA	Others ID	Others NID	Higher Alcohols
300	1	1	0	0	0	0	0	0	0
350	9	3	1	2	2	0	0	1	0
400	28	9	3	4	8	1	0	1	1
450	71	17	11	6	12	9	5	7	4

By studying the reaction temperature effect at a higher value of contact time than the previous conditions (Figure 40, table 23), namely 1 g_{CAT}/mL·s instead of 0.4 g_{CAT}/mL·s, the trends observed of the reaction results changed. Ethanol conversion increased with increasing temperature as expected, while both acetaldehyde and dehydration products of ethanol selectivity decreased with increasing temperature. At the lowest temperature studied 300ºC, with an ethanol conversion of 1%,

n-butanol was already detected with a selectivity value of 10%. Then, *n*-butanol selectivity presented a maxim value at 400ºC reaching the value of 28% and then decreased to 17% at 450ºC. This suggests that at higher temperature *n*-butanol is converted to others products. Indeed, at higher temperature the butyraldehyde and higher alcohols selectivity increased reaching the value of 13% and 6% respectively. Accordingly, the effect of the contact time at 400ºC has been investigated, the results are presented in the next section.

4.3.2.4.1.4   WHSVs effect at 400ºC

The influence of the contact time on the activity and products distribution has been evaluated at 400ºC by varying the contact time between the ethanol fed and the catalysts in the range 0.2, 0.35, 1, 2, 3 g_{CAT}/mL·s (WHSV= 1.7, 1, 0.3, 0.17, 0.11 g_{EtOH}/(gcat·h)); the results are depicted in Figure 44 and Table 27. Figure 45 reports the catalytic results by means of the dependence of the products selectivity on the ethanol conversion.
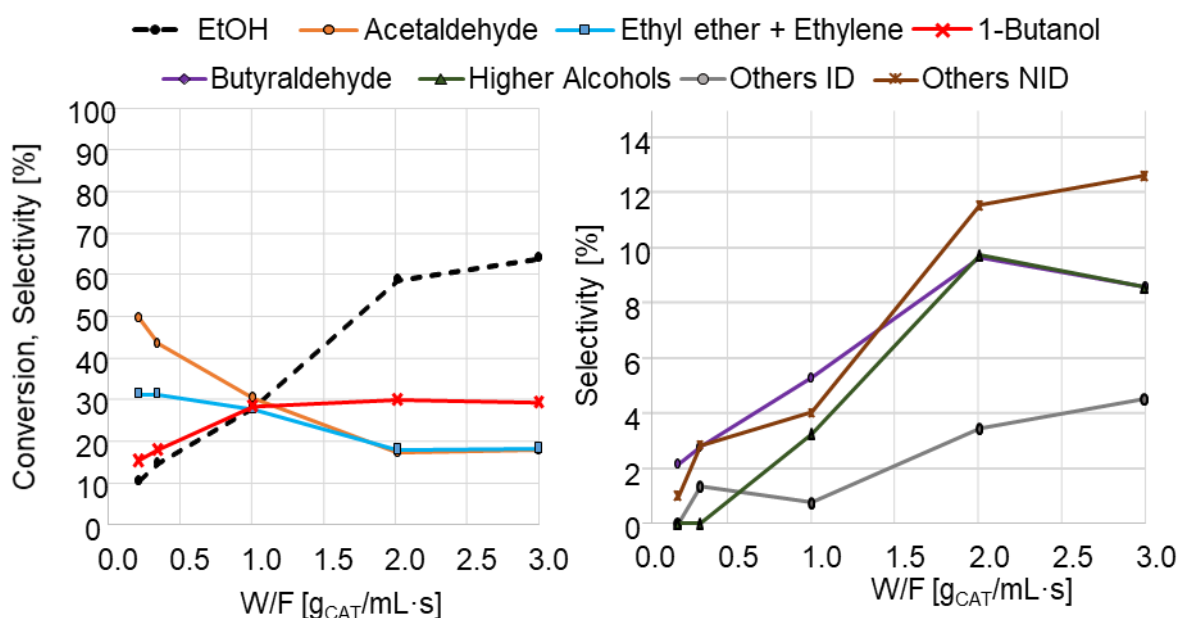
Figure 44   Ethanol conversion and products selectivities as a function of the contact time (W/F, g_{CAT}/mL·s) for the reaction performed over the 7Cs/Sep@500 catalyst. Higher alcohols: 2-ethyl-butanol, 1-hexanol, 2-ethyl-hexanol, 1-octanol. Others ID: acetone, 2-pentanone, CO_2, ethyl acetate. Reaction conditions: EtOH 5% v/v in N_2, T=**400ºC**, P= 1 atm, W/F= 0.2, 0.35, 1, 2, 3 g_{CAT}/mL·s; WHSV= 1.7, 1, 0.3, 0.17, 0.11 g_{EtOH}/(gcat·h).
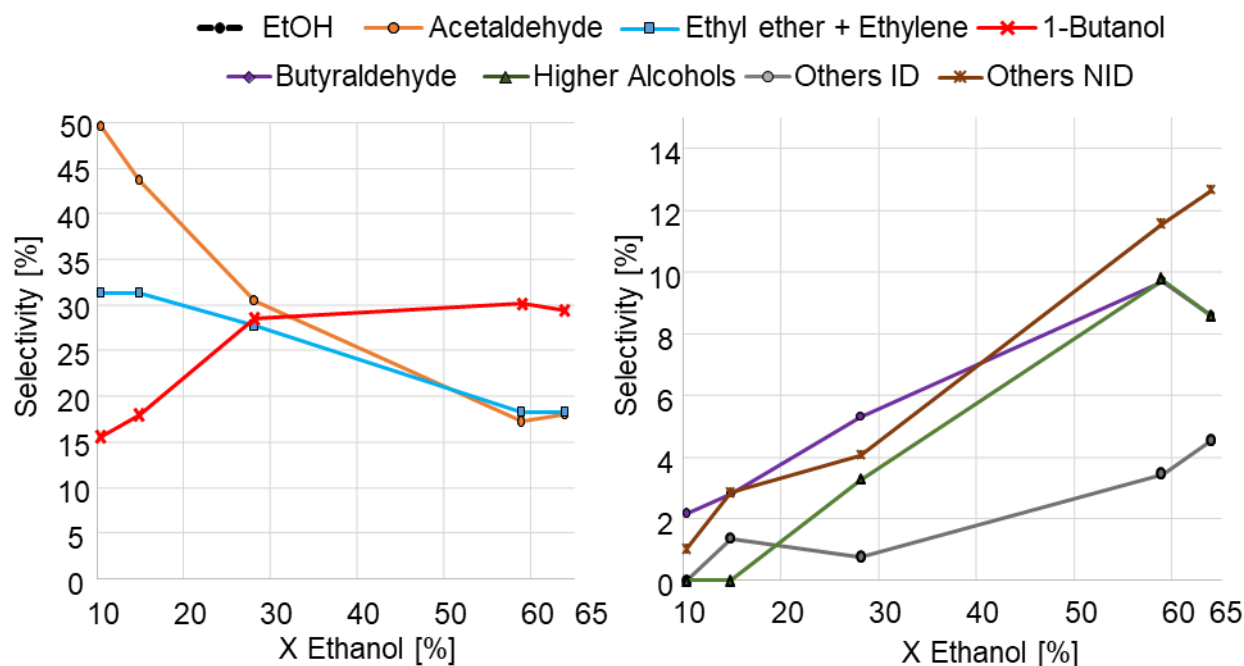
Figure 45   Products selectivity as a function of ethanol conversion over the 7Cs/Sep@500 catalyst. Higher alcohols: 2-ethyl-butanol, 1-hexanol, 2-ethyl-hexanol, 1-octanol. Others ID: acetone, 2-pentanone, CO_2, ethyl acetate, ethane. Reaction conditions: EtOH 5% v/v in N_2, T=**400ºC**, P= 1 atm, W/F= 0.2, 0.3, 1, 2, 3 g_{CAT}/mL·s.

By increasing contact time, ethanol conversion increased, reaching the value of 65% at W/F 3 g_{CAT}/mL·s. *n*-Butanol selectivity reached a maximum value of 30% while working at W/F 2 g_{CAT}/mL·s then dropped slightly to 29% at W/F=3 g_{CAT}/mL·s. Selectivity of both higher alcohols and BuA followed the same trend. By increasing the contact time, the selectivity of both the dehydration products of ethanol and acetaldehyde decreased, and concomitantly, the ones of the other products increased. Accordingly, the formation of Others NID products was favoured at higher contact time suggesting that their formation could come from consecutive side reactions. As stated before (Section 4.3.2.4.1.2), thanks to GC-MS analysis, their nature could be mainly aromatics and longer chains ketones. The quite specular trend of acetaldehyde and *n*-butanol selectivity with increasing ethanol conversion could suggest the nature of acetaldehyde as intermediate product for *n*-butanol formation.

Table 27. *Variation of products selectivities with contact time W/F [g_{CAT}/mL·s] and the ethanol conversion over the 7Cs/Sep@500 catalyst. Guerbet alcohols = n-butanol, higher alcohols (n-hexanol, 2-ethyl butanol, n-octanol, 2-ethyl hexanol); Others= others NID and ID (acetone, 2-pentanone, CO_2, ethyl acetate, ethane). Reaction conditions: EtOH 5% v/v in N_2, T=**400ºC**, P= 1 atm, W/F= 0.2, 0.3, 1, 2, 3 g_{CAT}/mL*s.*

		Selectivity [%]									
W/F [g_{CAT}/mL·s]	X EtOH [%]	AA	Ethylene	DEE	BuOH	BuA	Others ID	Others NID	Higher Alcohols	Guerbet Alcohols	Dehydration products
0.2	10	50	14	18	16	2	0	1	0	16	31
0.3	15	44	13	18	18	3	1	3	0	18	31
1.0	28	30	12	16	28	5	1	4	3	32	28
2.0	59	17	6	12	30	10	3	12	10	40	18
3.0	64	18	7	12	29	9	5	13	9	38	18
		Yield [%]									
W/F [g_{CAT}/mL·s]	X EtOH [%]	AA	Ethylene	DEE	BuOH	BuA	Others ID	Others NID	Higher Alcohols	Guerbet Alcohols	Dehydration products
0.2	10	5	1	2	2	0	0	0	0	2	3
0.3	15	6	2	3	3	0	0	0	0	3	5
1.0	28	9	3	4	8	1	0	1	1	9	8
2.0	59	10	3	7	18	6	2	7	6	23	11
3.0	64	12	4	7	19	5	3	8	5	25	12

Regardless, a relative high value of *n*-butanol selectivity have been obtained. From the point of view of the overall Guerbet alcohols production, the total alcohols selectivity followed the same trends manifested by *n*-butanol: the maximum value was reached at W/F=2 g_{CAT}/mL·s with a cumulative selectivity of 40% (figure 46). At that value of contact time the Guerbet reactions seemed faster than the dehydration of ethanol.
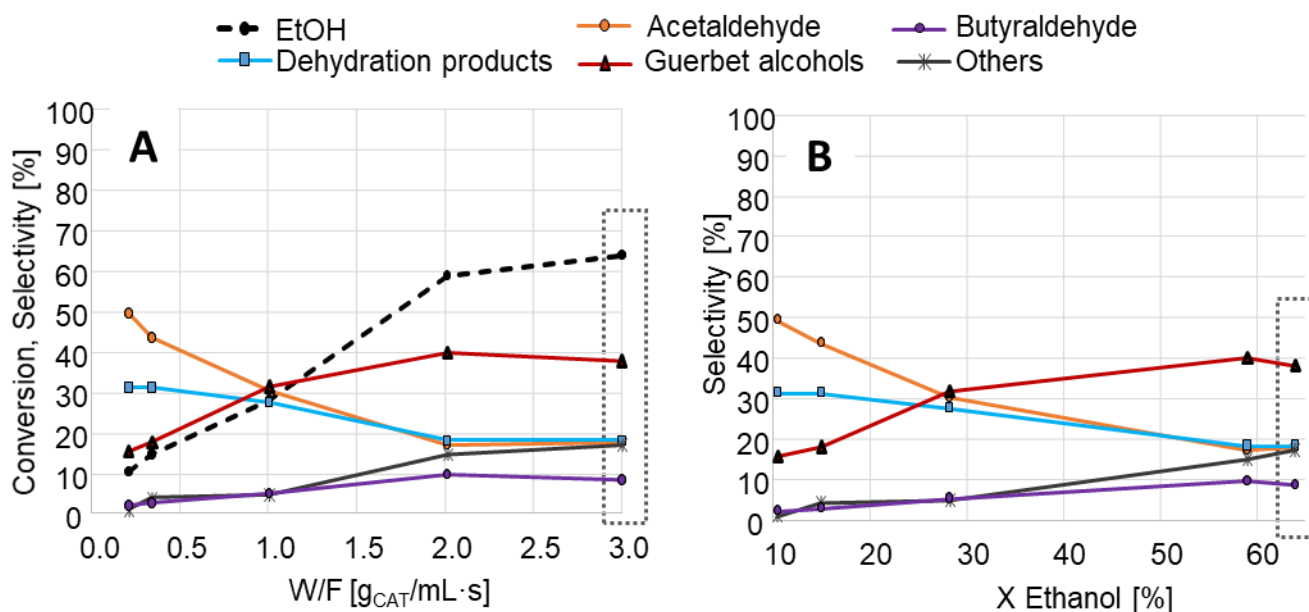
Figure 46 Variation of products selectivities with contact time W/F [g_{CAT}/mL·s](A) and the ethanol conversion (B) over the 7Cs/Sep@500 catalyst. Guerbet alchohols = *n*-butanol, higher alcohols (n-hexanol, 2-ethyl butanol, n-octanol, 2-ethyl hexanol); Others= others NID and ID (acetone, 2-pentanone, CO_2, ethyl acetate, ethane). Reaction conditions: EtOH 5% v/v in N_2, T=**400ºC**, P= 1 atm, W/F= 0.2, 0.3, 1, 2, 3 g_{CAT}/mL*s.

4.3.2.4.1.5 *Stability Test*

Finally, in order to evaluate the catalyst stability and deactivation, a 7.5 h test was carried out at 400°C and 3 g_{CAT}/mL·s, the same reaction conditions with the highest contact time used in the previous tests (framed in Figure 46). To do so, the reaction has been performed by keeping the reaction parameters constant over a time on stream of 7.5 hours, the results are depicted in Figure 47.
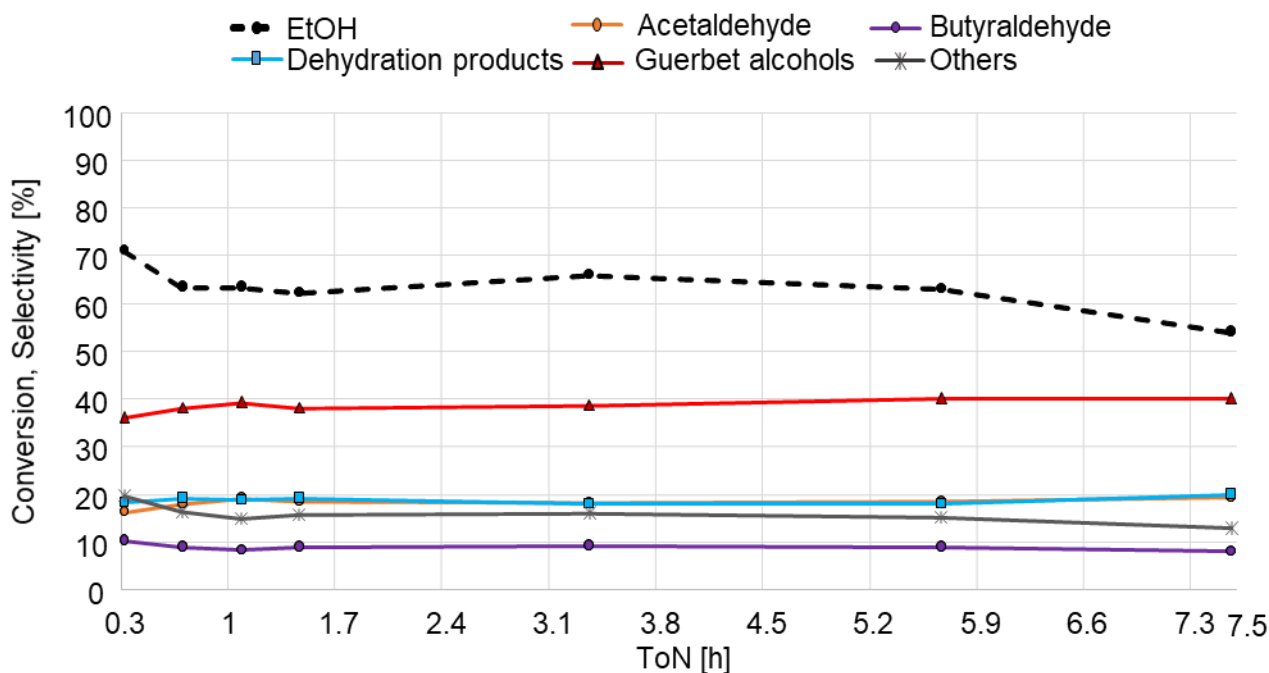
Figure 47   Catalytic results obtained in the Ethanol gas-phase conversion over the 7Cs/Sep@500 in terms of conversion of ethanol and main products selectivity as a function of the time on stream, TON (h). Guerbet products= *n*-butanol, butyraldehyde, higher alcohols (n-hexanol, 2-ethyl butanol, n-octanol, 2-ethyl hexanol); Others= others NID and ID (acetone, 2-pentanone, CO_2, ethyl acetate, ethane).Reaction conditions: EtOH 5% v/v in N_2, T=400°C, P= 1 atm, W/F =3 g_{CAT}/mL·s; WHSV= 0.11 g_{EtOH}/(gcat·h).

The stability has been reached after 0.5 h of time on stream (ToN), with an ethanol conversion of around 60%, it can be noticed a slight decrease of conversion after 7.5 h to 55%. The trend can be related to partial deactivation of the catalyst due to coke formation. While the overall Guerbet products selectivity has not changed, a simultaneous slight decrease of other products selectivity can be observed, suggesting that their productions is related to different reaction paths.

4.3.2.4.1.6   *Effect of reaction temperature and W/F, overview.*

Figure 48 resumes the results obtained while studying the effect of the reaction temperature and contact time on the activity and products production. In particular, the effect of the contact time studied (i.e., 0.2, 0.35, 1, 2, 3 g_{CAT}/mL·s) at 400 and 450ºC on ethanol conversion and products selectivity is depicted. It can be noticed a different behaviour of the product distribution with increasing contact time according to the reaction temperature employed. In particular, higher temperature (i.e 450ºC) seems to favour *n*-butanol conversion to consecutive reactions while rising the contact time employed.

200
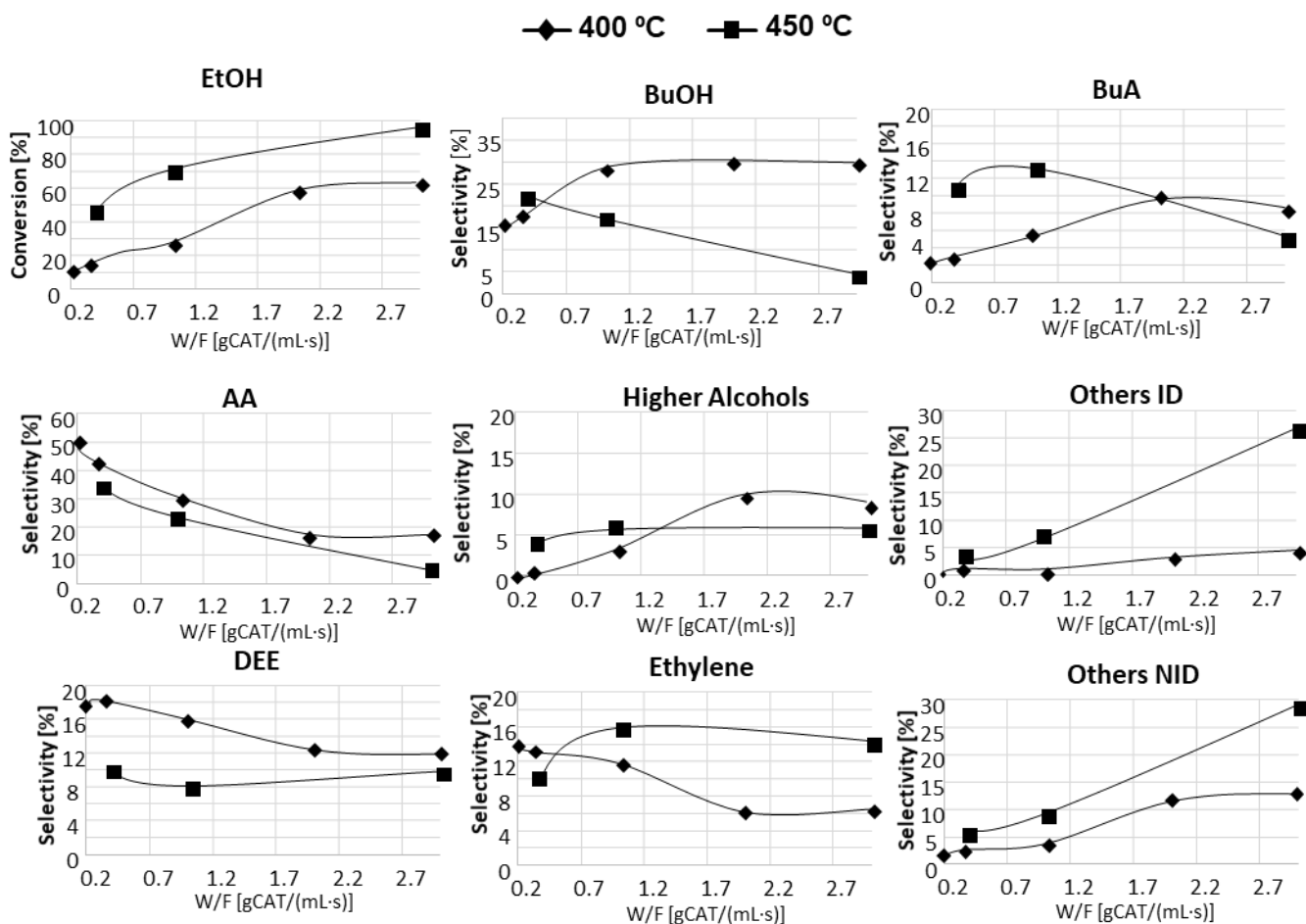
Figure 48   Conversion and selectivity of the main products as a function of the contact time W/F. (Others NID= other products unidentified; Others ID (acetone, 2-pentanone, CO_2, ethyl acetate, ethane). Reaction conditions: EtOH 5% v/v in N_2, T=400ºC, 450ºC; P= 1 atm, W/F= 0.2, 0.35, 1, 2, 3 g_{CAT}/mL·s.

The selectivity of the other unknown products (Other NID) is not completely trustworthy since they have been quantified through an artificial response factor (see section 3.2.3.1) that could overestimate or underestimate some products, according to their nature and number of carbon chain.

Regardless, since the slope at short contact time of *n*-butanol selectivity seemed to be higher than zero, it is reasonable to claim that this compound is a kinetic primary product. Thus, the reaction mechanism of its formation could not follow the one based on aldol condensation. The reaction mechanism that could take place over the alkali doped sepiolite will be discussed in the final section (section 4.3.3).

4.3.2.5 Double bed

For the production of *n*-butanol from ethanol, two main reaction mechanism has been proposed. The main accepted one rely on aldol condensation, with acetaldehyde as key intermediate while the second one involves the direct condensation of two molecules of ethanol. [46,62,283,291,303] To gain more

insight into the reaction pathway, a reaction over the most performing catalyst (7Cs/Sep@500) has been carried out by feeding a mixture of ethanol and acetaldehyde. Since acetaldehyde is difficult to handle at room temperature due to its low boiling point (20.2ºC), another strategy has been adopted, i.e. it has been produced in-situ. Therefore, aiming to study the effect of the presence of acetaldehyde in the feeding mixture, a reaction has been performed by using two catalysts, shaping a "double bed". The first catalyst used was the CuO/2Na/Sep@500 10 wt%, since by using it at 450ºC and 0.24 s of contact time, the ethanol conversion and acetaldehyde selectivity obtained where both 51%. In this way, a gaseous solution containing 2,5 v/v of ethanol and 1.25 v/v of acetaldehyde (EtOH:AA 2:1) was fed through the second catalyst, namely 7Cs/Sep@500. The reaction has been performed at 450ºC and with 1 g/(g$_{CAT}$·h) as WHSV for each catalyst. The results obtained are reported in Figure 49, 50 and Table 28.
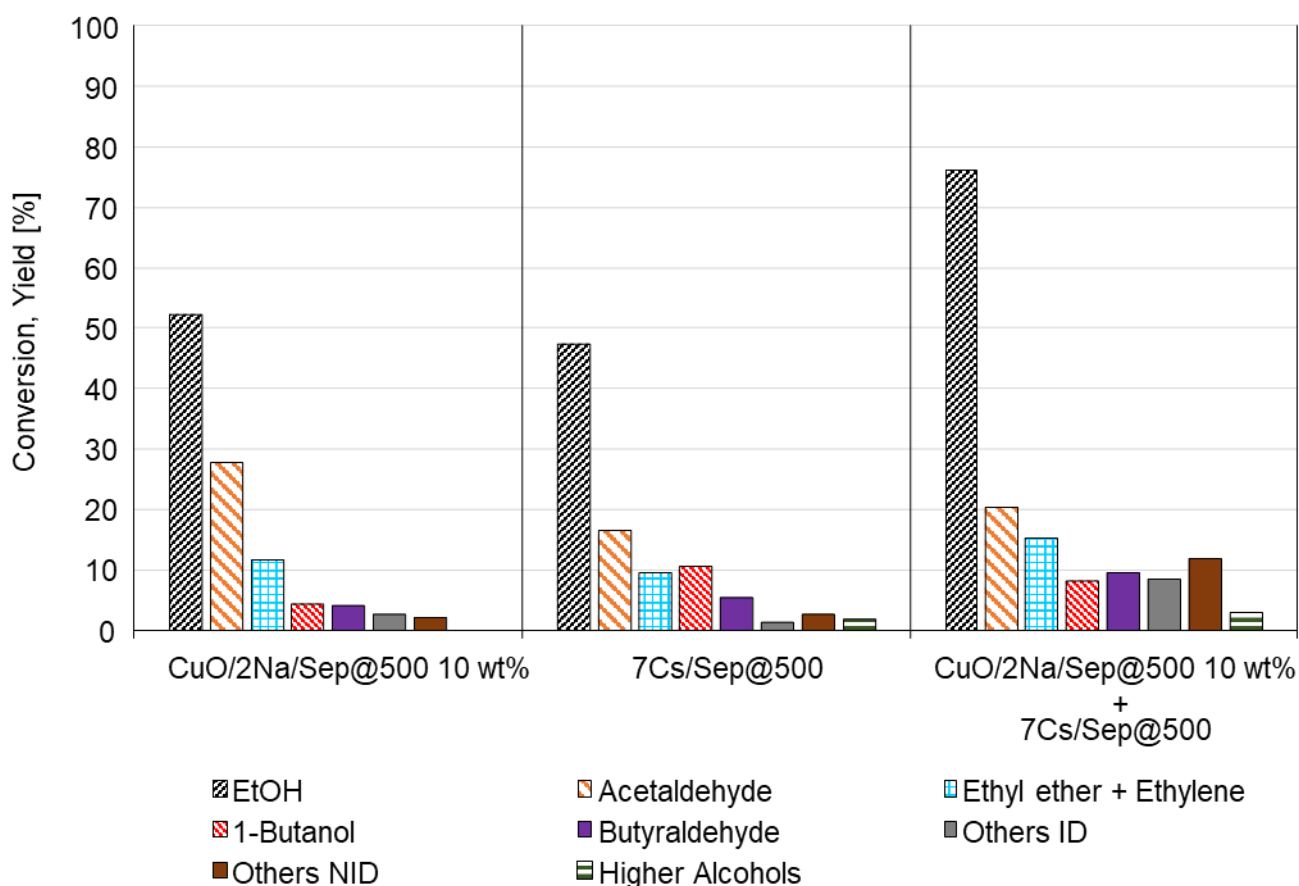
Figure 49 Products yield and ethanol conversion obtained for the ethanol gas-phase conversion over CuO/2Na/Sep@500 10 wt%, 7Cs/Sep@500 and the dual bed catalysts. Higher alcohols: n-hexanol, 2-ethyl butanol, n-octanol, 2-ethyl hexanol; Others ID: acetone, 2-pentanone, CO_2, 1,3-butadiene, ethane. Others NID: other products unidentified. Reaction conditions: EtOH 5% v/v in N_2, T= 450°C, P= 1 atm, WHSV$_1$= 1 g/(gcat·h), WHSV$_2$= 1 g/(gcat·h).

Table 28. *Catalytic results obtained in the Ethanol gas-phase conversion over CuO/2Na/Sep@500 10 wt%, 7Cs/Sep@500 and the dual bed catalysts. Higher alcohols: n-hexanol, 2-ethyl butanol, n-octanol, 2-ethyl hexanol; Others ID: acetone, 2-pentanone, CO₂, 1,3-butadiene (BD), ethane. Others NID: other products unidentified. Reaction conditions: EtOH 5% v/v in N₂, T= 450°C, P= 1 atm, WHSV₁= 1 g/(gcat·h), WHSV₂= 1 g/(gcat·h).*

Catalyst	X EtOH [%]	Yield[%]						
		AA	Ethylene	DEE	BuOH	BuA	Others NID	Higher Alcohols
CuO/2Na/Sep@500 10 wt%	52	28	4	7	4	4	2	0
7Cs/Sep@500	47	17	5	5	10	5	3	2
CuO/2Na/Sep@500 10 wt% + 7Cs/Sep@500	76	20	5	10	8	10	12	3

Catalyst	X EtOH [%]	Others ID					Total Others ID
		Acetone	2-Pentanone	BD	CO₂	Etane	
CuO/2Na/Sep@500 10 wt%	52	0.5	0.2	1.3	0.1	0.4	3
7Cs/Sep@500	47	0.3	0.4	0.0	0.1	0.3	1
CuO/2Na/Sep@500 10 wt% + 7Cs/Sep@500	76	1.5	2.0	3.4	0.6	0.9	8
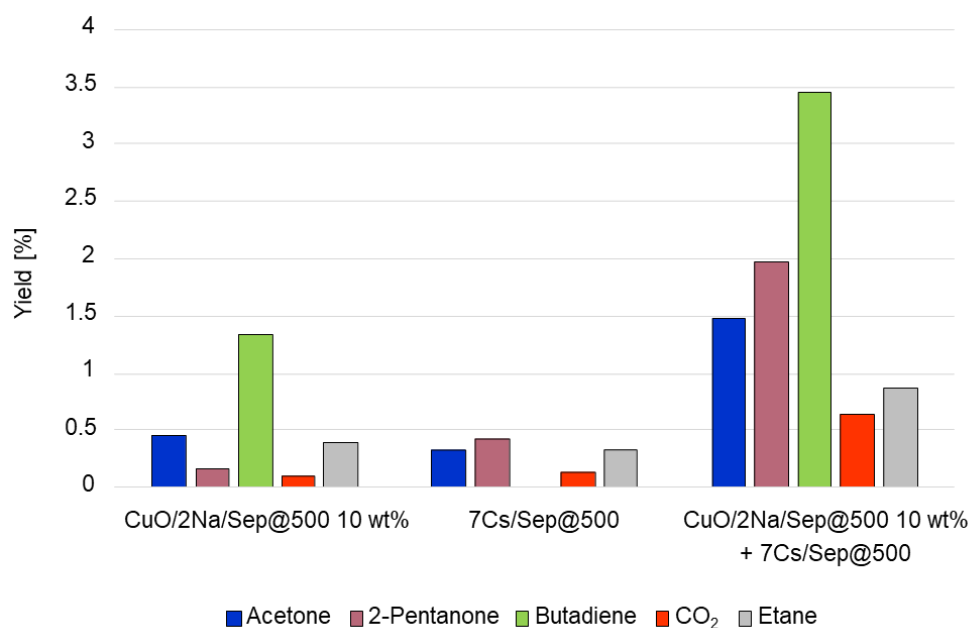
Figure 50 Catalytic results obtained, in terms of products yields (ID others), in the Ethanol gas-phase conversion over CuO/2Na/Sep@500 10 wt%, 7Cs/Sep@500 and the dual bed catalysts. EtOH 5% v/v in N₂, T= 450°C, P= 1 atm, WHSV₁= 1 g/(gcat·h), WHSV₂= 1 g/(gcat·h).

It can be noticed that by feeding acetaldehyde with ethanol the formation of *n*-butanol has not been favoured. On the contrary, a slight decrease of *n*-butanol yield was obtained. Considering that *n*-butanol was present in the "feeding" mixture obtained over the first catalyst, a decrease of *n*-butanol yield could be explained by its conversion subsequent conversion over the second catalyst. Indeed,

the yield of both higher alcohols and butyraldehyde increased, the formation of which can be explained by consecutive Guerbet reactions and its dehydrogenation, respectively. Acetaldehyde yield increased a bit, comparing the results between the ones obtained over 7Cs/Sep@500 and the dual bed set. On the other hand, the just-mentioned selectivity decreased if compared to the one obtained while performing the reaction over the CuO/2Na/Sep@500 10 wt% catalyst alone. Its final yields is a combination of the two catalytic results, but the fact that it has decreased could be related to its conversion to form other products. In particular, in Figure 50 are reported the yields obtained of the other identified products, namely acetone, 2-pentanone, CO_2, 1,3-butadiene, ethane. Except for ethane, the hydrogenation product of ethylene, the other products came from consecutive reactions that comprehends acetaldehyde as intermediate products (ketonization and Toussaint, see Scheme 4). [301] Moreover, it is well-known that acetaldehyde has a beneficial effect on 1,3-butadiene yield, which is why this aldehyde is recycled to the reactor in the industrial process. [317] Indeed, acetaldehyde has been reported as key intermediate product in ethanol conversion into butadiene.[302] The Ostromislensky process[318] consists of two reactors—a first one for partial dehydrogenation of ethanol to acetaldehyde followed by a second one, allocated for the conversion of the as-obtained ethanol–acetaldehyde mixtures to butadiene.
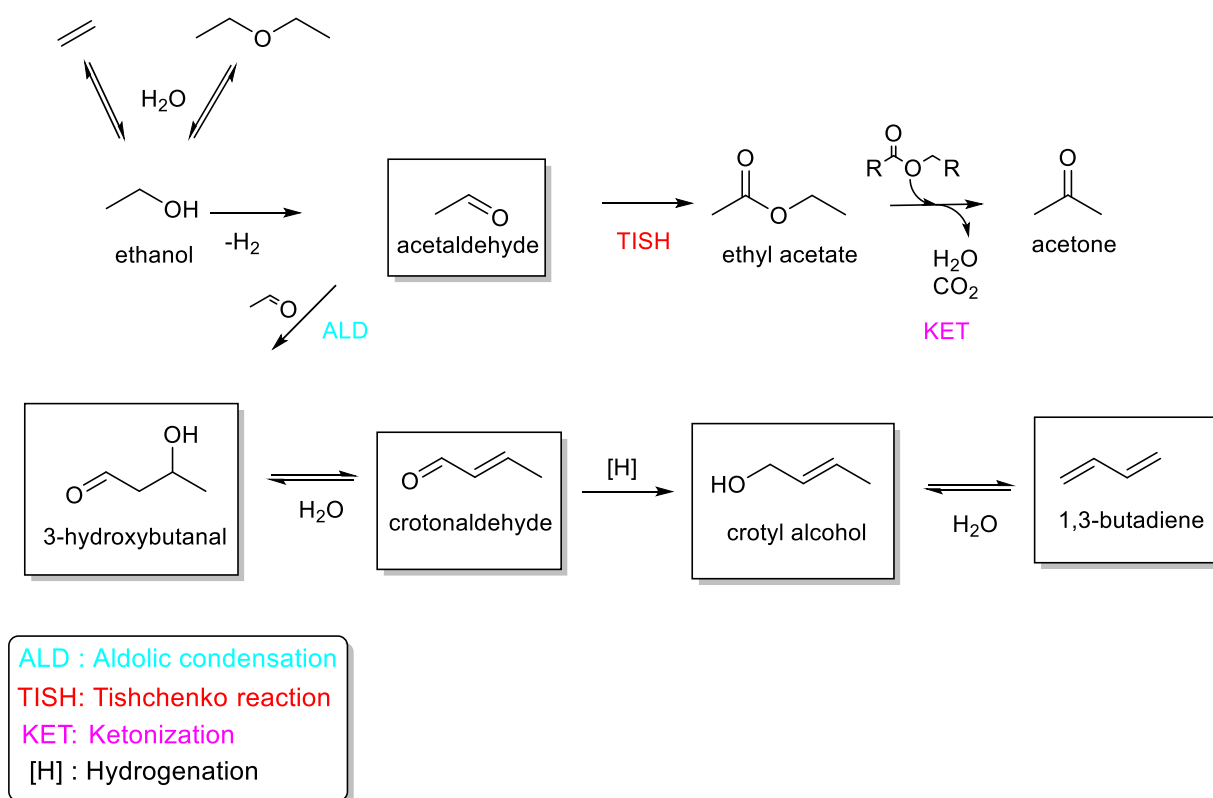
Scheme 4. Toussaint mechanism for ethanol conversion to butadiene. Some side reactions are depicted.

4.3.2.6 Catalysts screening in the best reaction conditions

From the previous catalytic tests, the highest *n*-butanol selectivity obtained, 30%, was reached by performing the reaction at 400ºC with a contact time of 2 g$_{CAT}$/mL·s over the catalyst 7Cs/Sep@500.

At the same time, it has been observed that the best alkali-metal:sepiolite moles/weight ratio was the one at around 0.6 mmol$_{MET}$/g$_{SEP}$. Accordingly, the catalysts containing this amount of sodium and potassium have been tested in the most performing reaction conditions in order to evaluate the effect of the different alkali metals. More specifically, catalytic tests at 400ºC, 1 atm and 2 g$_{CAT}$/mL·s, have been performed over the catalysts 2K/Sep@500 and 1.2Na/Sep@500 and the results obtained have been compared to the ones obtained over the 7Cs/Sep@500 catalyst. The results in terms of ethanol conversion and products selectivity are reported in Figure 51 and Table 29.
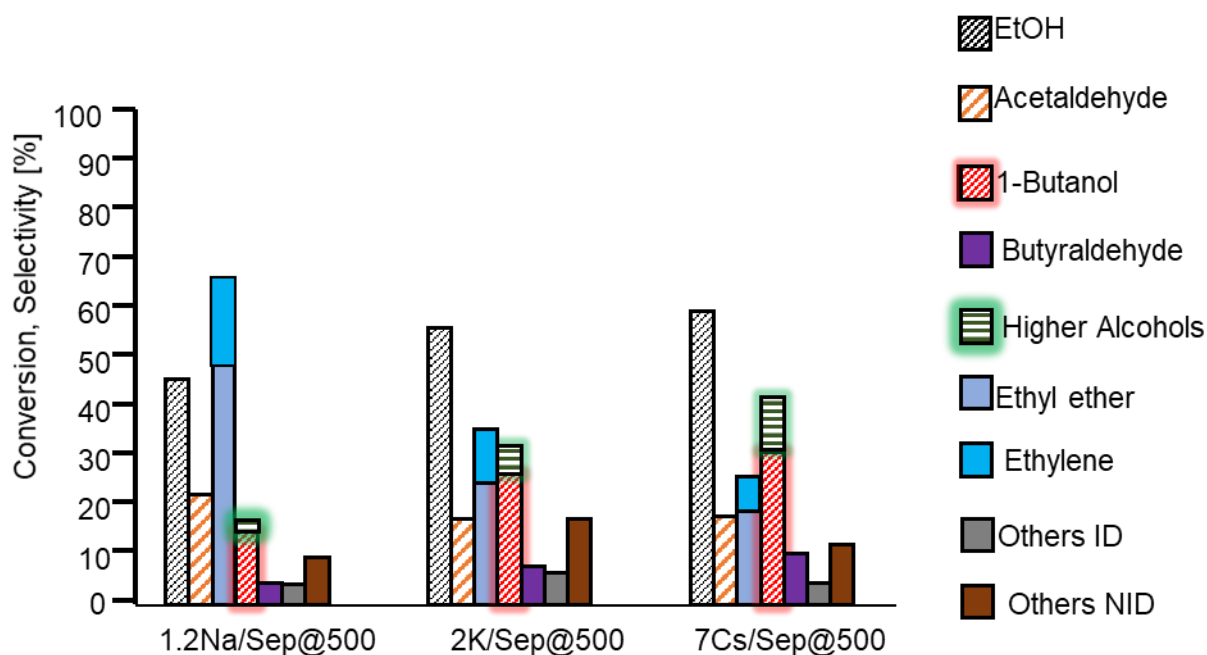
Figure 51   Catalytic results obtained, in terms of EtOH conversion and main products selectivity, in the Ethanol gas-phase conversion over the impregnated sepiolite samples with 1.2 wt% of Na (1.2Na/Sep@500), 2wt% of K (2K/Sep@500) and 7 wt% of Cs (7Cs/Sep@500). Higher alcohols: n-hexanol, 2-ethyl butanol, n-octanol, 2-ethyl hexanol; Others ID: acetone, 2-pentanone, CO_2, ethyl acetate; Others NID: other products unidentified. Reaction conditions: EtOH 5% v/v in N2, T= 400°C, P= 1 atm, W/F= 2 g/mL·s; WHSV= 0.2 g/(g$_{CAT}$·h).

Table 29. *Catalytic results obtained, in terms of EtOH conversion and main products selectivity and yields, in the Ethanol gas-phase conversion over the impregnated sepiolite samples with 1.2 wt% of Na (1.2Na/Sep@500), 2wt% of K (2K/Sep@500) and 7 wt% of Cs (7Cs/Sep@500). AA: acetaldehyde, BuA: butyraldehyde Higher alcohols: n-hexanol, 2-ethyl butanol, n-octanol, 2-ethyl hexanol; Others ID: acetone, 2-pentanone, CO_2, ethyl acetate; Others NID: other products unidentified. Guerbet alcohols: n-butanol + higher alcohols. Reaction conditions: EtOH 5% v/v in N_2, T= 400°C, P= 1 atm, W/F= 2 g/mL·s; WHSV= 0.2 g/(gCAT·h).*

| | Selectivity [%] | | | | | | | | | |
Metal	EtOH	AA	DEE	Ethylene	BuOH	BuA	Higher Alcohols	Guerbet alcohols	Others ID	Others NID
1.2Na	45.2	21.5	47.7	17	13.9	3.5	1.2	15.1	3.4	8.8
2K	55.7	16.6	24.0	9.8	25.8	6.9	4.9	30.7	5.7	16.6
7Cs	*59.0*	*17.2*	*18.2*	*5.9*	*30.1*	*9.7*	*9.8*	*39.9*	*3.5*	*11.5*
	Yields [%]									
Metal	EtOH	AA	DEE	Ethylene	BuOH	BuA	Higher Alcohols	Guerbet alcohols	Others ID	Others NID
1.2Na	45.2	9.7	21.6	7.7	6.3	1.6	0.5	6.8	1.5	4.0
2K	55.7	9.2	13.4	5.5	14.4	3.8	2.7	17.1	3.2	9.2
7Cs	**59.0**	**10.2**	**10.7**	**3.5**	**17.8**	**5.7**	**5.7**	**23.5**	**2.0**	**6.8**

The nature of the alkali metal exerts a great effect on ethanol conversion (Figure 5), especially with regards of the products distribution. Ethanol conversion obtained over the cesium-doped sepiolite is greater than the one containing sodium and potassium by 14% and 4% respectively. The products distribution could reflects the basicity of the metal ions. Accordingly, the selectivity of dehydration products decreased while the ones of *n*-butanol and higher alcohols increased. Butyraldehyde and others NID products formation seemed to be favoured over the 7Cs/Sep@500 catalyst as well.

4.3.3 Reaction mechanism

Along the aldol-condensation-based pathway for the Guerbet route, the intermediates that are formed starting from the aldol condensation of two molecules of acetaldehyde are the acetaldol (3-hydroxy-butanal), its dehydration product, the α,β-unsaturated aldehyde (crotonaldehyde) and then its hydrogenation products. From the hydrogenation of the double bond is formed butyraldehyde, while from the hydrogenation of the carbonyl group, crotyl alcohol is formed. Crotyl alcohol is reported to be a key product for butadiene formation, that should come from which its dehydration.[58] Butadiene have been detected mainly when transition metals (copper and nickel) where added to sepiolite, favouring acetaldehyde formation, suggesting that acetaldehyde it's a key compounds to form butadiene. Nevertheless, neither crotonaldehyde nor crotylalcohol, have been detected or quantified while conducting the catalytic tests. Then, the formation of butadiene could follow another route different from the aldol-condensation one. The fact that the addition of a transition metal only favoured the formation of acetaldehyde without favouring *n*-butanol formation could suggest that acetaldehyde is not the major intermediate in the mechanism, instead, it favoured the formation of

the side product 1,3-butadiene. Nevertheless, from the literature is reported that after transition metal addition, the aldol condensation step becomes the rate-limiting one.[148]

From the literature, along with the aldol-condensation based mechanism, another way to produce *n*-butanol from ethanol has been proposed by several authors[46,62,283,291,303], and it is based on the formation of *n*-butanol directly from two molecules of ethanol by condensation without any intermediates, the so-called "direct route". Yang and co-workers [46] in 1993 proposed a mechanism in which ethanol undergoes H-abstraction from a β- carbon atom generation a nucleophilic centre that attacks another molecule of ethanol , condensing to *n*-butanol and water. Ndou et al. [283] stated that the basic sites on the surface of the catalyst are necessary to activate the C-H bond in the β-position in ethanol in order to condense with another molecule of ethanol by dehydration to form *n*-butanol. Accordingly, the addition of the basic alkali metal ions Na^+, K^+ and Cs^+ promoted *n*-butanol formation. Indeed, by adding alkali metals it has been observed a related formation of new basic sites with different strength, which led to a general decrease of the acidity of the sepiolite surface and related lower values of the A/B ratios. Many authors [59,258] reported how important it is to tune the quantity and ratio of basic and acid sites of the catalyst in order to promote *n*-butanol formation from ethanol, regardless the overall activity differs from one catalyst to another due to its nature and related side reactions that can take place over its specific surface.

Scalbert et al. [62] reported that at least two reaction pathways take place simultaneously, the direct route and a secondary condensation reaction between ethanol and acetaldehyde (formed from ethanol dehydrogenation) to form butenols, which are dehydrogenated to *n*-butanol by H-transfer from a sacrificial ethanol molecule. Also, Chieregato et al. [303] stated that even the condensation features of the catalyst need to be adjusted by means of the distance of the active sites in order to properly bound the intermediates that lead selectively to *n*-butanol formation. Through DRIFTS and DFT calculations they proposed a different reaction mechanism. They studied the Guerbet reaction mechanism over a basic heterogeneous catalyst, MgO, and they claimed that the *n*-butanol formation from ethanol relay on the formation of a carbanion intermediate formed over the surface of the catalyst that directly yield *n*-butanol. If vicinal adsorbed acetaldehyde reacts with the carbanion, butadiene is formed. Moreover, the mechanism they proposed do not comprise hydrogenation reactions by H-transfer (Meerwein-Ponndorf-Verley).

As far as the side product butyraldehyde is concerned, some of the catalytic results obtained suggested its formation derived from consecutive dehydrogenation of *n*-butanol, rather than being an intermediate (as it should be considering the aldol condensation route). For instance, considering the effect of the contact time on the products distribution obtained at 400ºC (see Fig.44, 45 and 48), the increasing trend of the selectivity of butyraldehyde with the contact time suggested its nature of consecutive product. Nevertheless, considering the complexity of the reaction mechanism it is difficult to draw certain conclusions. Indeed, butyraldehyde may be formed even by direct condensation of a molecule of ethanol and one of acetaldehyde [46,283], then its hydrogenation could lead to form *n*-butanol.

By combining the catalytic results together with the reaction mechanisms proposed from the literature, a reaction mechanism for the Guerbet route that could take place over the alkali metal

doped sepiolite catalysts has been proposed and is depicted in Scheme 5. Further evidence will be required to support this proposal.
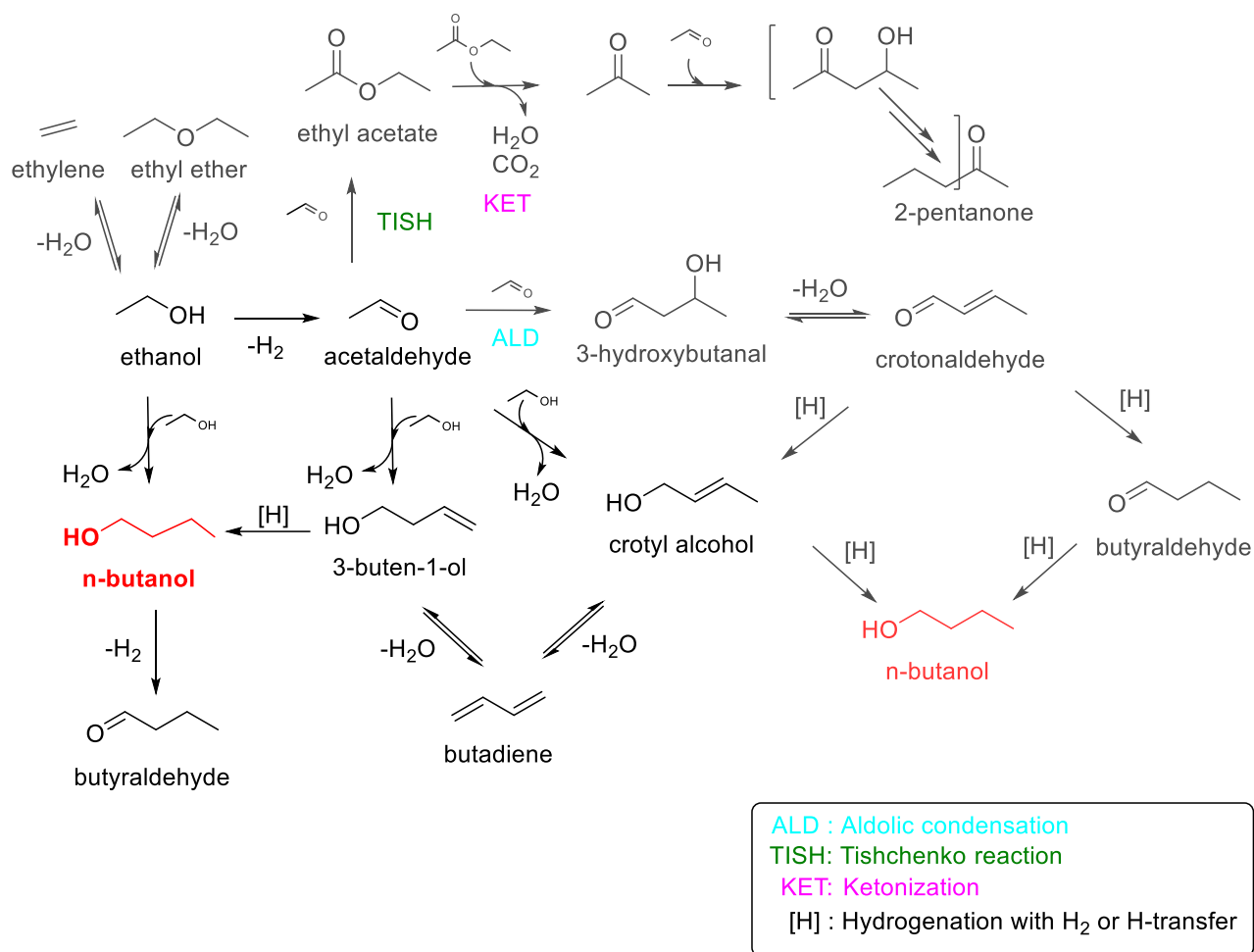
Scheme 5. Reaction mechanism hypothesized over the alkali-doped sepiolite catalyst.

4.3.4   CONCLUSIONS

The natural clay Sepiolite has been modified with the addition of alkali metals (i.e. Na, K and Cs) by incipient wetness impregnation with different amount (i.e., 2, 4, 5, 7, 14 wt%) and of transition metal oxides (i.e., CuO and NiO) with a metal loading of 5 or 10 wt%. The catalysts as prepared have then been tested for the ethanol continuous flow gas-phase conversion into a las-scale quartz reactor.

Since it is known that copper as a dopant could significantly speed up the rate of ethanol dehydrogenation, which is supposed to be the first step toward the formation of *n*-butanol, some samples impregnated with copper has been prepared and tested. The results obtained were not promising regarding the Guerbet pathway, since its addition only favoured acetaldehyde formation. Nevertheless, it has been observed an interesting synergic effect between transition metal and alkali metal, leading to higher acetaldehyde formation, to butadiene formation and even to an overall lower carbonaceous deposits formation over the catalyst surface. The formation of the latter has been linked to the ethylene oligomerization and consecutive coke formation. [267,312,313] Hence, the concomitant presence of transition metal and alkali metal should be better investigated in the optic of enhance butadiene selectivity, an important chemical compound for the polymer industry. In addition, the catalyst impregnated with nickel (i.e., NiO/2Na/Sep@500 5 wt%) has been more active and led to a slight increase of 1,3-butadiene formation, reaching a butadiene selectivity of 7% while performing the reaction at 400ºC and 1 g/(g$_{CAT}$·h) as WHSV.

Generally, it has been observed that the presence of an alkali metal over sepiolite favoured the formation of the Guerbet product of ethanol, *n*-butanol. Simultaneously, a decrease in the strength and concentration of acid sites responsible for the occurrence of a side reaction of ethanol dehydration to ethylene or ethyl ether has been observed. It is worth to note that the calcination temperature of the heating treatment of sepiolite was crucial, showing better results when calcined at 500ºC. Indeed, regarding the sodium-impregnated sepiolite, the best results in terms of *n*-butanol selectivity have been obtained over the 2Na/Sep@500, namely 14%, a 13% higher than the one obtained over 2Na/Sep@700, when tested in the same conditions.

Even the amount and the nature of the alkali metals played a role in the optimization of n-butanol selectivity. The catalytic results obtained over the different alkali metals have been compared through the molar amount of the metals per weight of sepiolite (mmol$_{MET}$/g$_{SEP}$), finding an optimal amount of ca. 0.6 mmol$_{MET}$/g$_{SEP}$. Indeed, with that amount, the maximum selectivity of *n*-butanol have been obtained over the catalysts, regardless the nature of the alkali metals. Between them, the maximum yield of *n*-butanol, namely 10.3%, has been obtained over the cesium-impregnated one (i.e., 7Cs/Sep@500). This catalyst had an acid/base sites ratio of 1.6, containing both of medium and strong basic sites. In contrast with the ones doped with sodium or potassium that, with the same alkali metal amount, showed a different basic sites distribution. The reason of such difference should be better investigate since the nature of the basic sites could be responsible for the enhanced *n*-butanol formation.

The subsequent reaction condition optimization performed over the catalyst 7Cs/Sep@500 (i.e., 400°C, atmospheric pressure and 0.2 g/(g$_{CAT}$·h) as WHSV) led to the achievement of a maximum

selectivity of *n*-butanol equal to 30% with 59% of ethanol conversion. Figure 52 summarizes the catalytic results obtained by several authors[59,61,97,99,181,283,293,319,319] for the ethanol gas-phase conversion through the Guerbet route performed at atmospheric pressure. It can be noticed an inverse relation between *n*-butanol selectivity and ethanol conversion, indeed the best result in terms of *n*-butanol selectivity (~80%) was obtained with an ethanol conversion of 4% over a strontium phosphate hydroxyapatite catalyst.[97] The results obtained over the 7Cs/Sep@500 let it be placed in a promising position.
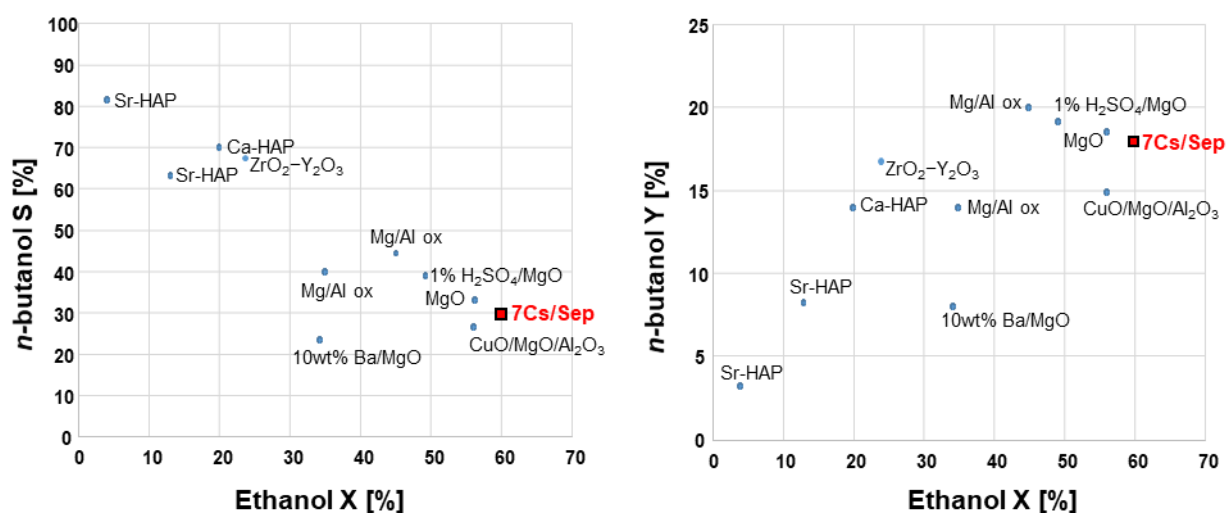
Figure 52   Relation between *n*-butanol selectivity (S%) and yield (Y%) with ethanol conversion (X%) for the best performing heterogeneous catalysts in the vapour-phase Guerbet reaction performed at atmospheric pressure and in the temperature range 260-450°C.[59,61,97,99,181,283,293,319,319]

In addition, considering the cumulative selectivity of *n*-butanol and higher Guerbet alcohols, which find suitability for advanced biofuel and lubricants applications, it was possible to reach a total Guerbet alcohols selectivity of 40%, corresponding to a total yield of ~24%.

A reaction mechanism by which the Guerbet reaction took place over the alkali-doped sepiolite catalyst has been proposed. Further studies are needed to better understand the overall mechanism. To shed more light on the reaction mechanism over the alkali-sepiolite catalysts, it could be useful perform reactions by feeding some intermediate molecules, such as butyraldehyde. Then, it would be interesting to perform in situ Diffuse Reflectance Infrared Fourier Transform (DRIFT) spectroscopy analysis over the sepiolite surface.

5 CONCLUSIONS

This Thesis, which represents the summary of the results collected during the three years of my PhD, reports on the investigation of the catalytic, gas-phase, continuous-flow, upgrading of ethanol to a wide range of added-value molecules. Three main topics have been addressed, with regards to the nature of the materials used as heterogeneous catalyst: hydroxyapatite, zirconium oxide and the natural clay sepiolite.

As far as the ion-exchanged hydroxyapatite based catalysts is concerned, the Sr-HAP system has been employed to study the formation of heavier products from ethanol in order to obtain a hydrocarbon mixture suitable for biofuel application. With this proposal, harsh reaction conditions such as high ethanol feeding concentration or relatively long contact time have been used. A final hydrocarbon mixture with composition resembling the one of gasoline has been obtained with a total yield of ca.50%. Nevertheless, the main product obtained was the dehydrogenation product of acetaldehyde. Another issue encountered was the percentage of aromatics products obtained, which should be diminished in order to reach the limits of 25% claimed in standard specification for jet fuel application.[106] Nevertheless, the reaction system has been upgraded in order to perform further investigations for this purpose.

The effect of various synthetic parameters over the zirconia phase formation have been evaluated. The incorporation of a 5% molar of a metal dopant (Ti and Y) permitted the stabilization of the metastable phases cubic and tetragonal over the monoclinic one. However, all the synthetized samples acted mainly as acid catalysts, promoting ethyl ether and ethylene formation, both dehydration product of ethanol. From the perspective of favouring the Guerbet mechanism, it would be interesting to study the effect of the addiction of a redox element, such as a transition metal, over the catalyst surface in order to catalyse the acetaldehyde formation, often reported the rate-limiting step of the reaction.

Natural sepiolite has been also studied as an alternative heterogeneous catalyst for the gas-phase ethanol selective conversion through the Guerbet route. It has been observed that the incorporation of an alkali metal as promoter (by means of incipient wetness impregnation) changes the acid-base properties of catalysts favouring the Guerbet from ethanol. In particular, it was possible to obtain n-butanol with a selectivity of 30% and ethanol conversion of 59% over the 7Cs/Sep@500 catalyst (with 7 wt% of Cs$^+$). Those results are interesting since, from the perspective of the "Green and Sustainable Development" concept, the use of naturally abundant clay minerals like sepiolite as catalyst has economical, eco-friendly and nontoxic advantages.[320] In this study, sepiolite has been used for the first time as heterogeneous catalyst for performing ethanol gas-phase Guerbet

conversion into higher alcohols with reasonable yields, opening new perspectives for future catalyst engineering for this kind of complex reaction mechanism.

6 REFERENCES

1 D. Martin Alonso, J. Q. Bond and J. A. Dumesic, *Green Chemistry*, 2010, **12**, 1493–1513.

2 Anastas P. T. and Warner J. C., *Green Chemistry: Theory and Practice*, Oxford University Press: New York, 1998.

3 M. Poliakoff, P. Licence and M. W. George, *Current Opinion in Green and Sustainable Chemistry*, 2018, **13**, 146–149.

4 F. Cavani, G. Centi, S. Perathoner and F. Trifirò, Eds., *Sustainable Industrial Chemistry: Principles, Tools and Industrial Examples*, Wiley-VCH, Weinheim, 1st edition., 2009.

5 J. Sun, Y. Wang, J. Li, G. Xiao, L. Zhang, H. Li, Y. Cheng, C. Sun, Z. Cheng, Z. Dong and L. Chen, *International Journal of Hydrogen Energy*, 2010, **35**, 3087–3091.

6 M. J. Hülsey, *Green Energy & Environment*, 2018, **3**, 318–327.

7 J. O. B. Carioca, *Biotechnology Journal*, 2010, **5**, 260–273.

8 D. Mohan, C. U. Pittman and P. H. Steele, *Energy Fuels*, 2006, **20**, 848–889.

9 E. Bolyos, D. Lawrence and A. Nordin, 7.

10 *Directive 2009/28/EC of the European Parliament and of the Council of 23 April 2009 on the promotion of the use of energy from renewable sources and amending and subsequently repealing Directives 2001/77/EC and 2003/30/EC (Text with EEA relevance)*, 2009, vol. 140.

11 J. H. Clark, in *Green and Sustainable Medicinal Chemistry*, 2016, pp. 1–11.

12 *Industrial Biotechnology*, 2012, **8**, 57–61.

13 A. T. Ubando, C. B. Felix and W.-H. Chen, *Bioresource Technology*, 2020, **299**, 122585.

14 G. Centi and R. A. van Santen, Eds., *Catalysis for Renewables: From Feedstock to Energy Production*, Wiley, 1st edn., 2007.

15 L. Nogueira, J. Seabra, G. Best, M. R. Leal and M. Poppe, *Sugarcane based bioethanol: energy for sustainable development*, 2008.

16 F. Dumeignil, M. Capron, B. Katryniok, R. Wojcieszak, A. Löfberg, J.-S. Girardon, S. Desset, M. Araque-Marin, L. Jalowiecki-Duhamel and S. Paul, *Journal of the Japan Petroleum Institute*, 2015, **58**, 257–273.

17 P. Lanzafame, S. Perathoner, G. Centi, S. Gross and E. J. M. Hensen, *Catalysis Science & Technology*, 2017, **7**, 5182–5194.

18 J. M. Gómez, M. D. Romero and V. Callejo, *Catalysis Today*, 2013, **218–219**, 143–147.

19 L. Zhang, C. (Charles) Xu and P. Champagne, *Energy Conversion and Management*, 2010, **51**, 969–982.

20 K. Robak and M. Balcerek, *Food Technol Biotechnol*, 2018, **56**, 174–187.

21 M. E. Dias De Oliveira, B. E. Vaughan and E. J. Rykiel, *BioScience*, 2005, **55**, 593–602.

22 R. F. Service, *Science*, 2010, **329**, 784–785.

23 T. Tsuchida, S. Sakuma, T. Takeguchi and W. Ueda, *Ind. Eng. Chem. Res.*, 2006, **45**, 8634–8642.

24 C. A. Cardona and O. J. Sánchez, *Bioresour Technol*, 2007, **98**, 2415–2457.

25 L. Panella, *Sugar Tech*, 2010, **12**, 288–293.

26 C. S. Goh and K. T. Lee, *Renewable and Sustainable Energy Reviews*, 2010, **14**, 842–848.

27 R. P. John, G. S. Anisha, K. M. Nampoothiri and A. Pandey, *Bioresour Technol*, 2011, **102**, 186–193.

28 M. Y. Menetrez, *Environ. Sci. Technol.*, 2012, **46**, 7073–7085.

29 V. Menon and M. Rao, *Progress in Energy and Combustion Science*, 2012, **38**, 522–550.

30 R. C. Saxena, D. K. Adhikari and H. B. Goyal, *Renewable and Sustainable Energy Reviews*, 2009, **13**, 167–178.

31 A. Singh, P. S. Nigam and J. D. Murphy, *Bioresource Technology*, 2011, **102**, 10–16.

32 G. O. Ezinkwo, V. P. Tretyakov, A. Aliyu and A. M. Ilolov, *ChemBioEng Reviews*, 2014, **1**, 194–203.

33 J. J. Spivey and A. Egbebi, *Chem. Soc. Rev.*, 2007, **36**, 1514–1528.

34 F. R. Bengelsdorf, M. Straub and P. Dürre, *Environmental Technology*, 2013, **34**, 1639–1651.

35   J. R. Phillips, K. T. Klasson, E. C. Clausen and J. L. Gaddy, *Applied Biochemistry and Biotechnology*, 1993, **37**, 559–571.

36   A. M. Henstra, J. Sipma, A. Rinzema and A. J. Stams, *Current Opinion in Biotechnology*, 2007, **18**, 200–206.

37   D. W. Griffin and M. A. Schultz, *Environ. Prog. Sustainable Energy*, 2012, **31**, 219–224.

38   M. Köpke, C. Mihalcea, J. C. Bromley and S. D. Simpson, *Current Opinion in Biotechnology*, 2011, **22**, 320–325.

39   G. W. Huber, S. Iborra and A. Corma, *Chem. Rev.*, 2006, **106**, 4044–4098.

40   J. R. Rostrup-Nielsen, *Catalysis Reviews*, 2004, **46**, 247–270.

41   B. G. Harvey and H. A. Meylemans, *Journal of Chemical Technology & Biotechnology*, 2011, **86**, 2–9.

42   R. Johansson, S. L. Hruby, J. Rass-Hansen and C. H. Christensen, *Catal Lett*, 2008, **127**, 1.

43   J. Coombs, *Enzyme and Microbial Technology*, 1981, **3**, 171–173.

44   C. A. Cardona Alzate and O. J. Sánchez Toro, *Energy*, 2006, **31**, 2447–2459.

45   M. J. Taherzadeh and K. Karimi, *BioResources*, 2007, **2**, 472–499.

46   C. Yang and Z. Y. Meng, *Journal of Catalysis*, 1993, **142**, 37–44.

47   Kirk-Othmer Encyclopedia of Chemical Technology, Index to Volumes 1 - 26, 5th Edition | Wiley,   https://www.wiley.com/en-ie/Kirk+Othmer+Encyclopedia+of+Chemical+Technology%2C+Index+to+Volumes+1+26%2C+5th+Edition-p-9780471484967.

48   A. S. Ndou, N. Plint and N. J. Coville, *Applied Catalysis A: General*, 2003, **251**, 337–345.

49   E. M. Green, *Current Opinion in Biotechnology*, 2011, **22**, 337–343.

50   C. Jin, M. Yao, H. Liu, C. F. F. Lee and J. Ji, *Renewable and Sustainable Energy Reviews*, 2011, **15**, 4080–4106.

51   United States, US2762847A, 1956.

52   A. J. O'Lenick, *J Surfact Deterg*, 2001, **4**, 311–315.

53   Y. Xie, Y. Ben-David, L. J. W. Shimon and D. Milstein, *J. Am. Chem. Soc.*, 2016, **138**, 9077–9080.

54   J. Campos-Fernández, J. M. Arnal, J. Gómez and M. P. Dorado, *Applied Energy*, 2012, **95**, 267–275.

55   Q. Liu, G. Xu, X. Wang, X. Liu and X. Mu, *ChemSusChem*, 2016, **9**, 3465–3472.

56   J. Pang, M. Yin, P. Wu, X. Li, H. Li, M. Zheng and T. Zhang, *Green Chemistry*, 2021, **23**, 7902–7916.

57   Y. Injongkol, T. Maihom, S. Choomwattana, B. Boekfa and J. Limtrakul, *RSC Advances*, 2017, **7**, 38052–38058.

58   C. R. Ho, S. Shylesh and A. T. Bell, *ACS Catalysis*, 2016, **6**, 939–948.

59   T. Tsuchida, J. Kubo, T. Yoshioka, S. Sakuma, T. Takeguchi and W. Ueda, *Journal of Catalysis*, 2008, **259**, 183–189.

60   D. Gabriëls, W. Y. Hernández, B. Sels, P. V. D. Voort and A. Verberckmoes, *Catal. Sci. Technol.*, 2015, **5**, 3876–3902.

61   L. Silvester, J.-F. Lamonier, C. Lamonier, M. Capron, R.-N. Vannier, A.-S. Mamede and F. Dumeignil, *ChemCatChem*, 2017, **9**, 2250–2261.

62   J. Scalbert, F. Thibault-Starzyk, R. Jacquot, D. Morvan and F. Meunier, *Journal of Catalysis*, 2014, **311**, 28–32.

63   J. I. Di Cosimo, C. R. Apesteguıa, M. J. L. Ginés and E. Iglesia, *Journal of Catalysis*, 2000, **190**, 261–275.

64   A. Chieregato, J. Velasquez Ochoa, C. Bandinelli, G. Fornasari, F. Cavani and M. Mella, *ChemSusChem*, 2015, **8**, 377–388.

65   C. F. de Graauw, J. A. Peters, H. van Bekkum and J. Huskens, *Synthesis*, 1994, **1994**, 1007–1017.

66   CH. WEIZMANN, E. BERGMANN and M. SULZBACHER, *J. Org. Chem.*, 1950, **15**, 54–57.

67   J. T. Kozlowski and R. J. Davis, *Journal of Energy Chemistry*, 2013, **1**, 58–64.

68   T. L. Jordison, C. T. Lira and D. J. Miller, *Ind. Eng. Chem. Res.*, 2015, **54**, 10991–11000.

69   T. Tsuchida, T. Yoshioka, S. Sakuma, T. Takeguchi and W. Ueda, *Ind. Eng. Chem. Res.*, 2008, **47**, 1443–1452.

70   J. I. Di Cosimo, V. K. Díez, M. Xu, E. Iglesia and C. R. Apesteguía, *Journal of Catalysis*, 1998, **178**, 499–510.

71   A. Ciftci, D. Varisli, K. Cem Tokay, N. Aslı Sezgi and T. Dogu, *Chemical Engineering Journal*, 2012, **207–208**, 85–93.

72   D. Fan, D.-J. Dai and H.-S. Wu, *Materials*, 2013, **6**, 101–115.

73   A. Morschbacker, *Polymer Reviews*, 2009, **49**, 79–84.

74   E. V. Makshina, M. Dusselier, W. Janssens, J. Degrève, P. A. Jacobs and B. F. Sels, *Chem. Soc. Rev.*, 2014, **43**, 7917–7953.

75   E. Santacesaria, G. Carotenuto, R. Tesser and M. Di Serio, *Chemical Engineering Journal*, 2012, **179**, 209–220.

76   H. Liu and M. S. Eisen, *Eur. J. Org. Chem.*, 2017, **2017**, 4852–4858.

77   M. E. Sad, M. Neurock and E. Iglesia, *J. Am. Chem. Soc.*, 2011, **133**, 20384–20398.

78   H. Idriss, K. S. Kim and M. A. Barteau, *Journal of Catalysis*, 1993, **139**, 119–133.

79   M. Gliński, W. Szymański and D. Łomot, *Applied Catalysis A: General*, 2005, **281**, 107–113.

80   N. Plint, D. Ghavalas, T. Vally, V. D. Sokolovski and N. J. Coville, *Catalysis Today*, 1999, **49**, 71–77.

81   N. D. Plint, N. J. Coville, D. Lack, G. L. Nattrass and T. Vallay, *Journal of Molecular Catalysis A: Chemical*, 2001, **165**, 275–281.

82   L. M. Orozco, M. Renz and A. Corma, *ChemSusChem*, 2016, **9**, 2430–2442.

83   A. Gangadharan, M. Shen, T. Sooknoi, D. E. Resasco and R. G. Mallinson, *Applied Catalysis A: General*, 2010, **385**, 80–91.

84   H. Aitchison, R. L. Wingad and D. F. Wass, *ACS Catal.*, 2016, **6**, 7125–7132.

85   K. Koda, T. Matsu-ura, Y. Obora and Y. Ishii, *Chem. Lett.*, 2009, **38**, 838–839.

86   United States, US8318990B2, 2012.

87   C. Cesari, A. Gagliardi, A. Messori, N. Monti, V. Zanotti, S. Zacchini, I. Rivalta, F. Calcagno, C. Lucarelli, T. Tabanelli, F. Cavani and R. Mazzoni, *Journal of Catalysis*, 2022, **405**, 47–59.

88   E. Farnetti, *INORGANIC CHEMISTRY*, 10.

89   M. K. Lam and K. T. Lee, in *Biofuels from Algae*, eds. A. Pandey, D.-J. Lee, Y. Chisti and C. R. Soccol, Elsevier, Amsterdam, 2014, pp. 261–286.

90   W. Ueda, T. Ohshida, T. Kuwabara and Y. Morikawa, *Catal Lett*, 1992, **12**, 97–104.

91   A. S. Ndou and N. J. Coville, *Applied Catalysis A: General*, 2004, **275**, 103–110.

92   J. T. Kozlowski and R. J. Davis, *ACS Catal.*, 2013, **3**, 1588–1600.

93   S. Hanspal, Z. D. Young, H. Shou and R. J. Davis, *ACS Catalysis*, 2015, **5**, 1737–1746.

94   I.-C. Marcu, N. Tanchoux, F. Fajula and D. Tichit, *Catal Lett*, 2013, **143**, 23–30.

95   T. Riittonen, E. Toukoniitty, D. K. Madnani, A.-R. Leino, K. Kordas, M. Szabo, A. Sapi, K. Arve, J. Wärnå and J.-P. Mikkola, *Catalysts*, 2012, **2**, 68–84.

96   Z. D. Young and R. J. Davis, *Catal. Sci. Technol.*, 2018, **8**, 1722–1729.

97   S. Ogo, A. Onda and K. Yanagisawa, *Applied Catalysis A: General*, 2011, **402**, 188–195.

98   J. H. Earley, R. A. Bourne, M. J. Watson and M. Poliakoff, *Green Chem.*, 2015, **17**, 3018–3025.

99   D. L. Carvalho, R. R. de Avillez, M. T. Rodrigues, L. E. P. Borges and L. G. Appel, *Applied Catalysis A: General*, 2012, **415–416**, 96–100.

100   V. V. Ordomsky, V. L. Sushkevich and I. I. Ivanova, *Journal of Molecular Catalysis A: Chemical*, 2010, **333**, 85–93.

101   M. A. Díaz-Pérez and J. C. Serrano-Ruiz, *Molecules*, 2020, **25**, 802.

102   F. Pradelle, S. L. Braga, A. R. F. A. Martins, F. Turkovics and R. N. C. Pradelle, *Energy Fuels*, 2015, **29**, 7753–7770.

103   D. Stratiev, *Oxidation Communications*, 2011, **34**, 183–192.

104   ExxonMobil, 2017.

105   E. Jamalzade, K. Kashkooli, L. Griffin, G. P. van Walsum and T. J. Schwartz, *React. Chem. Eng.*, 2021, **6**, 845–857.

106   N. M. Eagan, M. D. Kumbhalkar, J. S. Buchanan, J. A. Dumesic and G. W. Huber, *Nat Rev Chem*, 2019, **3**, 223–249.

107   K. P. Brooks, L. J. Snowden-Swan, S. B. Jones, M. G. Butcher, G.-S. J. Lee, D. M. Anderson, J. G. Frye, J. E. Holladay, J. Owen, L. Harmon, F. Burton, I. Palou-Rivera, J. Plaza, R. Handler and D. Shonnard, in *Biofuels for Aviation*, ed. C. J. Chuck, Academic Press, 2016, pp. 109–150.

108   J. Yang, Z. Xin, Q. (Sophia) He, K. Corscadden and H. Niu, *Fuel*, 2019, **237**, 916–936.

109   M. Wang, Raf. Dewil, K. Maniatis, J. Wheeldon, T. Tan, J. Baeyens and Y. Fang, *Progress in Energy and Combustion Science*, 2019, **74**, 31–49.

110   D. Biello, "Fatted Eagle" Joins "Green Hornet" in U.S. Military's Alternative Fuels Fighter Fleet, https://www.scientificamerican.com/article/fatted-eagle-biofuel-flight-air-force-fighter/.

111   James D. Kinder and Timothy Rahmes, 2009.

112   Naphthalene Removal Assessment – Ascent, https://ascent.aero/project/naphthalene-removal-assessment/.

113   J. P. Ford, J. G. Immer and H. H. Lamb, *Topics in Catalysis*, 2012, **55**, 175–184.

114   J. C. Serrano-Ruiz, E. V. Ramos-Fernández and A. Sepúlveda-Escribano, *Energy Environ. Sci.*, 2012, **5**, 5638–5652.

115   S. A. Nikolaev, A. V. Chistyakov, M. V. Chudakova, E. P. Yakimchuk, V. V. Kriventsov and M. V. Tsodikov, *Journal of Catalysis*, 2013, **297**, 296–305.

116   N. Viswanadham, S. K. Saxena, J. Kumar, P. Sreenivasulu and D. Nandan, *Fuel*, 2012, **95**, 298–304.

117   Alliance BioEnergy Plus, Vertimass sign technology license agreement, https://www.canadianbiomassmagazine.ca/alliance-bioenergy-plus-vertimass-sign-technology-license-agreement/.

118   Gevo Flies High with USAF Alcohol-to-Jet Test Flight, https://www.businesswire.com/news/home/20120703005409/en/Gevo-Flies-High-with-USAF-Alcohol-to-Jet-Test-Flight.

119   K. Ben Tayeb, L. Pinard, N. Touati, H. Vezin, S. Maury and O. Delpoux, *Catalysis Communications*, 2012, **27**, 119–123.

120   A. Galadima and O. Muraza, *Journal of Industrial and Engineering Chemistry*, 2015, **31**, 1–14.

121   S. Svelle, S. Kolboe and O. Swang, *J. Phys. Chem. B*, 2004, **108**, 2953–2962.

122   J. Hannon, 24.

123   ExxonMobil, https://corporate.exxonmobil.com/.

124   K. K. Ramasamy and Y. Wang, *Catalysis Today*, 2014, **237**, 89–99.

125   K. K. Ramasamy, H. Zhang, J. Sun and Y. Wang, *Catalysis Today*, 2014, **238**, 103–110.

126   J. S. Lopez, R. A. Dagle, V. L. Dagle, C. Smith and K. O. Albrecht, *Catal. Sci. Technol.*, 2019, **9**, 1117–1131.

127   D. E. Bryant and W. L. Kranich, *Journal of Catalysis*, 1967, **8**, 8–13.

128   C. B. Phillips and R. Datta, *Ind. Eng. Chem. Res.*, 1997, **36**, 4466–4475.

129   K. Dossumov, D. Kh. Churina, G. Y. Yergaziyeva, M. M. Telbayeva and S. Zh. Tayrabekova, *IJCEA*, 2016, **7**, 128–132.

130   A. Mohsenzadeh, A. Zamani and M. J. Taherzadeh, *ChemBioEng Reviews*, 2017, **4**, 75–91.

131   M. Zhang and Y. Yu, *Ind. Eng. Chem. Res.*, 2013, **52**, 9505–9514.

132   T. Kito-Borsa, D. A. Pacas, S. Selim and S. W. Cowley, *Ind. Eng. Chem. Res.*, 1998, **37**, 3366–3374.

133   I. Takahara, M. Saito, M. Inaba and K. Murata, *Catal Lett*, 2005, **105**, 249–252.

134   D. Varisli, T. Dogu and G. Dogu, *Chemical Engineering Science*, 2007, **62**, 5349–5352.

135   A. Corma and J. Perez-Pariente, *Clay Minerals*, 1987, **22**, 423–433.

136   G. Garbarino, G. Pampararo, T. K. Phung, P. Riani and G. Busca, *Energies*, 2020, **13**, 3587.

137   M. Almohalla, I. Rodríguez-Ramos and A. Guerrero-Ruiz, *Catal. Sci. Technol.*, 2017, **7**, 1892–1901.

138   T. K. R. de Oliveira, M. Rosset and O. W. Perez-Lopez, *Catalysis Communications*, 2018, **104**, 32–36.

139   V. V. Bokade and G. D. Yadav, *Applied Clay Science*, 2011, **53**, 263–271.

140   N. L. Morrow, *Environmental Health Perspectives*, 1990, **86**, 7–8.

141   W. C. White, *Chem Biol Interact*, 2007, **166**, 10–14.

142   Chemicals and Fuels from Bio-Based Building Blocks | Wiley, https://www.wiley.com/en-gb/Chemicals+and+Fuels+from+Bio+Based+Building+Blocks-p-9783527338979.

143   C. Angelici, B. M. Weckhuysen and P. C. A. Bruijnincx, *ChemSusChem*, 2013, **6**, 1595–1614.

144   W. M. Quattlebaum, W. J. Toussaint and J. T. Dunn, *J. Am. Chem. Soc.*, 1947, **69**, 593–599.

145   H. Niiyama, S. Morii and E. Echigoya, *Bulletin of the Chemical Society of Japan*, 1972, **45**, 655–659.

146   G. Pomalaza, M. Capron, V. Ordomsky and F. Dumeignil, *Catalysts*, 2016, **6**, 203.

147   J. Velasquez Ochoa, C. Bandinelli, O. Vozniuk, A. Chieregato, A. Malmusi, C. Recchi and F. Cavani, *Green Chemistry*, 2016, **18**, 1653–1663.

148   C. Angelici, M. E. Z. Velthoen, B. M. Weckhuysen and P. C. A. Bruijnincx, *ChemSusChem*, 2014, **7**, 2505–2515.

149   A. D. Patel, K. Meesters, H. den Uil, E. de Jong, K. Blok and M. K. Patel, *Energy Environ. Sci.*, 2012, **5**, 8430–8444.

150   S. S. Bhat, U. V. Waghmare and U. Ramamurty, *Crystal Growth & Design*, 2014, **14**, 3131–3141.

151   N. I. Agbeboh, I. O. Oladele, O. O. Daramola, A. A. Adediran, O. O. Olasukanmi and M. O. Tanimola, *Heliyon*, 2020, **6**, e03765.

152   M. Ferri, S. Campisi, M. Scavini, C. Evangelisti, P. Carniti and A. Gervasini, *Applied Surface Science*, 2019, **475**, 397–409.

153   A. Fihri, C. Len, R. S. Varma and A. Solhy, *Coordination Chemistry Reviews*, 2017, **347**, 48–76.

154   L. Silvester, J.-F. Lamonier, R.-N. Vannier, C. Lamonier, M. Capron, A.-S. Mamede, F. Pourpoint, A. Gervasini and F. Dumeignil, *J. Mater. Chem. A*, 2014, **2**, 11073–11090.

155   J. Dobosz, S. Hull and M. Zawadzki, *Studia Universitatis Babeş-Bolyai Chemia*, 2018, **63**, 215–237.

156   S. Diallo-Garcia, D. Laurencin, J.-M. Krafft, S. Casale, M. E. Smith, H. Lauron-Pernot and G. Costentin, *J. Phys. Chem. C*, 2011, **115**, 24317–24327.

157   M. J. Robles-Águila, J. A. Reyes-Avendaño and M. E. Mendoza, *Ceramics International*, 2017, **43**, 12705–12709.

158   S. Campisi, M. G. Galloni, F. Bossola and A. Gervasini, *Catalysis Communications*, 2019, **123**, 79–85.

159   G. Chen, X. Zheng, C. Wang, J. Hui, X. Sheng, X. Xu, J. Bao, W. Xiu, L. Yuwen and D. Fan, *RSC Adv.*, 2017, **7**, 56537–56542.

160   S. Pai, M. S. Kini and R. Selvaraj, *Environ Sci Pollut Res*, 2021, **28**, 11835–11849.

161   E. Pecheva and L. Pramatarova, *Modified Inorganic Surfaces as a Model for Hydroxyapatite Growth*, 2006.

162   M. G. Galloni, S. Campisi, S. G. Marchetti and A. Gervasini, *Catalysts*, 2020, **10**, 1415.

163   C. L. Kibby and W. K. Hall, *Journal of Catalysis*, 1973, **31**, 65–73.

164   L. Silvester, J.-F. Lamonier, J. Faye, M. Capron, R.-N. Vannier, C. Lamonier, J.-L. Dubois, J.-L. Couturier, C. Calais and F. Dumeignil, *Catal. Sci. Technol.*, 2015, **5**, 2994–3006.

165   US 8,187,347 B2, 2012.

166   J. J. Lovón-Quintana, J. K. Rodriguez-Guerrero and P. G. Valença, *Applied Catalysis A: General*, 2017, **542**, 136–145.

167   V. F. Tret'yakov, Yu. I. Makarfi, K. V. Tret'yakov, N. A. Frantsuzova and R. M. Talyshinskii, *Catal. Ind.*, 2010, **2**, 402–420.

168   Y. Han and J. Zhu, *Top Catal*, 2013, **56**, 1525–1541.

169   D. L. Porter and A. H. Heuer, *Journal of the American Ceramic Society*, 1979, **62**, 298–305.

170   S. N. Basahel, T. T. Ali, M. Mokhtar and K. Narasimharao, *Nanoscale Res Lett*, 2015, **10**, 73.

171   Y. Murase and E. Kato, *Journal of the American Ceramic Society*, 1983, **66**, 196–200.

172   R. H. Nielsen and G. Wilfing, in *Ullmann's Encyclopedia of Industrial Chemistry*, ed. Wiley-VCH Verlag GmbH & Co. KGaA, Wiley-VCH Verlag GmbH & Co. KGaA, Weinheim, Germany, 2010, p. a28_543.pub2.

173   M. C. Muñoz, S. Gallego, J. I. Beltrán and J. Cerdá, *Surface Science Reports*, 2006, **61**, 303–344.

174   R. Grau-Crespo, N. C. Hernández, J. F. Sanz and N. H. de Leeuw, *J. Phys. Chem. C*, 2007, **111**, 10448–10454.

175   G. Teufer, *Acta Cryst*, 1962, **15**, 1187–1187.

176   D. K. Smith and W. Newkirk, *Acta Cryst*, 1965, **18**, 983–991.

177   A. Pissenberger and G. Gritzner, *J Mater Sci Lett*, 1995, **14**, 1580–1582.

178   Y. Sugizaki, S. Yamaguchi, S. Hashimoto, M. Hirabayashi and Y. Ishikawa, *J. Phys. Soc. Jpn.*, 1985, **54**, 2543–2551.

179   J. P. Abriata, J. Garcés and R. Versaci, *Bulletin of Alloy Phase Diagrams*, 1986, **7**, 116–124.

180   P. D. L. Mercera, J. G. Van Ommen, E. B. M. Doesburg, A. J. Burggraaf and J. R. H. Ross, *Applied Catalysis*, 1990, **57**, 127–148.

181   N. V. Vlasenko, P. I. Kyriienko, K. V. Valihura, G. R. Kosmambetova, S. O. Soloviev and P. E. Strizhak, *ACS Omega*, 2019, **4**, 21469–21476.

182   T. Yamaguchi, *Catalysis Today*, 1994, **20**, 199–217.

183   A. Benedetti, G. Fagherazzi and F. Pinna, *Journal of the American Ceramic Society*, 1989, **72**, 467–469.

184   P. Turlier, J. A. Dalmon, G. A. Martin and P. Vergnon, *Applied Catalysis*, 1987, **29**, 305–310.

185   W. Zhang, Z. Wang, J. Huang and Y. Jiang, *Energy & Fuels*, , DOI:10.1021/acs.energyfuels.1c00709.

186   C. T. Campbell and C. H. F. Peden, *Science*, 2005, **309**, 713–714.

187   N. V. Vlasenko, P. I. Kyriienko, O. I. Yanushevska, K. V. Valihura, S. O. Soloviev and P. E. Strizhak, *Catal Lett*, 2020, **150**, 234–242.

188   Y. Nakano, T. Iizuka, H. Hattori and K. Tanabe, *Journal of Catalysis*, 1979, **57**, 1–10.

189   S. Axpuac, M. A. Aramendía, J. Hidalgo-Carrillo, A. Marinas, J. M. Marinas, V. Montes-Jiménez, F. J. Urbano and V. Borau, *Catalysis Today*, 2012, **187**, 183–190.

190   P. B. Vásquez, T. Tabanelli, E. Monti, S. Albonetti, D. Bonincontro, N. Dimitratos and F. Cavani, *ACS Sustainable Chem. Eng.*, 2019, **7**, 8317–8330.

191   J. Tai and R. J. Davis, *Catalysis Today*, 2007, **123**, 42–49.

192   M. Angeles Aramendía, V. Boráu, C. Jiménez, J. M. Marinas, A. Porras and F. J. Urbano, *Journal of the Chemical Society, Faraday Transactions*, 1997, **93**, 1431–1438.

193   I. Ferino, M. F. Casula, A. Corrias, M. G. Cutrufello, R. Monaci and G. Paschina, *Phys. Chem. Chem. Phys.*, 2000, **2**, 1847–1854.

194   M. G. Cutrufello, I. Ferino, R. Monaci, E. Rombi and V. Solinas, *Topics in Catalysis*, 2002, **19**, 225–240.

195   K. Tanabe and T. Yamaguchi, *Catalysis Today*, 1994, **20**, 185–197.

196   M. Comotti, W.-C. Li, B. Spliethoff and F. Schüth, *J. Am. Chem. Soc.*, 2006, **128**, 917–924.

197   X. Zhang, H. Shi and B.-Q. Xu, *Catalysis Today*, 2007, **122**, 330–337.

198   X. Zhang, H. Wang and B.-Q. Xu, *J. Phys. Chem. B*, 2005, **109**, 9678–9683.

199   J. Li, N. Ta, W. Song, E. Zhan and W. Shen, *Gold Bull*, 2009, **42**, 48–60.

200   F. Pinna, A. Olivo, V. Trevisan, F. Menegazzo, M. Signoretto, M. Manzoli and F. Boccuzzi, *Catalysis Today*, 2013, **203**, 196–201.

201   X. Zhang, H. Shi and B.-Q. Xu, *Angewandte Chemie*, 2005, **117**, 7294–7297.

202   B. Nagy and W. Bradle, *The structural scheme of sepiolite*, 1955, **40**, 885–892.

203   G. Tian, G. Han, F. Wang and J. Liang, in *Nanomaterials from Clay Minerals*, eds. A. Wang and W. Wang, Elsevier, 2019, pp. 135–201.

204   B. F. Jones and E. Galan, in *Chapter 16. SEPIOLITE AND PALYGORSKITE*, De Gruyter, 2018, pp. 631–674.

205   E. Galán and M. Pozo, in *Developments in Clay Science*, eds. E. Galàn and A. Singer, Elsevier, 2011, vol. 3, pp. 125–173.

206   E. Galan and A. Castillo, in *Developments in Sedimentology*, eds. A. Singer and E. Galan, Elsevier, 1984, vol. 37, pp. 87–124.

207   D. K. Dutta, in *Developments in Clay Science*, eds. R. Schoonheydt, C. T. Johnston and F. Bergaya, Elsevier, 2018, vol. 9, pp. 289–329.

208   A. J. Dandy and M. S. Nadiye-tabbiruka, *Surface Properties of Sepiolite from Amboseli, Tanzania, and Its Catalytic Activity for Ethanol Decomposition*, .

209   United States, US5051202A, 1991.

210   M. Mora, M. Isabel López, M. Ángeles Carmona, C. Jiménez-Sanchidrián and J. Rafael Ruiz, *Polyhedron*, 2010, **29**, 3046–3051.

211   Y. Kitayama and A. Abe, *Nippon Kagaku Kaishi*, 1989, **1989**, 1824–1829.

212   M. Suárez and E. García-Romero, in *Developments in Clay Science*, eds. E. Galàn and A. Singer, Elsevier, 2011, vol. 3, pp. 33–65.

213   E. Duquesne, S. Moins, M. Alexandre and P. Dubois, *Macromol. Chem. Phys.*, 2007, **208**, 2542–2550.

214   R. W. Mccabe and J. M. Adams, in *Developments in Clay Science*, eds. F. Bergaya and G. Lagaly, Elsevier, 2013, vol. 5, pp. 491–538.

215   M. R. Weir, E. Rutinduka, C. Detellier, C. Y. Feng, Q. Wang, T. Matsuura and R. Le Van Mao, *Journal of Membrane Science*, 2001, **182**, 41–50.

216   R. Nehra, S. N. Maiti and J. Jacob, *Polymers for Advanced Technologies*, 2018, **29**, 234–243.

217   H. Chen, M. Zheng, H. Sun and Q. Jia, *Materials Science and Engineering: A*, 2007, **445**, 725–730.

218   S. Hojati and K. Hossein, *Journal of Sciences, Islamic Republic of Iran*, 2013, **24**, 129–134.

219   Y. Sarıkaya, M. Önal and A. D. Pekdemir, *J Therm Anal Calorim*, 2020, **140**, 2667–2672.

220   G. Tian, G. Han, F. Wang and J. Liang, in *Nanomaterials from Clay Minerals*, eds. A. Wang and W. Wang, Elsevier, 2019, pp. 135–201.

221   M. A. V. Rodriguez, J. D. D. L. Gonzalez and M. A. B. Muñoz, *Clay Minerals*, 1994, **29**, 361–367.

222   M. Myriam, M. Suárez and J. M. Martín-Pozas, *Clays Clay Miner.*, 1998, **46**, 225–231.

223   J. Pérez Pariente, V. Fornés, A. Corma and A. Mifsud, *Applied Clay Science*, 1988, **3**, 299–306.

224   United States, US4542002A, 1985.

225   A. Corma and R. M. Martín-Aranda, *Journal of Catalysis*, 1991, **130**, 130–137.

226   A. Corma, H. García, A. Leyva and A. Primo, *Applied Catalysis A: General*, 2004, **257**, 77–83.

227   A. Corma and R. M. Martín-Aranda, *Applied Catalysis A: General*, 1993, **105**, 271–279.

228   N. Degirmenbasi, N. Boz and D. M. Kalyon, *Applied Catalysis B: Environmental*, 2014, **150–151**, 147–156.

229   Y. Kitayama and A. Michishita, *J. Chem. Soc., Chem. Commun.*, 1981, 401.

230   V. Gruver, A. Sun and J. J. Fripiat, *Catal Lett*, 1995, **34**, 359–364.

231   E. Arundale and L. A. Mikeska, *Chem. Rev.*, 1952, **51**, 505–555.

232   M. Chen, C. Wang, Y. Wang, Z. Tang, Z. Yang, H. Zhang and J. Wang, *Fuel*, 2019, **247**, 344–355.

233   M. E. Zilm, L. Chen, V. Sharma, A. McDannald, M. Jain, R. Ramprasad and M. Wei, *Phys. Chem. Chem. Phys.*, 2016, **18**, 16457–16465.

234   Y. Matsumura, J. B. Moffat, S. Sugiyama, H. Hayashi, N. Shigemoto and K. Saitoh, *J. Chem. Soc., Faraday Trans.*, 1994, **90**, 2133–2140.

235   C. R. Ho, S. Zheng, S. Shylesh and A. T. Bell, *Journal of Catalysis*, 2018, **365**, 174–183.

236   M. Schiavoni, S. Campisi, P. Carniti, A. Gervasini and T. Delplanche, *Applied Catalysis A: General*, 2018, **563**, 43–53.

237   S. Campisi, M. G. Galloni, F. Bossola and A. Gervasini, *Catalysis Communications*, 2019, **123**, 79–85.

238   A. W. Burton, K. Ong, T. Rea and I. Y. Chan, *Microporous and Mesoporous Materials*, 2009, **117**, 75–90.

239   Evaluation of the Capacity of Hydroxyapaptite Prepared from Concrete Sludge to Remove Lead from Water | Industrial & Engineering Chemistry Research, https://pubs.acs.org/doi/abs/10.1021/ie200233s?casa_token=e-n8ktTuFlcAAAAA:ZtFUXa9H_6FO2xuf9jlUhB5WDk1uhA0x3mAd2HLxNvFxqhT1XQCU2FazzWLVlQe7er3WyJ3nM1wWmeE.

240   M. Okada, K. Fujiwara, M. Uehira, N. Matsumoto and S. Takeda, *Journal of Colloid and Interface Science*, 2013, **405**, 58–63.

241   Investigation of HA Nanocrystallite Size Crystallographic Characterizations in NHA, BHA and HA Pure Powders and their Influence on Biodegradation of HA | Scientific.Net, https://www.scientific.net/AMR.829.314.

242   B. Locardi, U. E. Pazzaglia, C. Gabbi and B. Profilo, *Biomaterials*, 1993, **14**, 437–441.

243   L. Kumari, W. Li and D. Wang, *Nanotechnology*, 2008, **19**, 195602.

244   A. Corma, V. Form and M. I. Juan-Rajadell, 1994, 13.

245   A. Corma, J. M. L. Nieto and N. Paredes, *Journal of Catalysis*, 1993, **144**, 425–438.

246   M. Gauna, S. Conconi, S. Gómez, G. Suarez, E. Aglietti and N. Rendtorff, *Ceramics Silikaty*, 2015, **59**, 318–325.

247   A. Corma, V. Fornés, M. I. Juan-Rajadell and J. M. L. Nieto, *Applied Catalysis A: General*, 1994, **116**, 151–163.

248   D. J. Gardiner, in *Practical Raman Spectroscopy*, eds. D. J. Gardiner and P. R. Graves, Springer, Berlin, Heidelberg, 1989, pp. 1–12.

249   D. A. Skoog, F. J. Holler and S. R. Crouch, *Principles of Instrumental Analysis*, Cengage Learning, Belmont, CA, 6th edition., 2006.

250   S. Ebnesajjad, in *Surface Treatment of Materials for Adhesive Bonding*, Elsevier, 2014, pp. 39–75.

251   O. D. Neikov and N. A. Yefimov, in *Handbook of Non-Ferrous Metal Powders*, Elsevier, 2019, pp. 3–62.

252   C. O. Colpan, Y. Nalbant and M. Ercelik, in *Comprehensive Energy Systems*, Elsevier, 2018, pp. 1107–1130.

253   P. D. Srinivasan, S. R. Nitz, K. J. Stephens, E. Atchison and J. J. Bravo-Suarez, *Applied Catalysis A: General*, 2018, **561**, 7–18.

254   R. e. Hummel, in *Encyclopedia of Analytical Chemistry*, John Wiley & Sons, Ltd, 2006.

255   S. Benomar, A. Chieregato, A. Masso, M. D. Soriano, J. A. Vidal-Moya, T. Blasco, R. Issaadi and J. M. López Nieto, *Catal. Sci. Technol.*, 2020, **10**, 8064–8076.

256   E. Costa, A. Uguina, J. Aguado and P. J. Hernandez, *Ind. Eng. Chem. Proc. Des. Dev.*, 1985, **24**, 239–244.

257   W.-C. Wang and L. Tao, *Renewable and Sustainable Energy Reviews*, 2016, **53**, 801–822.

258   H. Brasil, A. F. B. Bittencourt, K. C. E. S. Yokoo, P. C. D. Mendes, L. G. Verga, K. F. Andriani, R. Landers, J. L. F. Da Silva and G. P. Valença, *Journal of Catalysis*, , DOI:10.1016/j.jcat.2021.08.050.

259   S. Hanspal, Z. D. Young, J. T. Prillaman and R. J. Davis, *Journal of Catalysis*, 2017, **352**, 182–190.

260   C.-J. Liao, F.-H. Lin, K.-S. Chen and J.-S. Sun, *Biomaterials*, 1999, **20**, 1807–1813.

261   K. Tõnsuaadu, K. A. Gross, L. Plūduma and M. Veiderma, *J Therm Anal Calorim*, 2012, **110**, 647–659.

262   M. Khachani, M. Kacimi, A. Ensuque, J.-Y. Piquemal, C. Connan, F. Bozon-Verduraz and M. Ziyad, *Applied Catalysis A: General*, 2010, **388**, 113–123.

263   M. Sasidharan, S. G. Hegde and R. Kumar, *Microporous and Mesoporous Materials*, 1998, **24**, 59–67.

264   J. J. Lovón-Quintana, J. K. Rodriguez-Guerrero and P. G. Valença, *Applied Catalysis A: General*, 2017, **542**, 136–145.

265   E. G. Rodrigues, T. C. Keller, S. Mitchell and J. Pérez-Ramírez, *Green Chem.*, 2014, **16**, 4870–4874.

266   L. Silvester, J.-F. Lamonier, C. Lamonier, M. Capron, R.-N. Vannier, A.-S. Mamede and F. Dumeignil, *ChemCatChem*, 2017, **9**, 2250–2261.

267   E. A. Uslamin, H. Saito, N. Kosinov, E. Pidko, Y. Sekine and E. J. M. Hensen, *Catalysis Science & Technology*, 2020, **10**, 2774–2785.

268   V. F. Tret'yakov, Yu. I. Makarfi, K. V. Tret'yakov, N. A. Frantsuzova and R. M. Talyshinskii, *Catal. Ind.*, 2010, **2**, 402–420.

269   T. Tsuchida, S. Sakuma, T. Takeguchi and W. Ueda, *Ind. Eng. Chem. Res.*, 2006, **45**, 8634–8642.

270   T. J. Pilusa and E. Muzenda, 2013.

271   C. Angelici, F. Meirer, A. M. J. van der Eerden, H. L. Schaink, A. Goryachev, J. P. Hofmann, E. J. M. Hensen, B. M. Weckhuysen and P. C. A. Bruijnincx, *ACS Catal.*, 2015, **5**, 6005–6015.

272   In *Studies in Inorganic Chemistry*, Elsevier, 1994, vol. 18, pp. 111–189.

273   Y. Dahman, in *Nanotechnology and Functional Materials for Engineers*, ed. Y. Dahman, Elsevier, 2017, pp. 121–144.

274   S. N. Basahel, T. T. Ali, M. Mokhtar and K. Narasimharao, *Nanoscale Res Lett*, 2015, **10**, 73.

275   G. Rothenberg, *Catalysis: concepts and green applications*, WILEY-VCH, Weinheim, 2008.

276   R. Srinivasan, R. J. De Angelis, G. Ice and B. H. Davis, *J. Mater. Res.*, 1991, **6**, 1287–1292.

277   C. N. Chervin, B. J. Clapsaddle, H. W. Chiu, A. E. Gash, Satcher Joe H. and S. M. Kauzlarich, *Chem. Mater.*, 2005, **17**, 3345–3351.
278   A. Mohsenzadeh, A. Zamani and M. J. Taherzadeh, *ChemBioEng Reviews*, 2017, **4**, 75–91.
279   D. Gabriëls, W. Y. Hernández, B. Sels, P. Van Der Voort and A. Verberckmoes, *Catal. Sci. Technol.*, 2015, **5**, 3876–3902.
280   M. D. Jones, *Chemistry Central Journal*, 2014, **8**, 53.
281   A. Corma and J. Perez-Pariente, *Clay Minerals*, 1987, **22**, 423–433.
282   M. Mora, M. Isabel López, M. Ángeles Carmona, C. Jiménez-Sanchidrián and J. Rafael Ruiz, *Polyhedron*, 2010, **29**, 3046–3051.
283   A. Ndou, *Applied Catalysis A: General*, 2003, **251**, 337–345.
284   S. Hojati and H. Khademi, *Journal of Sciences, Islamic Republic of Iran*, 2013, **24**, 129–134.
285   C. A. d'Azevedo, F. M. S. Garrido and M. E. Medeiros, *J Therm Anal Calorim*, 2006, **83**, 649–655.
286   B. M. Nagaraja, V. Siva Kumar, V. Shashikala, A. H. Padmasri, S. Sreevardhan Reddy, B. David Raju and K. S. Rama Rao, *Journal of Molecular Catalysis A: Chemical*, 2004, **223**, 339–345.
287   P. Putanov, E. Kis, G. Boskovic and K. Lázár, *Applied Catalysis*, 1991, **73**, 17–26.
288   K. S. W. Sing, *Pure and Applied Chemistry*, 1985, **57**, 603–619.
289   R. Bal, B. B. Tope, T. K. Das, S. G. Hegde and S. Sivasanker, *Journal of Catalysis*, 2001, **204**, 358–363.
290   A. Walczyk, A. Michalik, B. D. Napruszewska, J. Kryściak-Czerwenka, R. Karcz, D. Duraczyńska, R. P. Socha, Z. Olejniczak, A. Gaweł, A. Klimek, M. Wójcik-Bania, K. Bahranowski and E. M. Serwicka, *Applied Clay Science*, 2020, **195**, 105740.
291   J. I. Di Cosimo, C. R. Apesteguıa, M. J. L. Ginés and E. Iglesia, *Journal of Catalysis*, 2000, **190**, 261–275.
292   T. Yan, W. Bing, M. Xu, Y. Li, Y. Yang, G. Cui, L. Yang and M. Wei, *RSC Adv.*, 2018, **8**, 4695–4702.
293   S. Cimino, L. Lisi and S. Romanucci, *Catalysis Today*, 2018, **304**, 58–63.
294   G. Busca, *Physical Chemistry Chemical Physics*, 1999, **1**, 723–736.
295   Z. Sun, A. C. Vasconcelos, G. Bottari, M. C. A. Stuart, G. Bonura, C. Cannilla, F. Frusteri and K. Barta, *ACS Sustainable Chemistry & Engineering*, 2017, **5**, 1738–1746.
296   K. Gotoh, S. Nakamura, T. Mori and Y. Morikawa, in *Studies in Surface Science and Catalysis*, Elsevier, 2000, vol. 130, pp. 2669–2674.
297   M. Kayanuma, Y. Shinke, T. Miyazawa, T. Fujitani and Y.-K. Choe, *Catalysis Communications*, 2021, **149**, 106239.
298   S. Veibel and J. I. Nielsen, *Tetrahedron*, 1967, **23**, 1723–1733.
299   S. Ogo, A. Onda, Y. Iwasa, K. Hara, A. Fukuoka and K. Yanagisawa, *Journal of Catalysis*, 2012, **296**, 24–30.
300   P. E. Hathaway and M. E. Davis, *Journal of Catalysis*, 1989, **119**, 497–507.
301   W. E. Taifan, T. Bučko and J. Baltrusaitis, *Journal of Catalysis*, 2017, **346**, 78–91.
302   G. Pomalaza, P. A. Ponton, M. Capron and F. Dumeignil, *Catalysis Science & Technology*, 2020, **10**, 4860–4911.
303   A. Chieregato, J. Velasquez Ochoa, C. Bandinelli, G. Fornasari, F. Cavani and M. Mella, *ChemSusChem*, 2015, **8**, 377–388.
304   J. J. Bravo-Suárez, B. Subramaniam and R. V. Chaudhari, Ultraviolet–Visible Spectroscopy and Temperature-Programmed Techniques as Tools for Structural Characterization of Cu in CuMgAlOx Mixed Metal Oxides, https://pubs.acs.org/doi/pdf/10.1021/jp303631v.
305   C. Negri, M. Signorile, N. G. Porcaro, E. Borfecchia, G. Berlier, T. V. W. Janssens and S. Bordiga, *Applied Catalysis A: General*, 2019, **578**, 1–9.
306   K. Shimizu, H. Maeshima, H. Yoshida, A. Satsuma and T. Hattori, *Phys. Chem. Chem. Phys.*, 2000, **2**, 2435–2439.
307   J. Goetze, F. Meirer, I. Yarulina, J. Gascon, F. Kapteijn, J. Ruiz-Martínez and B. M. Weckhuysen, *ACS Catal.*, 2017, **7**, 4033–4046.
308   K. Hemelsoet, Q. Qian, T. De Meyer, K. De Wispelaere, B. De Sterck, B. M. Weckhuysen, M. Waroquier and V. Van Speybroeck, *Chemistry – A European Journal*, 2013, **19**, 16595–16606.
309   S. V. Konnov, V. S. Pavlov, P. A. Kots, V. B. Zaytsev and I. I. Ivanova, *Catal. Sci. Technol.*, 2018, **8**, 1564–1577.

310   J. C. López-Curiel, G. I. Hernández-Salgado, M. E. Hernández-Terán, G. A. Fuentes, J. C. López-Curiel, G. I. Hernández-Salgado, M. E. Hernández-Terán and G. A. Fuentes, *Journal of the Mexican Chemical Society*, 2021, **65**, 74–83.

311   A. N. Pestryakov, V. P. Petranovskii, A. Kryazhov, O. Ozhereliev, N. Pfänder and A. Knop-Gericke, *Chemical Physics Letters*, 2004, **385**, 173–176.

312   M. Inaba, K. Murata, M. Saito and I. Takahara, *React Kinet Catal Lett*, 2006, **88**, 135–141.

313   M. Ghashghaee, *Reviews in Chemical Engineering*, 2018, **34**, 595–655.

314   J. C. Morris, *J. Am. Chem. Soc.*, 1944, **66**, 584–589.

315   E. Gil-Av, J. Shabtai and F. Steckel, *Ind. Eng. Chem.*, 1960, **52**, 31–32.

316   T. Tsuchida, T. Yoshioka, S. Sakuma, T. Takeguchi and W. Ueda, *Ind. Eng. Chem. Res.*, 2008, **47**, 1443–1452.

317   United States, US2421361A, 1947.

318   R. A. L. Baylon, J. Sun and Y. Wang, *Catalysis Today*, 2016, **259**, 446–452.

319   United States, US20090054705A1, 2009.

320   J. Baloyi, T. Ntho and J. Moma, *RSC Advances*, 2018, **8**, 5197–5211.